CONVECTIVE BOUNDARY LAYER FLOW OF VISCOELASTIC MICROPOLAR FLUID OVER BLUFF BODY WITH ALIGNED MAGNETIC EFFECT

LAILA AMERA AZIZ

DOCTOR OF PHILOSOPHY

UNIVERSITI MALAYSIA PAHANG
AL-SULTAN ABDULLAH

UNIVERSITI MALAYSIA PAHANG AL-SULTAN ABDULLAH

DECLARATION OF THESIS AND COPYRIGHT

Author's Full Name	:	LAILA AMERA AZIZ
Date of Birth	:	14/08/1988
Title	:	CONVECTIVE BOUNDARY LAYER FLOW OF VISCOELASTIC MICROPOLAR FLUID OVER BLUFF BODY WITH ALIGNED MAGNETIC EFFECT
Academic Session	:	SEMESTER II 2023/2024

I declare that this thesis is classified as:

☐	CONFIDENTIAL	(Contains confidential information under the Official Secret Act 1997)*
☐	RESTRICTED	(Contains restricted information as specified by the organization where research was done)*
☒	OPEN ACCESS	I agree that my thesis to be published as online open access (Full Text)

I acknowledge that Universiti Malaysia Pahang Al-Sultan Abdullah reserves the following rights:

1. The Thesis is the Property of Universiti Malaysia Pahang Al-Sultan Abdullah
2. The Library of Universiti Malaysia Pahang Al-Sultan Abdullah has the right to make copies of the thesis for the purpose of research only.
3. The Library has the right to make copies of the thesis for academic exchange.

Certified by:

(Student's Signature)

(Supervisor's Signature)

New IC/Passport Number
Date: 04/08/2024

ASSOC. PROF. DR ABDUL RAHMAN MOHD KASIM
Name of Supervisor
Date: 04/08/2024

NOTE : * If the thesis is CONFIDENTIAL or RESTRICTED, please attach a thesis declaration letter.

اونيۏرسيتي مليسيا ڤهڠ السلطان عبدالله
UNIVERSITI MALAYSIA PAHANG
AL-SULTAN ABDULLAH

SUPERVISOR'S DECLARATION

We hereby declare that we have checked this thesis and in our opinion, this thesis is adequate in terms of scope and quality for the award of the degree of Doctor of Philosophy.

____

(Supervisor's Signature)

Full Name : DR. ABDUL RAHMAN BIN MOHD KASIM

Position : ASSOCIATE PROFESSOR

Date : 04/08/2024

____

(Co-supervisor's Signature)

Full Name : DR. MOHD ZUKI BIN SALLEH

Position : PROFESSOR

Date : 04/08/2024

STUDENT’S DECLARATION

I hereby declare that the work in this thesis is based on my original work except for quotations and citations which have been duly acknowledged. I also declare that it has not been previously or concurrently submitted for any other degree at Universiti Malaysia Pahang Al-Sultan Abdullah or any other institutions.

____

(Student’s Signature)

Full Name : LAILA AMERA AZIZ

ID Number : PSE15001

Date : 04/08/2024

CONVECTIVE BOUNDARY LAYER FLOW
OF VISCOELASTIC MICROPOLAR FLUID
OVER BLUFF BODY WITH ALIGNED
MAGNETIC EFFECT

LAILA AMERA AZIZ

Thesis submitted in fulfillment of the requirements
for the award of the degree of
Doctor of Philosophy

Centre for Mathematical Sciences

UNIVERSITI MALAYSIA PAHANG AL-SULTAN ABDULLAH

AUGUST 2024

In dedication to:

My beloved parents,
Encik Aziz Mamat and Puan Haslina Abu Hasan

My beloved brothers,
Ahmad Mustakim Aziz and Ahmad Mukhlis Aziz

PhD is not about brilliance but resilience

ACKNOWLEDGEMENTS

All praise to Allah S.W.T, The Almighty for giving me the chance, blessing and strength to complete this study. May Allah's blessing goes to His final Prophet Muhammad (peace be up on him), his family and his companions.

Alhamdulillah that after a long way, I have finally come to end of this journey. In fact, it is still dreamlike to me that this thesis is finally completed. When I decided to pursue my PhD on a part time basis with my full-time job as a lecturer, I was absolutely clueless about the endless challenges awaiting me until they came kicking, taxing me both physically and mentally. The things that kept me going are the fact that the only way to continue my career path is by having this qualification and most importantly, my own team of cheerleaders who keep rooting for me.

Among the most important figures behind this achievement is definitely my main supervisor, Associate Prof. Dr. Abdul Rahman Mohd Kasim. Thank you for not giving up on me despite all the time I took to complete this thesis. He never fails to give me the push I needed whenever I drifted away from my study, drowned in work. He also taught me to embrace new challenges and opportunities, making me realise my worth. Special thanks also to my co-supervisor, Prof. Dr. Mohd Zuki bin Salleh. Thank you for the encouragement and faith that you have in me. Your kindness will be forever etched in my memories.

I also would like to express my gratitude to the two pillars in my life, my dad, Encik Aziz Mamat and my mum, Puan Haslina Abu Hasan. I will never find the light of the tunnel without your endless support and prayers. Not to be forgotten, my dearest brothers, Ahmad Mustakim Aziz and Ahmad Mukhlis Aziz.

I would also like to extend my gratitude to Mr. Mohammed Abdul Qawi for always being there for me through countless tears. Thank you for lending me your strength and confidence when I drained mine, helping me to get back on my feet again as I stumble along the way to reach the end of this journey.

Last but not least, thank you to the younger sisters I never had, Mila and Wani for being with me for three quarters of my PhD journey, planning and dragging me to conferences. My babes and rays of sunshine, Syi, Ilah and Fizah for the readiness to cheering me up and your unwavering support.

Thank you everyone.

ABSTRAK

Bendalir viskoelastik mikropolar adalah sejenis bendalir bukan Newtonian dengan ciri-ciri likat dan elastik serta mengandungi struktur mikro. Pelbagai bahan seperti darah, cecair sinovial, kristal cecair dan sebahagian pelincir mempamerkan ciri-ciri bendalir mickropolar viskoelastik, menjadikan kajian ini bermanfaat untuk pelbagai aplikasi industri, kejuruteraan dan bioperubatan. Sebagai contoh, kajian ini boleh membantu memahami tingkah laku bendalir sekitar penyemperit silinder dalam pemprosesan polimer. Disebabkan sifat kompleks bendalir ini, persamaan yang mengawal cecair mikropolar viskoelastik mencapai sehingga tertib keempat dalam persamaan momentum yang memerlukan syarat sempadan tambahan untuk mendapatkan penyelesaian lengkap. Tesis ini mengkaji tingkah laku aliran bendalir mikropolar viskoelastik melewati jasad tumpul, khususnya silinder bulat mendatar dan sfera dibincangkan untuk fenomena olakan bebas dan campuran. Pada mulanya, kajian ini memberi tumpuan kepada aliran lapisan sempadan dan kemudiannya analisis dikembangkan untuk merangkumi olakan bebas dan campuran. Olakan bebas terjadi kerana perbezaan ketumpatan dalam bendalir yang disebabkan oleh kecerunan suhu, kebiasaannya melibatkan tingkah laku bendalir di sekitar permukaan yang dipanaskan atau disejukkan, manakala olakan campuran melibatkan kedua-dua olakan bebas dan gerakan bendalir paksa, lazimnya dari sumber luaran. Persamaan menakluk lapisan sempadan ditukar ke bentuk tanpa dimensi sebelum ditukar kepada set persamaan lapisan sempadan ketakserupaan. Kemudian, kaedah kotak-Keller, iaitu skim perbezaan terhingga, digunakan untuk menyelesaikan persamaan ini secara berangka menggunakan bahasa pengaturcaraan Fortran. Keputusan dipaparkan dalam bentuk jadual dan grafik yang merangkumi profil halaju, suhu dan putaran mikro, geseran permukaan dan pemindahan haba untuk pelbagai parameter seperti viskoelastik, mikropolar, olakan campuran, magnetik serta sudut sejajar medan magnet bagi kes suhu permukaan malar. Kajian mendapati bahawa kelajuan, suhu dan ciri mikro-putaran bendalir viskoelastik mikropolar dipengaruhi oleh sifat viskoelastiknya serta kehadiran mikrostruktur dalam bendalir. Secara umum, viskoelastisiti dan mikrostruktur cenderung melambatkan halaju aliran tetapi meningkatkan profil suhu dan putaran mikro. Ciri-ciri ini juga mempengaruhi sifat pemindahan haba dan geseran permukaan aliran bendalir serta mengawal pemisahan lapisan sempadan pada jasad tumpul. Kelikatanjalan yang lebih tinggi mengakibatkan pengurangan dalam pekali pemindahan haba dan geseran permukaan, sementara mikropolariti yang lebih tinggi menghasilkan kesan yang sebaliknya. Selain itu, parameter sudut sejajar juga dikenal pasti sebagai faktor pembatas untuk kekuatan medan magnet di mana kekuatan adalah maksimum apabila garis medan magnet dan vektor kelajuan aliran bersilang. Parameter olakan campuran menunjukkan kesan yang sama pada silinder bulat mendatar dan sfera. Peningkatan parameter olakan campuran menyebabkan peningkatan halaju aliran, pekali geseran permukaan dan pemindahan haba di samping merendahkan profil putaran mikro dan suhu. Secara keseluruhannya, masalah yang dibincangkan dalam tesis ini tidak terhad kepada geometri dan kesan aliran bendalir yang dikaji ini, malah idea ini juga boleh diekstrapolasi kepada geometri alternatif dan kesan tambahan lain.

ABSTRACT

Viscoelastic micropolar fluid is a non-Newtonian fluid that exhibits both viscous and elastic properties along with the presence of microstructures. Diverse materials such as blood, synovial fluid, liquid crystals, and certain lubricants exhibit the characteristics of viscoelastic micropolar fluids, rendering this study advantageous for a broad spectrum of industrial, engineering, and biomedical applications. For instance, this study could help to understand fluid behaviour around cylinder extruders in polymer processing. Due to the complex nature of this fluid its governing equations involve fourth-order derivatives in the momentum equations that require an additional boundary condition to obtain a complete solution. This thesis investigates the behaviour of viscoelastic micropolar fluid flow over bluff bodies, specifically horizontal circular cylinders and spheres. Initially, the study focuses on boundary layer flow, and subsequently extends its analysis to encompass free and mixed convection scenarios. Free convection occurs due to density differences in the fluid caused by temperature gradients, often involving fluid behaviour around heated or cooled surfaces, while mixed convection involves both free convection and forced fluid motion, typically from an external source. The governing boundary layer equations are transformed into the non-dimensional form before they are converted into a set of non-similar boundary layer equations. Then, the Keller-box scheme, which is a finite-difference method, was used to solve these equations numerically employing the Fortran programming language. The results are displayed in both tabular and graphical forms include velocity, temperature and microrotation profiles, skin friction and heat transfer for various parameters such as viscoelastic, micropolar, mixed convection, magnetic as well as the aligned angle of the magnetic field for the case of constant wall temperature. From the study, it is found that velocity, temperature and micro-rotation behaviour of viscoelastic micropolar fluid is influenced by its viscoelastic nature as well as the presence of microstructures in the fluid. In general, viscoelasticity and microstructures tend to retard the velocity of the flow but enhance the temperature and microrotation profiles. These characteristics also have a leverage on the heat transfer and skin friction properties of the fluid flow while exerting control on the boundary layer separation on the bluff body. Higher viscoelasticity leads to a reduction in heat transfer and skin friction coefficient, while higher micropolarity results in the opposite behavior. In addition, the aligned angle parameter is also recognized as a limiting factor for the strength of the magnetic field and the strength is maximised when the magnetic field lines and flow velocity vectors are orthogonal. The mixed convection parameter has the same effect on horizontal circular cylinder and sphere. Elevating the mixed convection parameter leads to augmented flow velocity, skin friction coefficient, and heat transfer, while simultaneously impeding microrotation and temperature profiles. Overall, the issue addressed in this thesis is not solely confined to the present geometry and fluid flow impact; rather, it can be extrapolated to encompass alternative geometries and supplementary effects.

TABLE OF CONTENT

LIST OF TABLES

LIST OF FIGURES

LIST OF SYMBOLS

$\mathbf{a}$	acceleration
a	radius of a cylinder (or sphere)
$\mathbf{b}$	induced magnetic field
$\mathbf{B}$	total magnetic field
$\mathbf{B_0}$	uniform magnetic field
c_p	specific heat at constant pressure
C_f	local skin friction coefficient
$\mathbf{d}$	deformation rate
$\mathbf{D}$	rate of strain tensor
$\mathbf{E}$	electric field
$\mathbf{F}$	force
$\mathbf{F_b}$	body force
$\mathbf{F_s}$	surface force
f_x	x-component of body force
f_y	y-component of body force
f_z	z-component of body force
$\mathbf{g}$	gravitational force
$\mathbf{H}$	microrotation vector
H	microrotation component / angular velocity of micropolar fluid
$\mathbf{I}$	identity vector
$\mathbf{J}$	electric current density
j	microinertia per unit mass
k	thermal conductivity
k_0	short-memory coefficient
K	viscoelastic parameter
K_1	micropolar parameter of micropolar fluid
M	magnetic parameter
n	coupling number
p	pressure of fluid phase
p_h	hydrostatic pressure
p_d	dynamic pressure
Pr	Prandtl number
$\dot{q}$	volumetric heat rate addition per unit mass
$\mathbf{r}$	position vector
r	radial distance from symmetrical axis to surface of sphere
Re	Reynolds number
Re_L	Reynold number based on the length of plate
$\mathbf{T}$	total stress tensor
T_{ij}	stress tensor in index notation
T	temperature
T_∞	ambient temperature of fluid
u	velocity of fluid in x-direction
u_e	velocity outside boundary layer

U_∞	free stream velocity
v	velocity of fluid in y-direction
$\mathbf{V}$	velocity vector field of fluid
W	work done on or by the system
$\dot{W}$	work rate done by force acting on moving fluid element
x	coordinate in direction of surface motion
y	coordinate in direction normal to surface motion

Greek letters

α	aligned angle
β^*	thermal expansion coefficient
δ	boundary layer thickness
δ_{ij}	Kronecker Delta
η	dimensionless similarity variable
θ	dimensionless temperature
κ	vortex viscosity
λ	mixed convection parameter
μ	dynamic viscosity
ν	kinematic viscosity
ρ	density of fluid
σ	electric conductivity of fluid
σ_x	normal stress in x-direction
σ_y	normal stress in y-direction
σ_z	normal stress in z-direction
τ_w	reduced skin friction parameter
τ_{xx}	shear stress in x-direction exerted on a face normal to x-axis
τ_{xy}	shear stress in y-direction exerted on a face normal to x-axis
τ_{xz}	shear stress in z-direction exerted on a face normal to x-axis
τ_{yx}	shear stress in x-direction exerted on a face normal to y-axis
τ_{yy}	shear stress in y-direction exerted on a face normal to y-axis
τ_{yz}	shear stress in z-direction exerted on a face normal to y-axis
τ_{zx}	shear stress in x-direction exerted on a face normal to z-axis
τ_{zy}	shear stress in y-direction exerted on a face normal to z-axis
τ_{zz}	shear stress in z-direction exerted on a face normal to z-axis
$\boldsymbol{\tau}$	viscous stress tensor
$\boldsymbol{\tau}_e$	viscoelastic stress tensor
$\boldsymbol{\tau}_p$	couple stress tensor
ϕ	rate of viscous dissipation
ψ	stream function
χ	thermal diffusivity

LIST OF ABBREVIATIONS

MHD	Magnetohydrodynamics
ODE	Ordinary differential equation
PDE	Partial differential equation
CNT	Carbon nanotube
UV	Ultraviolet
GDQLLM	Generalized differential quadrature local linearisation method
pH	Potential of hydrogen

LIST OF APPENDICES

CHAPTER 1

INTRODUCTION

1.1 Research Background

Fluid dynamics is a study related to movement of fluid and gas which can be affected by different forces. This field of study is pertinent to numerous disciplines and has enabled scientists to explore natural occurrences such as ocean current, plate tectonics as well as the theoretical foundations of technological advancements such as oil pipelines, conditioning systems and aircraft design. The discipline that is devoted to solving mathematically challenging fluid flow problem is known as computational fluid dynamics where Navier-Stokes is solved numerically using computer software to simulate fluidic system (Raman et al., 2018). Computational fluid dynamics has been proven to assist engineers in the designing process to maximize performance and ensure consumers' safety in addition to detecting damage to machinery components that is undetectable by instruments.

Most studies in fluid dynamics focus on an important region of the fluid known as the boundary layer, driven by the fact that what happens on the boundary layer will affect the outer flow. Reflecting upon the boundary layer theory, the outstanding research by Prandtl (1928) needs to be addressed. Introducing the idea of existence of a thin transition layer, or better known as the boundary layer that is adjacent to the wall of solid boundary in a fluid flow, Prandtl has opened a new paradigm in terms of applications in aerodynamics and fluid dynamics. He hypothesized that due to the adhesion of fluid on the wall caused by friction effect, the fluid would assume the wall velocity, which is also known as the no-slip condition and a large velocity gradient exists within the layer (Anderson, 2005). Since the velocity gradient is proportional to the shear stress, the local shear stress will also be large, hence the skin friction drag force on the body within this region is prominent. However, outside the boundary layer, viscosity has no effect, and it is known as the free flow.

Besides, Prandtl also raised the idea of the presence of a separation point where the flow detached from the wall into the free flow because of external conditions (Tani, 1977) which leads to a relevant contribution in aviation as boundary layer separation is an important factor for aircraft wings (Svorcan et al., 2022). In airplane design, the main goal is to reduce the pressure drag which opposes the forward motion or also known as aircraft stall by delaying the boundary layer separation area. Among the ways to achieve this are by keeping the aircraft body smooth to reduce the air and surface friction and using the optimum angle of attack for the wing.

The physical phenomenon of boundary layer initiates two possible sources of drag. The first type of drag is the frictional drag which is caused by frictional shear stress between fluid and solid surface, while the other is the pressure drag that is formed due to boundary layer separation. The shape of the body is the indicator whether the flow is dominated by frictional, or pressure drag. For bluff body like cylinder and sphere, which are of interest in this study, pressure drag has the upper hand. With practical importance, for example in design of sports equipment (e.g. dimple on golf balls to delay separation) (Mehta, 1985), and in reducing wind noise in car design (Watkins, 2010), the topic of fractional and pressure drag at various types of body are always relevant and crucial to be discussed in studies related to boundary layer for any types of fluid.

Different types of fluid require different sets of equations as the model accentuates the predominant characteristics of the fluid. Viscoelastic fluid is a type of non-Newtonian fluid, used to classify fluids that are both viscous and elastic in nature. These fluids are semi-permanently deformed when force is exerted on them but would go back to the original state when the force is removed. Unset cement, honey and egg-white are examples of viscoelastic fluid. The most common viscoelastic fluid in our daily life is toothpaste. When we press the tube, the paste deforms following the force from our hand, but when force is released, the fluid goes back into the tube to its initial state. Some industrial polymers are viscoelastic in nature and even biofluids like blood and saliva are mostly viscoelastic ((Rock et al., 2020); and (Plan et al., 2020)).

Besides resembling industrial fluid like polymer, non-linear viscoelastic fluid model can also be used to model brain injury since about 83% of total brain mass is made up of water. The initial investigation commenced in the 1940s with Holbourn (1943), presents utilization of brain and cranium anatomy, in conjunction with Newton's law of motion, to approximate the likelihood of an injury occurring and its precise location based on the shear strain within the brain. This pioneer study has then inspired Cotter et al. (2002) to propose his model and his numerical results suggest that brain injury is actually a brain turbulence phenomenon. Furthermore, Kainz et al. (2023) conducted an experimental study using a tailor-made polyvinyl alcohol-based hydrogel to mimic the brain tissue. These studies evident the importance of the viscoelastic fluid model for medical purpose in neurodevelopment and neurosurgery.

Similar to viscoelastic, micropolar fluid also belongs to the non-Newtonian family. It is a new class of fluid that responds to micro-rotational motion and spin inertia triggered by small, rigid and randomly oriented cylindrical elements in the form of dumbbell-shaped molecules suspended in viscous fluid (Saleem et al., 2012). Examples of micropolar fluid include lubricants, blood and liquid crystals. Red blood cells are one of the components in blood, along with white blood cell and platelets in plasma. They are small, semi rigid particles for which microrotation is substantial to increase blood viscosity, thus changing the blood rheology. The presence of microstructure would affect the physical and mechanical properties of any fluid. Hence, it motivates researchers to re-examine the classical flows in order to reveal the effects of the microstructure on how it alters the behavior of the flow.

When it comes to micropolar fluid, Eringen is a significant figure that paves the way for a new class of fluids that responds to micro-rotational motion and spin inertia. His work on micropolar fluid model (Eringen, 1966) and a more recent version (Eringen, 2001), basically serves as a user manual for any model of micropolar fluid and has been cited continuously. In the study, Eringen highlighted how the classical Navier-Stokes theory is incapable of acknowledging the unique characteristic of micropolar fluid. Thus, by incorporating the microfluid theorem from his own work (Eringen, 1964), he introduced the micropolar fluid model. Since the foundation has been laid, research opportunities are created to explore on this fluid and improvise previous studies that do not consider the presence of microstructures.

The mathematical concept of micropolar fluid has also been discussed in detail by Lukaszewicz (1999) in his work and besides lubrication theory, other real-life applications of the fluid had also been highlighted. Among them is how micropolar model can serve to represent biological flows such as the blood flow in our body and lubrication in human joints which could be a life-changing contribution in biomedical engineering.

To date, numerous studies have attempted to describe the blood flow model as micropolar (Beg et al., 2022); (Reddy et al., 2023) and (Vilchevskaya et al., 2023), thus convincing the author on the importance of micropolar fluid for medical sciences break through. Prasad and Yasa (2021) and Abdullah and Norsarahaida (2010) were both intrigued by the blood flow through a stenosis-related narrowing of a tapered artery caused by the accumulation of adipose deposits. The consensus among these studies is that the micropolar fluid model most accurately represents blood flow due to the rotating suspended microelements that comprise blood.

Micropolar fluid has also been proven to be better lubricants compared to other fluids with the same viscosity. According to Tipei (1979), lubricants with micro rotational properties generate higher pressure and load carrying capacity while enhancing bearing performance. Zu-gan and Zhang-ji (1987) from their study revealed that the scale of suspended materials or the additive in the lubricants affects the performance of the lubricant. Additive with smaller scale is preferred as it works better at decreasing the friction coefficient and increasing the heat dissipation effect. Similar studies on micropolar fluids as lubricants have also been published by Mukutadze et al. (2022) and Sharma et al. (2023).

Magnetohydrodynamics (MHD) is among the sought-after effect in fluid flow problems. MHD is the study that concerns the behaviour of electrically conducting fluid under the exposure of electric and magnetic field. The Lorentz force or electromagnetic force is the outcome of the motion when current is induced into the fluid causing the magnetic field itself to be altered. In astrophysics, humans are protected from the harmful UV radiation by the earth's magnetic field that is self-produced from the motion of earth's liquid core. Besides, the important role of MHD in industrial process is a major motivation to study MHD especially in metallurgical industry. The versatility of Lorentz force and magnetic field is recognized by metallurgists and now is part of the regular process to heat, pump, stir, stabilize, repel and levitate liquid metals (Davidson, 2016).

Convection is a mode of heat transfer that occurs due to fluid movement from hotter to colder region. The simplest example of convection in daily life is how the air condition works to cool a room. During the process, the less dense hot air will go up and replaced by the cooler air from the air conditioner that will sink to the lower part of the room due to higher buoyancy. The cycle continues generating a convection current that will keep the room at the desired temperature. This also explains the reason why air conditioner is positioned high on the wall instead of at the bottom like a heater.

Convection is applied in the mechanism of refrigerators, air-cooled engines, convection oven and even for heat exchanger in industrial machines as well as nuclear facilities. Heat exchanger works by allowing interactions between fluid at different temperatures and as a result, heat is transferred to one another to achieve equilibrium. The industrial furnace that are used in petroleum refining and other chemical process industries, for example, have two specific chambers: one section is where radiation heat transfer is dominant while the other chamber uses the mechanism of convection heat transfer.

There are three types of convection which are free or natural, forced and mixed convection. Free convection occurs due to buoyancy forces. Cooling a hot cup of water by exposing it to room temperature is an example of free convection. The heat from the hot water is gradually transferred to the outer layer of air and as a result, the water cools down. Forced convection is when fluid movement is externally driven by another source like a fan or pump. Refrigerators, for example use fans to blow away the heat and retain the cold temperature. This concept could also work in our favour on a cold winter day. Turning on a ceiling fan on low speed would circulate the air and force the hotter air to come down instead of drifting on the ceiling and leaving the colder air at the bottom due to the density. Mixed convection, as the name suggests is the combination of both free and forced convections. The concept is applied in the cooling system of photovoltaic or solar panels to remove excess heat and enhance electrical efficiency which is attainable using the nano-cooling fluid as studied by Al-Waeli et al. (2018).

Putting all the above elements together, this study focuses on the boundary layer flow of viscoelastic micropolar fluid subject to aligned MHD effect, considering two distinct geometries, namely the horizontal circular cylinder and sphere, in the context of free and mixed convection modes. To the best of the author's knowledge, the study of viscoelastic micropolar model over bluff body has not yet received much attention. This complex fluid model is anticipated to compensate the weakness of the existing models and become a three-in-one model for viscoelastic, micropolar and viscoelastic micropolar fluid flow.

1.2 Problem Statement

Advancements in industrial and engineering applications over recent decades have highlighted the limitations of classical Navier-Stokes equation on describing complex fluid behaviours, which require the discovery of non-Newtonian fluid model (Bafakeeh et al., 2023). These scenarios include mathematical models that represent complex fluid with characteristics that is implausible to be captured by simpler model. One such model is the viscoelastic micropolar model. Since many fluids used in polymer processing, biotechnology and advanced material manufacturing exhibit both viscoelastic and micropolar properties, the viscoelastic micropolar model addresses limitation and could provide better predictions in scenarios where the existing model that separate viscoelastic and micropolar characteristics fall short (Gaffar et al., 2020).

Boundary layer flow over bluff bodies such as circular cylinder and spheres are of particular interest due to their prevalence in real-word scenarios. These shapes generate complex flow pattern and understanding the phenomena is crucial for optimizing designs in aerospace, civil and marine engineering (Arjun & Kumar, 2017). Investigating the behaviour of viscoelastic micropolar fluid around these geometries can provide insight to enhance efficiency, reducing drag and improve performance in wide range of technology and processes . On those grounds, this study aims to explore the following problems:

i. Boundary layer flow of viscoelastic micropolar fluid over a circular cylinder.

ii. Free convection boundary layer flow of viscoelastic micropolar fluid with aligned MHD over a horizontal circular cylinder.

iii. Mixed convection boundary layer flow of viscoelastic micropolar fluid with aligned MHD over horizontal circular cylinder.

iv. Free convection boundary layer flow over solid sphere in viscoelastic micropolar fluid with aligned MHD.

v. Mixed convection boundary layer flow of viscoelastic micropolar fluid over solid sphere with aligned MHD.

1.3 Research Questions

For this thesis, the research questions that will guide the investigation for all the problems outlined in Section 1.2 are:

i. How to formulate mathematical model for the following proposed problems?

ii. How to solve the governing nonlinear differential equations of the proposed problems by using Keller-box method?

iii. What are the effects of viscoelastic, micropolar, magnetic and aligned angle effect on the skin friction and heat transfer coefficient as well as the velocity, microrotation and temperature profiles of the fluid?

1.4 Research Objectives

This study investigates the complex dynamics of viscoelastic micropolar fluid flow in bluff body. The research begins by examining the boundary layer flow over a circular cylinder to provide a foundation for subsequent analyses. Building upon this initial investigation, the study expands to explore free and mixed convection boundary layer flow over both horizontal circular cylinders and solid spheres with aligned MHD effect. The objectives of this study are as follows:

i. To introduce a viscoelastic model with microstructures that exhibit viscous and elastic characteristics as it passes over a horizontal circular cylinder and solid sphere.
ii. To improve the existing models of non-Newtonian fluid that can be a generalized model for complex fluid.
iii. To develop numerical codes for solving the complex fluid using Keller-box method.
iv. To obtain numerical solutions of the viscoelastic micropolar fluid model and conduct validation test over existing literatures.
v. To investigate the effect of the parameters involved in the model to the skin friction and heat transfer of the fluid as well as the temperature, velocity and microrotation profiles.

1.5 Research Framework

The transformed governing equations have been solved numerically using the Keller-box method coded in Fortran language. The research framework of this study is shown in the following figure.

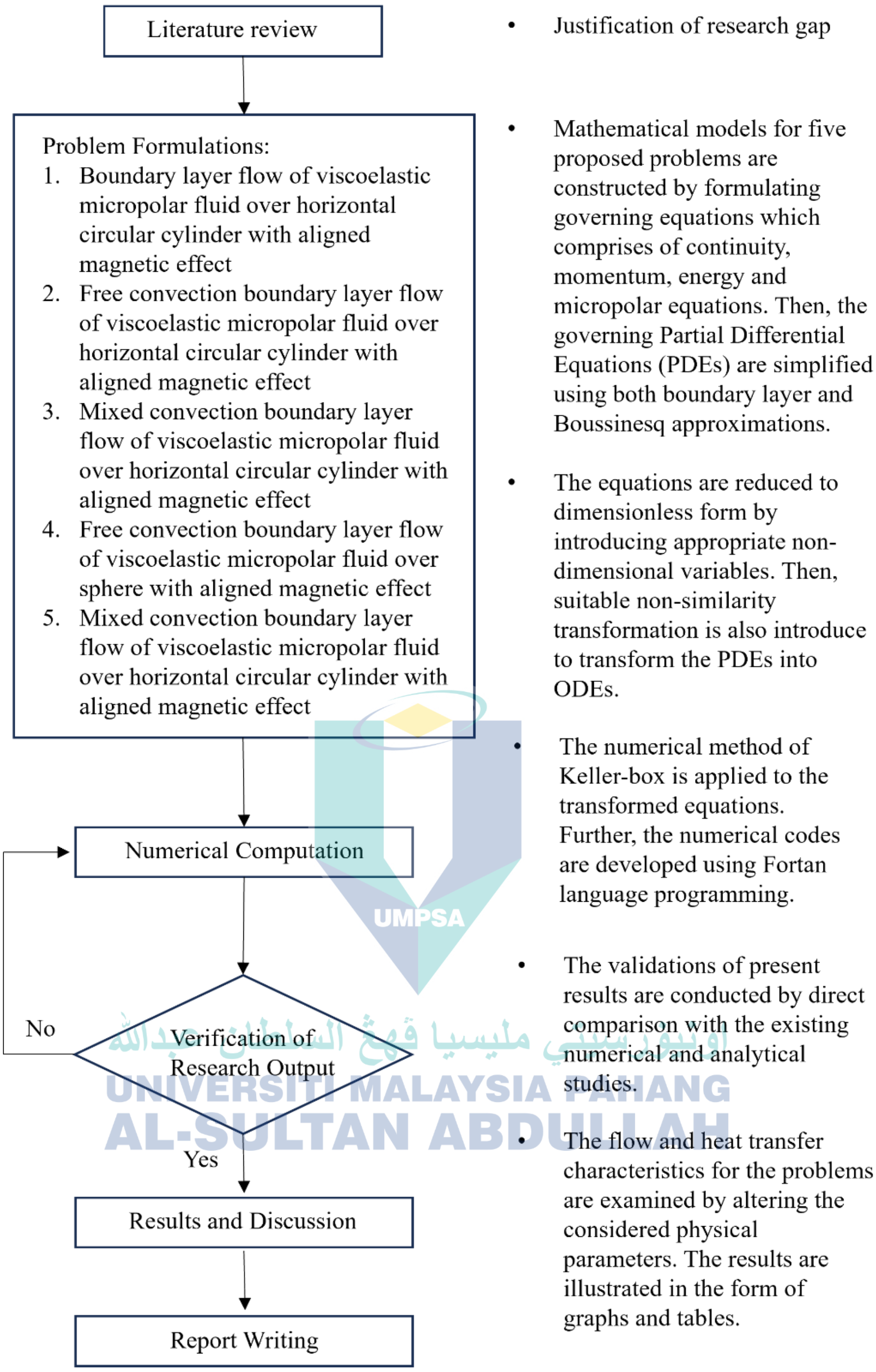

Figure 1.1 Research framework

1.6 Research Scope

The focus of this study is on two-dimensional incompressible boundary layer flow of viscoelastic micropolar fluid as it goes over horizontal circular cylinder and solid sphere. Viscoelastic micropolar fluid is a complex fluid that exhibits both viscous and elastic properties, while also containing microstructures that can undergo rotation independent of the fluid's overall motion. Non-similarity transformation variables are applied to the dimensionless governing equations which results in the equations being reduced to a set of partial differential equations with less complexity. Due to the complication of the differential equations, exact solutions are non-existent and only numerical solutions are attainable.

In this study, only the behaviour of the flow at the boundary layer will be considered as the boundary layer region has been proven to be crucial in various fields. Throughout the analysis, blood is utilised as a representative model for viscoelastic micropolar fluid due to its unique composition of cellular components, primarily red blood cells, that can rotate independently within the plasma. In addition, its nature that can partially recover its shape after deformation is consistent with the behaviour of viscoelastic fluid.

1.7 Research Significance

Micropolar and viscoelastic fluid are both from the non-Newtonian family. Viscoelastic is a renowned type of fluid in industrial-manufacturing processes and engineering field with practicality in petroleum drilling, manufacturing of foods and paper, as well as reducing frictional drag on the hulls of ships and submarines. Typical applications for viscoelastic boundary layer flow includes polymer sheet extrusion from a dye, glass fibre and paper production, and drawing of plastic films (Jafar et al., 2019) and (Veena et al., 2023).

Micropolar fluid is equally interesting and plays a significant role in chemical and biomedical industry. In the chemical industry, the micropolar fluid theory can be used to visualize the flow of lubricants, liquid crystal and polymeric fluids. Meanwhile, in medicine, the synovial fluid in knee that plays an important role to reduce friction between the articular cartilages of synovial joints during movements exhibit micropolar traits (Florea & Roşca, 2015).

However, there exists certain liquids such as human blood and synovial fluid that fall into both categories of being viscoelastic and micropolar. The existing models of viscoelastic or micropolar fluid are inadequate to describe the flow of such fluid. If viscoelastic model is considered, the presence of suspended particles that rotate in the fluid are neglected. On the other hand, micropolar fluid model fails to embrace the elasticity nature of the viscous fluid. These characteristics require utmost consideration since the presence of the particles and the viscoelasticity have paramount effect on the behaviour of the fluid flow and heat transfer. To put it briefly, choosing the existing model means that we have to abandon one characteristic or another and hence will not be the greatest option since the model is not the best representation of the fluid.

Therefore, in this study, the non-Newtonian viscoelastic and micropolar fluid will not be considered separately as prior studies, but together as a complex fluid known as viscoelastic micropolar. This study is motivated by the existence of certain fluids that could fit both characteristics as being viscoelastic as well as micropolar fluid, for example, human and animal blood. The outcome produced from the mathematical model proposed will give a more accurate representation of viscoelastic fluid with the presence of microrotating particles. With the existence of viscoelastic micropolar model, the previous models are improvised for a better representation of these types of fluid to explain the motion of such fluid.

Convection is the main method of heat transfer in fluids. Free convection is a method of heat transfer due to temperature differences without the assistance of any external mechanism. Convection is especially significant in food industry. Free convection assists in sterilization of liquid food material in still retorts with steam flowing around the surface of the can. The process occurs by exposing the hot surface with or without insulation to colder ambience air (Koribilli et al., 2011). It also takes place when food is placed inside a chiller or freezer store in which circulation is not assisted by fans. Besides these examples, free convection is also common in nature and engineering applications.

Mixed convection, on the other hand, occurs in many technological and industrial applications such as solar central receivers that are exposed to wind currents, cooling of nuclear reactors during emergency shutdown, heat exchangers placed in low-velocity environments, boundary-layer control on air foil, lubrication of ceramic machine parts and food processing. Mixed convection flows arise when the free stream, inertial and near wall buoyant forces have strong effects on the resulting convective heat transport.

The MHD effect will also be considered for all problems in this study. However, instead of transverse MHD, which is common in the study of fluid flow, the main focus will be on the effect of aligned MHD. By considering aligned MHD, the mathematical models proposed are more generalized and valid for both transverse and aligned MHD. Aligned MHD is more industrially befitting since the exposure of the magnetic field could be at any arbitrary angle not only limited to being perpendicular to the fluid flow.

From the previous arguments, the significance of the study of free and mixed convections of viscoelastic micropolar boundary layer flow problems with aligned MHD effect is justified due to its imperative applications in real life. For instance, the viscoelastic micropolar fluid model over sphere could be used to analyse the blood flow in human body when microsphere is used as drug carrier so that the drug can be released at specific parts of our body as the microsphere can be pH responsive (Singh & Nayak, 2023). Besides, the vortex flow meter also works based on the concept of vortex formation that occurs when the fluid flow separates from bluff body (Li et al., 2020).

Considering these facts, the output from this research could enhance the understanding of the fluid flow phenomena and improve the development of related fields, for example the manufacturing industries. Besides, the generation of efficient algorithm of the viscoelastic micropolar problem will help in solving the problem of computational fluid dynamics in the future and improve the existing models.

1.8 Thesis Organization

This thesis comprises of a total of nine chapters. The first three chapters are the preliminary part of this study while the rest of the chapters will elaborate each of the problem in detail. The essence of each chapter is summarized as follows:

Chapter 1: The introductory part where the research background, problem statement research objectives, research scope and research significance are explained in detail.

Chapter 2 : The literature that leads toward the establishment of the problems are acknowledged and research gaps are addressed in this particular chapter.

Chapter 3: This chapter focuses on the derivation part of the problems which centres around the conservation of mass, momentum, energy and angular momentum. From the derivation, the governing equations which consist of continuity, momentum, angular momentum and energy equation are obtained and to be solved numerically in the upcoming chapters.

Chapter 4: For the first problem, we will look at the boundary layer problem of viscoelastic micropolar fluid over circular cylinder. The constitutive equations are solved using Keller-box method in Fortran and compared to previous results. Then, the effects of viscoelastic, micropolar, magnetic and aligned angle parameters on the velocity and microrotation profiles as well as skin friction coefficient are observed.

Chapter 5: Free convection boundary layer flow of viscoelastic micropolar fluid over horizontal circular cylinder will be discussed. There will be an additional energy equation in the governing equations. Hence, outcome will also include temperature profile and heat transfer coefficient.

Chapter 6: In this chapter mixed convection boundary layer flow of viscoelastic micropolar fluid over horizontal circular cylinder is investigated. This leads to an additional parameter for mixed convection to be inspected.

Chapter 7: This chapter will discuss the free convection boundary layer flow of viscoelastic micropolar fluid over sphere. Effects of viscoelastic, micropolar, magnetic and aligned angle parameter on the velocity, temperature and microrotation profiles as well as skin friction coefficient and heat transfer will be observed.

Chapter 8: The problem to be discussed is the mixed convection boundary layer flow of viscoelastic micropolar fluid over sphere. The same profiles and physical parameters as in Chapter 7 are evaluated for all parameters on top of the mixed convection parameter.

Chapter 9: This chapter will conclude this study and provide recommendations for future research opportunities related to this topic.

CHAPTER 2

LITERATURE REVIEW

2.1 Introduction

In this chapter, the previous work of other researchers that incited this study and made it possible are reviewed. Viscoelastic and micropolar fluid are the main interests in various studies and the same goes for magnetohydrodynamics effect. The numerical scheme chosen for this study is also highlighted. Reviewing these works provided insights into the missing pieces in the fluidic system that is worth putting together for application purposes.

2.2 Viscoelastic Fluid

The study of viscoelastic fluid is familiar in fluid mechanics due to the possible important discoveries that could be huge contributions to various fields of interest as these non-Newtonian fluid covers a significant range of fluid. Among the earliest viscoelastic fluid models is the Oldroyd-B model (Oldroyd, 1950) that is a decent approximation of the fluid but inappropriate at high stress levels because of singularity in the equation (Denn, 1990). It is then trailed by the Walter-B model (Beard & Walters, 1964), where Prandtl's idea of boundary layer theory is extended to the case of idealized viscoelastic fluid where the fluid is assumed to be incompressible and inviscid. This study provides fellow researchers with the insight that fluid elasticity is directly proportional to the velocity at boundary layer as well as the stress on the solid boundary.

The study of flow for viscoelastic fluid has started as early as 1980s by Rajagopal et al. (1984), focusing on the flow of the second order fluid on stretching sheet due to its significance in polymer processing. The study has theoretically proven that power expenditure to stretch the sheets is affected by the viscoelasticity property of the fluid as the skin friction decreases when the viscoelastic parameter gets higher. The idea is then extended by Dandapat and Gupta (1989) who consider the flow and heat transfer of the above-mentioned study thus acquiring an exact analytical solution of the problem. However, these results come with a restriction that the viscoelastic parameter must be generally small.

Limitation is imposed on the above-mentioned models due to the reason that the equation of the motion of viscoelastic fluid is of higher order than the classical Navier-Stokes equations. As a result, complete solution is unattainable from the existing boundary conditions. Inspired by Bourgin and Tichy (1989), where extra velocity boundary condition is added to a fifth order differential equation to represent second-order fluid, Garg and Rajagopal (1990) overcome the restriction by including additional boundary conditions at infinity in their study of the motion of non-Newtonian fluid. This study creates opportunities for further investigations of viscoelastic fluid where the dimensionless viscoelastic parameter, K is no longer limited to only small values.

Later, in her study of mixed convection flow of viscoelastic fluid over a wedge, Kumari et al. (1995) adopted the idea of boundary conditions augmentation where an extra condition is incorporated since the momentum equation is one order higher than the classical boundary layer equation. The work of Anwar et al. (2008) also benefitted from the idea where the analysis is valid for arbitrary value of K after additional boundary condition $f''(\infty)=0$ is included. This study which focuses on the boundary layer flow of viscoelastic fluid over a heated and cooled horizontal circular cylinder reveals that heated cylinder delays separation of the boundary layer from the solid surface while cooling the cylinder brings the separation point closer to the lower stagnation point.

Since the earliest study has demonstrated that less power is required to stretch a sheet in viscoelastic fluid compared to one in Newtonian fluid, to date, the publications on the topic of boundary layer flow of viscoelastic fluid along a stretching sheet have developed rapidly. Using the momentum integral technique, Bujurke et al. (1987) focused on the momentum and heat transfer of the flow and the results showed that skin friction can be minimized by choosing the right fluid with particular viscoelasticity and speed of drawing the sheet. On the other hand, Andersson (1992) conducted a study on the magnetic effect on viscoelastic fluid flow over a stretching sheet and successfully obtained the exact analytical solution. The finding disclosed that both external magnetic field and viscoelasticity had the same effect on the flow where velocity and boundary layer thickness were reduced, while on the contrary, the surge in values of the parameters increased the skin friction.

Other notable example of viscoelastic flow over stretching body is the study of hydromagnetic flow for viscoelastic fluid over an oscillatory stretching surface where the analytical result from homotopy analysis method was compared to numerical results from a finite difference scheme and both undoubtedly yielded similar results (Abbas et al., 2008). Similar interest on magnetic effect on viscoelastic fluid flow has also motivated Misra et al. (2008) to study the flow and heat transfer in channels with stretching walls for which the model is applicable to simulate the flow of blood in arteries with stretchable walls upon exposure to magnetic field.

Aside from the stretching sheet problem, the effect of viscoelastic fluid flow on other geometrics are also pursued to match the diversity of application problems. Among them are the published work of Bodart and Crochet (1994) which aimed to compute the motion of a sphere released along the axis of a circular cylinder filled with a specific viscoelastic fluid, namely the Oldroyd-B fluid. Sets of material parameters were thoughtfully chosen in this study to replicate laboratory experiments and the result showed that the retardation to relaxation time ratio, a numeric value used to quantify the elasticity property, affects the time-dependent velocity of the sphere. The study also investigated the same geometrical body but with drag reduction as the primary interest of the study where the outcome of the study confirms the breakthrough of viscoelastic fluid in industrial application as it theoretically validates that fluid elasticity and shear-thinning have remarkable effects in reducing drag coefficient.

In addition, Minaeian et al. (2020) and Ma et al. (2023) examined the flow of viscoelastic fluid over horizontal circular cylinder. Both studies utilized numerical techniques to analyse viscoelastic fluid flow around a circular cylinder oscillating transversely to the flow direction. The former study focused on heat transfer characteristics, implementing a finite volume method to solve the governing equations. They found that increasing Reynolds and Bingham numbers enhances heat transfer, while raising Prandtl number reduces it. The effects of fluid elasticity were significant, especially near the cylinder surface. In contrast, the latter study investigated the lock-in phenomenon and wake topology. Using a high-order dual splitting scheme, they simulated Oldroyd-B fluid flow at low and moderate Reynolds numbers.

Other fluid rheology of viscoelastic fluid in other bluff body geometrics had also been explored. For instance, Khan et al. (2020) and Ramzan et al. (2022) investigated the fluid motion between rotating parallel disks, Badami et al. (2021) observe the flow of viscoelastic fluid in an axisymmetric pipe. Meanwhile Kudenatti & Amrutha (2022) and (Sun et al., 2024), evaluated the boundary layer flow of viscoelastic fluid over a moving or static wedge and triangular cylinders, respectively. These studies have contributed to the idea of solving the complex viscoelastic micropolar fluid when the terms related to the viscoelasticity is concerned. The idea of augmented boundary condition is adopted along with some general ideas of how the viscoelastic characteristics of the fluid will affect the flow and heat transfer.

2.3 Micropolar Fluid

As mentioned in the introduction, Eringen is the main figure behind the flow of micropolar model that his study is the ultimate framework for any research involving micropolar fluid. Since his breakthrough, the study of micropolar fluid started to gain momentum with Willson (1970) and Peddieson (1970) being among the earliest researchers to actively pursue the topic of micropolar fluid. Both researchers explored the concept of boundary layer theory in micropolar at stagnation points by re-examining the existing classical flows but taking the existence of microstructure into consideration.

Various other studies for this uniquely structured fluid include the work of Ariman and Cakmak (1968) which focused on the motion of micropolar fluid between two parallel plates and Ahmadi (1976) whose finding is applicable to the flow of suspension solutions over a flat plate. Although the attention is mostly on two-dimensional body where the solution is attainable with less complication, Nath (1975) took the alternative to solve the similar equation for the steady incompressible laminar boundary layer equations for micropolar fluids over a two-dimensional body at stagnation point as well as non-similarity equations for three-dimensional body, namely sphere and cylinder (Nath, 1976).

According to the micropolar fluid theory, the micropolar fluid model should include an extra set of transport equation to represent the conservation of local angular momentum on top of the classical fluid dynamic equations (Ishak et al., 2006). This angular momentum equation and the micropolar parameter, or also known as material parameter sets apart the model from other fluid flow and becomes an additional puzzle to solve when dealing with micropolar fluid where these problems can be approached analytically and numerically.

Researchers started covering various modes of heat transfer, geometrics and effects as soon as it was proven that the micropolar model is an ideal representation for fluids with various physical structures which is a common trait in non-Newtonian fluid. Studies on micropolar flow dynamics are evenly favoured for both stretching and shrinking sheets. Sankara and Watson (1985) initiated the study of micropolar flow over a permeable stretching sheet using a globally convergent homotopy method coupled with a more robust and efficient optimization method called the Quasi-Newton method. Then, this work is further extended by Heruska et al. (1986) who examined the flow over a porous stretching sheet by applying the same method thus enabling the comparison of the flow pattern between the impermeable porous stretching sheet.

The idea of fluid flow over a shrinking sheet is founded by Wang (1990) who briefly presented the solution of a specific unsteady shrinking film before the complete idea is published by Miklavcic and Wang (2006) and later, adopted for micropolar flow due to the importance in paper production, metal spinning and drawing of plastic films. The study of micropolar flow over shrinking sheet had been conducted by Azizah Tukiran and Ishak (2012) while Aurangzaib et al. (2016) came out with an original model of the flow and heat transfer over an exponentially permeable stretching sheet. Both studies affirmed that micropolar fluid requires stronger mass suction compared to the classical Newtonian fluid for the solution to exist because of the microrotation affect.

Thus far, the studies of micropolar fluid is not only limited to these cases but has been extended by other researchers with more effects and relevant geometrics that is related to real-life applications. Kumar et al. (2022) investigated the impact of micropolar parameter on the flow of CNT-blood nanofluid through a squeezing channel where the results obtained is applicable for drug delivery system in our body. Meanwhile, Wang and Chu (2023) proposed a model that can be used to simulate the flow of micropolar fluids in geological engineering applications. Simulating the behaviours of geological phenomena is very important for understanding how they were formed and preventing potential dangers. Besides these real-life models, micropolar model also allows detailed simulation of complex fluid flows in the microscopic geometries found in stomach anatomy, which can provide biological insights that could be risky to be tested experimentally (Saleem et al., 2021).

For engineering processes that happen in high temperature environment, radiation effect has also appealed as a topic of interest. Ishak (2010), Siddiqa et al. (2021) and Alao et al. (2024) had analysed the fluid flow of micropolar flow over unmoving horizontal plate through porous medium, vertical and stretchable surface, respectively, by using Rosseland diffusion approximation to describe the radiative heat transfer in the energy equation. Furthermore, Rana et al. (2021) explored nano-micropolar fluids with magnetohydrodynamic effects and porous media with applications in simulation and control of microfluidic devices, biomedical engineering, microelectronics cooling, and nanomaterial manufacturing. The outcome of the study inferred that increasing magnetic field and micropolar effects suppress the velocity but enhance the temperature.

From the review, there has also been a growing interest in the study of complex fluid and several models that include micropolar fluid had been identified. Among them is the popular micropolar nanofluid published by Hsiao (2017), Rashad et al. (2019), Dawar et al. (2020) and Guedri et al. (2023). There is a valid reason for such interest in micropolar nanofluid and according to Sadiq et al. (2019), micropolar and nanofluid are highly compatible duo as micropolar fluid contain microelements that are highly likely nano-size particles which will make the micropolar to behave like nanofluids. This combined fluid model could accurately characterize fluids with microscale structures and embedded nanoparticles to imitate the flow of engineered smart fluids, biological fluids and microgel suspensions.

Besides micropolar nanofluid, there is also the Casson micropolar fluid that represents Casson fluid model with microrotation. Mehmood et al. (2017) observed the flow of Casson micropolar fluid for a system undergoing internal heating phenomenon, Ali et al. (2020) examined the behaviour of the pulsatile flow of micropolar-Casson fluid in a constricted channel in the existence of magnetic field, while Al-Sharifi et al. (2023) computationally investigated the boundary layer flow of non-Newtonian Casson micropolar fluid, analysing the effects of rheological parameters on velocity and thermal fields.

Further review also revealed the existence of a hybrid model known as Casson micropolar nanofluid that has also been introduced and published by Shah et al. (2019) and Amjad et al. (2021). In addition to the ones mentioned above, there are still other complex micropolar models such as Jeffrey micropolar (Al-Sharifi et al., 2017), micropolar Brinkman (Faltas et al., 2020), micropolar ferrofluid model (Rauf et al., 2023) as well as micropolar-casson model (Abbas et al., 2024). The existence of these joint micropolar fluid is an attempt to develop a model that is as close as possible to representing the physics of complex real-world fluids.

2.4 Bluff Body

Bluff body refers to a shape that creates substantial drag and flow separation due to its non-streamlined geometry, in contrast to streamlined teardrop shapes designed for low drag. Bluff bodies have broad, rounded shapes rather than sleek, tapered shapes. Circular cylinders, spheres, cubes and prisms are examples of bluff bodies and in real life these can be visualized as tall structures like buildings, bridges as well as offshore pipelines. However, any aerodynamic body could be bluff body depending on the orientation flow such as the airplane wing at high angles of attack (Verma & Govardhan, 2011). According to Bearman (1997), advances in computer technology have greatly enabled studies involving bluff body geometry, as the numerical solutions to the complex Navier-Stokes equations for these flows have become more tractable. With high-performance computing, research groups can now obtain solutions for bluff body problems that were previously impossible or impractical to solve numerically.

Bluff body is less resistant of frictional drag but comes with significant pressure drag which depends on the shape of the forebody and afterbody that might lead to a large wake region. Wake region refers to the large low-pressure turbulent region behind the body which contributes to pressure drag. Flow separation and vortex shedding are two important phenomena in bluff-body aerodynamics that are incredibly important and play vital roles in various processes such as vehicle design (Nath et al., 2021) and wind engineering especially in structural engineering (Buresti & Piccardo, 2022). Driven by the importance of the study of bluff body hydrodynamics, a variety of work on bluff body had been published.

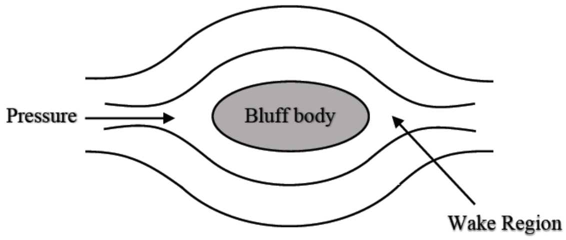

Figure 2.1 Boundary layer flow of fluid over bluff body

Experimental study is the traditional approach to observe and predict the turbulent flows around bluff bodies before technology takes over and numerical solution is readily available. Among the earliest experimental studies on bluff body is conducted by Parkinson (1971) whose findings revealed that the vortex formation length and width of the wake size are influenced by Reynolds number and cross-section of the cylinder while Saha et al. (2000) also conducted an experimental study which revealed that the separation mechanism and the related integral parameters for the flow over circular and square cylinder are non-identical. On the other hand, Yagmur et al. (2015) conducted a thorough study by looking at both angles experimentally and numerically, for the flow in the wake region for diverse bluff bodies. The experiment was conducted using the Particle Image Velocimetry (PIV) method in an open water channel and the experimental results obtained are consistent with the numerical analysis.

Since experimental studies require extensive knowledge and comes with many potential limitations, computational fluid dynamics seems to be a more convenient option for researchers. The analytical study of mixed convection boundary layer on a sphere by Hieber and Gebhart (1969) was inspired by the first experimental study of the same topic by Yuge (1960). Afterwards, Chen and Mucoglu (1977) and Mucoglu and Chen (1978) used an implicit finite difference scheme to investigate the heat transfer results of the laminar mixed force and free convection flow over a sphere. Their work was then extended by Lien and Chen (1987) who examined the case when the flow is subjected to constant mass transfer and uniform surface temperature.

Many works on boundary layer flow and heat transfer for different types of fluid flow over a sphere are available for review. Nazar and Amin (2002) and Nazar et al. (2002), for example, proposed a model for free convection boundary layer flow of micropolar fluid over sphere for constant wall temperature and constant heat flux boundary conditions, respectively. Followed by these studies, Cheng (2008) examined the natural convection heat transfer near sphere with constant wall temperature and concentration while Salleh et al. (2012) did a similar study with Newtonian heating. Recent study on hybrid micropolar fluid over sphere is also conducted by Alkasasbeh et al. (2023) to investigate how magnetic field impacts the flow while Boodoo (2024) developed a mathematical model to analyse the flow of micropolar fluid around porous shell for better understanding of the behaviour of drug-carrying microspheres in the body for more effective drug delivery method.

The study of viscoelastic fluid over a solid sphere is also fairly popular. Kasim et al. (2012) and Kasim et al. (2013) investigated the behaviour of fluid for natural convection boundary layer flow over sphere with constant heat flux and Newtonian heating, respectively. In the meantime, the same case of mixed convection boundary layer flow of viscoelastic fluid was published by Ghani and Rumite (2021) with MHD effect while Pimenta and Alves (2021) added viscous dissipation to the flow model.

According to Schlichting and Kestin (1960), the study of boundary layer is pioneered by Ludwig Prandtl in 1904. His early work is acknowledged as the most significant concept in fluid rheology and the flow over circular cylinder is one of his domains. Prandtl's work was then extended by Blasius (1908), who successfully came out with the first solution of the steady forced convection momentum boundary layer flow over circular cylinder using the series method. The thermal equation of the same problem was solved by Frossling (1958) by considering the case when the surface temperature of the circular cylinder is constant using the series expansion technique. Then, Sparrow and Lee (1976) solved the problem of flow of a vertical stream over a heated horizontal circular cylinder with constant wall temperature. Their achievement is trailed by Merkin (1977), who solved the problem of mixed convection from a horizontal circular cylinder held at constant temperature numerically.

Now that this problem has proven attainability, the concept is implemented for other significant new ideas. Javed et al. (2018), for instance, decided to approach on the axisymmetric flow of Casson fluid upon noticing that swirling cylinder has yet been widely discussed. In their recent study, Hosseinzadeh et al. (2020), performed an analysis of flow over a horizontal and three-dimensional cylinder for a fascinating cross-fluid that originally belongs to the Newtonian subclass with the presence of gyrotactic microorganisms and nanoparticles. While Khan et al. (2021) and Khan et al. (2022) investigated the flow of hybrid nanofluid and Johnson-Segalman fluid over a vertical cylinder, respectively, an experimental study of structure turbulent flow behind a square cylinder had also been conducted as opposed to the conventional streamlined cylinder in cross-flow (Yanovych et al., 2021).

Many researchers who study bluff body fluid dynamics are driven by the fact that, while there is extensive literature on one-dimensional flows, very little research exists on two-dimensional flows around bluff body geometries. Bluff body problems have been largely overlooked due to their greater complexity compared to one-dimensional scenarios. However, this presents an opportunity for this study, as the boundary layer flows and heat transfer with viscoelastic micropolar fluid specifically over a sphere and circular cylinder have not yet been fully explored.

2.5 Magnetohydrodynamic (MHD)

During the review for the previous subtopics, it is noticeable that a great number of literatures mentioned about the MHD effect. MHD is a field that study the dynamics of electrically conducting fluids. The phenomenon of magnetic field in convection flow is remarkably significant in the advancement of technology and industry with important role in insulation of nuclear reactor, solar energy collection and cooling of electronic chips and devices as well as petroleum production (Tamoor et al., 2017). MHD was first discovered by Hannes Alfven, an engineer-cum-physicist who was awarded the Nobel Prize in Physics for his extraordinary discovery. In his article, Alfven (1942) described

MHD as a combined electromagnetic-hydro-dynamic wave that changes fluid motion when electrically conducting fluid is exposed to a constant magnetic field, causing the fluid motion to generate electromotive force thus producing electric current.

Among the earliest work on MHD effect was published by Goldsworthy (1961), who in continuation of Alfven's work, presented an extensive theory that enables for the MHD flow of perfectly conducting viscous fluid over three different obstacles which are sphere, circular cylinder and semi-infinite flat plate to be predicted. As for non-Newtonian fluid, the first study of magnetic field effect on the flow was published by Sarpkaya (1961), elevated by earlier studies on Newtonian fluid. The two non-Newtonian models that were considered in the study were Bingham plastic model and power-law model where the flow of these fluid between two parallel plates in the presence of a transverse magnetic field was observed. Later, the study was extended by Kapur (1962) for the flow of Reiner-Rivlin fluid.

To date, the effect of MHD has been studied for the flow of almost all existed fluid and mode of heat transfer, even coupled with other effects to match with the actual applications. Ramzan et al. (2016) and Yasmin et al. (2020) are both interested in the MHD effect on micropolar fluid on stretched surface. The results from the prior study which focused on the combination of thermal radiation and Joule heating showed that microrotation and magnetic field intensity are directly related which can be justified physically, as higher magnetic field will speed up the rotation of the fluid particles and as a result, increase microrotation velocity. The latter study revealed that the magnetic field and micropolar parameters show opposing effects on the flow velocity, but both enhance heat transfer.

More examples of studies of MHD effect include Bibi et al. (2019) whose study focussed on solving the flow of MHD tangent hyperbolic fluid on variable conductive heat flow with convective boundary condition. The high nonlinearity of the problem called for numerical solution as the best option and this problem was solved using bvp4c in MATLAB. Other than that, Muhammad et al. (2021) did a comparison study of two different numerical methods which are the bvp4c function and shooting technique to solve three-dimensional Eyring–Powell nanofluid nonlinear thermal radiation with modified heat plus mass fluxes. The comparison of tables and graphs presented in the paper indicates that both techniques produce exactly the same result. Meanwhile, instead of using existing method, Wakif (2020) came out with a novel numerical procedure using a new unconventional GDQLLM algorithm that integrates local linearization technique with the generalized differential quadrature method to study convective flows of radiative Casson fluids moving over a nonlinearly elongating elastic sheet with a nonuniform thickness with MHD effect.

So far, all the above listed literatures analyse the case when the fluid flow is perpendicular to the magnetic field. However, imposing such limitations on the study will restrict the practicality. With the aim for more general and applicable result, researchers started exploring the idea of aligned MHD. In their numerical study of structure of oblique hydromagnetic shock waves, Dixon and Woods (1976) addressed that majority of studies are devoted on the limiting case of $\alpha = 0^{\circ}$ and $\alpha = 90^{\circ}$ where α represents the angle of magnetic field that oblique angles $(0^{\circ} < \alpha < 90^{\circ})$ seems neglected. The same idea was emphasised by Chandna et al. (1982) when he solved the flow of variably inclined MHD plane where the angle and velocity field were diversified using hodograph transformation.

Later, Josserand et al. (1993) conducted a study on liquid metal flow over a cylinder under the effect of aligned MHD where the pressure and drag measurements on the body was observed. The result from the experimental study showed that the rear and global pressure drag are proportional to $\sqrt{N}$, where N is the interaction parameter, a ratio between electromagnetic force and inertia forces yields. Sekhar et al. (2007) also investigated the flow on circular cylinder with aligned MHD but with particular interest on viscous fluid. The study concluded that magnetic field and drag coefficient are positively correlated and that the magnetic field has greater effect on downstream base pressure compared to the upstream base pressure.

A comparison study between aligned and non-aligned MHD flow for two types of water-based ferrofluids over a flat plate was pursued by Ilias et al. (2016). The outcome of the study revealed that increasing angle of magnetic field increases the heat transfer rate on the plate surface and that the transfer rate is higher for kerosene-ferrofluid compared to water. In the meantime, studies of aligned MHD on nanofluid flow by Rosaidi et al. (2022) and Ali et al. (2022) concluded that the surge of magnetic field and aligned magnetic field accelerated the temperature and fluid velocity.

However, it was shown by (Ilias et al., 2023) for Jeffry hybrid nanofluid flow, the magnetic effect tends to retard the flow velocity but increase the temperature and that the aligned magnetic parameter displays identical effect on the flow as the magnetic parameter. Alternatively, Ali et al. (2024), who investigates the effect of MHD on micropolar fluid over stretching wedge surface concludes that the magnetic field oppose fluid motion, increasing the temperature profiles but reduce the velocity and microrotation profiles.

In summary, the aligned MHD field could provide a simpler starting point to reveal the basic influences of the magnetic field on the boundary layer flow and heat transfer prior to adding the extra complexities of the transverse orientation. This aids fundamental understanding and control of MHD systems that motivates incorporating aligned magnetic effect in this study.

2.6 Keller-box Method

The Navier-Stokes equation that is used to describe the motion of fluid are in the form of differential equations, so the key to solving fluid dynamics problems lies within solving the differential equations. The complexity and method chosen to solve the equations depend on whether the equations are in the form of ordinary or partial differential equations where partial differentials equation are more challenging to deal with. The function bvp4c in MATLAB and shooting method are popular options among researchers when it comes to ordinary differential equations while for partial differential equations, finite difference and finite elements methods are implemented. Finite difference method has been used to solve wide range of boundary value problems since 1940s. The principle of the method is to convert the partial differential equations into a set of simultaneous equations for which the solution is the approximate solution of the boundary value problem (Zhou, 1993).

For finite difference approaches, Keller-box method has been a popular option to solve fluid flow and heat transfer problems. The method was first introduced by Keller and Cebeci (1972), claiming that it is faster, simpler to program and more versatile than other such numerical methods where the governing partial differential equations are reduced to first-order system. Furthermore, the method also allows for calculation that is extremely close to the boundary-layer separation without any restraint and has proven to be applicable to three-dimensional boundary layer flows. Afterwards, the method has been discussed extensively by Cebeci and Bradshaw (1984) and widely adopted by other researchers for various boundary value problems.

In his work, Cebeci et al. (1986) has also demonstrated that the Keller-box method can also be used to represent flows that have regions of reverse flow which is common when dealing with opposed forced and free convection. Motivated by the desirable features of Keller-box method, Poulikakos and Renken (1987) implemented the method to find the numerical solution of the energy equation for their general model for flow in porous medium with variable porosity, flow inertia, and Brinkman friction effects. Then, the same method was utilized in the published works of Lin and Yu (1988) and Lin and Chen (1988), where the free convection flow on horizontal plate and a general model of mixed convection flow on vertical plate were discussed, respectively.

To date, the numerical scheme has been applied to various geometric bodies. For instance, Hossain et al. (1996) applied the method to solve free convection flow near rotating round-nosed bodies with the presence of transverse magnetic field despite the non-similarity in the constitutive equations due to the buoyancy force field on top of the magnetic field and the transverse curvature of the bodies. The numerical scheme has also been chosen by Habib et al. (2022) to visualise the effects of chemical reaction, variable suction, activation energy, and heat-generation over a non-linear static and moving wedge with heat transfer properties, chosen for its rapid algorithm and adaptability for most problems. To further illustrate the versatility of Keller-box method, the method has also been adopted by Mohamed et al. (2023) and Habib et al. (2024) to examine the MHD effect on boundary layer flow of Casson ferrofluid over vertical truncated cone and nanofluid over a paraboloid, respectively.

Thus far, the finite difference scheme is still relevant for current and ongoing fluid dynamics problems as proven by Bilal et al. (2017) to which the numerical results of his study for the flow of Williamson fluid along cylindrical stretching surface showed excellent agreement with a previous study using Homotopy analysis method, hence validating the reliability of this technique. Furthermore, a comparison study of two different numerical approaches, namely the Keller-box and shooting method by Shabbir et al. (2020) has also demonstrated the consistency of the technique when almost identical figures are obtained from both methods.

According to Ahmed et al. (2021), compared to other numerical techniques, Keller-box is speedier and more efficient when dealing with cases of higher order nonlinear differential equations. His numerical results on unsteady squeezing flow between two infinite parallel plates were authenticated by comparing the solution of the simplest case of his work obtained using Keller-box method and the built-in function bvp4c in MATLAB. All things considered, due to the flexibility and reliability of the Keller-box method, this method has been chosen to solve the problems in this study using the Fortran programming language.

2.7 Summary

In this chapter, previous studies related to the current research interest has been reviewed to identify the gap that can be filled in. It has been determined through the evaluation that studies on the heat transfer and flow characteristics of viscoelastic micropolar are scarce. Given the considerable quantity of non-Newtonian fluids that exhibit these dual characteristics, it is prudent to consider investigating this issue. In addition to examining the flow of a complex fluid, one of the challenges in the present study will be determining the solution of fourth-order partial differential equations, given that the bluff body has been selected as the geometric subject of interest. Despite this, this study is made feasible by the concepts compiled from prior research and the encouraging outcomes produced by the Keller-box method.

CHAPTER 3

METHODOLOGY

3.1 Introduction

In this chapter, the derivation of the constitutive equations of the flow for viscoelastic micropolar fluid with MHD effect that consists of continuity, momentum, angular momentum and energy equations are elaborated. Generally, those equations are based on the three fundamental physical principles which are conservation of mass, Newton's second law and first law of thermodynamics which describe the relationship between velocity, pressure, temperature and density to the parameters that characterise the flow of a fluid. From the literature review in Chapter 2, the studies concerning the flow of viscoelastic micropolar fluid over horizontal circular cylinder and sphere are extremely limited. However, the closest literatures that guided these problems are the cases when viscoelastic and micropolar flow are considered separately. This chapter is divided into four sections where Section 3.1 is the introduction to the chapter, 3.2 presents the detailed derivation of the governing equations, 3.3 demonstrates the derivation of the boundary layer equations of the viscoelastic micropolar fluid and 3.4 summarizes the governing equations of the flow for viscoelastic micropolar fluid.

3.2 Governing Equation for Newtonian Fluid with MHD Effect

This section covers the derivation of continuity, momentum, energy and angular momentum equations where the details are explained in Section 3.2.1 to 3.2.4, respectively. Subsequently, it is followed by the description of the concept of boundary layer approximation in Section 3.2.5.

3.2.1 Continuity Equation

The law of conservation of mass declares that mass can neither be created nor destroyed, hence constant amount of matter is present in a system over time for an isolated system (Coleman, 2010). The fluid flow has to obey this law since material does not simply disappear nor does new material would simply emerge during the flows. According to Oertel (2010), the rate of mass accumulation in a volume element equals the difference between the rate of mass in and out of the volume element or

$$\begin{array}{c}\text{The rate of change of mass}\\\text{in a volume element}\end{array} = \begin{array}{c}\sum \text{the mass fluxes into the volume element}\\ - \\ \sum \text{the mass fluxes out of the volume element}\end{array} \quad 3.1$$

This can be visualised as in Figure 3.1 where in the x-direction, the mass flux entering the volume element is given by:

$$(\rho u)\,dy\,dz \quad 3.2$$

and when the position shifts from x to $x+dx$ in the x-direction, the quantity change is depicted by:

$$\frac{\partial \rho u}{\partial x}dx \quad 3.3$$

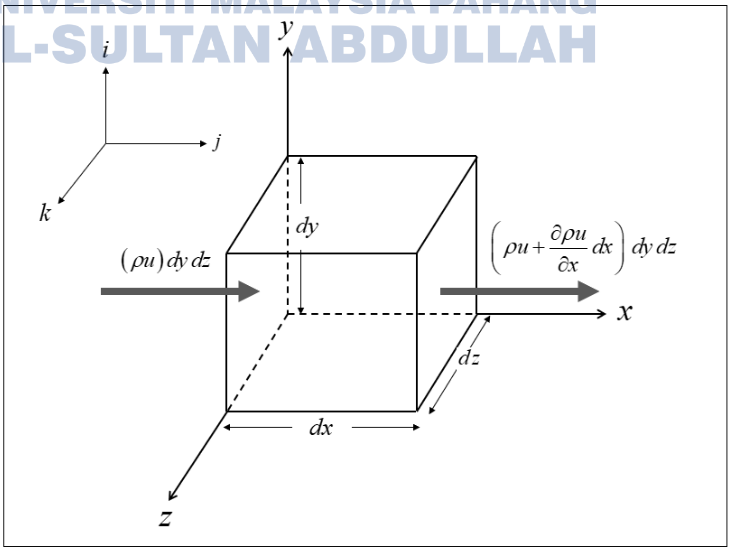

Figure 3.1 Mass fluxes entering and leaving volume element in x-direction

Hence, the net outflow in x-direction is given by:

$$\rho u\, dy dz - \left[\rho u + \frac{\partial(\rho u)}{\partial x} dx \right] dy dz = -\frac{\partial(\rho u)}{\partial x} dx\, dy\, dz \qquad 3.4$$

while net outflow in y-direction is:

$$\rho v\, dx dz - \left[\rho v + \frac{\partial(\rho v)}{\partial y} dy \right] dx dz = -\frac{\partial(\rho v)}{\partial y} dx\, dy\, dz \qquad 3.5$$

and in z-direction, net outflow is:

$$\rho w\, dx dy - \left[\rho w + \frac{\partial(\rho w)}{\partial z} dz \right] dx dy = -\frac{\partial(\rho w)}{\partial z} dx\, dy\, dz \qquad 3.6$$

In the Cartesian space, the vector velocity field is defined as $\mathbf{V} = u\mathbf{i} + v\mathbf{j} + w\mathbf{k}$ and the density of the fluid element is $\rho = \rho(x, y, z, t)$. Therefore, net flow mass is:

$$\text{net mass flow} = -\left[\frac{\partial(\rho u)}{\partial x} + \frac{\partial(\rho v)}{\partial y} + \frac{\partial(\rho w)}{\partial z} \right] dx dy dz \qquad 3.7$$

Since the rate of change of mass inside the volume element is equivalent to the sum of net flow mass, then,

$$\frac{\partial(\rho\, dx\, dy\, dz)}{\partial t} = -\left[\frac{\partial(\rho u)}{\partial x} + \frac{\partial(\rho v)}{\partial y} + \frac{\partial(\rho w)}{\partial z} \right] dx dy dz \qquad 3.8$$

Considering that dV, that is physically defined as total mass of fluid in volume element is given by $dV = dx\, dy\, dz$, the equation can be simplified to:

$$-\frac{\partial \rho}{\partial t} = \frac{\partial(\rho u)}{\partial x} + \frac{\partial(\rho v)}{\partial y} + \frac{\partial(\rho w)}{\partial z} \qquad 3.9$$

After rearranging the equation and using the operator, $\nabla = \frac{\partial}{\partial x} i + \frac{\partial}{\partial y} j + \frac{\partial}{\partial z} k$, the equation is transformed to:

$$\frac{\partial \rho}{\partial t} + \nabla \cdot \rho \mathbf{V} = 0 \tag{3.10}$$

Considering that the material derivative of the density is $\frac{D\rho}{Dt} = \frac{\partial \rho}{\partial t} + \mathbf{V} \cdot \nabla \rho$ and applying the vector identity $\nabla \cdot (\rho \mathbf{V}) = \rho(\nabla \cdot \mathbf{V}) + \mathbf{V} \cdot \nabla \rho$, alternatively, Equation (3.10) can also be expressed in the form:

$$\frac{D\rho}{Dt} + \rho(\nabla \cdot \mathbf{V}) = 0 \tag{3.11}$$

Since for incompressible fluid the density remains constant throughout the flow, hence Equation (3.11) becomes:

$$\nabla \cdot \mathbf{V} = 0 \tag{3.12}$$

For two-dimensional case, the continuity equation can be written as:

$$\frac{\partial u}{\partial x} + \frac{\partial u}{\partial y} = 0 \tag{3.13}$$

3.2.2 Momentum Equation

Momentum equation, or better known as the Navier-Stokes equation is named after Claude-Louis Navier and Sir George Stokes where the differential equations serve the purpose of expressing the motion of a particle immersed in a fluid or the motion of the fluid itself. The equation is constructed from the Newton's second law of motion in the form below:

$$\mathbf{F} = m\mathbf{a} \tag{3.14}$$

which describes that the net force of fluid element, **F** is equivalent to the product of its mass, m and the acceleration of the element, **a**.

According to Katopodes (2019), the type of forces that must be considered correspond to normal and tangential stresses exerted on the element's surfaces by the surrounding fluid as well as the body forces that act through the centroid of the element. Body forces, $\mathbf{F}_b$ result from immersing fluid element is a force field such as gravitational and electromagnetic field. The forces are proportional to the mass of the fluid and spread across the fluid element without physical contact. Meanwhile, the surface forces, $\mathbf{F}_s$ includes pressure that act inward and normal to the surface element and viscous forces that acts in any direction on the surface caused by the viscosity of the fluid.

In his detail derivation of Navier Stokes equation with consideration of all forces acting on the fluid, Subramanian (2019a) stated that the following equation can be casted to represent the principle of conservation of momentum applied to a control volume.

$$\rho\left[\frac{\partial \mathbf{V}}{\partial t}+\left(\mathbf{V}\cdot\nabla\right)\mathbf{V}\right]=\nabla\cdot\mathbf{T}+\rho\mathbf{F}_b \qquad 3.15$$

In the equation, **T** embodied the stress tensor of the fluid where motion is initiated due to horizontal friction and shear stresses. The stress at a point in a fluid is described by nine components that can be written in matrix form as follows:

$$\mathbf{T}=\begin{pmatrix}\sigma_x & \tau_{xy} & \tau_{xz}\\ \tau_{yx} & \sigma_y & \tau_{yz}\\ \tau_{zx} & \tau_{zy} & \sigma_z\end{pmatrix} \qquad 3.16$$

where the main diagonal elements σ_x, σ_y and σ_z represent the normal stresses. The remaining six elements in the form τ_{ij} express the shear stresses, where *i* represents the surface upon which it is acting on while *j* specifies the direction where the stress acts on as illustrated in Figure 3.2.

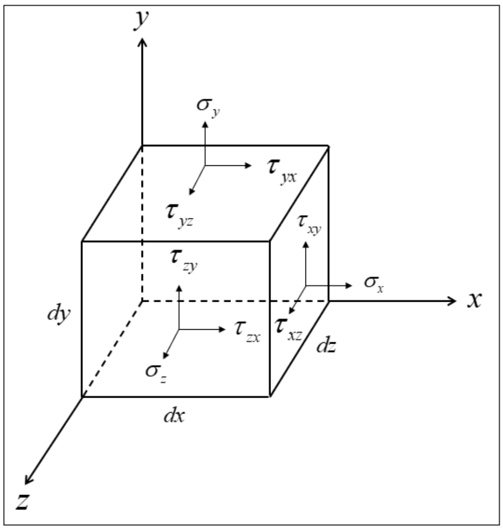

Figure 3.2 Normal stresses and shear stresses of fluid element

Following Papanastasiou et al. (2021), total stress tensor is generally expressed as the sum of isotropic pressure and viscous distributions or mathematically,

$$\mathbf{T} = -p\mathbf{I} + \boldsymbol{\tau} \tag{3.17}$$

Taking Equation (3.16) into consideration, Equation (3.15) in each direction, respectively, can be written as follows:

x-direction:

$$\rho\left(\frac{\partial u}{\partial t} + u\frac{\partial u}{\partial x} + v\frac{\partial u}{\partial y} + w\frac{\partial u}{\partial z}\right) = -\frac{\partial p}{\partial x} + \frac{\partial \tau_{xx}}{\partial x} + \frac{\partial \tau_{yx}}{\partial y} + \frac{\partial \tau_{zx}}{\partial z} + \rho f_x \tag{3.18}$$

y-direction:

$$\rho\left(\frac{\partial v}{\partial t} + u\frac{\partial v}{\partial x} + v\frac{\partial v}{\partial y} + w\frac{\partial v}{\partial z}\right) = -\frac{\partial p}{\partial y} + \frac{\partial \tau_{xy}}{\partial x} + \frac{\partial \tau_{yy}}{\partial y} + \frac{\partial \tau_{zy}}{\partial z} + \rho f_y \tag{3.19}$$

z-direction:

$$\rho\left(\frac{\partial w}{\partial t} + u\frac{\partial w}{\partial x} + v\frac{\partial w}{\partial y} + w\frac{\partial w}{\partial z}\right) = -\frac{\partial p}{\partial z} + \frac{\partial \tau_{xz}}{\partial x} + \frac{\partial \tau_{yz}}{\partial y} + \frac{\partial \tau_{zz}}{\partial z} + \rho f_z \tag{3.20}$$

or subsequently, in their vector form,

$$\rho\left(\frac{\partial \mathbf{V}}{\partial t}+\mathbf{V}\cdot\nabla\mathbf{V}\right)=-\nabla p+\nabla\cdot\boldsymbol{\tau}+\mathbf{F}_b \qquad 3.21$$

where $\mathbf{F}_b=\left(\rho f_{x,}\rho f_y,\rho f_z\right)$. They also stated that for Newtonian fluid, $\boldsymbol{\tau}=2\mu\mathbf{D}$ for which μ is the dynamic viscosity of the fluid and the rate-of-strain tensor, **D** is equivalent to $\frac{1}{2}\left[\nabla\mathbf{V}+\left(\nabla\mathbf{V}\right)^T\right]$. Hence, it follows from Equation (3.17) that the stress tensor may be defined by:

$$\mathbf{T}=-p\mathbf{I}+2\mu\mathbf{D}=-p\mathbf{I}+\mu\left[\nabla\mathbf{V}+\left(\nabla\mathbf{V}\right)^T\right] \qquad 3.22$$

In Cartesian coordinate system, Equation (3.22) is made up of nine components in the form:

$$T_{ij}=-p\delta_{ij}+\mu\left(\frac{\partial v_i}{\partial x_j}+\frac{\partial v_j}{\partial x_i}\right), \quad i,j=x,y,z \qquad 3.23$$

where δ_{ij} is the Kronecker Delta, which is defined such that $\delta_{ij}=1$ when $i=j$ and $\delta_{ij}=0$ when $i\neq j$. As a result of the symmetric nature of viscous stress tensor, i.e., $\tau_{ij}=\tau_{ji}$, there are only six independent stress components which are:

$$\begin{aligned} &\sigma_x=2\mu\frac{\partial u}{dx}, && \sigma_y=2\mu\frac{\partial v}{dy}, && \sigma_z=2\mu\frac{\partial w}{dz} \\ &\tau_{xy}=\tau_{yx}=\mu\left(\frac{\partial u}{dy}+\frac{\partial v}{dx}\right), && \tau_{xz}=\tau_{zx}=\mu\left(\frac{\partial u}{dz}+\frac{\partial w}{dx}\right), && \tau_{yz}=\tau_{zy}=\mu\left(\frac{\partial v}{dz}+\frac{\partial w}{dy}\right) \end{aligned} \qquad 3.24$$

As a result, **T** can be written in matrix form as:

$$\mathbf{T} = -\begin{pmatrix} p & 0 & 0 \\ 0 & p & 0 \\ 0 & 0 & p \end{pmatrix} + \mu \begin{pmatrix} 2\dfrac{\partial u}{dx} & \left(\dfrac{\partial u}{\partial y} + \dfrac{\partial v}{\partial x}\right) & \left(\dfrac{\partial u}{\partial z} + \dfrac{\partial w}{\partial x}\right) \\ \left(\dfrac{\partial u}{\partial y} + \dfrac{\partial v}{\partial x}\right) & 2\dfrac{\partial v}{\partial y} & \left(\dfrac{\partial v}{\partial z} + \dfrac{\partial w}{\partial y}\right) \\ \left(\dfrac{\partial u}{\partial z} + \dfrac{\partial w}{\partial x}\right) & \left(\dfrac{\partial v}{\partial z} + \dfrac{\partial w}{\partial y}\right) & 2\dfrac{\partial w}{\partial z} \end{pmatrix} \qquad 3.25$$

Hence, the divergence of total stress tensor in Cartesian coordinate system can be defined as:

$$\nabla \mathbf{T} = \begin{pmatrix} -\dfrac{\partial p}{\partial x} + 2\mu \dfrac{\partial^2 u}{dx^2} + \mu\left(\dfrac{\partial^2 u}{\partial y^2} + \dfrac{\partial^2 v}{\partial x \partial y}\right) + \mu\left(\dfrac{\partial^2 u}{\partial z^2} + \dfrac{\partial^2 w}{\partial x \partial z}\right) \\ -\dfrac{\partial p}{\partial y} + \mu\left(\dfrac{\partial^2 u}{\partial x \partial y} + \dfrac{\partial^2 v}{\partial x^2}\right) + 2\mu \dfrac{\partial^2 v}{\partial y^2} + \mu\left(\dfrac{\partial^2 v}{\partial z^2} + \dfrac{\partial^2 w}{\partial y \partial z}\right) \\ -\dfrac{\partial p}{\partial z} + \mu\left(\dfrac{\partial^2 u}{\partial x \partial z} + \dfrac{\partial^2 w}{\partial x^2}\right) + \mu\left(\dfrac{\partial^2 v}{\partial y \partial z} + \dfrac{\partial^2 w}{\partial y^2}\right) + 2\mu \dfrac{\partial^2 w}{\partial z^2} \end{pmatrix} \qquad 3.26$$

Concurrently, gravitational and magnetic field are the components of body force, $\mathbf{F}_b$ where the force can be expressed as:

$$\mathbf{F}_b = \rho \mathbf{g} + \mathbf{J} \times \mathbf{B} \qquad 3.27$$

given that ρ is the average density of the element, $\mathbf{g}$ is the gravitational vector, defined as $\mathbf{g} = \left(-g_x, -g_y, 0\right)$, $\mathbf{J}$ is the electric current density and $\mathbf{B}$ represents the magnetic field. The magnetic force is incorporated by implying Lorentz force in the equation. According to the generalized Ohm's law, the density of the induced current, $\mathbf{J}$ can also be written in the form:

$$\mathbf{J} = \sigma\left(\mathbf{E} + \mathbf{V} \times \mathbf{B}\right), \qquad 3.28$$

assuming that σ represents the electrical conductivity of the fluid, **E** is the electrical field and $\mathbf{B} = \mathbf{B_0} + \mathbf{b}$ where **b** indicates the induced magnetic field, while **B₀** is the uniform magnetic field at aligned angle α in the form $(0, B_0 \sin\alpha, 0)$. In this study, it is of interest to investigate how different values of acute angle, α could affect the fluid flow.

Under the assumptions that $\mathbf{E} = 0$ since there is no applied or polarization voltage, and that **b** is insignificant compared to the value of the magnetic field $\mathbf{B_0}$ so that the magnetic Reynolds number is small (Zakaria & Amin, 2014), Equation (3.28) becomes:

$$\mathbf{J} = \sigma(\mathbf{V} \times \mathbf{B}) = \begin{vmatrix} \boldsymbol{i} & \boldsymbol{j} & \boldsymbol{k} \\ u & v & 0 \\ 0 & 0 & B_0 \sin\alpha \end{vmatrix} = (\sigma v B_0 \sin\alpha, -\sigma u B_0 \sin\alpha, 0) \qquad 3.29$$

From the result,

$$\mathbf{J} \times \mathbf{B} = \begin{vmatrix} \boldsymbol{i} & \boldsymbol{j} & \boldsymbol{k} \\ \sigma v B_0 \sin\alpha & -\sigma u B_0 \sin\alpha & 0 \\ 0 & 0 & B_0 \sin\alpha \end{vmatrix} = \left(-\sigma u B_0^2 \sin^2\alpha, -\sigma v B_0^2 \sin^2\alpha, 0\right) \qquad 3.30$$

Hence, the body force equation in Equation (3.27) can be written as:

$$\begin{aligned} \mathbf{F}_b &= \rho\left(-g_x, -g_y, 0\right) + \left(-\sigma u B_0^2 \sin^2\alpha, -\sigma v B_0^2 \sin^2\alpha, 0\right) \\ &= \left(-\rho g_x - \sigma u B_0^2 \sin^2\alpha, -\rho g_y - \sigma v B_0^2 \sin^2\alpha, 0\right) \end{aligned} \qquad 3.31$$

Following the derivations of the body force components in Equation (3.31) and the stress tensor in Equation (3.26), Equation (3.18) which is the steady two- dimensional flow for Newtonian fluid in *x*-direction is now in the form as follows:

$$\rho\left(u\frac{\partial u}{\partial x} + v\frac{\partial u}{\partial y}\right) = -\frac{\partial p}{\partial x} + 2\mu\frac{\partial^2 u}{\partial x^2} + \mu\left(\frac{\partial^2 u}{\partial y^2} + \frac{\partial^2 v}{\partial x \partial y}\right) - \sigma u B_0^2 \sin^2\alpha - \rho g_x \qquad 3.32$$

or similarly,

$$\rho\left(u\frac{\partial u}{\partial x}+v\frac{\partial u}{\partial y}\right)=-\frac{\partial p}{\partial x}+\mu\left(\frac{\partial^2 u}{\partial x^2}+\frac{\partial^2 u}{\partial y^2}\right)+\mu\frac{\partial}{\partial x}\left(\frac{\partial u}{\partial x}+\frac{\partial v}{\partial y}\right)-\sigma uB_0^2\sin^2\alpha-\rho g_x \quad 3.33$$

Taking into account Equation (3.13), the above equation can be simplified to:

$$\rho\left(u\frac{\partial u}{\partial x}+v\frac{\partial u}{\partial y}\right)=-\frac{\partial p}{\partial x}+\mu\left(\frac{\partial^2 u}{\partial x^2}+\frac{\partial^2 u}{\partial y^2}\right)-\sigma uB_0^2\sin^2\alpha-\rho g_x \quad 3.34$$

and correspondingly, the momentum equation for *y*-direction is:

$$\rho\left(u\frac{\partial v}{\partial x}+v\frac{\partial v}{\partial y}\right)=-\frac{\partial p}{\partial y}+\mu\left(\frac{\partial^2 v}{\partial y^2}+\frac{\partial^2 v}{\partial x^2}\right)-\sigma vB_0^2\sin^2\alpha-\rho g_y \quad 3.35$$

In the equations, the total pressure in the flow, p is the sum of hydrostatic pressure, p_h and dynamic pressure, p_d or mathematically written in the form $p = p_h + p_d$. Outside the boundary layer, the hydrostatics pressure that is due to the weight of the fluid can be expressed as:

$$\frac{\partial p_h}{\partial x}=-\rho_\infty g_x \quad 3.36$$

where ρ_∞ corresponds to the fluid density. Hence,

$$-\rho g_x-\frac{\partial p_h}{\partial x}-\frac{\partial p_d}{\partial x}=(\rho_\infty-\rho)g_x-\frac{\partial p_d}{\partial x} \quad 3.37$$

and substituting these terms into Equation (3.34), we obtain:

$$\rho\left(u\frac{\partial u}{\partial x}+v\frac{\partial u}{\partial y}\right)=-\frac{\partial p_d}{\partial x}+\mu\left(\frac{\partial^2 u}{\partial x^2}+\frac{\partial^2 u}{\partial y^2}\right)-\sigma uB_0^2\sin^2\alpha+(\rho_\infty-\rho)g_x \quad 3.38$$

However, according to Padet et al. (2015), the equation can be simplified by adopting the Boussinesq approximation, where the density can be described as a linear function of the temperature alongside a reference value, which for this case refers to the ambient temperature of the fluid, T_∞ in the following form:

$$p_\infty - \rho = \rho\beta^*\left(T - T_\infty\right) \quad 3.39$$

Rearranging and substituting the equation into Equation (3.38), the following equation is acquired:

$$\rho\left(u\frac{\partial u}{\partial x} + v\frac{\partial u}{\partial y}\right) = -\frac{\partial p_d}{\partial x} + \mu\left(\frac{\partial^2 u}{\partial x^2} + \frac{\partial^2 u}{\partial y^2}\right) - \sigma u B_0^2 \sin^2\alpha + \rho\beta^*\left(T - T_\infty\right)g_x \quad 3.40$$

In the equation, β^* represents the thermal expansion coefficient and defined as $\beta^* = -\frac{1}{\rho}\left(\frac{\partial \rho}{\partial T}\right)_p$. Concurrently, in *y*-direction the momentum equation will be in the form as follows:

$$\rho\left(u\frac{\partial v}{\partial x} + v\frac{\partial v}{\partial y}\right) = -\frac{\partial p}{\partial y} + \mu\left(\frac{\partial^2 v}{\partial y^2} + \frac{\partial^2 v}{\partial x^2}\right) - \sigma v B_0^2 \sin^2\alpha + \rho\beta^*\left(T - T_\infty\right)g_y \quad 3.41$$

after the subscript *d* in the dynamic pressure term is dropped for the sake of simplicity.

3.2.3 Energy Equation

The energy equation of flow is derived from the first law of thermodynamics that is a vital concept for chemical reaction including for nuclear power plant. The law states that even if energy is converted from one form to another, the total energy remains constant. According to Zohuri (2018), this relationship can be expressed as:

$$\Delta E = Q + W \quad 3.42$$

where ΔE is the change of internal energy in the system, Q is the heat transferred in or out of the system and W represents the work done on or by the system.

In the equation, the term system corresponds to the control volume where the working fluid passes through. The total energy inside a control volume which is also known as stored energy per unit mass is a combination of kinetic energy corresponding to the bulk motion of the fluid, $\frac{V^2}{2}$ and the internal energy of the fluid from the molecular motion, e. Hence, the total internal energy is $e+\frac{V^2}{2}$. Since the internal and kinetic energy flow are defined as:

i. internal energy flow = (mass flow) × (internal energy/mass),
ii. kinetic energy flow = (mass flow) × (kinetic energy/mass)

and the mas flow is $\rho\, dxdydz$ therefore the total energy flow rate of a given fluid element in space can be expressed in substantial derivative as follows:

$$\Delta E = \rho \frac{D}{Dt}\left(e+\frac{V^2}{2}\right) dx\, dy\, dz \qquad 3.43$$

Meanwhile, the next element, Q represents the heat energy from volumetric heating and heat transfer across the surface. Volumetric heating refers to a condition where an entire volume (of a flowing fluid in this case) is uniformly heated thus delivering energy evenly throughout the body and this phenomenon can be mathematically interpreted as:

$$\text{volumetric heating of the element} = \rho \dot{q}\, dx\, dy\, dx \qquad 3.44$$

where the term $\dot{q}$ represents the volumetric heat rate addition per unit mass. As for the surface heating in the x-direction, the amount of heat transported into the moving fluid is $\dot{q}_x\, dy\, dz$ per unit time per unit area while the heat transferred out is given by $\left(\dot{q}_x + \frac{\partial \dot{q}_x}{\partial x} dx\right) dy\, dz.$ This can be demonstrated by Figure 3.3.

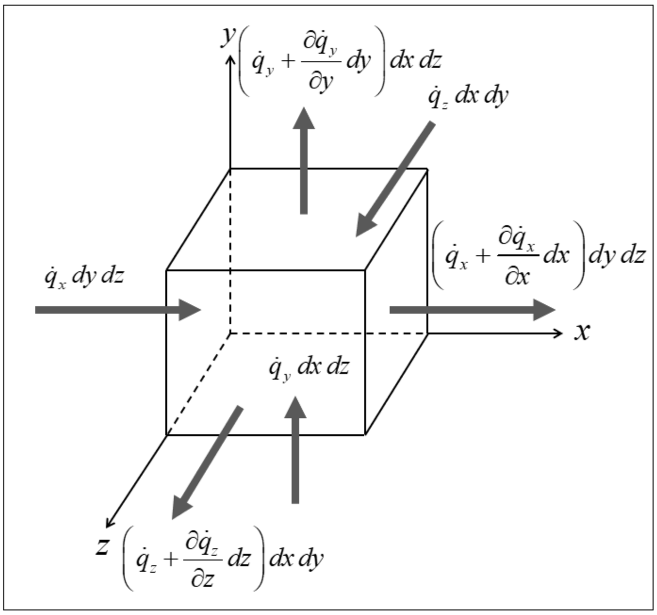

Figure 3.3 Heat fluxes flow in and out of volume element

From the figure, the net heat flux in the *x*-direction can be written as:

$$\dot{q}_x dy\, dz - \left(\dot{q}_x + \frac{\partial \dot{q}_x}{\partial x} dx\right) dy\, dz = -\frac{\partial \dot{q}_x}{\partial x} dx\, dy\, dz \qquad 3.45$$

While in the *y*-direction the net heat flux is:

$$\dot{q}_y dx\, dz - \left(\dot{q}_y + \frac{\partial \dot{q}_y}{\partial y} dy\right) dx\, dz = -\frac{\partial \dot{q}_y}{\partial y} dx\, dy\, dz \qquad 3.46$$

and in z-direction, the net heat flux is:

$$\dot{q}_z\, dx\, dy - \left(\dot{q}_z + \frac{\partial \dot{q}_z}{\partial z} dz\right) dx\, dy = -\frac{\partial \dot{q}_z}{\partial z} dx\, dy\, dz \qquad 3.47$$

It follows from Equations (3.45) to (3.47) that the heat transferred in and out of the moving fluid is:

$$Q = \left[\rho \dot{q} - \left(\frac{\partial \dot{q}_x}{\partial x} + \frac{\partial \dot{q}_y}{\partial y} + \frac{\partial \dot{q}_z}{\partial z}\right)\right] dx\, dy\, dz \qquad 3.48$$

Aside from the law of conservation of energy, Fourier's law also plays a vital role in the derivation of heat energy. The law states that the rate of heat transfer through a material is proportional to the negative gradient in the temperature and to the area, at right angles to that gradient, through which the heat flows (Arfken et al., 1984). The differential form is given by:

$$\dot{\mathbf{q}} = -k\nabla T \tag{3.49}$$

or can be written separately for individual component as:

$$\dot{q}_x = -k\frac{\partial T}{\partial x}; \quad \dot{q}_y = -k\frac{\partial T}{\partial y}; \quad \dot{q}_z = -k\frac{\partial T}{\partial z} \tag{3.50}$$

where the proportionality constant, k is known as thermal conductivity. Consequently, substituting Equation (3.50) into Equation (3.48), the new form is:

$$Q = \left[\rho\dot{q} + \frac{\partial}{\partial x}\left(k\frac{\partial T}{\partial x}\right) + \frac{\partial}{\partial y}\left(k\frac{\partial T}{\partial y}\right) + \frac{\partial}{\partial z}\left(k\frac{\partial T}{\partial z}\right)\right]dx\,dy\,dz \tag{3.51}$$

The work rate is performed by a force, **F** moving at velocity **V**. The two forces that will be considered are body forces that act on fluid inside the volume and surface forces which consists of pressure, shear and normal forces that act on the volume surface. A force pointing towards the positive coordinate direction is positive while the opposite direction will be in negative sign. The work rate done by a force acting on a moving fluid element is:

$$\dot{W} = \rho\mathbf{g}\cdot V\,dx\,dy\,dz = \rho\left(uf_x + vf_y + wf_z\right)dx\,dy\,dz \tag{3.52}$$

given that force, $\mathbf{F} = \left(f_x, f_y, f_z\right)$ includes gravitational, electric and magnetic forces. Referring to Figure 3.4, the work rate done by pressure in x-direction is:

$$\left[up - \left(up + \frac{\partial(up)}{\partial x}dx\right)\right]dy\,dz = -\frac{\partial(up)}{\partial x}dx\,dy\,dz \tag{3.53}$$

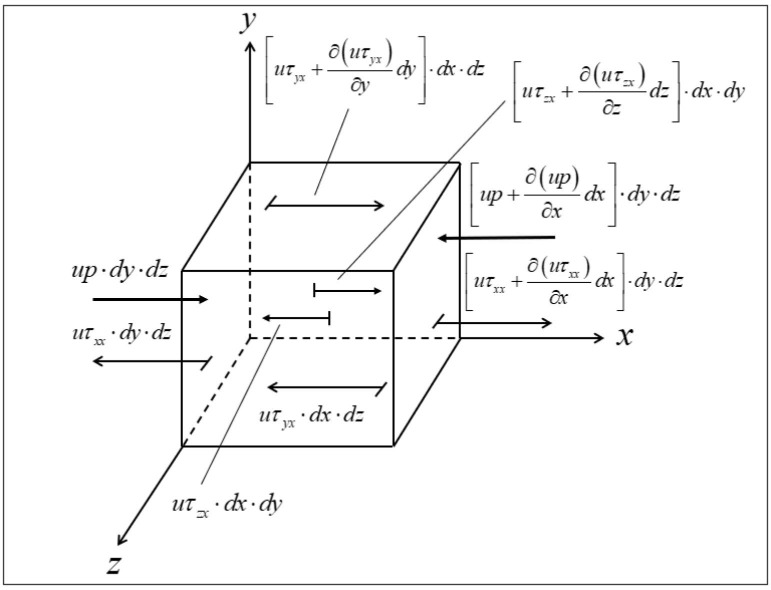

Figure 3.4 Work done by surface force in x-direction

Considering that τ_{xx}, τ_{yx} and τ_{zx} are the components of the stress acting on the surface which outward normal is pointing towards the x-direction, the net rate of work done by the surface forces in the x-direction is:

$$\left[\left(u\sigma_x+\frac{\partial(u\sigma_x)}{\partial x}dx\right)-u\sigma_x\right]dy\,dz+\left[\left(u\tau_{yx}+\frac{\partial(u\tau_{yx})}{\partial y}dy\right)-u\tau_{yx}\right]dx\,dz$$
$$+\left[\left(u\tau_{zx}+\frac{\partial(u\tau_{zx})}{\partial z}dz\right)-u\tau_{zx}\right]dx\,dy=\left[\frac{\partial(u\sigma_x)}{\partial x}+\frac{\partial(u\tau_{yx})}{\partial y}+\frac{\partial(u\tau_{zx})}{\partial z}\right]dx\,dy\,dz \qquad 3.54$$

Cumulatively, the total net rate of work done by the forces in the x-direction is:

$$\left[-\frac{\partial(up)}{\partial x}+\frac{\partial(u\sigma_x)}{\partial x}+\frac{\partial(u\tau_{yx})}{\partial y}+\frac{\partial(u\tau_{zx})}{\partial z}\right]dx\,dy\,dz \qquad 3.55$$

Therefore, the total of net rate of work done in all directions of the moving fluid due to the body and surface force can be represented by the following equation.

$$W=\begin{bmatrix} -\left(\frac{\partial(up)}{\partial x}+\frac{\partial(vp)}{\partial y}+\frac{\partial(wp)}{\partial z}\right)+\frac{\partial(u\sigma_x)}{\partial x}+\frac{\partial(u\tau_{yx})}{\partial y}+\frac{\partial(u\tau_{zx})}{\partial z} \\ +\frac{\partial(v\tau_{xy})}{\partial x}+\frac{\partial(v\sigma_y)}{\partial y}+\frac{\partial(v\tau_{zy})}{\partial z}+\frac{\partial(w\tau_{xz})}{\partial x}+\frac{\partial(w\tau_{yz})}{\partial y}+\frac{\partial(w\sigma_z)}{\partial z} \\ +\rho\left(uf_x+vf_y+wf_z\right) \end{bmatrix} dx\,dy\,dz \qquad 3.56$$

Hence, putting together all the individual elements, the final energy equation is obtained as follows:

$$\begin{aligned}\rho\frac{D}{Dt}\left(e+\frac{V^2}{2}\right)=\rho\dot{q}&+\frac{\partial}{\partial x}\left(k\frac{\partial T}{\partial x}\right)+\frac{\partial}{\partial y}\left(k\frac{\partial T}{\partial y}\right)+\frac{\partial}{\partial z}\left(k\frac{\partial T}{\partial z}\right)\\ &-\left(\frac{\partial(up)}{\partial x}+\frac{\partial(vp)}{\partial y}+\frac{\partial(wp)}{\partial z}\right)+\frac{\partial(u\sigma_x)}{\partial x}+\frac{\partial(u\tau_{yx})}{\partial y}\\ &+\frac{\partial(u\tau_{zx})}{\partial z}+\frac{\partial(v\tau_{xy})}{\partial x}+\frac{\partial(v\sigma_y)}{\partial y}+\frac{\partial(v\tau_{zy})}{\partial z}+\frac{\partial(w\tau_{xz})}{\partial x}\\ &+\frac{\partial(w\tau_{yz})}{\partial y}+\frac{\partial(w\sigma_z)}{\partial z}+\rho\left(uf_x+vf_y+wf_z\right)\end{aligned} \qquad 3.57$$

Equation (3.57) is the non-conservation form of energy equation since there are differentiated variables in the equation that exist as the coefficients of a certain derivative, for example the term $\frac{\partial(up)}{\partial x}$. When equations are solved numerically, the conservation form is more favourable. Therefore, in order to convert the energy equation to conservation form, chain rule is applied to the terms on the right side of the equation which results in the following equation:

$$\rho\frac{D}{Dt}\left(e+\frac{V^2}{2}\right)=\rho\dot{q}+\frac{\partial}{\partial x}\left(k\frac{\partial T}{\partial x}\right)+\frac{\partial}{\partial y}\left(k\frac{\partial T}{\partial y}\right)+\frac{\partial}{\partial z}\left(k\frac{\partial T}{\partial z}\right)-\left(p\frac{\partial u}{\partial x}+u\frac{\partial p}{\partial x}\right)$$
$$-\left(p\frac{\partial v}{\partial y}+v\frac{\partial p}{\partial y}\right)-\left(p\frac{\partial w}{\partial z}+w\frac{\partial p}{\partial z}\right)+\left(\sigma_x\frac{\partial u}{\partial x}+u\frac{\partial \sigma_x}{\partial x}\right)$$
$$+\left(\tau_{yx}\frac{\partial u}{\partial y}+u\frac{\partial \tau_{yx}}{\partial y}\right)+\left(\tau_{zx}\frac{\partial u}{\partial z}+u\frac{\partial \tau_{zx}}{\partial z}\right)+\left(\tau_{xy}\frac{\partial u}{\partial x}+v\frac{\partial \tau_{xy}}{\partial x}\right) \quad 3.58$$
$$+\left(\sigma_y\frac{\partial u}{\partial y}+v\frac{\partial \sigma_y}{\partial y}\right)+\left(\tau_{zy}\frac{\partial u}{\partial z}+v\frac{\partial \tau_{zy}}{\partial z}\right)+\left(\tau_{xz}\frac{\partial u}{\partial x}+w\frac{\partial \tau_{xz}}{\partial x}\right)$$
$$+\left(\tau_{yz}\frac{\partial u}{\partial y}+w\frac{\partial \tau_{yz}}{\partial y}\right)+\left(\sigma_z\frac{\partial u}{\partial z}+w\frac{\partial \sigma_z}{\partial z}\right)+\rho\left(uf_x+vf_y+wf_z\right)$$

Equation (3.58) can also be rearranged as:

$$\rho\frac{D}{Dt}\left(e+\frac{V^2}{2}\right)=\rho\dot{q}+\frac{\partial}{\partial x}\left(k\frac{\partial T}{\partial x}\right)+\frac{\partial}{\partial y}\left(k\frac{\partial T}{\partial y}\right)+\frac{\partial}{\partial z}\left(k\frac{\partial T}{\partial z}\right)-p\left(\frac{\partial u}{\partial x}+\frac{\partial v}{\partial y}+\frac{\partial w}{\partial z}\right)$$
$$+u\left(\frac{\partial \sigma_x}{\partial x}+\frac{\partial \tau_{yx}}{\partial y}+\frac{\partial \tau_{zx}}{\partial z}\right)+v\left(\frac{\partial \tau_{xy}}{\partial x}+\frac{\partial \sigma_y}{\partial y}+\frac{\partial \tau_{zy}}{\partial z}\right)$$
$$+w\left(\frac{\partial \tau_{xz}}{\partial x}+\frac{\partial \tau_{yz}}{\partial y}+\frac{\partial \sigma_z}{\partial z}\right)-u\frac{\partial p}{\partial x}-v\frac{\partial p}{\partial y}-w\frac{\partial p}{\partial z}+\sigma_x\frac{\partial u}{\partial x}+\tau_{yx}\frac{\partial u}{\partial y} \quad 3.59$$
$$+\tau_{zx}\frac{\partial u}{\partial z}+\tau_{xy}\frac{\partial v}{\partial x}+\sigma_y\frac{\partial v}{\partial y}+\tau_{zy}\frac{\partial v}{\partial z}+\tau_{xz}\frac{\partial w}{\partial x}+\tau_{yz}\frac{\partial w}{\partial y}+\sigma_z\frac{\partial w}{\partial z}$$
$$+\rho\left(uf_x+vf_y+wf_z\right)$$

However, it is also common for the energy equation to be expressed in terms of the internal energy, *e* only instead of the combination of internal and kinetic energy as shown in the equation. This can be achieved by using Equations (3.18) to (3.20) from Section 3.2.2. The first step is to multiply the equations by *u*, *v*, and *w*, respectively, from which these equations are obtained.

$$\rho\frac{D\left(\frac{u^2}{2}\right)}{Dt}=-u\frac{\partial p}{\partial x}+u\frac{\partial \sigma_x}{\partial x}+u\frac{\partial \tau_{yx}}{\partial y}+u\frac{\partial \tau_{zx}}{\partial z}+\rho uf_x \quad 3.60$$

$$\rho\frac{D\left(\frac{v^2}{2}\right)}{Dt}=-v\frac{\partial p}{\partial x}+v\frac{\partial\tau_{xy}}{\partial x}+v\frac{\partial\sigma_y}{\partial y}+v\frac{\partial\tau_{zy}}{\partial z}+\rho vf_y \tag{3.61}$$

$$\rho\frac{D\left(\frac{w^2}{2}\right)}{Dt}=-w\frac{\partial p}{\partial x}+w\frac{\partial\tau_{xz}}{\partial x}+w\frac{\partial\tau_{yz}}{\partial y}+w\frac{\partial\sigma_z}{\partial z}+\rho wf_z \tag{3.62}$$

Now, given that $u^2+v^2+w^2=V^2$, the sum of the equations can be simplified to:

$$\begin{aligned}\rho\frac{D\left(\frac{V^2}{2}\right)}{Dt}=&-u\frac{\partial p}{\partial x}-v\frac{\partial p}{\partial x}-w\frac{\partial p}{\partial x}+u\left(\frac{\partial\sigma_x}{\partial x}+\frac{\partial\tau_{yx}}{\partial y}+\frac{\partial\tau_{zx}}{\partial z}\right)+v\left(\frac{\partial\tau_{xy}}{\partial x}+\frac{\partial\sigma_y}{\partial y}+\frac{\partial\tau_{zy}}{\partial z}\right)\\&+w\left(\frac{\partial\tau_{xz}}{\partial x}+\frac{\partial\tau_{yz}}{\partial y}+\frac{\partial\sigma_z}{\partial z}\right)+\rho\left(uf_x+vf_y+wf_z\right)\end{aligned} \tag{3.63}$$

By subtracting Equation (3.63) from Equation (3.59), the following equation is obtained:

$$\begin{aligned}\rho\frac{D}{Dt}(e)=&\rho\dot{q}+\frac{\partial}{\partial x}\left(k\frac{\partial T}{\partial x}\right)+\frac{\partial}{\partial y}\left(k\frac{\partial T}{\partial y}\right)+\frac{\partial}{\partial z}\left(k\frac{\partial T}{\partial z}\right)-p\left(\frac{\partial u}{\partial x}+\frac{\partial v}{\partial y}+\frac{\partial w}{\partial z}\right)\\&+\sigma_x\frac{\partial u}{\partial x}+\tau_{yx}\frac{\partial u}{\partial y}+\tau_{zx}\frac{\partial u}{\partial z}+\tau_{xy}\frac{\partial v}{\partial x}+\sigma_y\frac{\partial v}{\partial y}+\tau_{zy}\frac{\partial v}{\partial z}+\tau_{xz}\frac{\partial w}{\partial x}\\&+\tau_{yz}\frac{\partial w}{\partial y}+\sigma_z\frac{\partial w}{\partial z}\end{aligned} \tag{3.64}$$

In the above equation, even though the terms related to body force are already eliminated, the equation is still in non-conservative form. The equation can be reduced further by recognizing the symmetricity of the stress tensor i.e. $\tau_{xy}=\tau_{yx},\tau_{xz}=\tau_{zx}$ and $\tau_{yz}=\tau_{zy}$ As reported by Oertel (2010), from the definition of enthalpy, *h* and equation of state of ideal gas, the internal energy can be expressed as:

$$e=c_p\cdot T-\frac{p}{\rho} \tag{3.65}$$

where c_p is the specific heat at constant pressure. Substituting this thermodynamic relation and Equation (3.24) into Equation (3.65), while also taking into account that pressure is constant, the energy equation becomes:

$$\rho c_p \frac{DT}{Dt} = \rho \dot{q} + k\frac{\partial^2 T}{\partial x^2} + k\frac{\partial^2 T}{\partial y^2} + k\frac{\partial^2 T}{\partial z^2} + \mu\left[2\left(\frac{\partial u}{\partial x}\right)^2 + 2\left(\frac{\partial v}{\partial y}\right)^2 + 2\left(\frac{\partial w}{\partial z}\right)^2 + \left(\frac{\partial u}{\partial y} + \frac{\partial v}{\partial x}\right)^2 + \left(\frac{\partial u}{\partial z} + \frac{\partial w}{\partial x}\right)^2 + \left(\frac{\partial v}{\partial z} + \frac{\partial w}{\partial y}\right)^2\right] \quad 3.66$$

The terms in the square brackets are expressed in velocity gradient and they represent the rate of viscous dissipation, ϕ. Hence, the equation can be written as:

$$\rho c_p \frac{DT}{Dt} = \rho \dot{q} + k\frac{\partial^2 T}{\partial x^2} + k\frac{\partial^2 T}{\partial y^2} + k\frac{\partial^2 T}{\partial z^2} + \mu\phi \quad 3.67$$

According to Bejan (2013), many convection problems comply with simple models where the fluid conductivity, k is a constant value, volumetric heat addition, $\dot{q}$ is zero and viscous dissipation, $\mu\phi$ is negligible. With these assumptions, those related terms are discarded, and the equation becomes:

$$\rho c_p \left(\frac{\partial T}{\partial t} + u\frac{\partial T}{\partial x} + v\frac{\partial T}{\partial y} + w\frac{\partial T}{\partial z}\right) = k\left(\frac{\partial^2 T}{\partial x^2} + \frac{\partial^2 T}{\partial y^2} + \frac{\partial^2 T}{\partial z^2}\right) \quad 3.68$$

For a two-dimensional steady incompressible flow, the conservative form of the energy equation is:

$$u\frac{\partial T}{\partial x} + v\frac{\partial T}{\partial y} = \chi\left(\frac{\partial^2 T}{\partial x^2} + \frac{\partial^2 T}{\partial y^2}\right) \quad 3.69$$

given that $\chi = \dfrac{k}{\rho c_p}$ and it is known as thermal diffusivity.

3.2.4 Angular Momentum Equation

When micropolar fluid is considered, an additional equation that represents the conservation of angular momentum is needed with the rest of the governing equations to describe the fluid flow in terms of the microrotation of the suspended microelements. This equation is a result from the fact that for polar fluid, stress tensor is not symmetric and the conservation law of linear momentum is independent of the law of conservation of mass and momentum (Lukaszewicz, 1999).

Lukaszewicz (1999) also mentioned that for micropolar fluid, the angular momentum is made up of two components, which are the spin angular momentum from the particle rotation and the orbital angular momentum due to the fluid flow. According to the principle of conservation of angular momentum, the rate of change of angular momentum is equal to the sum of moments of external forces. Therefore, this can be expressed mathematically as

$$\frac{D}{Dt}\left(\rho j\mathbf{H}+\mathbf{r}\times\rho\mathbf{V}\right)=\mathbf{M} \tag{3.70}$$

where j is microinertia per unit mass, $\mathbf{H}$ is the microrotation vector, $\mathbf{r}$ is the position vector and $\mathbf{M}$ is the sum of the moments acting on the fluid element. The moments, $\mathbf{M}$ can be broken down into three elements which are body couples, surface couples and antisymmetric part of the stress tensor. As a result, Equation (3.70) can be updated to

$$\begin{aligned}&\rho j\left(\frac{\partial\mathbf{H}}{\partial t}+\mathbf{V}\cdot\nabla\mathbf{H}\right)+\rho j\left(\mathbf{H}\times\mathbf{H}\right)+\mathbf{r}\times\rho\left(\frac{\partial\mathbf{V}}{\partial t}+\mathbf{V}\cdot\nabla\mathbf{V}\right)=\rho\mathbf{l}+\gamma\nabla^{2}\mathbf{H}\\&+\kappa\left(-2\mathbf{H}+\nabla\times\mathbf{V}\right)\end{aligned} \tag{3.71}$$

given that $\mathbf{l}$ is body couple per unit mass, κ is vortex viscosity and γ is the spin gradient viscosity defined as $\gamma=\left(1+\frac{\kappa}{2}\right)j$. Since $\mathbf{H}\times\mathbf{H}=0$ and assuming no body couple, i.e $\rho\mathbf{l}=0$, these terms can be dismissed from the equation. The third term, $\mathbf{r}\times\rho\left(\frac{\partial\mathbf{V}}{\partial t}+\mathbf{V}\cdot\nabla\mathbf{V}\right)$ can also be omitted because it is related to the linear momentum equation and is balanced by the moment of the stress tensor divergence. Hence, the equation is now in the form

$$\rho j\left(\frac{\partial \mathbf{H}}{\partial t}+\mathbf{V}\cdot\nabla\mathbf{H}\right)=\gamma\nabla^2\mathbf{H}+\kappa\left(-2\mathbf{H}+\nabla\times\mathbf{V}\right) \tag{3.72}$$

For steady two-dimensional flow, the angular momentum equation can be written as

$$\rho j\left(u\frac{\partial H}{\partial x}+v\frac{\partial H}{\partial y}\right)=\gamma\left(\frac{\partial^2 H}{\partial x^2}+\frac{\partial^2 H}{\partial y^2}\right)+\kappa\left(-2H+\frac{\partial v}{\partial x}-\frac{\partial u}{\partial y}\right) \tag{3.73}$$

3.2.5 Boundary Layer Approximation

Prandtl's boundary layer theory is the fundamental of the existence of boundary layer equations, which are the simpler form of Navier-Stokes equations that is only applicable on the boundary layer (Anderson, 2005). The concept originated from Prandtl's assumptions that when fluid flows over a surface at large value of Reynold number $(\mathrm{Re}\to\infty)$, the flow region is split into two regions. The first region is the region away from the object surface where viscous effect is negligible while the other region is known as the boundary layer region where viscous effect and inertia are equally significant.

In rectangular Cartesian form, the inertia and viscous terms are defined as $\rho u\frac{\partial u}{\partial x}$ and $\mu\frac{\partial^2 u}{\partial y^2}$, respectively. Since both are comparable, their order of magnitude would also be identical. Order of magnitude refers to a quantity that is used in scaling analysis to decide whether a term should remain or to be dropped from the equation. According to Subramanian (2019b), for inertia and viscous term of a plate with length *L*, their order of magnitude is given by:

$$\rho u\frac{\partial u}{\partial x}\sim\rho\frac{U_\infty^2}{L}\qquad\qquad \mu\frac{\partial^2 u}{\partial y^2}\sim\mu\frac{U_\infty}{\delta^2} \tag{3.74}$$

From the relationship, $\delta^2 \sim \dfrac{\mu L}{\rho U_\infty}$ or $\dfrac{\delta}{L} \sim \dfrac{1}{\sqrt{\mathrm{Re}_L}}$ where $\mathrm{Re}_L = \dfrac{U_\infty L}{\nu}$ is the Reynold number based on the length of the plate. Consequently, δ which represents the boundary layer thickness will have a very small value if $\mathrm{Re}_L \gg 1$. Since the terms of order δ will be relatively small, those terms can be discarded from the equations. Following Ozisik (1985) and Arifin (2019),

$$u \sim \mathrm{o}(1), \;\; x \sim \mathrm{o}(1), \;\; y \sim \mathrm{o}(\delta) \qquad 3.75$$

Performing the scaling analysis to the continuity equation in Equation (3.13), the following is obtained.

Table 3.1 Order of magnitude analysis for continuity equation

Terms	**Order of Magnitude**
$\dfrac{\partial u}{\partial x}$	$\dfrac{\mathrm{o}(1)}{\mathrm{o}(1)} = \mathrm{o}(1)$
$\dfrac{\partial v}{\partial y}$	$\dfrac{v}{\mathrm{o}(\delta)} = \mathrm{o}(1)$

According to Biswas (2003), it is the general rule of incompressible fluid mechanics that for continuity equation, none of the terms should be dismissed. Hence, from the rule it can be concluded that v is of order δ. Additionally, he also stated the term $-\dfrac{\partial p}{\partial y}$ will not exceed order 1 while the order of the rest of the quantities has been verified by and Abdul Rahman Mohd Kasim (2014) and Schlichting and Gersten (2016) as the following:

Table 3.2 Order of magnitude analysis for quantities

Terms	**Order of Magnitude**
$\dfrac{\mu}{\rho}$	$\mathrm{o}(\delta^2)$
σ	$\mathrm{o}\left(\dfrac{1}{\delta^2}\right)$
B_0^2	$\mathrm{o}(\delta^2)$
$\mathbf{g}$	$\mathrm{o}(1)$

For the momentum equation in x-direction as stated in Equation (3.40),

Table 3.3 Order of magnitude analysis for x-momentum equation

Terms	Order of Magnitude	Decision
$u\frac{\partial u}{\partial x}$	$o(1)\frac{o(1)}{o(1)}=o(1)$	remain
$v\frac{\partial u}{\partial y}$	$o(\delta)\frac{o(1)}{o(\delta)}=o(1)$	remain
$\frac{\mu}{\rho}\frac{\partial^2 u}{\partial x^2}$	$o(\delta^2)\frac{o(1)}{o(1)}=o(\delta^2)$	≈ 0
$\frac{\mu}{\rho}\frac{\partial^2 u}{\partial y^2}$	$o(\delta^2)\frac{o(1)}{o(\delta^2)}=o(1)$	remain
$\frac{\sigma}{\rho}B_0^2 u\sin^2\alpha$	$\frac{o(1)}{o(\delta^2)}o(\delta^2)o(1)=o(1)$	remain
$\beta^* g_x(T-T_\infty)$	$o(1)$	remain

Hence, from the analysis, the term $\frac{\mu}{\rho}\frac{\partial^2 u}{\partial x^2}$ that is of order δ^2 will be dropped from the equation. As for the momentum equation in y-direction in Equation (3.41), the analysis is as follows.

Table 3.4 Order of magnitude analysis for y-momentum equation

Terms	Order of Magnitude	Decision
$u\frac{\partial v}{\partial x}$	$o(1)\frac{o(\delta)}{o(1)}=o(\delta)$	remain
$v\frac{\partial v}{\partial y}$	$o(\delta)\frac{o(\delta)}{o(\delta)}=o(\delta)$	remain
$\frac{\mu}{\rho}\frac{\partial^2 v}{\partial y^2}$	$o(\delta^2)\frac{o(\delta)}{o(\delta^2)}=o(\delta)$	remain
$\frac{\mu}{\rho}\frac{\partial^2 v}{\partial x^2}$	$o(\delta^2)\frac{o(\delta)}{o(1)}=o(\delta^3)$	≈ 0
$\frac{\sigma}{\rho}vB_0^2\sin^2\alpha$	$\frac{o(1)}{o(\delta^2)}o(\delta^2)o(1)=o(1)$	remain
$\beta^* g_y(T-T_\infty)$	$o(1)$	remain

From the scaling analysis, only the aligned magnetic and buoyancy terms are of order 1 but the rest of the terms are of order δ and δ^3. Therefore, the momentum equation in the y-direction can be secluded from the constitutive equations.

For the momentum equation to be balanced, the term $-\frac{\partial p}{\partial y}$ must be of order δ. This can be physically interpreted as the pressure remains unchanged in the boundary layer which implies that p is only a function of x. Hence, $\frac{\partial p}{\partial x} = \frac{dp}{dx}$. However, since Prandtl has declared that pressure on the surface is almost identical to pressure at the edge of the boundary layer, therefore across boundary layer, pressure is negligible (Arakeri & Shankar, 2000). Hence, $\frac{dp}{dx} = 0$ and for simplification purpose, the term g_x is replaced by g. As a result, the boundary layer equations of Newtonian fluid are:

$$\frac{\partial u}{\partial x} + \frac{\partial v}{\partial y} = 0 \qquad 3.76$$

$$u\frac{\partial u}{\partial x} + v\frac{\partial u}{\partial y} = \frac{\mu}{\rho}\frac{\partial^2 u}{\partial y^2} - \frac{\sigma}{\rho}B_0^2 u \sin^2\alpha + \beta^* g\left(T - T_\infty\right) \qquad 3.77$$

As for the energy equation, the quantities in Equation (3.69) with their orders are:

$$T \sim \mathrm{o}(1), \quad \alpha \sim \mathrm{o}\left(\delta^2\right) \qquad 3.78$$

The order of magnitude analysis on the equation is as follows:

Table 3.5 Order of magnitude analysis for energy equation

Terms	Order of Magnitude	Decision
$u\frac{\partial T}{\partial x}$	$\mathrm{o}(1)\ \frac{\mathrm{o}(1)}{\mathrm{o}(1)} = \mathrm{o}(1)$	remain
$v\frac{\partial T}{\partial y}$	$\mathrm{o}(\delta)\frac{\mathrm{o}(1)}{\mathrm{o}(\delta)} = \mathrm{o}(1)$	remain
$\chi\frac{\partial^2 T}{\partial x^2}$	$\mathrm{o}\left(\delta^2\right)\frac{\mathrm{o}(1)}{\mathrm{o}(1)} = \mathrm{o}\left(\delta^2\right)$	≈ 0

Table 3.5 Continued

Terms	Order of Magnitude	Decision
$\chi \frac{\partial^2 T}{\partial y^2}$	$o\left(\delta^2\right)\frac{o(1)}{o\left(\delta^2\right)} = o(1)$	remain

From the analysis, the third term will be discarded, hence the thermal boundary layer equation is:

$$u\frac{\partial T}{\partial x} + v\frac{\partial T}{\partial y} = \chi \frac{\partial^2 T}{\partial y^2} \qquad 3.79$$

For the angular momentum equation in Equation (3.73), following Biswas et al. (2012), $\rho j \sim o(1), \gamma \sim o\left(\delta^2\right)$ and $\kappa \sim o(\delta)$. The order of magnitude for the equation is presented in the following table.

Table 3.6 Order of magnitude analysis for angular momentum equation

Terms	Order of Magnitude	Decision
$\rho ju \frac{\partial H}{\partial x}$	$o(1)\,o(1)\frac{o(1)}{o(1)} = o(1)$	remain
$\rho jv \frac{\partial H}{\partial y}$	$o(1)\,o(\delta)\frac{o(\delta)}{o(\delta)} = o(\delta)$	remain
$\gamma \frac{\partial^2 H}{\partial x^2}$	$o\left(\delta^2\right)\frac{o(1)}{o(1)} = o\left(\delta^2\right)$	≈ 0
$\gamma \frac{\partial^2 H}{\partial y^2}$	$o\left(\delta^2\right)\frac{o(1)}{o\left(\delta^2\right)} = o(1)$	remain
$\kappa \frac{\partial v}{\partial x}$	$o(\delta)\frac{o(\delta)}{o(1)} = o\left(\delta^2\right)$	≈ 0
$\kappa \frac{\partial u}{\partial y}$	$o(\delta)\frac{o(1)}{o(1)} = o(\delta)$	remain
$H\kappa$	$o(1)\,o(1) = o(1)$	remain

From the analysis, after discarding two of the terms, the angular momentum equation is:

$$\rho j\left(u\frac{\partial H}{\partial x}+v\frac{\partial H}{\partial y}\right)=-\kappa\left(2H+\frac{\partial u}{\partial y}\right)+\gamma\frac{\partial^2 H}{\partial y^2} \quad 3.80$$

3.3 Governing Equation for Viscoelastic Micropolar Fluid

In Section 3.2, the derivation of the governing equations for Newtonian fluid is shown in detail. Newtonian fluid model is presented as the model is simple which makes it convenient to explain how the equations of fluid flow are derived from the conservation of mass, momentum and energy as well as how other concepts are utilized in order to construct the equations in the simplest solvable form. Moreover, the Newtonian fluid model is the basic framework of any fluid model and even our complex model can be reduced to Newtonian fluid model by discarding all the parameters that describe the viscoelasticity and polar characteristics. Based on the idea that has been presented in the previous section, Section 3.3 will elaborate in detail the derivation of the governing equation for viscoelastic micropolar fluid.

The continuity and energy equations for viscoelastic micropolar fluid are identical to respective equations of the Newtonian fluid that are stated in Equations (3.76) and (3.79). Since the fluid is polar, an additional angular momentum is also necessary to describe the fluid flow as derived in Section 3.2.4. However, the major contribution of this study will be in terms of the Navier-Stokes equation that represents the conservation of momentum and due to the intricate nature of the fluid, the derivation will be much more complicated since there will be more terms involved compared to the Newtonian model. Furthermore, the order of the derivatives will be as high as fourth order, and it is widely recognized that for differential equations, the order and the level of difficulty to solve the equations work in parallel.

Referring to Jafar et al. (2019) as well as Idowu and Falodun (2020), the Cauchy stress tensor for viscoelastic fluid is given by:

$$\boldsymbol{\tau}_e=\mu(2\mathbf{d})-k_0\left(2\overset{\nabla}{\mathbf{d}}\right) \quad 3.81$$

where $\mathbf{I}$, $\mathbf{d}$ and k_0 represent the identity vector, deformation rate tensor and short-memory coefficient, respectively. In the equation, $\overset{\nabla}{\mathbf{d}}$ is the upper-convected derivative of a tensor, defined as:

$$\overset{\nabla}{\mathbf{d}} = \mathbf{V}\cdot\nabla(\mathbf{d}) - (\mathbf{d})\cdot(\nabla\mathbf{V})^T - \nabla\mathbf{V}\cdot(\mathbf{d}) \tag{3.82}$$

which is equivalent to:

$$2\overset{\nabla}{\mathbf{d}} = \mathbf{V}\cdot\nabla(2\mathbf{d}) - (2\mathbf{d})\cdot(\nabla\mathbf{V})^T - \nabla\mathbf{V}\cdot(2\mathbf{d}) \tag{3.83}$$

Hence, in steady condition the stress component in two-dimension is:

$$\tau_{ij} = \mu\left(2d_{ij}\right) - k_0\left[\mathbf{V}\cdot\nabla(2d_{ij}) - (2d_{ij})\cdot(\nabla\mathbf{V})^T - \nabla\mathbf{V}\cdot(2d_{ij})\right] \tag{3.84}$$

where

$$2d_{ij} = \frac{\partial \mathbf{V}_j}{\partial x_i} + \frac{\partial \mathbf{V}_i}{\partial x_j}, \quad i = x, y, \quad j = x, y \tag{3.85}$$

The individual elements of the stress tensor are as follows:

$$\tau_{xx} = 2\mu\frac{\partial u}{\partial x} - 2k_0\left[u\frac{\partial^2 u}{\partial x^2} + v\frac{\partial^2 u}{\partial x\partial y} - 2\left\{\left(\frac{\partial u}{\partial x}\right)^2 + \frac{1}{2}\frac{\partial u}{\partial y}\left(\frac{\partial u}{\partial y} + \frac{\partial v}{\partial x}\right)\right\}\right] \tag{3.86}$$

$$\begin{aligned}\tau_{xy} = \tau_{yx} &= \mu\left(\frac{\partial v}{\partial x} + \frac{\partial u}{\partial y}\right) \\ &\quad - 2k_0\left[\frac{u}{2}\left(\frac{\partial^2 v}{\partial x^2} + \frac{\partial^2 u}{\partial x\partial y}\right) + \frac{v}{2}\left(\frac{\partial^2 v}{\partial y\partial x} + \frac{\partial^2 u}{\partial y^2}\right) - \left(\frac{\partial u}{\partial x}\cdot\frac{\partial v}{\partial x} + \frac{\partial v}{\partial y}\cdot\frac{\partial u}{\partial y}\right)\right]\end{aligned} \tag{3.87}$$

$$\tau_{yy} = 2\mu\frac{\partial v}{\partial y} - 2k_0\left[u\frac{\partial^2 v}{\partial x\partial y} + v\frac{\partial^2 v}{\partial y^2} - 2\left\{\left(\frac{\partial v}{\partial y}\right)^2 + \frac{1}{2}\frac{\partial v}{\partial x}\left(\frac{\partial v}{\partial x} + \frac{\partial u}{\partial y}\right)\right\}\right] \tag{3.88}$$

However, the stress tensor in Equation (3.93) is insufficient for this problem as it does not count into the couple stress that is vital for model with rotating microelements. Therefore, for the case of viscoelastic micropolar fluid, the total stress tensor of the fluid is:

$$\mathbf{T} = -p\mathbf{I} + \boldsymbol{\tau}_e + \boldsymbol{\tau}_p \tag{3.89}$$

where $\boldsymbol{\tau}_p$ is the additional couple stress from the microrotation. According to Alzahrani et al. (2022), given that $\mathbf{H} = (0, 0, H)$, in vector form the couple stress can be defined as:

$$\boldsymbol{\tau}_p = \kappa \nabla (\nabla \cdot \mathbf{V}) + \kappa (\nabla \times \mathbf{H}) \tag{3.90}$$

Following Equation (3.18) and (3.19), the momentum equations for viscoelastic micropolar fluid with the corresponding order of magnitude analysis are:

x-direction:

$$\begin{aligned} u\frac{\partial u}{\partial x} + v\frac{\partial u}{\partial y} &= -\frac{1}{\rho}\frac{\partial p}{\partial x} + \left(\frac{\mu+\kappa}{\rho}\right)\left(\frac{\partial^2 u}{\partial x^2} + \frac{\partial^2 u}{\partial y^2}\right) + \kappa\frac{\partial H}{\partial y} \\ &+ \frac{k_0}{\rho}\left[\begin{aligned} & u\left(\frac{\partial^3 u}{\partial x^3} + \frac{\partial^3 u}{\partial x \partial y^2}\right) + v\left(\frac{\partial^3 u}{\partial x^2 \partial y} + \frac{\partial^3 u}{\partial y^3}\right) + \frac{\partial u}{\partial x}\left(3\frac{\partial^2 v}{\partial x \partial y} + \frac{\partial^2 u}{\partial y^2}\right) - \frac{\partial u}{\partial y}\left(\frac{\partial^2 u}{\partial x \partial y} + \frac{\partial^2 v}{\partial x^2}\right) \\ & -2\frac{\partial v}{\partial x}\frac{\partial^2 u}{\partial x \partial y} \end{aligned}\right] \end{aligned} \tag{3.91}$$

Table 3.7 Order of magnitude analysis for *x*-momentum of viscoelastic micropolar fluid

Terms	**Order of Magnitude**	**Decision**
$u\frac{\partial u}{\partial x}$	$\text{o}(1)\frac{\text{o}(1)}{\text{o}(1)} = \text{o}(1)$	remain
$v\frac{\partial u}{\partial y}$	$\text{o}(\delta)\frac{\text{o}(1)}{\text{o}(\delta)} = \text{o}(1)$	remain
$\left(\frac{\mu+\kappa}{\rho}\right)\frac{\partial^2 u}{\partial x^2}$	$\text{o}(2\delta^2)\frac{\text{o}(1)}{\text{o}(1)} = \text{o}(2\delta^2)$	≈ 0

Table 3.7 Continued

Terms	Order of Magnitude	Decision
$\left(\frac{\mu+\kappa}{\rho}\right)\frac{\partial^2 u}{\partial y^2}$	$\mathrm{o}\left(2\delta^2\right)\frac{\mathrm{o}(1)}{\mathrm{o}\left(\delta^2\right)}=\mathrm{o}(2)$	remain
$\kappa\frac{\partial H}{\partial y}$	$\mathrm{o}\left(\delta^2\right)\frac{\mathrm{o}(1)}{\mathrm{o}\left(\delta^2\right)}=\mathrm{o}(1)$	remain
$\frac{k_0}{\rho}u\frac{\partial^3 u}{\partial x^3}$	$\mathrm{o}\left(\delta^2\right)\mathrm{o}(1)\frac{\mathrm{o}(1)}{\mathrm{o}(1)}=\mathrm{o}\left(\delta^2\right)$	≈ 0
$\frac{k_0}{\rho}u\frac{\partial^3 u}{\partial x\partial y^2}$	$\mathrm{o}\left(\delta^2\right)\mathrm{o}(1)\frac{\mathrm{o}(1)}{\mathrm{o}(1)\,\mathrm{o}\left(\delta^2\right)}=\mathrm{o}(1)$	remain
$\frac{k_0}{\rho}v\frac{\partial^3 u}{\partial x^2\partial y}$	$\mathrm{o}\left(\delta^2\right)\mathrm{o}(\delta)\frac{\mathrm{o}(1)}{\mathrm{o}(1)\,\mathrm{o}(\delta)}=\mathrm{o}\left(\delta^2\right)$	≈ 0
$\frac{k_0}{\rho}v\frac{\partial^3 u}{\partial y^3}$	$\mathrm{o}\left(\delta^2\right)\mathrm{o}(\delta)\frac{\mathrm{o}(1)}{\mathrm{o}\left(\delta^3\right)}=\mathrm{o}(1)$	remain
$\frac{k_0}{\rho}\frac{\partial u}{\partial x}3\frac{\partial^2 v}{\partial x\partial y}$	$\mathrm{o}\left(\delta^2\right)\frac{\mathrm{o}(1)}{\mathrm{o}(1)}\frac{\mathrm{o}(\delta)}{\mathrm{o}(1)\,\mathrm{o}(\delta)}=\mathrm{o}\left(\delta^2\right)$	≈ 0
$\frac{k_0}{\rho}\frac{\partial u}{\partial x}\frac{\partial^2 u}{\partial y^2}$	$\mathrm{o}\left(\delta^2\right)\frac{\mathrm{o}(1)}{\mathrm{o}(1)}\frac{\mathrm{o}(1)}{\mathrm{o}\left(\delta^2\right)}=\mathrm{o}(1)$	remain
$\frac{k_0}{\rho}\frac{\partial u}{\partial y}\frac{\partial^2 u}{\partial x\partial y}$	$\mathrm{o}\left(\delta^2\right)\frac{\mathrm{o}(1)}{\mathrm{o}(\delta)}\frac{\mathrm{o}(1)}{\mathrm{o}(1)\,\mathrm{o}(\delta)}=\mathrm{o}(1)$	remain
$\frac{k_0}{\rho}\frac{\partial u}{\partial y}\frac{\partial^2 v}{\partial x^2}$	$\mathrm{o}\left(\delta^2\right)\frac{\mathrm{o}(1)}{\mathrm{o}(\delta)}\frac{\mathrm{o}(\delta)}{\mathrm{o}(1)}=\mathrm{o}\left(\delta^2\right)$	≈ 0

y-direction:

$$u\frac{\partial v}{\partial x}+v\frac{\partial v}{\partial y}=-\frac{1}{\rho}\frac{\partial p}{\partial y}+\left(\frac{\mu+\kappa}{\rho}\right)\left(\frac{\partial^2 v}{\partial x^2}+\frac{\partial^2 v}{\partial y^2}\right)$$
$$+\frac{k_0}{\rho}\left[\begin{array}{l} u\left(\frac{\partial^3 v}{\partial x\partial y^2}+\frac{\partial^3 v}{\partial x^3}\right)+v\left(\frac{\partial^3 v}{\partial y^3}+\frac{\partial^3 v}{\partial x^2\partial y}\right)-\frac{\partial v}{\partial x}\left(\frac{\partial^2 u}{\partial y^2}+\frac{\partial^2 v}{\partial x\partial y}\right)+\frac{\partial v}{\partial y}\left(\frac{\partial^2 v}{\partial x^2}-3\frac{\partial^2 v}{\partial y^2}\right) \\ -2\frac{\partial u}{\partial y}\frac{\partial^2 v}{\partial x\partial y} \end{array}\right] \quad 3.92$$

Table 3.8 Order of magnitude analysis for *y*-momentum of viscoelastic micropolar fluid

Terms	Order of Magnitude	Decision
$u\dfrac{\partial v}{\partial x}$	$o(1)\dfrac{o(\delta)}{o(1)}=o(\delta)$	≈ 0
$v\dfrac{\partial v}{\partial y}$	$o(\delta)\dfrac{o(\delta)}{o(\delta)}=o(\delta)$	≈ 0
$\left(\dfrac{\mu+\kappa}{\rho}\right)\dfrac{\partial^2 v}{\partial x^2}$	$o\left(2\delta^2\right)\dfrac{o(\delta)}{o(1)}=o\left(2\delta^3\right)$	≈ 0
$\left(\dfrac{\mu+\kappa}{\rho}\right)\dfrac{\partial^2 v}{\partial y^2}$	$o\left(2\delta^2\right)\dfrac{o(\delta)}{o\left(\delta^2\right)}=o(2\delta)$	≈ 0
$\dfrac{k_0}{\rho}u\dfrac{\partial^3 v}{\partial x\partial y^2}$	$o\left(\delta^2\right)o(1)\dfrac{o(\delta)}{o(1)\,o\left(\delta^2\right)}=o(\delta)$	≈ 0
$\dfrac{k_0}{\rho}u\dfrac{\partial^3 v}{\partial x^3}$	$o\left(\delta^2\right)o(1)\dfrac{o(\delta)}{o(1)}=o\left(\delta^3\right)$	≈ 0
$\dfrac{k_0}{\rho}v\dfrac{\partial^3 v}{\partial y^3}$	$o\left(\delta^2\right)o(\delta)\dfrac{o(\delta)}{o\left(\delta^3\right)}=o(\delta)$	≈ 0
$\dfrac{k_0}{\rho}v\dfrac{\partial^3 v}{\partial x^2\partial y}$	$o\left(\delta^2\right)o(\delta)\dfrac{o(\delta)}{o(1)\,o(\delta)}=o\left(\delta^3\right)$	≈ 0
$\dfrac{k_0}{\rho}\dfrac{\partial v}{\partial x}\dfrac{\partial^2 u}{\partial y^2}$	$o\left(\delta^2\right)\dfrac{o(\delta)}{o(1)}\dfrac{o(1)}{o\left(\delta^2\right)}=o(\delta)$	≈ 0
$\dfrac{k_0}{\rho}\dfrac{\partial v}{\partial x}\dfrac{\partial^2 v}{\partial x\partial y}$	$o\left(\delta^2\right)\dfrac{o(\delta)}{o(1)}\dfrac{o(\delta)}{o(1)\,o(\delta)}=o\left(\delta^3\right)$	≈ 0
$\dfrac{k_0}{\rho}\dfrac{\partial v}{\partial y}\dfrac{\partial^2 v}{\partial x^2}$	$o\left(\delta^2\right)\dfrac{o(\delta)}{o(\delta)}\dfrac{o(\delta)}{o(1)}=o\left(\delta^3\right)$	≈ 0
$\dfrac{k_0}{\rho}\dfrac{\partial v}{\partial y}3\dfrac{\partial^2 v}{\partial y^2}$	$o\left(\delta^2\right)\dfrac{o(\delta)}{o(\delta)}\dfrac{o(\delta)}{o\left(\delta^2\right)}=o(\delta)$	≈ 0
$\dfrac{k_0}{\rho}2\dfrac{\partial u}{\partial y}\dfrac{\partial^2 v}{\partial x\partial y}$	$o\left(\delta^2\right)\dfrac{o(1)}{o(\delta)}\dfrac{o(\delta)}{o(1)\,o(\delta)}=o(\delta)$	≈ 0

After the boundary layer approximation, all the terms in *y*-direction can be discarded and as for the momentum equation in *x*-direction, the equation is simplified to:

$$u\frac{\partial u}{\partial x}+v\frac{\partial u}{\partial y}=-\frac{1}{\rho}\frac{\partial p}{\partial x}+\left(v+\frac{\kappa}{\rho}\right)\frac{\partial^2 u}{\partial y^2}+\frac{\kappa}{\rho}\frac{\partial H}{\partial y} + \frac{k_0}{\rho}\left[u\frac{\partial^3 u}{\partial x\partial y^2}+v\frac{\partial^3 u}{\partial y^3}+\frac{\partial u}{\partial x}\frac{\partial^2 u}{\partial y^2}-\frac{\partial u}{\partial y}\frac{\partial^2 u}{\partial x\partial y}\right] \quad 3.93$$

where $v=\frac{\mu}{\rho}$ is the kinematic viscosity. Furthermore, adding the term that corresponds to the MHD effect as derived in Equation (3.31), the momentum equation of viscoelastic micropolar fluid with aligned MHD effect is:

$$u\frac{\partial u}{\partial x}+v\frac{\partial u}{\partial y}=-\frac{1}{\rho}\frac{\partial p}{\partial x}+\left(v+\frac{\kappa}{\rho}\right)\frac{\partial^2 u}{\partial y^2}+\frac{\kappa}{\rho}\frac{\partial H}{\partial y}-\frac{\sigma}{\rho}uB_0^2\sin^2\alpha+\beta^* g\left(T-T_\infty\right) + \frac{k_0}{\rho}\left[u\frac{\partial^3 u}{\partial x\partial y^2}+v\frac{\partial^3 u}{\partial y^3}+\frac{\partial u}{\partial x}\frac{\partial^2 u}{\partial y^2}-\frac{\partial u}{\partial y}\frac{\partial^2 u}{\partial x\partial y}\right] \quad 3.94$$

3.4 Summary

In this chapter, the derivation of the governing equations of the flow for viscoelastic micropolar fluid has been presented in detail. The main idea in this chapter is to come out with a set of equations that would be the best representation of the complex fluid where the equations should obey the conservation laws and at the same time, embody the viscoelasticity and micropolar characteristics of the fluid. The formulation also included the influence of aligned magnetic field. The basic equations of the proposed model are initially displayed in vector form before they are simplified by applying the boundary layer and Boussinesq approximations so that only the significant terms remain. Table 3.9 provides a summary of the basic governing equations that have been derived throughout this chapter.

Table 3.9 Governing equations of viscoelastic micropolar fluid with MHD effect

Name	Equation
Continuity equation	$\frac{\partial u}{\partial x}+\frac{\partial v}{\partial y}=0$
Momentum equation	$u\frac{\partial u}{\partial x}+v\frac{\partial u}{\partial y}=-\frac{1}{\rho}\frac{\partial p}{\partial x}+\left(\nu+\frac{\kappa}{\rho}\right)\frac{\partial^2 u}{\partial y^2}+\frac{\kappa}{\rho}\frac{\partial H}{\partial y}-\frac{\sigma}{\rho}uB_0^2\sin^2\alpha$ $+\beta^* g\left(T-T_\infty\right)+\frac{k_0}{\rho}\left[u\frac{\partial^3 u}{\partial x\partial y^2}+v\frac{\partial^3 u}{\partial y^3}+\frac{\partial u}{\partial x}\frac{\partial^2 u}{\partial y^2}-\frac{\partial u}{\partial y}\frac{\partial^2 u}{\partial x\partial y}\right]$
Angular momentum equation	$\rho j\left(u\frac{\partial H}{\partial x}+v\frac{\partial H}{\partial y}\right)=-\kappa\left(2H+\frac{\partial u}{\partial y}\right)+\gamma\frac{\partial^2 H}{\partial y^2}$
Energy equation	$u\frac{\partial T}{\partial x}+v\frac{\partial T}{\partial y}=\chi\left(\frac{\partial^2 T}{\partial x^2}+\frac{\partial^2 T}{\partial y^2}\right)$

CHAPTER 4

FLOW OF VISCOELASTIC MICROPOLAR FLUID OVER A HORIZONTAL CIRCULAR CYLINDER WITH ALIGNED MHD EFFECT

4.1 Introduction

The primary focus of this chapter is the problem involving the flow of viscoelastic micropolar fluid under the influence of aligned magnetic effect over a horizontal circular cylinder. This problem will serve as the pilot study for the rest of the problems especially in Chapters 5 and 6. Therefore in this chapter, only the behaviour of the flow will be analysed without considering the heat effect for our initial encounter with this model. The model will be presented in Section 4.2 where non-dimensional variables and non-similarity transformation will be introduced to the viscoelastic micropolar equation that had been derived in Chapter 3.

Following the outcomes obtained from applying the Keller-box method to the solvable form of the governing equations, the results will be presented and discussed in Section 4.3. The references used to affirm the reliability of the results in this chapter mainly come from Ariel (2002) and Anwar et al. (2008). While both studies focus on the boundary layer flow of viscoelastic fluid, the prior study specifically examines the flow, while the latter delves into the problem when mixed convection is considered. After the validation, the behavioural effect of the viscoelastic micropolar flow is then evaluated from the velocity and microrotation profiles as well as the skin friction coefficient that will be discussed in Section 4.4.

4.2 Mathematical Formulation

Consider a horizontal circular cylinder with radius a that is aligned to a free stream velocity given by U_∞. A steady, two-dimensional incompressible viscoelastic micropolar fluid flows over the circular cylinder as the cylinder is imposed to a uniform magnetic field at an acute, aligned angle, α, that is measured clockwise from the vertical downward. The Cartesian coordinate $\bar{x}$ is measured along the circumference of the cylinder starting from the lower stagnation point while $\bar{y}$ is perpendicular to the surface of the body as illustrated in Figure 4.1.

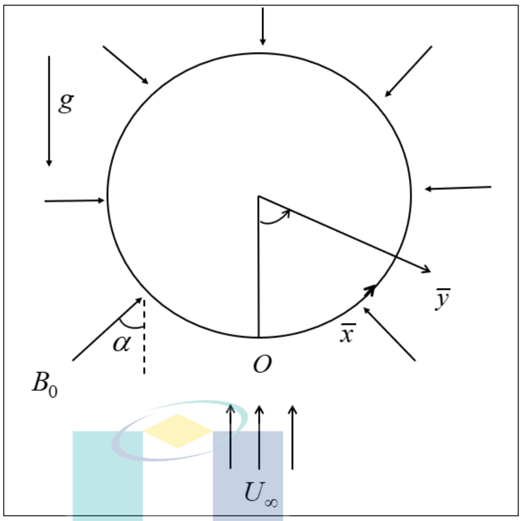

Figure 4.1 Schematic diagram for flow of viscoelastic micropolar fluid over a horizontal circular cylinder

This problem governed by Equations (3.76) and (3.80) is denoted by ‘ ¯ ’ as an indication that these equations are still in dimensional form as presented below:

$$\frac{\partial \bar{u}}{\partial \bar{x}}+\frac{\partial \bar{v}}{\partial \bar{y}}=0 \tag{4.1}$$

$$\rho j\left(\bar{u}\frac{\partial \bar{H}}{\partial \bar{x}}+v\frac{\partial \bar{H}}{\partial \bar{y}}\right)=-\kappa\left(2\bar{H}+\frac{\partial \bar{u}}{\partial \bar{y}}\right)+\gamma\frac{\partial^2 \bar{H}}{\partial \bar{y}^2} \tag{4.2}$$

As for the momentum equation, following Equation (3.94) while discarding heat related terms, the following equation is obtained:

$$\begin{aligned}\bar{u}\frac{\partial \bar{u}}{\partial \bar{x}}+\bar{v}\frac{\partial \bar{u}}{\partial \bar{y}}&=\frac{1}{\rho}\frac{\partial \bar{p}}{\partial \bar{x}}+\left(\nu+\frac{\kappa}{\rho}\right)\frac{\partial^2 \bar{u}}{\partial \bar{y}^2}+\frac{\kappa}{\rho}\frac{\partial \bar{H}}{\partial \bar{y}}-\frac{\sigma}{\rho}\bar{u}B_0^2\sin^2\alpha\\&+\frac{k_0}{\rho}\left[\bar{u}\frac{\partial^3 \bar{u}}{\partial \bar{x}\partial \bar{y}^2}+\bar{v}\frac{\partial^3 \bar{u}}{\partial \bar{y}^3}+\frac{\partial \bar{u}}{\partial \bar{x}}\frac{\partial^2 \bar{u}}{\partial \bar{y}^2}-\frac{\partial \bar{u}}{\partial \bar{y}}\frac{\partial^2 \bar{u}}{\partial \bar{x}\partial \bar{y}}\right]\end{aligned} \tag{4.3}$$

Outside the boundary layer region, the momentum equation of the flow is defined as:

$$\bar{u}_e \frac{\partial \bar{u}_e}{\partial \bar{x}} + \bar{v} \frac{\partial \bar{u}_e}{\partial \bar{y}} = \frac{1}{\rho} \frac{\partial \bar{p}}{\partial \bar{x}} + \left(\nu + \frac{\kappa}{\rho} \right) \frac{\partial^2 \bar{u}_e}{\partial \bar{y}^2} + \frac{\kappa}{\rho} \frac{\partial \bar{H}}{\partial \bar{y}} - \frac{\sigma}{\rho} \bar{u}_e B_0^2 \sin^2 \alpha$$
$$+ \frac{k_0}{\rho} \left[\bar{u}_e \frac{\partial^3 \bar{u}_e}{\partial \bar{x} \partial \bar{y}^2} + \bar{v} \frac{\partial^3 \bar{u}_e}{\partial \bar{y}^3} + \frac{\partial \bar{u}_e}{\partial \bar{x}} \frac{\partial^2 \bar{u}_e}{\partial \bar{y}^2} - \frac{\partial \bar{u}_e}{\partial \bar{y}} \frac{\partial^2 \bar{u}_e}{\partial \bar{x} \partial \bar{y}} \right] \quad 4.4$$

where $\bar{u}_e(\bar{x}) = U_\infty \sin\left(\bar{x}/a\right)$ and it represents the velocity outside the boundary layer. Since the velocity is only dependent on *x*, Equation (4.4) can be reduced to:

$$\frac{1}{\rho} \frac{\partial \bar{p}}{\partial \bar{x}} = \bar{u}_e \frac{\partial \bar{u}_e}{\partial \bar{x}} + \frac{\sigma}{\rho} \bar{u}_e B_0^2 \sin^2 \alpha \quad 4.5$$

Substituting Equation (4.5) into Equation (4.3), the following momentum equation is obtained:

$$\bar{u} \frac{\partial \bar{u}}{\partial \bar{x}} + \bar{v} \frac{\partial \bar{u}}{\partial \bar{y}} = \bar{u}_e \frac{d\bar{u}_e}{d\bar{x}} + \left(\frac{\mu + \kappa}{\rho} \right) \frac{\partial^2 \bar{u}}{\partial \bar{y}^2} + \frac{\kappa}{\rho} \frac{\partial \bar{H}}{\partial \bar{y}} - \frac{\sigma}{\rho} \left(\bar{u} - \bar{u}_e \right) B_0^2 \sin^2 \alpha$$
$$+ \frac{k_0}{\rho} \left[\frac{\partial}{\partial \bar{x}} \left(\bar{u} \frac{\partial^2 \bar{u}}{\partial \bar{y}^2} \right) + \bar{v} \frac{\partial^3 \bar{u}}{\partial \bar{y}^3} - \frac{\partial \bar{u}}{\partial \bar{y}} \frac{\partial^2 \bar{u}}{\partial \bar{x} \partial \bar{y}} \right] \quad 4.6$$

The governing equations are subjected to the boundary conditions:

$$\bar{u} = \bar{v} = 0, \quad \bar{H} = -n \frac{\partial \bar{u}}{\partial \bar{y}} \quad \text{on } \bar{y} = 0,$$
$$\bar{u} \to \bar{u}_e(x), \ \frac{\partial \bar{u}}{\partial \bar{y}} \to 0, \ \bar{H} \to 0 \quad \text{as } \bar{y} \to \infty \quad 4.7$$

This set of equations are then transformed into their non-dimensionless form where each term is stripped off its units by substituting relevant dimensionless variables. For this flow problem, the following variables are assumed:

$$x = \frac{\bar{x}}{a}, \ y = \frac{\mathrm{Re}^{1/2} \bar{y}}{a}, \ u = \frac{\bar{u}}{U_\infty}, \ v = \frac{\mathrm{Re}^{1/2} \bar{v}}{U_\infty}, \ H = \frac{\mathrm{Re}^{-1/2} a\bar{H}}{U_\infty}, \ u_e = \frac{\bar{u}_e(\bar{x})}{U_\infty} \quad 4.8$$

Applying the variables in Equation (4.8) into Equations (4.1), (4.2) and (4.6), the dimensionless form of continuity remains in the same form as stated in Equations (3.76) while the momentum and angular momentum equations are as follows:

$$\begin{aligned} u\frac{\partial u}{\partial x}+v\frac{\partial u}{\partial y} &= u_e\frac{du_e}{dx}+\left(1+K_1\right)\frac{\partial^2 u}{\partial y^2}+K_1\frac{\partial N}{\partial y}-M\left(u-u_e\right)\sin^2\alpha \\ &+K\left[\frac{\partial}{\partial x}\left(u\frac{\partial^2 u}{\partial y^2}\right)+v\frac{\partial^3 u}{\partial y^3}-\frac{\partial u}{\partial y}\frac{\partial^2 u}{\partial x\partial y}\right] \end{aligned} \quad 4.9$$

$$u\frac{\partial H}{\partial x}+v\frac{\partial H}{\partial y}=-K_1\left(2H+\frac{\partial u}{\partial y}\right)+\left(1+\frac{K_1}{2}\right)\frac{\partial^2 H}{\partial y^2} \quad 4.10$$

The dimensionless governing equations are bounded to the following conditions:

$$\begin{aligned} &u=v=0,\ \ H=-\frac{1}{2}\frac{\partial u}{\partial y} \quad \text{at } y=0 \\ &u\to u_e(x),\ \ \frac{\partial u}{\partial y}\to 0,\ \ H\to 0 \ \ \text{as } y\to\infty \end{aligned} \quad 4.11$$

And the parameters that express the special characteristics of the flow in the governing equations can be defined as:

$$j=\frac{av}{U_\infty},\quad K=\frac{k_0U_\infty}{a\rho\nu},\quad K_1=\frac{\kappa}{\mu},\quad M=\frac{\sigma B_0^2 a}{\rho U_\infty} \quad 4.12$$

where K, K_1 and M, represent the dimensionless viscoelastic, micropolar and magnetic parameter, respectively. Then, the equations can be further simplified by reducing the dependence of some terms to a single variable instead of two. For this problem, the following set of non-similarity equations is introduced for the mentioned purpose:

$$\psi = xf(x,y),\quad H=xh(x,y) \quad 4.13$$

The non-dimensional stream function, ψ is defined as:

$$u=\frac{\partial\psi}{\partial y},\quad v=-\frac{\partial\psi}{\partial x} \tag{4.14}$$

and it satisfies the continuity equation in Equation (3.76). After the non-similarity variables are applied, the momentum and angular momentum equations in Equations (4.9) and (4.10) will be in the form below:

$$\begin{aligned}&(1+K_1)\frac{\partial^3 f}{\partial y^3}+f\frac{\partial^2 f}{\partial y^2}-\left(\frac{\partial f}{\partial y}\right)^2+\frac{\sin x\cos x}{x}+K_1\frac{\partial h}{\partial y}-M\left(\frac{\partial f}{\partial y}-\frac{\sin x}{x}\right)\sin^2\alpha\\&+K\left\{2\frac{\partial f}{\partial y}\frac{\partial^3 f}{\partial y^3}-f\frac{\partial^4 f}{\partial y^4}-\left(\frac{\partial^2 f}{\partial y^2}\right)^2+x\left(\begin{gathered}\frac{\partial^2 f}{\partial x\partial y}\frac{\partial^3 f}{\partial y^3}-\frac{\partial f}{\partial x}\frac{\partial^4 f}{\partial y^4}\\+\frac{\partial f}{\partial y}\frac{\partial^4 f}{\partial x\partial y^3}-\frac{\partial^2 f}{\partial y^2}\frac{\partial^3 f}{\partial x\partial y^2}\end{gathered}\right)\right\}\\&=x\left(\frac{\partial f}{\partial y}\frac{\partial^2 f}{\partial x\partial y}-\frac{\partial f}{\partial x}\frac{\partial^2 f}{\partial y^2}\right)\end{aligned} \tag{4.15}$$

and

$$\left(1+\frac{K_1}{2}\right)\frac{\partial^2 h}{\partial y^2}+f\frac{\partial h}{\partial y}-h\frac{\partial f}{\partial y}-K_1\left(2h+\frac{\partial^2 f}{\partial y^2}\right)=x\left(\frac{\partial f}{\partial y}\frac{\partial h}{\partial x}-\frac{\partial f}{\partial x}\frac{\partial h}{\partial y}\right) \tag{4.16}$$

Referring to Lukaszewicz (1999), the dimensionless quantity, n in the boundary condition is known as the coupling number which measures the ratio between microinertia and the angular viscosity of the fluid where $0\le n\le 1$. For micropolar fluid, microinertia explains the stress experienced by the microstructures in the fluid to rotate around its axis where higher microinertia indicates more resistance for the particles to change their speed during rotation. Both Lukaszewicz (1999) and Vijaya et al. (2016) mentioned that the case $n=0$ corresponds to Newtonian fluid where microinertia is negligible compared to the angular velocity or in simpler terms, the value describes fluid with miniscule to no microstructures. Meanwhile, $n=1$ defines micropolar fluid where the particles in the fluid and the micro-rotational vector are rotating harmoniously at the same angular velocity. As this behavior indicates that fluid does not oppose the rotation, this is a special case of polar fluid with the characteristics of Newtonian fluid that is unaffected by shear rate.

Due to these arguments, for all the problems in this study, the value $n = 1/2$ is chosen to describe the viscoelastic micropolar model that belongs to the non-Newtonian family. This value indicates that both microinertia and angular viscosity are present, hence implying that the rotation is opposed by the fluid which is consistent to the nature of non-Newtonian fluid. As a result, the boundary conditions of this problem in non-dimensionless form are:

$$\begin{aligned} & f = \frac{\partial f}{\partial y} = 0, \quad h = -\frac{1}{2}\frac{\partial^2 f}{\partial y^2} \quad \text{on } y = 0 \\ & \frac{\partial f}{\partial y} = \frac{\sin x}{x}, \quad \frac{\partial^2 f}{\partial y^2} = 0, \quad h = 0 \quad \text{as } y \to \infty \end{aligned} \tag{4.17}$$

Considering the flow near the lower stagnation point of the cylinder where $x \approx 0$, Equations (4.15) and (4.16) will reduce to the following ODEs

$$(1+K_1) f''' + ff'' - f'^2 + 1 + K_1 h' - M(f'-1)\sin^2\alpha + K\left(2f'f''' - f f^{iv} - f''^2\right) = 0 \tag{4.18}$$

$$\left(1+\frac{K_1}{2}\right)h'' + f h' - f' h - K_1\left(2h + f''\right) = 0 \tag{4.19}$$

bounded to the conditions below:

$$\begin{aligned} & f(0) = f'(0) = 0, \quad h(0) = -\frac{1}{2} f''(0) \\ & f' \to 1, \quad f'' \to 0, \quad h \to 0 \quad \text{as } y \to \infty \end{aligned} \tag{4.20}$$

where the derivatives are with respect to variable y. For this problem, the physical quantity of interest is the local skin friction coefficient, C_f. Following Nazar (2004), the coefficient is defined as:

$$C_f = \frac{\mathrm{Re}^{1/2}\,\tau_w}{\rho U_\infty^2} \qquad 4.21$$

and for viscoelastic micropolar fluid, the reduced skin friction parameter, τ_w is:

$$\tau_w = \left(\left(\mu + \frac{\kappa}{2}\right)\frac{\partial \bar{u}}{\partial \bar{y}} + \kappa \bar{H}\right)_{\bar{y}=0} + k_0\left(\bar{u}\,\frac{\partial^2 \bar{u}}{\partial \bar{x}\partial \bar{y}} + \bar{v}\,\frac{\partial^2 \bar{u}}{\partial \bar{y}^2} + 2\frac{\partial \bar{u}}{\partial \bar{x}}\frac{\partial \bar{u}}{\partial \bar{y}}\right)_{\bar{y}=0} \qquad 4.22$$

Substituting Equations (4.8), (4.12) and (4.22) into Equation (4.21), the non-dimensional skin friction coefficient is:

$$C_f = \left(1 + \frac{K_1}{2}\right) x f''(x,0) \qquad 4.23$$

4.3 Results and Discussion

The ordinary differential equations in Equations (4.18) and (4.19) bounded by the conditions stated in Equation (4.20) are solved using the Keller-box method by implementing the Fortran algorithm. The numerical results obtained are tabulated and the velocity and microrotation profiles as well as the local skin friction coefficient are graphically illustrated to examine the effects of viscoelastic parameter, K, micropolar parameter, K_1, magnetic parameter, M and the aligned angle, α on the fluid as it flows over the circular cylinder.

The limiting case of the problem without the influence of viscoelastic, material and magnetic parameter is compared to the exact and numerical solution from published results for affirmation of results reliability. Current results are compared to the exact solution by Ariel (2002) and numerical solution by Anwar et al. (2008). The momentum equation and boundary conditions for both studies are listed in Table 4.1 where the current study and the study by Anwar included an augmented boundary condition, $f''(\infty) = 0$ while Ariel took a different approach and discarded the extra condition at infinity. Both approaches have the advantages over the other as having the extra boundary conditions will make the results valid for even large values of K (Garg & Rajagopal,

1990) whilst Ariel's algorithm is applicable in finite domains by perceiving the stress condition at the wall. Despite the fact that Anwar's study is on convective boundary layer flow, the equation is reduced to the limiting case for forced convection when $\lambda = 0$.

From the result comparison displayed in Table 4.2, it is evident that the current result concurs with those from the literatures. Furthermore, the current result shows extremely small relative error with the exact solution as compared to the numerical solution from the viscoelastic model. It is noteworthy that the purpose of this error analysis is to validate the accuracy of the current result given that the exact solution is known. The relative error recorded in Table 4.3 is calculated by taking the ratio of the absolute discrepancy between the exact and numerical value obtained with respect to the exact value itself. It can be observed that the error values are extremely small and negligible in comparison to the existing model. From this evaluation, it is justified that the numerical result for this flow problem is reliable so further analysis on the velocity and microrotation profiles are conducted.

The velocity profile in Figure 4.2 shows that the increase of viscoelastic parameter value, K reduces the speed of the flow. Due to no-slip condition, velocity of fluid at the wall is zero and increases as it moves further from the wall until it reaches free stream outside the boundary layer region. Higher value of viscoelastic parameter implies greater elasticity effect that would oppose the flow and resist deformation. As a result, the velocity is reduced as it fails to increase rapidly near the wall. This outcome has also been observed by Nazemi et al. (2019) for his comparison study between viscoelastic and Newtonian fluid.

The same effect is also observed with the growth of material parameter, K_1 as presented in Figure 4.5 with similar explanation but different stimulus. As discussed in Section 1.1, micropolar fluid contains tiny spinning particles or microelements that rotate on their own axes, isolated from the fluid velocity at the wall. Similar to the viscoelasticity behaviour, the microrotation also creates additional defiance to deformation that create resistance to the change of velocity. On the account that higher micropolar parameter means higher micropolarity, fluid with higher parameter consists of particles with greater tendency to rotate independently of the fluid's bulk motion, hence building more resistance to deformation. These particles refuse to align with the fluid flow and keep spinning independently, obstructing the development of the velocity boundary layer and causing the velocity gradient to decrease.

On the contrary, Figure 4.8 reveals that the increase of magnetic parameter, M and α has a boosting effect on the flow, causing the velocity to rise. Even though this result seems to contradict the expected behaviour of velocity in micropolar fluid from the literatures as observed by Yasmin et al. (2020) that lean towards magnetic field has retarding effect on the velocity, it cannot be generalized this way for this problem as despite the micropolarity, this complex fluid is also viscoelastic in nature. It has been shown in studies that for viscoelastic fluid, the presence of magnetic field could either increase or decrease the velocity of the flow (Bhukta et al., 2014) (Mahat et al., 2022).

As for the microrotation profile, it only existed for micropolar fluid where it describes the angular velocity of the particles in terms of the magnitude and direction of the spin. Figures 4.3, 4.6 and 4.9 show a standard pattern occurring in all three figures where reversal behaviour can be observed once it reaches a turning point at $y \approx 1.68$. All profiles show negative values of microrotation velocity indicating that for this problem, the particles are going against the vorticity of the fluid flow by spinning at anti-clockwise direction.

In Figure 4.3, increasing K stimulates the spinning velocity when the flow is reasonably close to the cylinder surface, but as it approaches y_{∞}, the opposite effect is observed. The rise of parameter K_1 also displays the same behaviour as shown in Figure 4.6 where at relatively small values, the velocity increases but for $y > 0.8$, increase of K_1 leads to lower spin velocity. The initial increase and subsequent decrease in angular velocity with increasing K and K_1 values is likely due to enhanced particle rotation followed by increased fluid structure resistance. On the contrary, M and α effects depict the reversal behaviour from the previous two parameters for the microrotation profile as illustrated in Figure 4.9. For $y < 1.8$, the velocity declines synchronously but for $1.8 < y < \infty$, the opposite behaviour is detected where h increases when M and α gets larger. This could result from the force exerted by the magnetic field that tends to orient the microscopic components of the fluid in a particular direction which can affect the particles' rotation followed by magnetically induced circulation at higher field strengths.

Aside from the velocity and microrotation profiles, Figures 4.4, 4.7 and 4.10 further analyse the behavioural flow over the bluff body in terms of how the parameters could influence the body and flow separation. Figure 4.4 illustrates the skin friction coefficient at different points on the cylinder for variety of K values. From the figure, higher values of K will contribute towards lower C_f and as the parameter becomes larger, the undesirable boundary layer separation is stalled. This is because higher viscoelastic parameter means higher resistance and stronger attachment on the wall to delay the separation. The same result is recorded by Jones and Lewis (1968) that higher viscoelasticity moves the separation point towards the front stagnation point.

Similar effect is observed for M and α effects, where the induced magnetic field also delays the separation time as M and α grow, while C_f surges in value. It is also illustrated in Figure 4.10 that when M gets significantly large, α no longer affects the boundary layer separation where the separation will occur at the same point on the wall for any value of α. The effect of material parameter is presented in Figure 4.7. The figure reveals that when K_1 elevates, C_f increases, and contrary to the other parameters, the separation is inclined to occur in advance which would result in a wider wake region after the separation point.

For the case of viscoelastic effect, its nature that resists deformation leads to the above observations. The opposition to the flow as mentioned previously has led to the reduction of velocity gradient and simultaneously, the magnitude of viscous stresses. As a result, the skin friction decreases.

Table 4.1 The momentum equation and boundary conditions of problems involved for result validation.

Author	Model
Present	$(1+K_1)f''' + ff'' - f'^2 + 1 + K_1 h' - M(f'-1)\sin^2\alpha$ $+K\left(2f'f''' - f f^{iv} - f''^2\right) = 0$ with boundary conditions $f(0) = f'(0) = 0, \quad h(0) = -\frac{1}{2}f''(0)$ $f' \to 1, \quad f'' \to 0, \quad h \to 0 \quad \text{as} \quad y \to \infty$
Ariel (2002)	$f''' + ff'' + 1 - f'^2 - K\left(ff^{iv} - 2f'f''' + f''^2\right) = 0$ with boundary conditions $f(0) = 0, \quad f'(0) = 0, \quad f'(\infty) = 1$
Anwar et al. (2008)	$f''' + ff'' - f'^2 + 1 + \lambda\theta + K\left(2f'f''' - ff^{iv} - f''^2\right) = 0$ with boundary conditions $f(0) = f'(0) = 0, \quad \theta(0) = 1$ $f' \to 1, \quad f'' \to 0, \quad \theta \to 0 \quad \text{as} \quad y \to \infty$

Table 4.2 Values of $f''(0)$ at different values of K when $M = K_1 = 0$

K	**Exact solution Ariel (2002)**	**Present**	**Viscoelastic model Anwar et al (2008)**
0	1.232588	1.232657	-
0.05	1.179830	1.179893	-
0.1	1.134114	1.134172	1.135982
0.2	1.058131	1.058180	1.045412
0.3	0.996844	0.996886	0.960922
0.4	0.945869	0.945907	0.882512
0.5	0.902500	0.902535	0.810182
1	0.752766	0.752803	-
100	0.099515	0.100783	-
500	0.044677	0.045487	-
1000	0.031607	0.032229	-

Table 4.3 The percentage error between present model and another viscoelastic model compared to an exact solution

K	**Present**	**Viscoelastic model Anwar et al (2008)**
0.1	0.0058	0.1868
0.2	0.0049	1.2719
0.3	0.0042	3.5922
0.4	0.0038	6.3357
0.5	0.0035	9.2318

Table 4.4 Variation of $f''(0)$ for various values of K, K_1, M and α

K	K_1	M	α	$f''(0)$
1	1	1	$\pi/6$	0.750093
2	1	1	$\pi/6$	0.615378
3	1	1	$\pi/6$	0.535845
4	1	1	$\pi/6$	0.481519
5	1	1	$\pi/6$	0.441285
1	1.5	1	$\pi/6$	0.720308
1	2	1	$\pi/6$	0.693973
1	2.5	1	$\pi/6$	0.670474
1	3	1	$\pi/6$	0.649327
1	3.5	1	$\pi/6$	0.630153
1	1	0	$\pi/6$	0.691474
1	1	1.5	$\pi/6$	0.750093
1	1	3	$\pi/6$	0.854826
1	1	4.5	$\pi/6$	0.902423
1	1	6	$\pi/6$	0.990432
1	1	1	$\pi/4$	0.804255
1	1	1	$\pi/3$	0.854826
1	1	1	$\pi/2$	0.902423

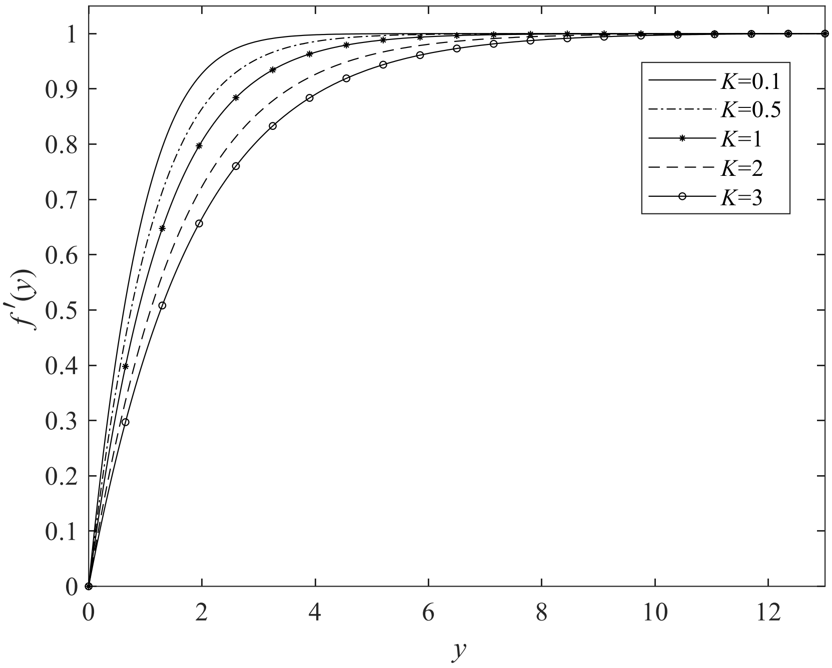

Figure 4.2 Variation of $f'(y)$ for various K at $K_1 = M = 1$ and $\alpha = \pi/6$

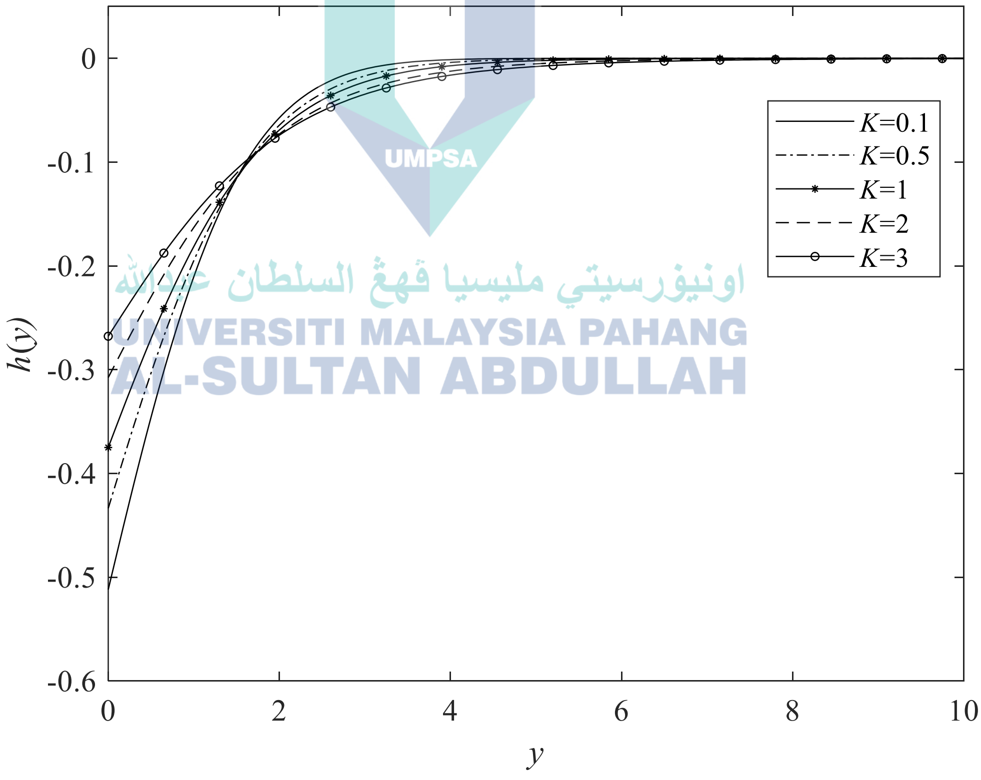

Figure 4.3 Variation of $h(y)$ for various K at $K_1 = M = 1$ and $\alpha = \pi/6$

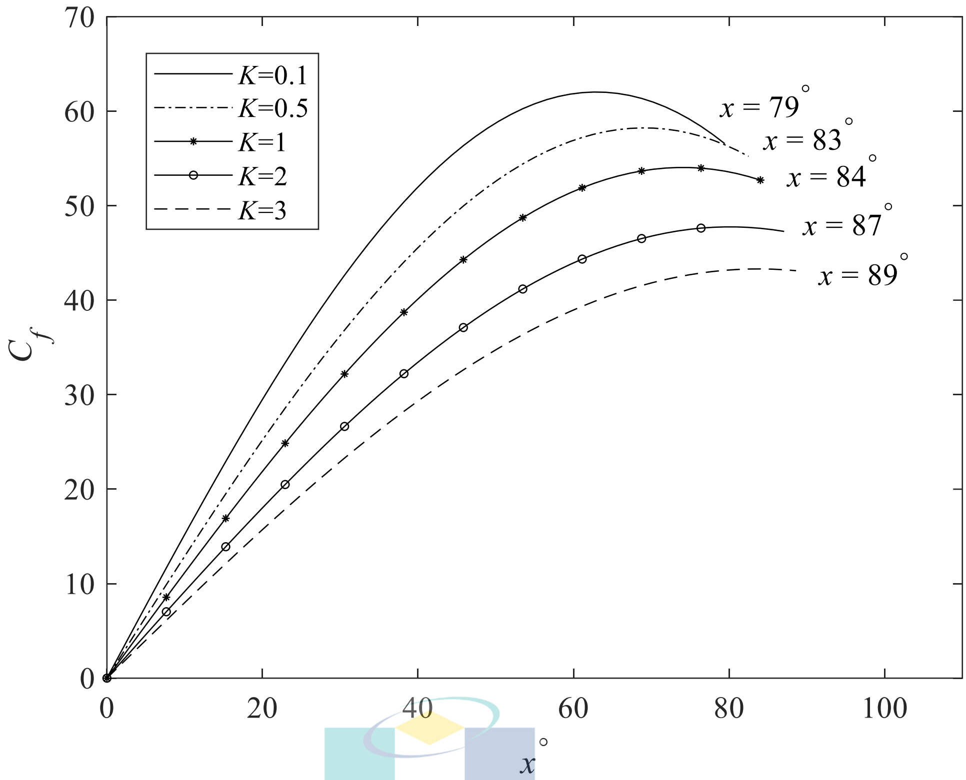

Figure 4.4 Variation of C_f for various K at $K_1 = M = 1$ and $\alpha = \pi/6$

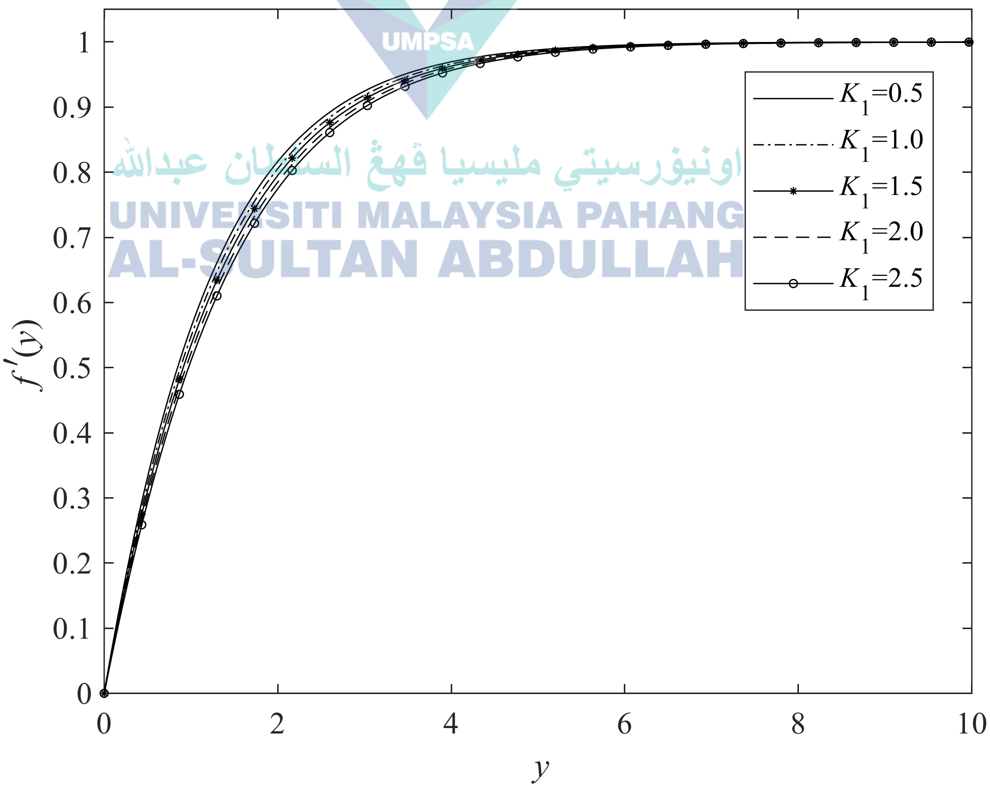

Figure 4.5 Variation of $f'(y)$ for various K_1 at $K = M = 1$ and $\alpha = \pi/6$

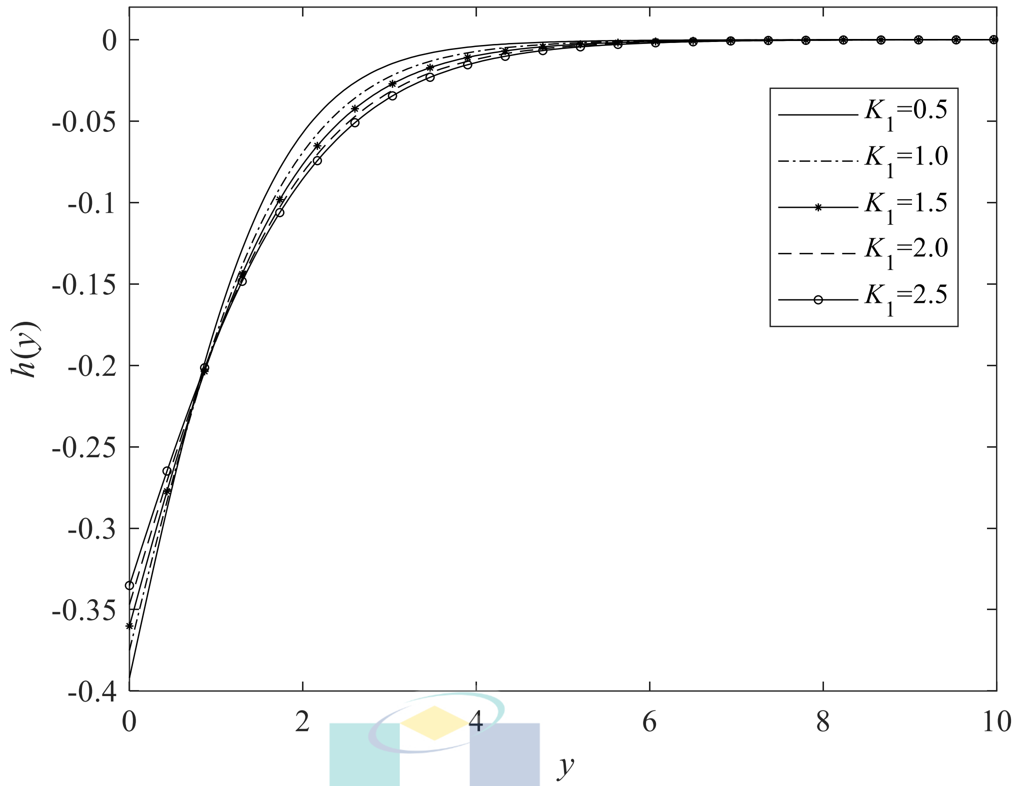

Figure 4.6 Variation of $h(y)$ for various K_1 at $K = M = 1$ and $\alpha = \pi/6$

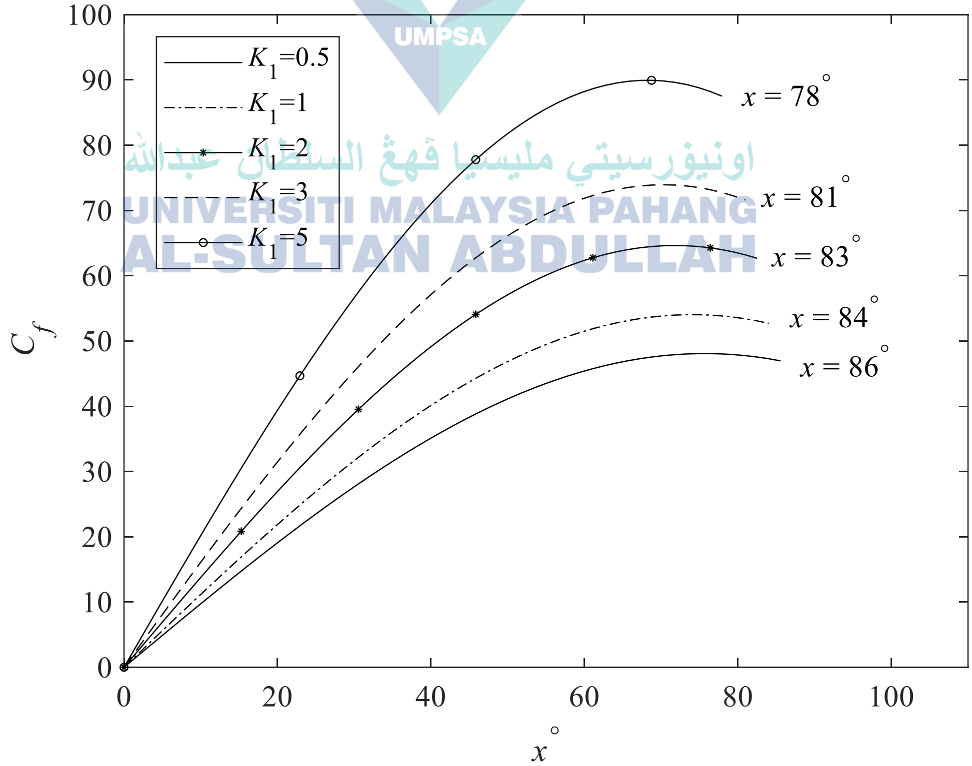

Figure 4.7 Variation of C_f for various K_1 at $K = M = 1$ and $\alpha = \pi/6$

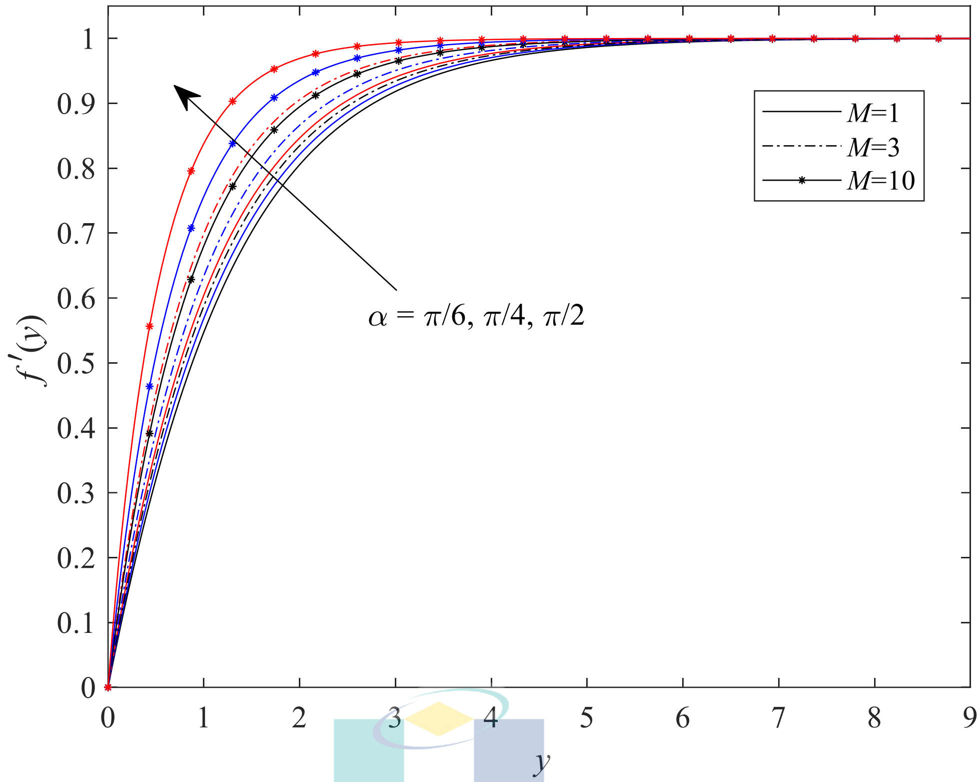

Figure 4.8 Variation of $f'(y)$ for various M and α at $K = K_1 = 1$

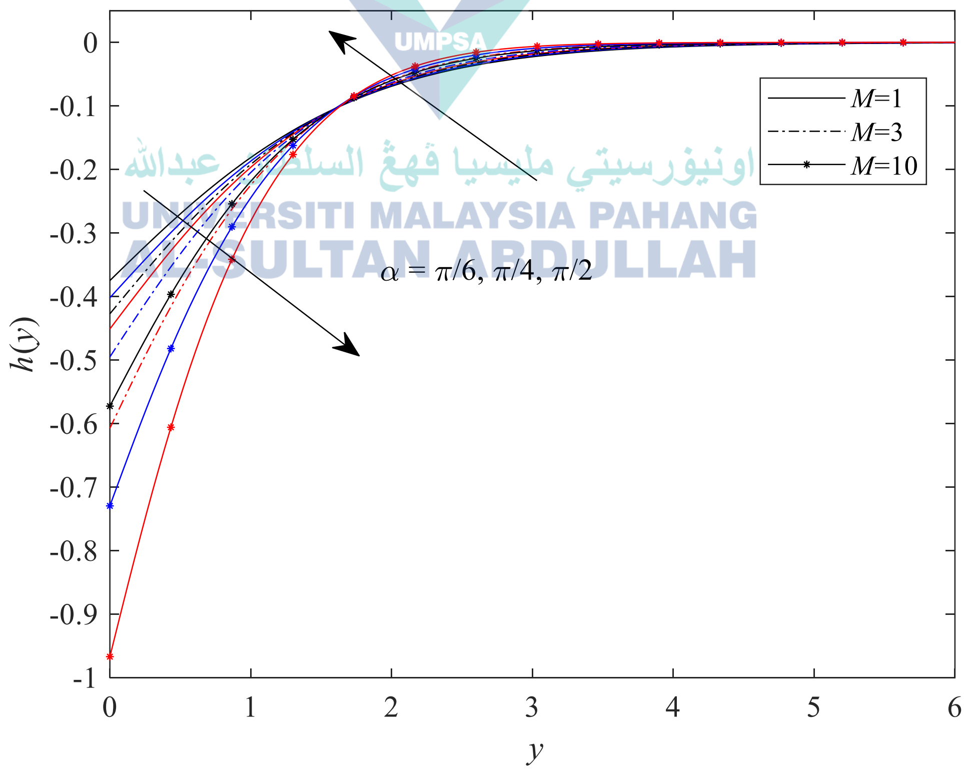

Figure 4.9 Variation of $h(y)$ for various M and α at $K = K_1 = 1$

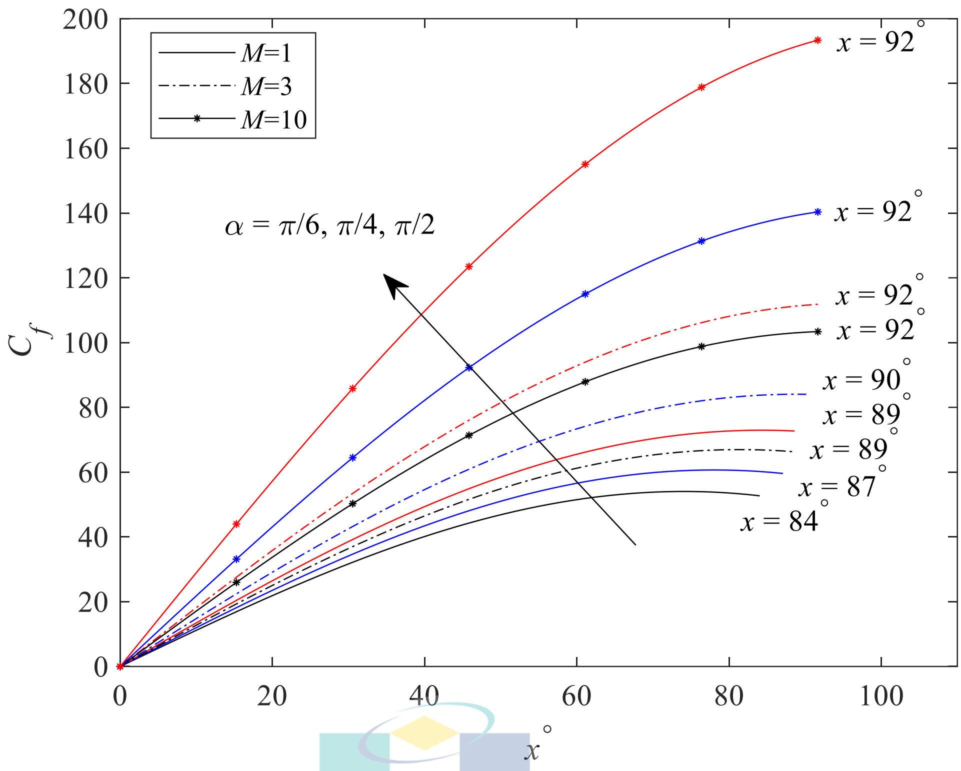

Figure 4.10 Variation of C_f for various M and α at $K = K_1 = 1$

4.4 Summary

In this chapter, the boundary layer flow of viscoelastic micropolar fluid over horizontal circular cylinder with aligned magnetic effect is discussed. The problem is solved numerically using the Keller-box method coded in Fortran programming language before the results are converted in graphical form in MATLAB software. The outline of all the steps involved for the mathematical formulation for this problem is presented in Table 4.6. The study of behavioral flow of the viscoelastic micropolar fluid will be further extended in Chapters 5 and 6 where free and mixed convections will be considered, respectively. The results presented in Section 4.3 can be summarized as follows:

i. Velocity profile decreases when K and K_1 increase, while the opposite trend is observed for M and α.

ii. Microrotation profile increases as K and K_1 increase for small values of y, but as y approaches infinity, h decreases. The reverse pattern is displayed by the microrotation profile when M and α get larger.

iii. The skin friction coefficient increases when K_1, M and α grow in value, but the opposite trend occurs when K increases. Boundary layer separation can be delayed by increasing K, M and α, as well as using smaller K_1.

Table 4.5 Summary of present results for boundary layer flow of viscoelastic micropolar on a circular cylinder

Distribution	$K\uparrow$	$K_1\uparrow$	$M\uparrow$	$\alpha\uparrow$
f'	$\downarrow$	$\downarrow$	$\uparrow$	$\uparrow$
h	$\uparrow\downarrow$	$\uparrow\downarrow$	$\downarrow\uparrow$	$\downarrow\uparrow$
C_f	$\downarrow$	$\uparrow$	$\uparrow$	$\uparrow$

$\uparrow$ increase $\downarrow$ decrease

Table 4.6 Solution procedure for mathematical formulation of boundary layer flow of viscoelastic micropolar fluid over horizontal circular cylinder

Steps	Equations
Governing Equations	$\frac{\partial u}{\partial x}+\frac{\partial v}{\partial y}=0$ $u\frac{\partial u}{\partial x}+v\frac{\partial u}{\partial y}=u_e\frac{du_e}{dx}(1+K_1)\frac{\partial^2 u}{\partial y^2}+K_1\frac{\partial H}{\partial y}-M\left(u-u_e\right)\sin^2\alpha_1$ $+K\left[\frac{\partial}{\partial x}\left(u\frac{\partial^2 u}{\partial y^2}\right)+v\frac{\partial^3 u}{\partial y^3}-\frac{\partial u}{\partial y}\frac{\partial^2 u}{\partial x\partial y}\right]$ $u\frac{\partial H}{\partial x}+v\frac{\partial H}{\partial y}=-K_1\left(2H+\frac{\partial u}{\partial y}\right)+\left(1+\frac{K_1}{2}\right)\frac{\partial^2 H}{\partial y^2}$
Boundary conditions	$u=v=0,\ H=-\frac{1}{2}\frac{\partial u}{\partial y}$ at $y=0$ $u\to u_e(x),\ \frac{\partial u}{\partial y}\to 0,\ H\to 0$ as $y\to\infty$
Non-similarity transformation	$\psi=xf(x,y),\quad H=xh(x,y)$
Ordinary differential equations	**At stagnation point:** $(1+K_1)f'''+ff''-f'^2+1+K_1h'-M\left(f'-1\right)\sin^2\alpha$ $+K\left(2f'f'''-f\,f^{iv}-f''^2\right)=0$ $\left(1+\frac{K_1}{2}\right)h''+f\,h'-f'h-K_1\left(2h+f''\right)=0$
Transformed boundary conditions	$f(0)=f'(0)=0,\ h(0)=-\frac{1}{2}f''(0)$ $f'\to 1,\quad f''\to 0,\quad h\to 0$ as $y\to\infty$

CHAPTER 5

FREE CONVECTION BOUNDARY LAYER FLOW OF VISCOELASTIC MICROPOLAR FLUID OVER A HORIZONTAL CIRCULAR CYLINDER WITH ALIGNED MHD EFFECT

5.1 Introduction

In this chapter, the free convection viscoelastic flow is taken into account with consideration of the influence of aligned magnetic field in the presence of microelements. Both the viscoelastic and micropolar properties are highlighted to describe the rheological behaviour of the fluid in this chapter, along with other parameters that have been discussed in Section 4.2 and 4.3. In the process of obtaining the numerical solutions, the steps include nondimensionalization and converting the governing equations into ordinary differential equation that will be shown in Section 5.2. The numerical solution is then presented and discussed in Section 5.3 before the concluding remarks in Section 5.4.

The two main references for this study are the free convection flow of viscoelastic fluid problem by Kasim et al. (2011) while another problem published by Nazar et al. (2002) concentrated on the free convection boundary layer flow over a circular cylinder immersed in micropolar fluid. Both studies were constructed around Merkin (1976) and Merkin and Pop (1988) where the complete solution of this problem was presented for the case of Newtonian fluid using a finite difference scheme. Most importantly, the results obtained had been validated to confirm the solidity of present model and numerical algorithm.

5.2 Mathematical Formulation

Free convection boundary layer flow of viscoelastic micropolar fluid over a horizontal circular cylinder with aligned magnetic field effect is investigated. The configuration considered for this problem is illustrated in Figure 5.1.

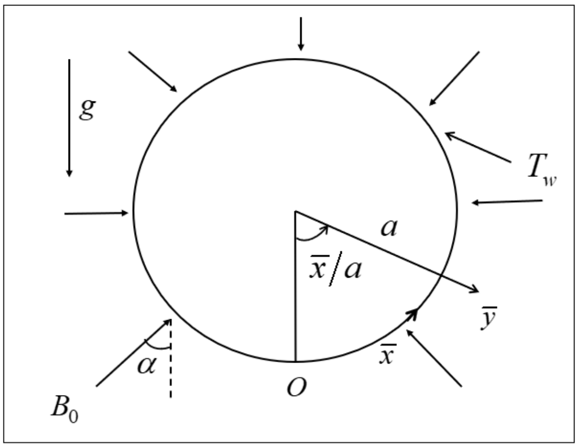

Figure 5.1 Schematic diagram for mixed convection boundary layer flow of viscoelastic micropolar fluid over a circular cylinder

The governing equations that represent the conservation of mass and angular momentum for the flow had been expressed in Equations (4.1) and (4.2), while the energy equation had been stated in Equation (3.79). The dimensional momentum equation, unique for this problem is in the form below:

$$\bar{u}\frac{\partial \bar{u}}{\partial \bar{x}}+\bar{v}\frac{\partial \bar{u}}{\partial \bar{y}}=\left(\frac{\mu+\kappa}{\rho}\right)\frac{\partial^2 \bar{u}}{\partial \bar{y}^2}+\frac{k_0}{\rho}\left[\frac{\partial}{\partial \bar{x}}\left(\bar{u}\frac{\partial^2 \bar{u}}{\partial \bar{y}^2}\right)+\bar{v}\frac{\partial^3 \bar{u}}{\partial \bar{y}^3}-\frac{\partial \bar{u}}{\partial \bar{y}}\frac{\partial^2 \bar{u}}{\partial \bar{x}\partial \bar{y}}\right]$$
$$+g\beta(T-T_\infty)\sin\left(\frac{\bar{x}}{a}\right)+\frac{\kappa}{\rho}\frac{\partial \bar{H}}{\partial \bar{y}}-\frac{\sigma}{\rho}\bar{u}B_0^2\sin^2\alpha \qquad 5.1$$

subject to the boundary conditions:

$$\bar{u}=\bar{v}=0,\ T=T_w,\ \bar{H}=-\frac{1}{2}\frac{\partial \bar{u}}{\partial \bar{y}} \quad \text{on } \bar{y}=0$$
$$\bar{u}\to 0,\ \frac{\partial \bar{u}}{\partial \bar{y}}\to 0,\ T\to T_\infty,\ \bar{H}\to 0 \quad \text{as } \bar{y}\to\infty \qquad 5.2$$

As proposed by Nazar (2004) and Mahat et al. (2021), the following variables are integrated into the equations to remove the physical dimensions while supplementarily, reducing the complexity of the model.

$$x=\frac{\bar{x}}{a},\ y=\frac{Gr^{1/4}\bar{y}}{a},\ u=\frac{aGr^{-1/2}\bar{u}}{\nu},\ v=\frac{aGr^{-1/4}\bar{v}}{\nu},\ H=\frac{a^2Gr^{-3/4}\bar{H}}{\nu},\ \theta=\frac{T-T_\infty}{T_w-T_\infty} \qquad 5.3$$

The outcomes of nondimensionalization for continuity and angular momentum equations are as stated in Equations (3.76) and (4.10), while the momentum and energy equations are as follows:

$$\begin{aligned}u\frac{\partial u}{\partial x}+v\frac{\partial u}{\partial y}&=\left(1+K_1\right)\frac{\partial^2 u}{\partial y^2}+K\left[\frac{\partial}{\partial x}\left(u\frac{\partial^2 u}{\partial y^2}\right)+v\frac{\partial^3 u}{\partial y^3}-\frac{\partial u}{\partial y}\frac{\partial^2 u}{\partial x\partial y}\right]\\&+\theta\sin x+K_1\frac{\partial H}{\partial y}-Mu\sin^2\alpha\end{aligned} \qquad 5.4$$

$$u\frac{\partial\theta}{\partial x}+v\frac{\partial\theta}{\partial y}=\frac{1}{\Pr}\frac{\partial^2\theta}{\partial y^2} \qquad 5.5$$

The governing equations are bounded by:

$$\begin{aligned}&u=v=0,\ \theta=1,\ H=-\frac{1}{2}\frac{\partial u}{\partial y}\ \text{ on }\ y=0\\&u\to 0,\ \frac{\partial u}{\partial y}\to 0,\ \theta\to 0,\ H\to 0\ \text{as}\ y\to\infty\end{aligned} \qquad 5.6$$

where the parameters in the equations are defined as:

$$j=a^2\mathrm{Gr}^{-1/2},\quad K=\frac{k_0\mathrm{Gr}^{1/2}}{a^2\rho},\quad K_1=\frac{\kappa}{\mu},\quad \mathrm{Gr}=\frac{g\beta\left(T_w-T_\infty\right)a^3}{\nu^2},\quad M=\frac{\sigma B_0{}^2a^2}{\rho\mathrm{Gr}^{1/2}\nu} \qquad 5.7$$

Subsequently, the identical stream function as in Equations (4.13) and (4.14) are introduced to the equations with an additional function for the energy equation in the form:

$$\theta=\theta(x,y) \qquad 5.8$$

As a result, the angular momentum equation is transformed into Equation (4.16) and the following is the new form of the momentum and energy equations.

$$
\left(1+K_1\right)\frac{\partial^3 f}{\partial y^3}+f\frac{\partial^2 f}{\partial y^2}-\left(\frac{\partial f}{\partial y}\right)^2+\frac{\sin x}{x}\theta+K_1\frac{\partial g}{\partial y}-M\frac{\partial f}{\partial y}\sin^2\alpha
$$

$$
+K\left\{2\frac{\partial f}{\partial y}\frac{\partial^3 f}{\partial y^3}-f\frac{\partial^4 f}{\partial y^4}-\left(\frac{\partial^2 f}{\partial y^2}\right)^2+x\left(\frac{\partial^2 f}{\partial x\partial y}\frac{\partial^3 f}{\partial y^3}-\frac{\partial f}{\partial x}\frac{\partial^4 f}{\partial y^4}+\frac{\partial f}{\partial y}\frac{\partial^4 f}{\partial x\partial y^3}-\frac{\partial^2 f}{\partial y^2}\frac{\partial^3 f}{\partial x\partial y^2}\right)\right\} \quad 5.9
$$

$$
=x\left(\frac{\partial f}{\partial y}\frac{\partial^2 f}{\partial x\partial y}-\frac{\partial f}{\partial x}\frac{\partial^2 f}{\partial y^2}\right)
$$

$$
\frac{1}{\Pr}\frac{\partial^2\theta}{\partial y^2}+f\frac{\partial\theta}{\partial y}=x\left(\frac{\partial f}{\partial y}\frac{\partial\theta}{\partial x}-\frac{\partial f}{\partial x}\frac{\partial\theta}{\partial y}\right) \quad 5.10
$$

These equations are subjected to the boundary conditions:

$$
\begin{aligned}
&f=\frac{\partial f}{\partial y}=0,\quad \theta=1,\ h=-\frac{1}{2}\frac{\partial^2 f}{\partial y^2}\quad \text{on}\quad y=0\\
&\frac{\partial f}{\partial y}\to 0,\quad \frac{\partial^2 f}{\partial y^2}\to 0,\quad \theta\to 0,\quad h\to 0\quad \text{as}\quad y\to\infty
\end{aligned} \quad 5.11
$$

Near the lower stagnation point of the cylinder, where $x\approx 0$, the angular momentum equation is reduced to Equation (4.19) while the momentum and energy equation become:

$$
\left(1+K_1\right)f'''+ff''-f'^2+1+\theta+K_1h'-Mf'\sin^2\alpha+K\left(2f'f'''-ff^{iv}-f''^2\right)=0 \quad 5.12
$$

$$
\frac{1}{\Pr}\theta''+f\,\theta'=0 \quad 5.13
$$

bounded to the following conditions:

$$
\begin{aligned}
&f(0)=f'(0)=0,\ \theta(0)=1,\ h(0)=-\frac{1}{2}f''(0)\\
&f'\to 0,\ f''\to 0,\ \theta\to 0,\ h\to 0,\ \text{as}\ y\to\infty
\end{aligned} \quad 5.14
$$

In this problem, the physical quantities of interest are the reduced skin friction coefficient, C_f and the heat transfer coefficient, Q_w. Whilst the dimensionless skin friction coefficient remains the same as the previous problem as stated in Equation (4.24), the dimensionless heat transfer coefficient, according to Kasim et al. (2011) is:

$$Q_w = -\theta'(x,0) \tag{5.15}$$

5.3 Results and Discussion

The ODE in Equations (5.12), (5.13) and (4.19), with the boundary conditions in (5.14) along with the PDE in Equations (5.9), (5.10) and (4.16) are solved using the Keller-box method coded in Fortran language and the numerical results are calculated. For this problem, all parameters that contribute towards the flow behaviour as expressed in the finalized equations are investigated. The effect of the physical parameters on velocity, temperature and microrotation profiles are evaluated with also special interest on their influence on the local skin friction coefficient, C_f and heat transfer coefficient, Q_w.

For validation purposes, results for the limiting case of this study are compared to the results documented by Merkin (1976), Molla et al. (2006) and Yasin et al. (2020). These studies have demonstrated the effects of free convective flow at the boundary layer of circular cylinder restricted by the same boundary conditions. In his study, Molla (2006) even justified his results using two different numerical methods, which are the Keller-box method and perturbation solution technique. The momentum equation from the governing equations of each problem is displayed in Table 5.1, while the result comparability is recorded in Tables 5.2 and 5.3. Present result shows high degree of similarity of $xf''(0)$ and $-\theta'(0)$ values to the above-mentioned studies as demonstrated in Figures 5.2 and 5.3. From both figures, it can be observed that all the markers that represent the values from different studies are overlapping, and they fall exactly on the line that represents the value from the current result. Hence, the figures have further justified the validity of the result from this study before further analysis.

The results of C_f and Q_w as the parameter values which varied at $\Pr = 21$ are presented in Table 5.4. This particular Prandtl number is applied throughout this study since according to Saeed et al. (2021), the dimensionless number represents pure human blood, that as aforementioned in Section 1.7, is a classic example of viscoelastic micropolar fluid. The table presents the distributions of heat transfer coefficients and local skin friction of the fluid on the circular cylinder's surface. The results are intended to provide insight into the behaviour of the viscoelastic micropolar fluid prior to the illustrative figures in which the figures depict the results.

The effect of increasing the value of K when other parameters are held constant is visualized in Figure 5.4 where the velocity of the fluid flow declines and then rises as the parameter is amplified. Similar effect is observed in Figure 5.9 that as K_1 rises, f' declines but as the flow moves further away from the wall and the momentum boundary layer thickness elevates, trend reversal is detected. Meanwhile, from Figures 5.6 and 5.11, it is evident that both parameters, K and K_1 intensify the microrotation profile, but the profile decreases at higher K and K_1 towards the free stream. This suggests that both viscoelasticity and micropolar properties enhance the rotational motion of fluid particles at the boundary layer. However, at higher values of both parameters, this effect diminishes towards the free stream, possibly as bulk flow effects begin to dominate over boundary interactions.

The temperature profiles for a range of values for K and K_1 also exhibit identical behaviour where Figures 5.5 and 5.10 show positive correlation between both parameters and the temperature. Viscoelasticity and temperatures are strongly related as the property itself is related to the time taken for molecular arrangement to occur inside the matter due to stress application. When the body undergoes deformation, a fraction of the total work is dissipated as heat through viscous losses but the remnant of the deformational energy is stored in elastic form Tschoegl (1989).

As for the trend of Q_w in Figure 5.7, it is apparent that higher K would reduce the amount of heat transfer but before boundary layer separation, which occurs in advance for lower value of K, the backward pattern is observed. The exact behavioural pattern is revealed in Figure 5.8 for C_f where the trend is explainable by the viscoelastic nature of the fluid that has the efficiency to reduce the frictional force between the body surface and the fluid. For the K_1 parameter, Figures 5.12 and 5.13 indicate that the parameter tends to enhance C_f but minimize Q_w on the surface and the separation for both quantities occurred faster as K_1 gets larger. These observations infer that the number of micro particles in the flow undeniably has significant impact on the physical quantities.

It has also been verified by Figures 5.14 and 5.15 that parameters M and α do hold substantial effect on the velocity and temperature of the flow. The velocity is suspended with the rise of M value, but the opposite effect is observed for temperature. The result also gives credence to the notion that different values of α will produce magnetic field with diversity of strength stemmed on its position on the flow region. For this problem, the increase of α value seems to enhance the effect of M thus broadening the Lorentz force on the surface of the cylinder. As a result, the force resists the movement of the fluid flow and its temperature increases.

For the microrotation profile in Figure 5.16, it is revealed that there exists positive relationship between M and the microrotation profile before the turning point. Furthermore, the microrotation is maximized when the magnetic field lines are perpendicular to the fluid flow. On the contrary, for Q_w and C_f, their values depleted when the angle expands from 0 to $\pi/2$. As for the magnetic effect, intensifying M also decreases Q_w and C_f These trends are illustrated in Figures 5.17 and 5.18. Overall, these results manifested that both parameters, M and α are correlated and can serve as limiting quantity for each other when either one is held constant.

Table 5.1 The momentum equation and boundary conditions of problems involved for result validation.

Author	Model
Present	$(1+K_1)f''' + ff'' - f'^2 + 1 + \theta + K_1 h' - Mf'\sin^2\alpha$ $+K\left(2f'f''' - ff^{iv} - f''^2\right) = 0$ with boundary conditions $f(0) = f'(0) = 0,\ \theta(0) = 1,\ h(0) = -\frac{1}{2}f''(0)$ $f' \to 0,\ f'' \to 0,\ \theta \to 0,\ h \to 0,\ \text{as } y \to \infty$
Merkin (1976)	$f''' + ff'' - f'^2 + \theta = 0$ with boundary conditions $f(0) = f'(0) = 0,\ \theta(0) = 1$ $f' \to 0,\ \theta \to 0,\ \text{as } y \to \infty$
Molla et al (2006)	$f''' + ff'' - f'^2 + \theta = 0$ with boundary conditions $f(0) = f'(0) = 0,\ \theta(0) = 1$ $f' \to 0,\ \theta \to 0,\ \text{as } y \to \infty$
Yasin et al (2020)	$\frac{1}{(1-\phi)^{2.5}\left[1-\phi+(\phi\rho_s)/(\rho_f)\right]}f''' + f\,f'' - f'^2 + \frac{(1-\phi)\rho_f + \phi(\rho\beta)_s/\beta_f}{(1-\phi)\rho_f + \phi\rho_s}\theta$ $-\frac{\sigma_{ff}/\sigma_f}{(1-\phi)+\phi(\rho_s/\rho_f)}Mf' = 0$ with boundary conditions $f(0) = f'(0) = 0,\ \theta(0) = 1$ $f' \to 0,\ \theta \to 0,\ \text{as } y \to \infty$

Table 5.2 Comparative values of skin friction coefficient $xf''(0)$ at different values of x when $\Pr = 1$

x	Merkin (1976)	Molla et al (2006)		Yasin et al (2020)	Present
		Finite difference	Series		
0	0.0000	0.0000	0.0000	0.0000	0.0000
$\pi/6$	0.4151	0.4145	0.4144	0.4121	0.4149
$\pi/3$	0.7558	0.7539	0.7544	0.7538	0.7549
$\pi/2$	0.9579	0.9541	0.9550	0.9563	0.9583
$2\pi/3$	0.9756	0.9696	0.9701	0.9743	0.9755
$5\pi/6$	0.7822	0.7739	0.7824	0.7813	0.7809

Table 5.3 Comparative values of $-\theta'(0)$ at different values of x when $\Pr = 1$

x	Merkin (1976)	Molla et al (2006)		Yasin et al (2020)	Present
		Finite difference	Series		
0	0.4214	0.4241	0.4216	0.4214	0.4214
$\pi/6$	0.4161	0.4161	0.4164	0.4163	0.4162
$\pi/3$	0.4007	0.4005	0.4009	0.4008	0.4007
$\pi/2$	0.3745	0.3740	0.3751	0.3744	0.3747
$2\pi/3$	0.3364	0.3355	0.3389	0.3364	0.3363
$5\pi/6$	0.2825	0.2812	0.2923	0.2824	0.2821

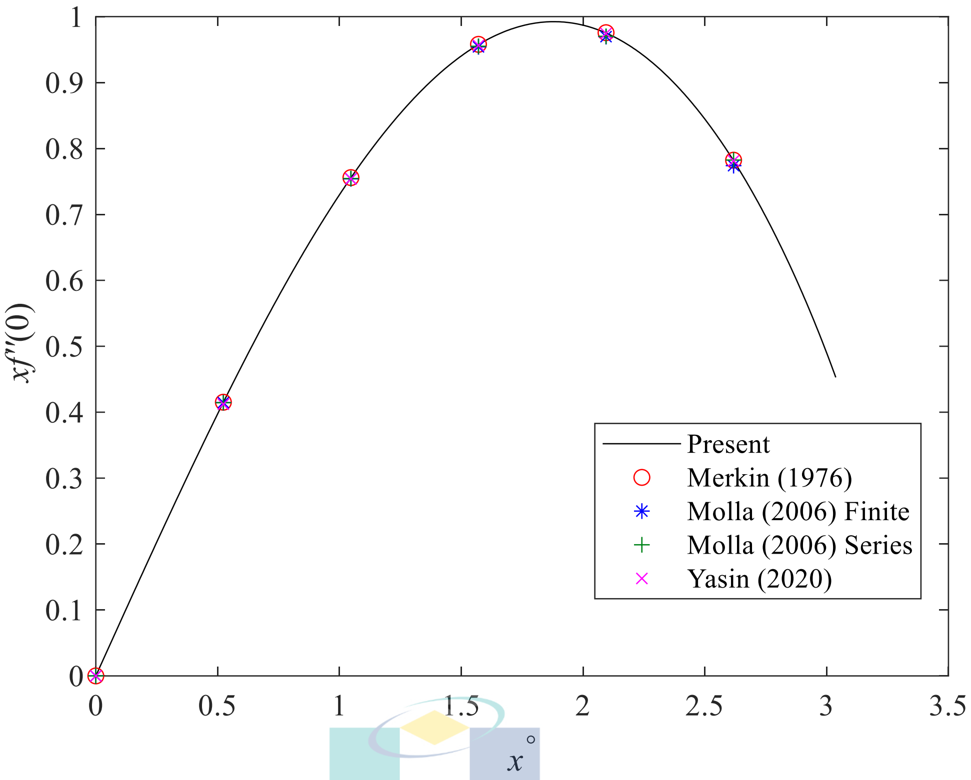

Figure 5.2 Comparative values of $xf''(0)$ at different values of x when $\Pr = 1$

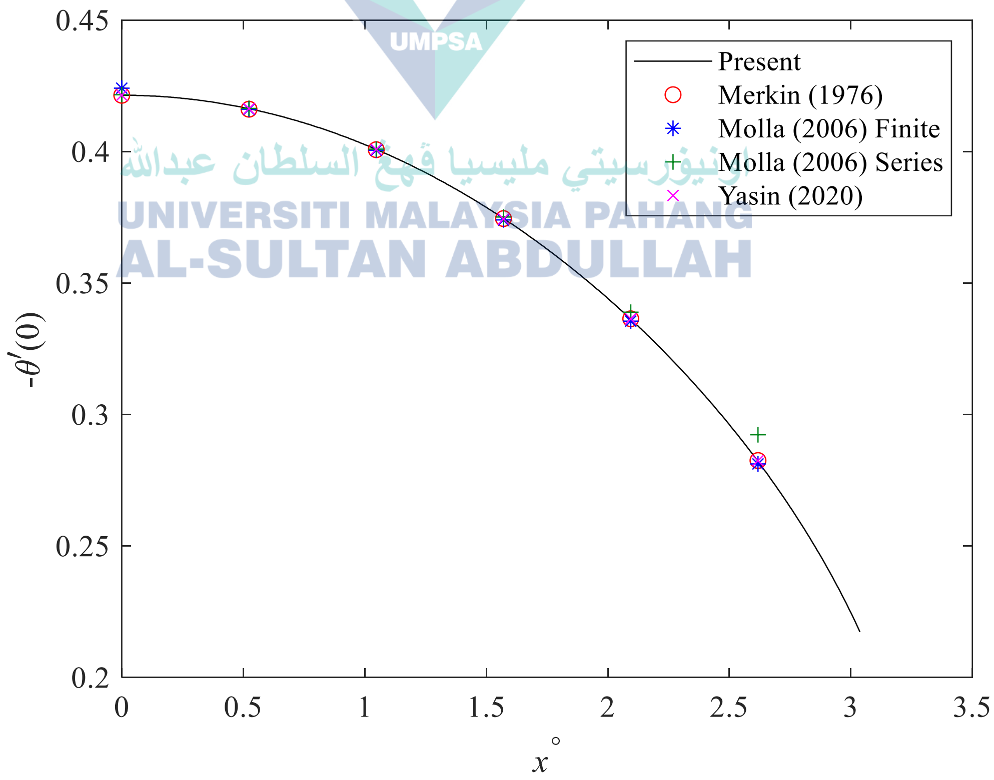

Figure 5.3 Comparative values of $-\theta'(0)$ at different values of x when $\Pr = 1$

Table 5.4 Variation of C_f and Q_w for various values of K, K_1, M and α for $\Pr = 21$ at $x = \pi/2$

K	**K1**	**M**	**α**	C_f	Q_w
1	1	1	$\pi/6$	0.513783	0.821961
2	1	1	$\pi/6$	0.490497	0.807547
3	1	1	$\pi/6$	0.469973	0.794194
4	1	1	$\pi/6$	0.452023	0.782125
5	1	1	$\pi/6$	0.436233	0.771238
1	1.5	1	$\pi/6$	0.539834	0.798068
1	2	1	$\pi/6$	0.563746	0.777162
1	2.5	1	$\pi/6$	0.585650	0.758645
1	3	1	$\pi/6$	0.605792	0.742075
1	3.5	1	$\pi/6$	0.624423	0.727116
1	1	0	$\pi/6$	0.541666	0.854099
1	1	1.5	$\pi/6$	0.513783	0.821961
1	1	3	$\pi/6$	0.477542	0.778424
1	1	4.5	$\pi/6$	0.463968	0.761661
1	1	6	$\pi/6$	0.441518	0.733355
1	1	1	$\pi/4$	0.493622	0.797958
1	1	1	$\pi/3$	0.477542	0.778424
1	1	1	$\pi/2$	0.463968	0.761661

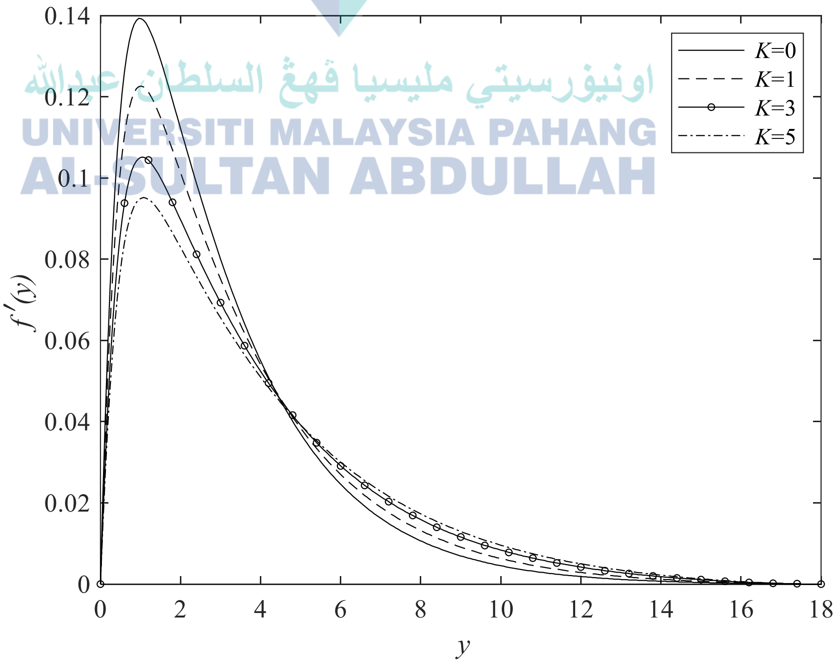

Figure 5.4 Variation of $f'(y)$ for various values of K at $K_1 = M = 0.5$ and $\alpha = \pi/6$

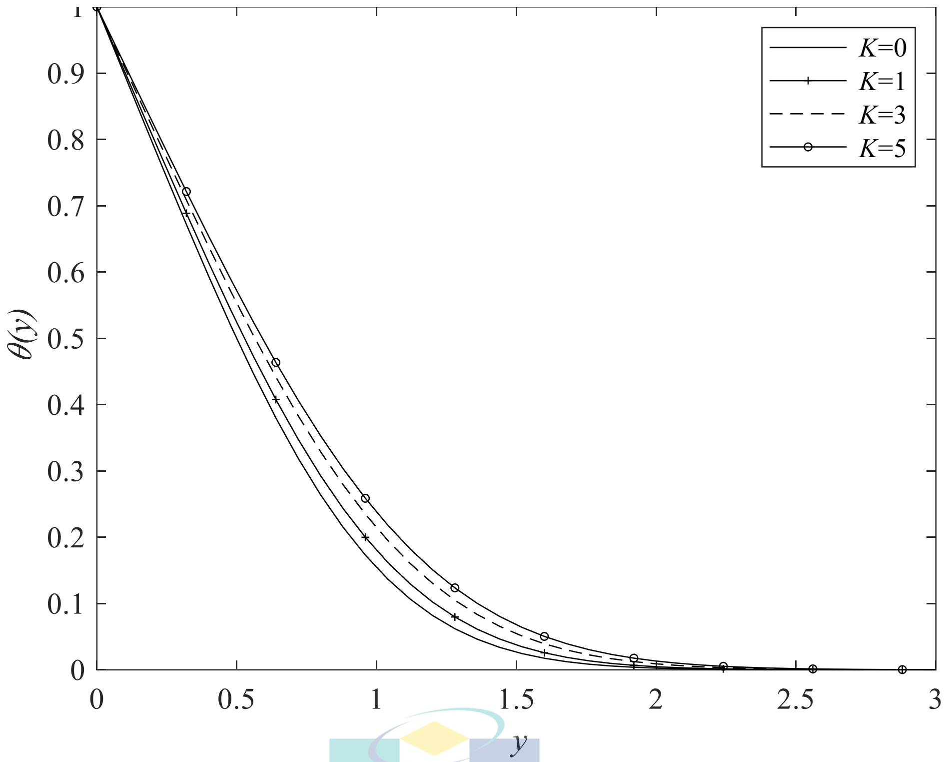

Figure 5.5 Variation of $\theta(y)$ for various values of K at $K_1 = M = 0.5$ and $\alpha = \pi/6$

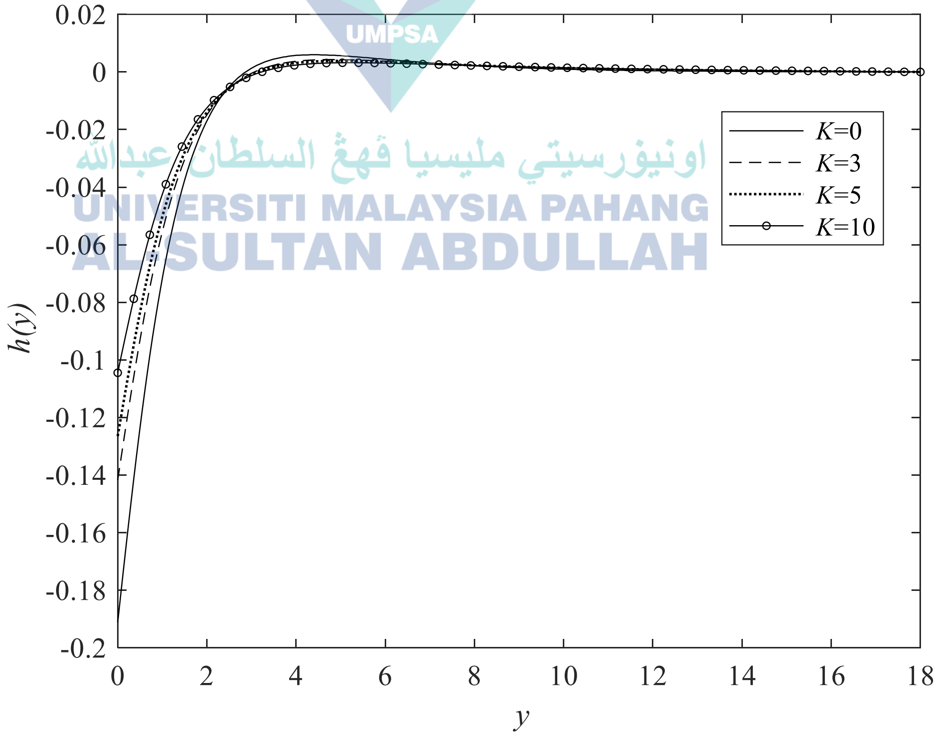

Figure 5.6 Variation of $h(y)$ at various values of K at $K_1 = M = 0.5$ and $\alpha = \pi/6$

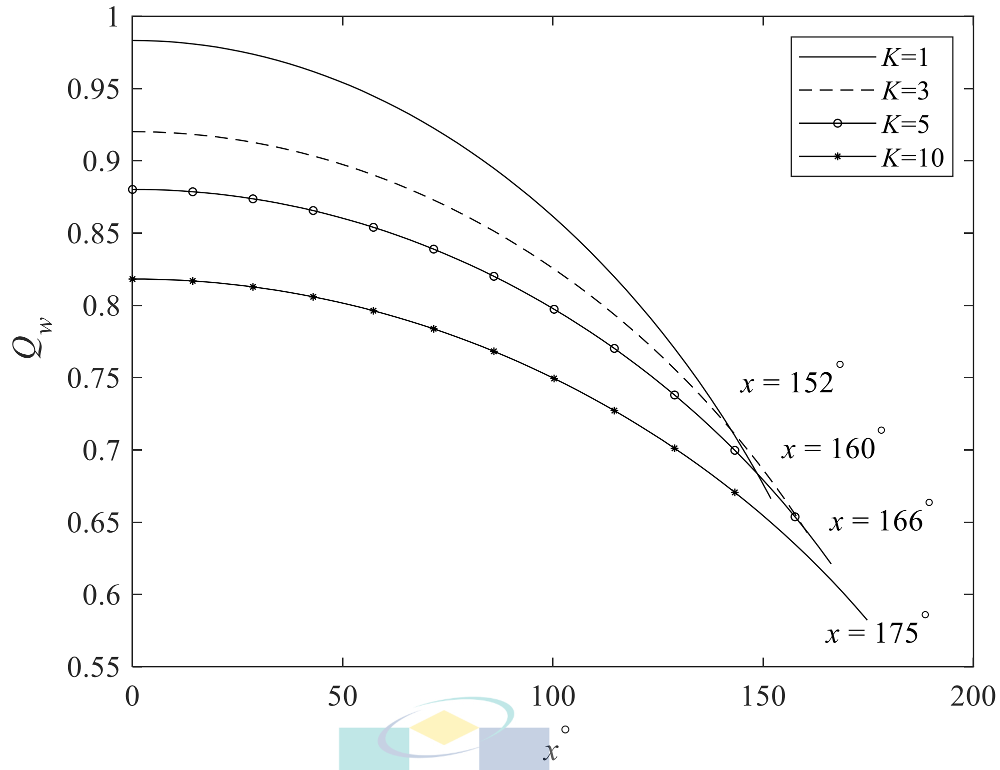

Figure 5.7 Variation of Q_w for various values of K at $K_1 = M = 0.5$ and $\alpha = \pi/6$

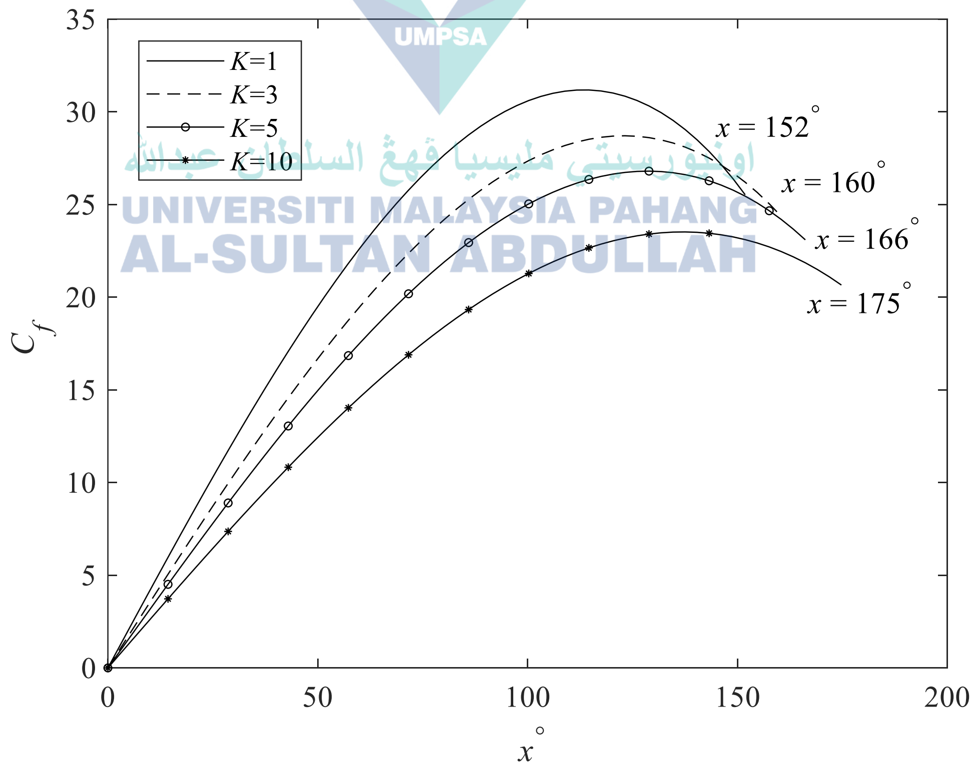

Figure 5.8 Variation of C_f for various values of K at $K_1 = M = 0.5$ and $\alpha = \pi/6$

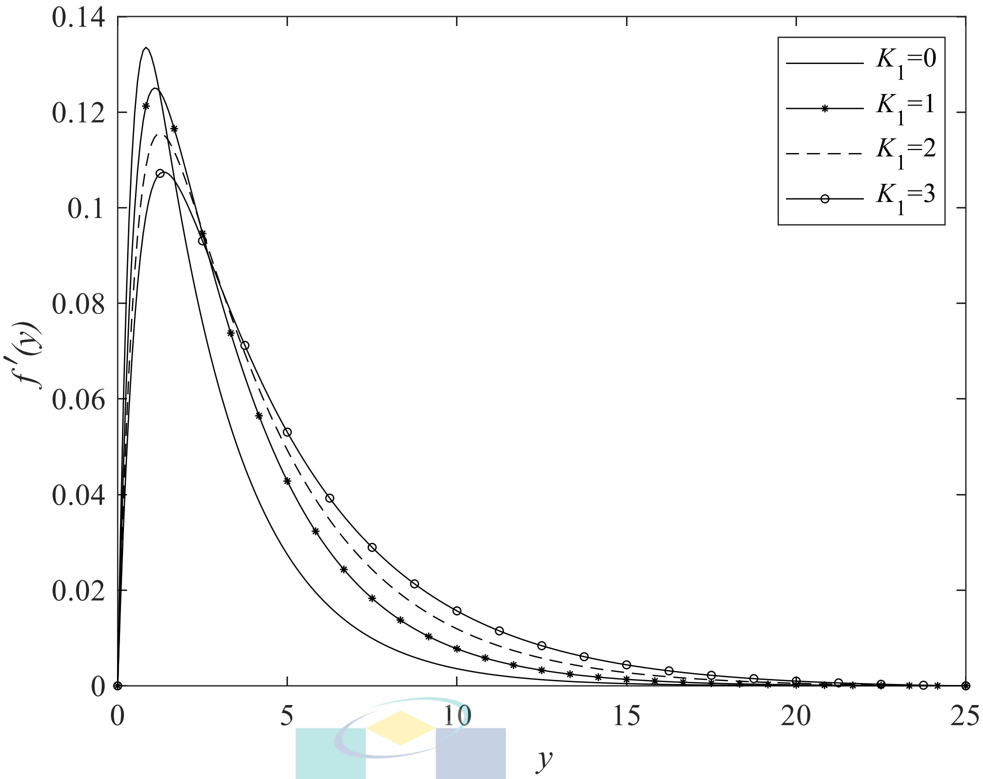

Figure 5.9 Variation of $f'(y)$ for various values of K_1 at $K = M = 0.5$ and $\alpha = \pi/6$

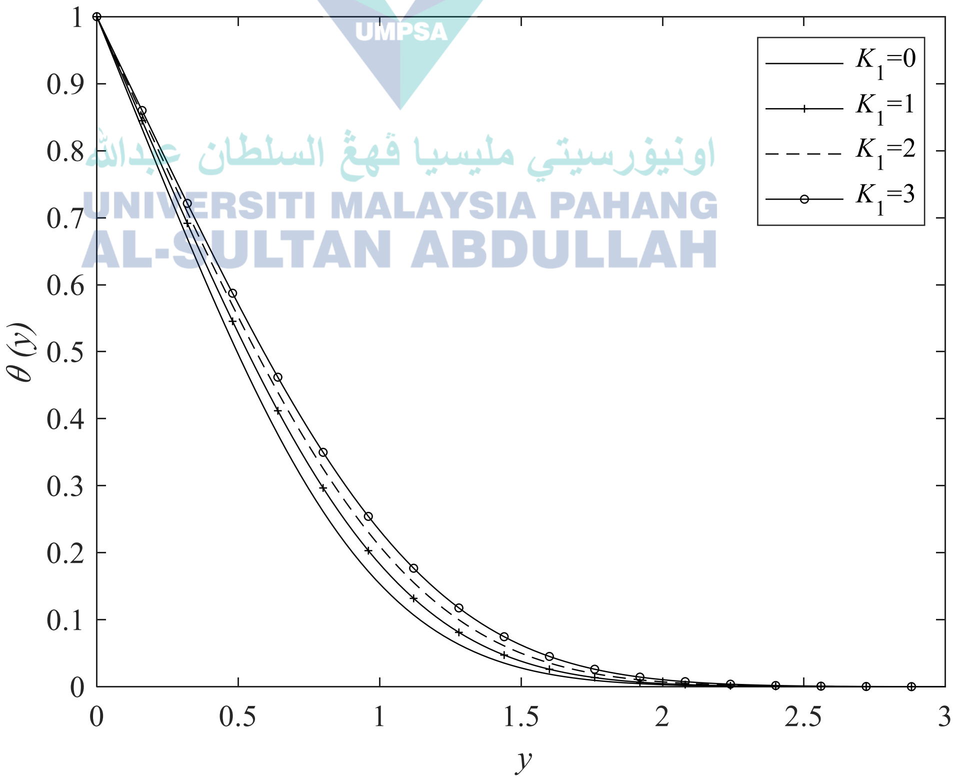

Figure 5.10 Variation of $\theta(y)$ for various values of K_1 at $K = M = 0.5$ and $\alpha = \pi/6$

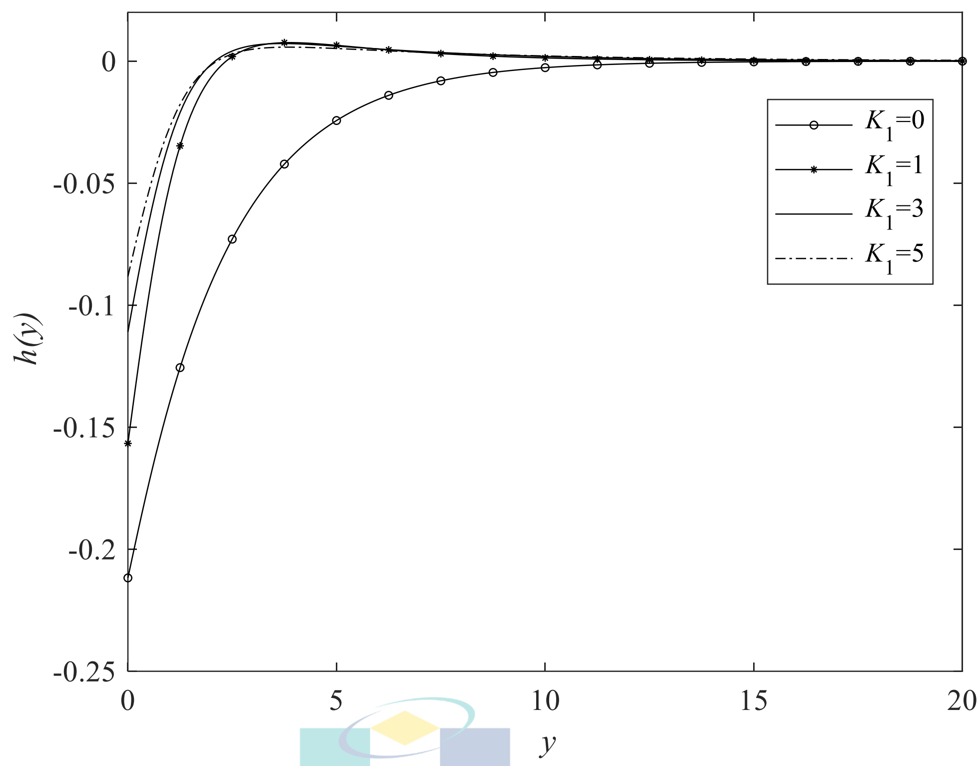

Figure 5.11 Variation of $h(y)$ at various values of K_1 at $K = M = 0.5$ and $\alpha = \pi/6$

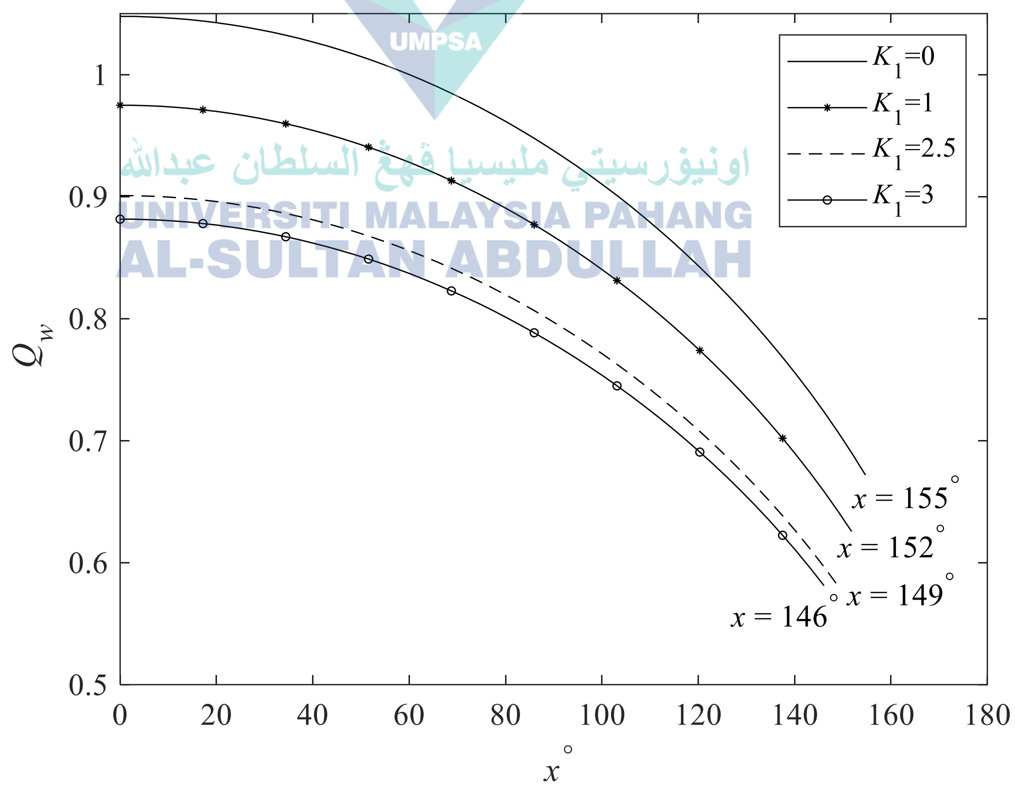

Figure 5.12 Variation of Q_w for various values of K_1 at $K = M = 0.5$ and $\alpha = \pi/6$

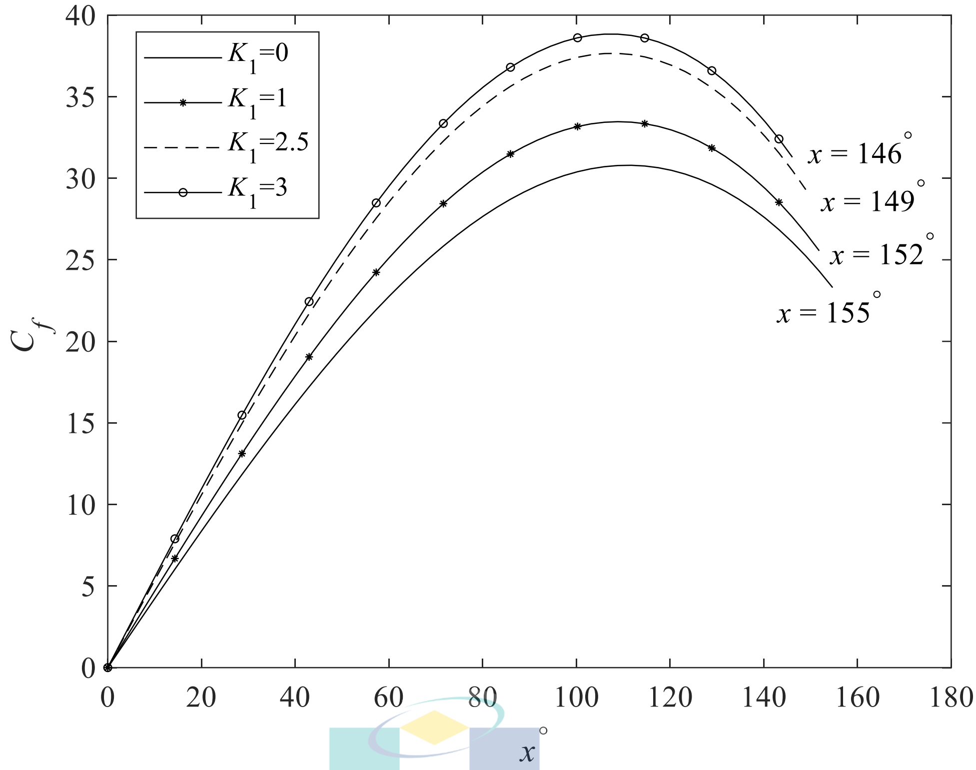

Figure 5.13 Variation of C_f for various values of K_1 at $K = M = 0.5$ and $\alpha = \pi/6$

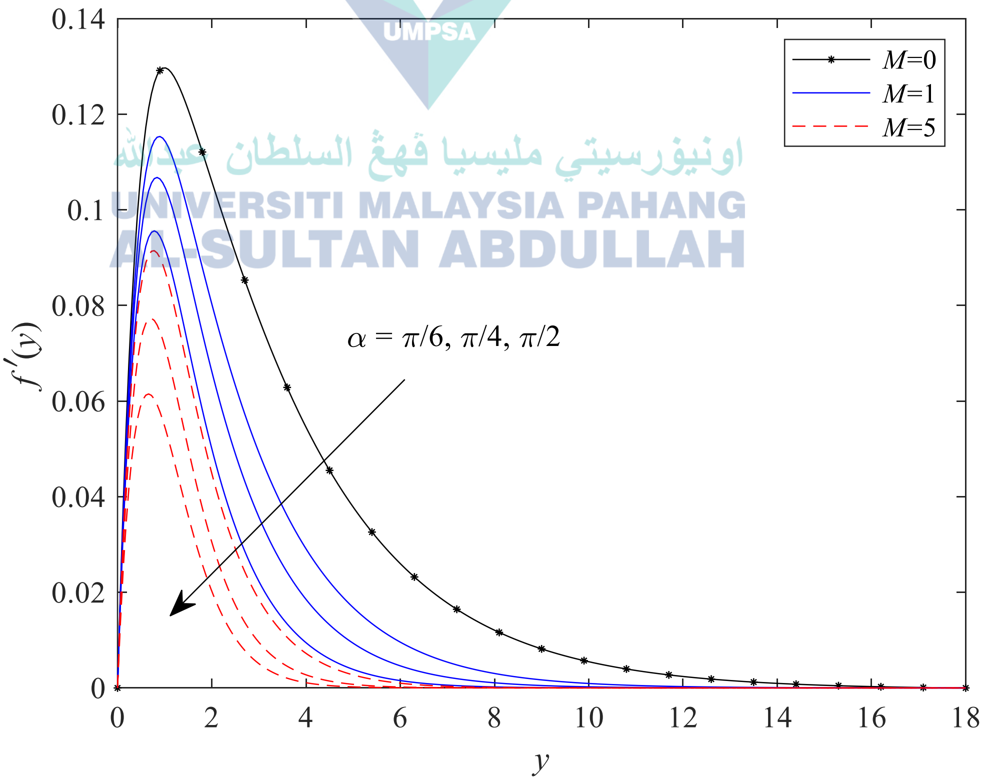

Figure 5.14 Variation of $f'(y)$ for various values of M and α at $K = K_1 = 0.5$

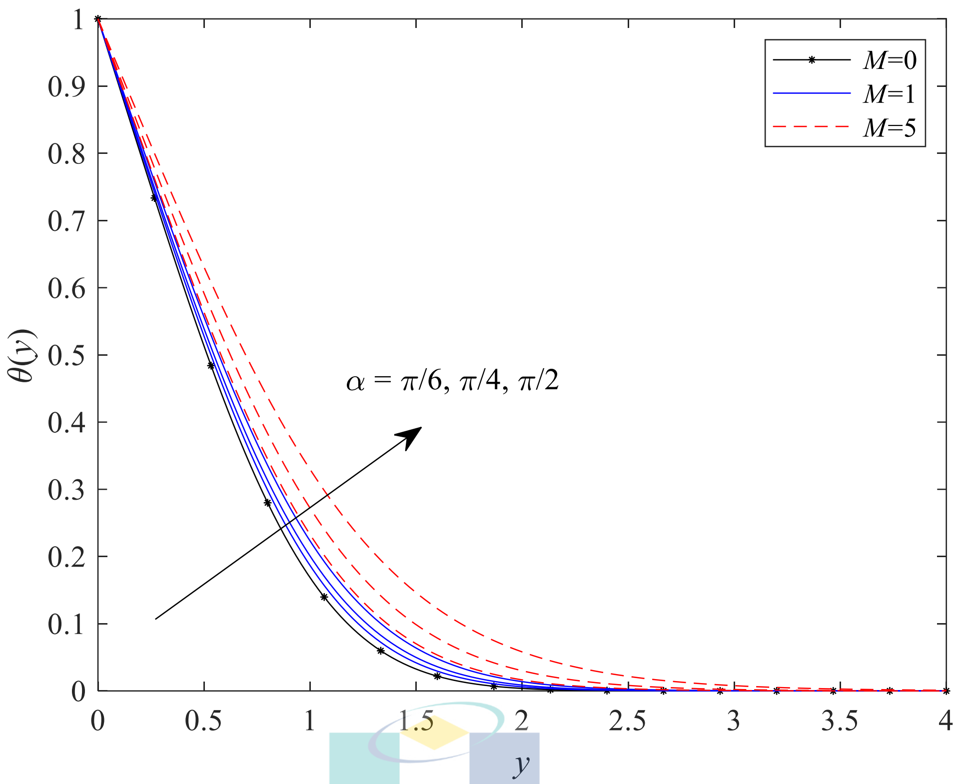

Figure 5.15 Variation of $\theta(y)$ for various values of M and α at $K = K_1 = 0.5$

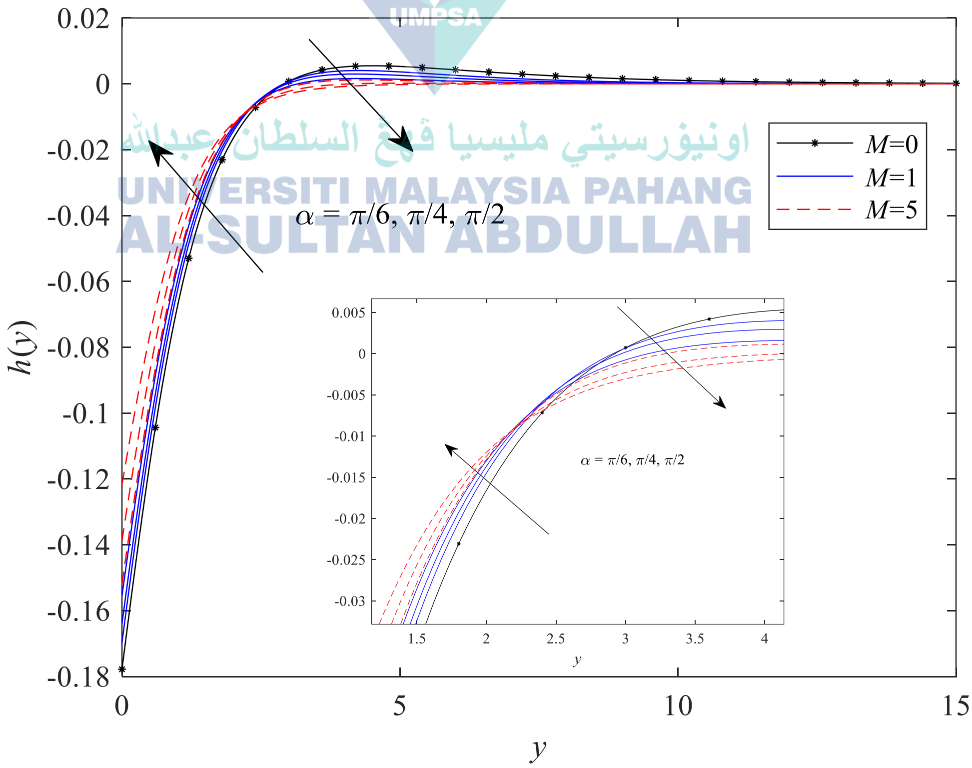

Figure 5.16 Variation of $h(y)$ for various values of M and α at $K = K_1 = 0.5$

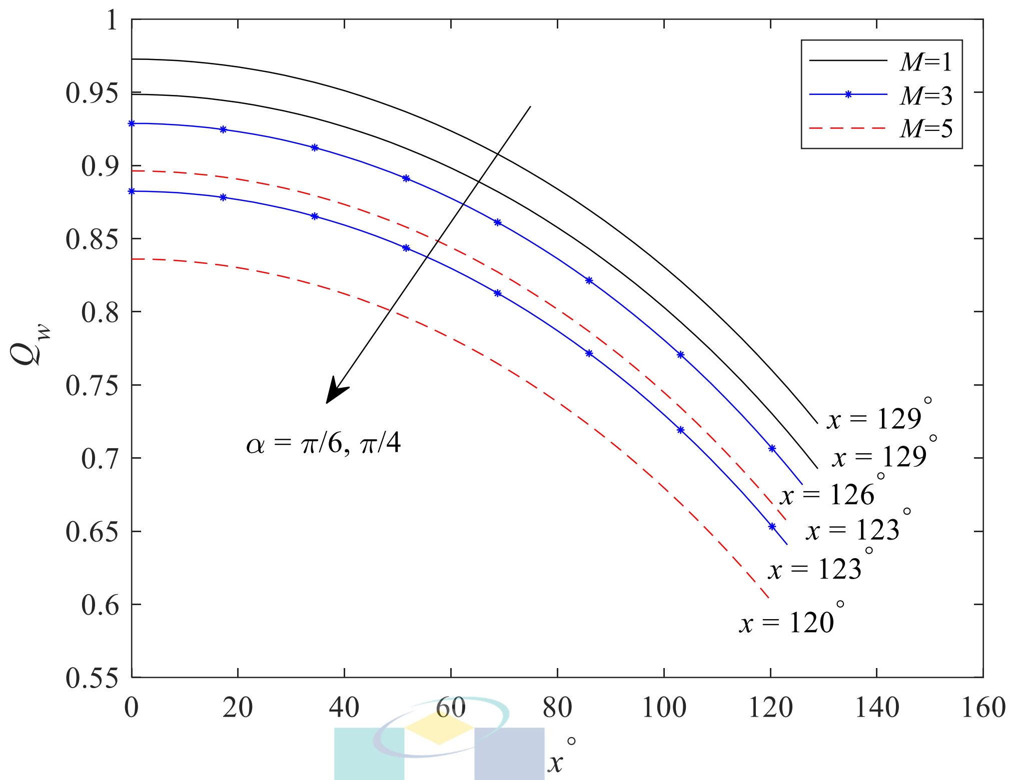

Figure 5.17 Variation of Q_w for various values of M and α at $K = K_1 = 0.5$

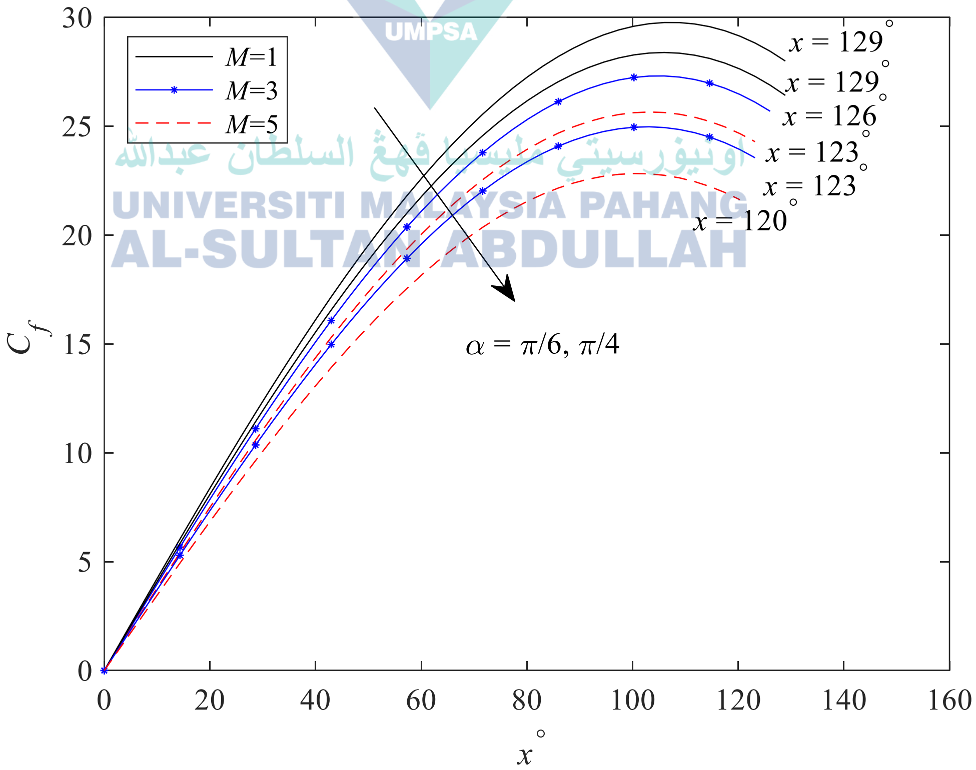

Figure 5.18 Variation of C_f for various values of M and α at $K = K_1 = 0.5$

5.4 Summary

This chapter has extended the problem from Chapter 4 by considering the boundary layer flow of viscoelastic micropolar fluid over a horizontal circular cylinder with the presence of magnetic effect for the case of free convection. The results are obtained using the Keller-box method, by employing Fortran programming and the change of trend for the physical quantities as well as the velocity, temperature and microrotation profiles influenced by parameters K, K_1, M and α had been discussed in Section 5.3. From the results obtained, the following are observed:

i. Velocity is inversely proportional to all the parameters, K, K_1, M and α. For K and K_1, as flow approaches the free stream, the trend reversed.

ii. Temperature is enhanced by the increase of K, K_1, M and α.

iii. Microrotation is positively correlated with all the parameters, but the profiles reverse towards the free stream.

iv. The rate of heat transfer is inversely proportional to all parameters.

v. The local skin friction coefficient rises with the decrease of K, M and α but the opposite occurs for K going towards the free stream. Meanwhile, the skin friction coefficient and K_1 are positively correlated.

Table 5.5 Summary of present results for free convection boundary layer flow of viscoelastic micropolar on a circular cylinder

Distribution	$K\uparrow$	$K_1\uparrow$	$M\uparrow$	$\alpha\uparrow$
f'	$\downarrow\uparrow$	$\downarrow\uparrow$	$\downarrow$	$\downarrow$
h	$\uparrow\downarrow$	$\uparrow\downarrow$	$\uparrow\downarrow$	$\uparrow\downarrow$
θ	$\uparrow$	$\uparrow$	$\uparrow$	$\uparrow$
C_f	$\downarrow$	$\uparrow$	$\downarrow$	$\downarrow$
Q_w	$\downarrow$	$\downarrow$	$\downarrow$	$\downarrow$

$\uparrow$ increase $\downarrow$ decrease

Table 5.6 Solution procedure for mathematical formulation of free convection boundary layer flow of viscoelastic micropolar on a horizontal circular cylinder

Steps	**Equation**
Governing equations	$\frac{\partial u}{\partial x}+\frac{\partial u}{\partial y}=0$ $u\frac{\partial u}{\partial x}+v\frac{\partial u}{\partial y}=(1+K_1)\frac{\partial^2 u}{\partial y^2}+K\left[\frac{\partial}{\partial x}\left(u\frac{\partial^2 u}{\partial y^2}\right)+v\frac{\partial^3 u}{\partial y^3}-\frac{\partial u}{\partial y}\frac{\partial^2 u}{\partial x\partial y}\right]$ $+\theta\sin x+K_1\frac{\partial H}{\partial y}-Mu\sin^2\alpha$ $u\frac{\partial H}{\partial x}+v\frac{\partial H}{\partial y}=-K_1\left(2H+\frac{\partial u}{\partial y}\right)+\left(1+\frac{K_1}{2}\right)\frac{\partial^2 H}{\partial y^2}$ $u\frac{\partial \theta}{\partial x}+v\frac{\partial \theta}{\partial y}=\frac{1}{\Pr}\frac{\partial^2 \theta}{\partial y^2}$
Boundary conditions	$u(0)=v(0)=0,\ \theta(0)=1,\ H(0)=-\frac{1}{2}\frac{\partial u}{\partial y}$ $u\to 0,\ \frac{\partial u}{\partial y}\to 0,\ \theta\to 0,\ H\to 0$ as $y\to\infty$
Non-similarity transformation	$\psi=xf(x,y),\ \ H=xh(x,y),\ \ \theta=\theta(x,y)$
Ordinary differential equations	At stagnation point: $(1+K_1)f'''+f\,f''-f'^2+1+\theta+K_1h'-M(f'-1)\sin^2\alpha$ $+K\left(2f'f'''-f\,f^{iv}-f''^2\right)=0$ $\left(1+\frac{K_1}{2}\right)h''+f\,h'-f'h-K_1(2h+f'')=0$ $\frac{1}{\Pr}\theta''+f\theta'=0$
Transformed boundary conditions	$f(0)=f'(0)=0,\ \theta(0)=1,\ h(0)=-\frac{1}{2}f''(0)$ $f'\to 0,\ f''\to 0,\ \theta\to 0,\ h\to 0,$ as $y\to\infty$

CHAPTER 6

MIXED CONVECTION BOUNDARY LAYER FLOW OF VISCOELASTIC MICROPOLAR FLUID OVER A HORIZONTAL CIRCULAR CYLINDER WITH ALIGNED MHD EFFECT

6.1 Introduction

This chapter is a continuation of Chapter 5 where in this study, the boundary layer flow of viscoelastic micropolar fluid over a horizontal circular cylinder with MHD effect, considering the case of mixed convection is discussed. When fluid motion is driven solely by buoyancy forces caused by density differences in the fluid due to temperature variations, this is considered as pure free convection. However, according to Incropera et al. (1996), when external forces such as fan or pump is introduced and the forced flow becomes comparable in magnitude to the natural buoyancy-driven flow, the system has entered a regime of mixed convection. The transition from forced convection to mixed convection could also happen when buoyancy forces become significant enough to affect the flow pattern alongside the forced flow. This typically happen when the forced flow velocity decreases or when temperature differences increase between the body and the flow.

The theoretical framework for this problem is primarily based on the viscoelastic models that were developed by Anwar et al. (2008) and Kasim et al. (2013) as well as the micropolar model by Nazar et al. (2003). The viscoelastic, micropolar, magnetic and aligned angle effect on the fluid flow will be discussed as the previous chapters on top of parameter λ which represents the mixed convection parameter. The results for the component skin friction, heat transfer as well as velocity, micropolar and temperature profiles are plotted for a wide range of parameters and the results will be reviewed and summarized.

6.2 Mathematical Formulation

Similar to the problem presented in Chapter 5, a horizontal circular cylinder is heated at constant temperature as it is immersed in viscoelastic micropolar fluid. As the free stream flows upward, its velocity at the boundary layer can be defined as $\bar{u}_e(\bar{x})$ while the temperature of the ambient is T_∞. The physical model of this study is as illustrated in Figure 6.1.

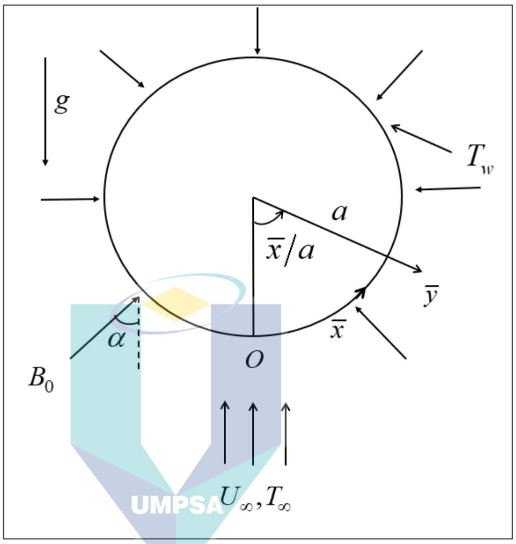

Figure 6.1 Schematic diagram for mixed convection boundary layer flow of viscoelastic micropolar fluid over a circular cylinder

The continuity, angular momentum and energy equations under boundary layer and Boussinesq approximation to represent the convective flow of viscoelastic micropolar fluid is as expressed in Equations (4.1), (4.2), and (3.79), respectively. The momentum equation, for this problem is defined by the following equation:

$$\bar{u}\frac{\partial \bar{u}}{\partial \bar{x}}+\bar{v}\frac{\partial \bar{u}}{\partial \bar{y}}=\bar{u}_e\frac{\partial \bar{u}_e}{\partial \bar{x}}+\left(\frac{\mu+\kappa}{\rho}\right)\frac{\partial^2 \bar{u}}{\partial \bar{y}^2}+\frac{k_0}{\rho}\left[\frac{\partial}{\partial \bar{x}}\left(\bar{u}\frac{\partial^2 \bar{u}}{\partial \bar{y}^2}\right)+\bar{v}\frac{\partial^3 \bar{u}}{\partial \bar{y}^3}-\frac{\partial \bar{u}}{\partial \bar{y}}\frac{\partial^2 \bar{u}}{\partial \bar{x}\partial \bar{y}}\right]$$
$$+\frac{\kappa}{\rho}\frac{\partial \bar{N}}{\partial \bar{y}}+g\beta\left(T-T_\infty\right)\sin\left(\frac{\bar{x}}{a}\right)-\frac{\sigma}{\rho}\left(\bar{u}-\bar{u}_e\right)B^2\sin^2\alpha \qquad 6.1$$

The governing equations are associated to the boundary conditions:

$$\bar{u} = \bar{v} = 0, \qquad T = T_w, \qquad \bar{H} = -\frac{1}{2}\frac{\partial \bar{u}}{\partial \bar{y}} \quad \text{on} \quad \bar{y} = 0,$$
$$\bar{u} \to \bar{u}_e(x), \quad \frac{\partial \bar{u}}{\partial \bar{y}} \to 0, \quad T \to T_\infty, \quad \bar{H} \to 0 \quad \text{as} \quad \bar{y} \to \infty \tag{6.2}$$

Then, the physical dimensions in the governing equations are dismissed by a set of dimensionless variables as proposed below:

$$x = \frac{\bar{x}}{a}, \quad y = \mathrm{Re}^{1/2}\left(\frac{\bar{y}}{a}\right), \quad u = \frac{\bar{u}}{U_\infty}, \quad v = \mathrm{Re}^{1/2}\left(\frac{\bar{v}}{U_\infty}\right)$$
$$H = \mathrm{Re}^{-1/2}\left(\frac{a}{U_\infty}\right)\bar{H}, \quad u_e = \frac{\bar{u}_e(\bar{x})}{U_\infty}, \quad \theta = \frac{T - T_\infty}{T_w - T_\infty} \tag{6.3}$$

As a result from the substitution of the dimensionless variable, the continuity, angular and energy equations are transformed to Equations (3.76), (4.10) and (5.5), respectively, while the momentum equation is as follows:

$$u\frac{\partial u}{\partial x} + v\frac{\partial u}{\partial y} = u_e\frac{\partial u_e}{\partial x} + (1 + K_1)\frac{\partial^2 u}{\partial y^2} + K\left(\frac{\partial}{\partial x}\left(u\frac{\partial^2 u}{\partial y^2}\right) + v\frac{\partial^3 u}{\partial y^3} - \frac{\partial u}{\partial y}\frac{\partial^2 u}{\partial x \partial y}\right)$$
$$+\lambda\theta \sin x + K_1\frac{\partial H}{\partial y} - M(u - u_e)\sin^2\alpha \tag{6.4}$$

The boundary conditions in Equation (6.3) are transformed to:

$$u = v = 0, \quad \theta = 1, \quad H = -\frac{1}{2}\frac{\partial u}{\partial y} \quad \text{on} \quad y = 0,$$
$$u \to u_e(x), \quad \frac{\partial u}{\partial y} \to 0, \quad \theta \to 0, \quad H \to 0 \quad \text{as} \quad y \to \infty \tag{6.5}$$

The parameters in the equations are as defined in Equation (4.12) and

$$\lambda = \frac{Gr}{\mathrm{Re}^2}, \; Gr = \frac{g\beta(T_w - T_\infty)a^3}{\nu^2} \tag{6.6}$$

Then, the same stream functions as stated in Equations (4.13) and (5.8) are applied to the momentum equation in Equation (6.4) and the boundary conditions in Equation (6.5). Consequently, the micropolar and energy equations are transformed to Equation (4.16) and (5.10). As for the momentum equation, it is now in the form below:

$$
\begin{aligned}
&(1+K_1)\frac{\partial^3 f}{\partial y^3}+f\frac{\partial^2 f}{\partial y^2}-\left(\frac{\partial f}{\partial y}\right)^2+\frac{\sin x\cos x}{x}+\lambda\frac{\sin x}{x}\theta+K_1\frac{\partial h}{\partial y} \\
&-M\left(\frac{\partial f}{\partial y}-\frac{\sin x}{x}\right)\sin^2\alpha \\
&+K\left\{2\frac{\partial f}{\partial y}\frac{\partial^3 f}{\partial y^3}-f\frac{\partial^4 f}{\partial y^4}-\left(\frac{\partial^2 f}{\partial y^2}\right)^2+x\left(\begin{aligned}&\frac{\partial^2 f}{\partial x\partial y}\frac{\partial^3 f}{\partial y^3}-\frac{\partial f}{\partial x}\frac{\partial^4 f}{\partial y^4}\\&+\frac{\partial f}{\partial y}\frac{\partial^4 f}{\partial x\partial y^3}-\frac{\partial^2 f}{\partial y^2}\frac{\partial^3 f}{\partial x\partial y^2}\end{aligned}\right)\right\} \\
&=x\left(\frac{\partial f}{\partial y}\frac{\partial^2 f}{\partial x\partial y}-\frac{\partial f}{\partial x}\frac{\partial^2 f}{\partial y^2}\right)
\end{aligned}
\qquad 6.7
$$

Subjected to the boundary conditions:

$$
\begin{aligned}
&f=\frac{\partial f}{\partial y}=0,\quad \theta=1,\ h=-\frac{1}{2}\frac{\partial^2 f}{\partial y^2}\quad \text{on}\quad y=0 \\
&\frac{\partial f}{\partial y}\to\frac{\sin x}{x},\ \frac{\partial^2 f}{\partial y^2}\to 0,\ \theta\to 0,\ h\to 0\ \text{as}\quad y\to\infty
\end{aligned}
\qquad 6.8
$$

Similarly to the previous cases, the value $n=1/2$ is chosen for this problem for which the value represents weak concentration and disappearance of the anti-symmetric part of the stress tensor (Majid et al., 2019). At lower stagnation point of the cylinder, where $x\approx 0$, Equation (6.7) is reduced to:

$$
\begin{aligned}
&(1+K_1)f'''+ff''-f'^2+1+\lambda\theta+K\left(2f'f'''-ff^{iv}-f''^2\right) \\
&+K_1h-M\left(f'-1\right)\sin^2\alpha=0
\end{aligned}
\qquad 6.9
$$

Meanwhile, the boundary conditions in Equation (6.8) are transformed to:

$$f(0)=f'(0)=0, \quad \theta(0)=1, \quad h(0)=-\frac{1}{2}f''(0)$$
$$f'\to 1, \quad f''\to 0, \quad \theta\to 0, \quad h=0 \quad \text{as } y\to\infty \tag{6.10}$$

Following Nazar et al. (2003), the skin friction and heat transfer coefficients of this problem are as stated in Equations (4.23) and (5.15), respectively.

6.3 Results and Discussion

In this section, the numerical result from the algorithm coded in Fortran language is developed for this problem to solve the finalized governing equations as stated in Equations (6.9), (5.13) and (4.19), bounded to the initial conditions in Equation (6.10). The solution obtained is compared to several studies that focus on different types of fluid including viscous fluid by Merkin (1977), micropolar fluid by Nazar et al. (2003) and viscoelastic by Anwar et al. (2008). The momentum equations and boundary conditions of these studies, as listed in Table 6.1, and the limiting case for current problem will conclusively reduce to the same equation when the parameter K, K_1 and M are all set to 0, invoking the comparability of the results.

The values of $f''(0)$ and Q_w were set side by side in Tables 6.2 and 6.3 between current result, Merkin (1977) and Nazar et al. (2003) at different positions on the wall when $\Pr=1$. The results showed high degree of similarity to the numerical results of both studies with the same limiting case. Further comparison was done for $f''(0)$ between current result and Anwar et al. for various values of K, and again, the results in Table 6.4 have shown high degree of consistency. After verification that the results are deemed valid, the values of C_f and Q_w at various parameters for this problem are generated and displayed in Table 6.5. From the table, the values generated show that except for K, the skin friction and heat transfer coefficients are directly proportional to the other parameters, K_1, M, λ and α.

For this problem, the behaviour of the flow under different mode of convection is monitored as the parameter changes by varying the mixed convection parameter, λ. When $\lambda>0$, the natural buoyancy assists the forced convection; cylinder is heated, hence, the coefficient represents mixed convection. In contrast, $\lambda < 0$ demonstrates opposing flow, where the natural convection opposed the forced flow; cylinder is cooled and ultimately, $\lambda = 0$ represents forced convection when there is absence of buoyancy force and flow is driven primarily by external force (Kakac et al., 2013).

As K surges in value, it can be observed from Figures 6.2, 6.5 and 6.6 that f', C_f and Q_w are diminished. Again, these circumstances can be explained by the enhancement of elastic properties of the fluid as K increases which acts against the momentum and thermal diffusion causing both f' and Q_w to decrease. Moreover, when λ keeps increasing, the forced convection becomes more dominant than the free convection and the external force strains the elastic microstructure thus increasing the viscosity and the resistance of the flow. The combined effect of these two factors results in poor momentum and heat transfer causing f', C_f and Q_w to decline.

As reported by Hayat et al. (2008), the growth of K value tends to increase the thermal boundary thus increasing the temperature as the viscoelasticity enhances the heat transfer properties as illustrated in Figure 6.3. It can also be observed that h and K are directly proportional, where the velocity of the particles were higher when buoyancy forces are dominant at $\lambda < 0$ as K increases. Further observation also revealed that boundary layer separation is delayed with increasing elasticity in assisting flow $(\lambda > 0)$.

As discussed in Chapter 4, the increase of K_1 indicates more resistance on the fluid where the resistance could exert shear stress on the wall that would increase C_f. This opposing nature can also explain the reduction of velocity and when λ increases simultaneously, the more dominant buoyance force also retarded the forced mainstream flow thus further reducing the velocity. A reversal behaviour can be noticed from Figure 6.9 where h increases then decreases when the value of K_1 grows. The reversal only occurs when micropolar element is present and at the beginning, the assisting flow retards the rotation but after the turning point, the opposite is observed.

The surge of K_1 value also results in the increment of θ and Q_w. While C_f and Q_w were enhanced by assisting flow, θ is restrained when $\lambda > 0$. The result shows that enhanced fluid particle rotation and microstructure results in greater heat transfer and skin friction, as the rotating particles create additional mechanisms for energy and momentum transfer within the fluid. The presence of both forced and natural convection restrains the temperature increase as a result from the additional fluid motion from mixed convection that helps to distribute heat more evenly, counteracting some of the localized heating effects from micropolar rotation.

It is also evident that boundary layer separation can be remanded by selecting higher values of K_1 and λ which suggests that the combination of micropolar effects and mixed convection enhances the fluid's ability to remain attached to the surface. This is the consequence of increased momentum transfer near the wall from particle rotation and the added energy from buoyancy forces, both of which help overcome adverse pressure gradients that typically cause separation.

The magnetic and mixed convection effect on the behavioural flow and heat transfer of the fluid is displayed in Figures 6.12 to 6.16. Similar to the previous two problems, interaction between magnetic field and electrically conducting fluid will generate Lorentz force (Asmat et al., 2023) that could have significant impact on the boundary layer flow. Additionally, for this case the convection effect is also integrated. Figure 6.12 shows how Lorentz force accelerated the fluid flow with the rise of both values of M and λ.

The increase of the intensity of the magnetic field also increases C_f and Q_w that also rise when λ grows. It can be seen from the microrotation profile in Figure 6.13 that the magnetic field curbs the rotation of the microelements thus reducing the microrotation velocity. On the contrary, h and λ are positively correlated. It has also been established from the result that as the magnetic field and buoyancy effect dominate, C_f and Q_w increase which indicates that the thermal energy transfer between fluid and cylinder wall is more effective as well as higher viscous drag force on the surface.

It is also of interest in this problem to see the combination effect of convection parameter and aligned angle. Judging from the result, aligned angle is a definite controlling factor for the magnetic force imposed to the flow. From Figure 6.16, it can be seen that f' increases as the angle is accentuated until the magnetic field is perpendicular to the flow and the same positive relationship is observed as λ increases. However, contrast behaviour is illustrated in Figures 6.18 and 6.19, where increasing aligned angle and λ cause a decrease in values of θ and h. If cooling down a system is of interest, then higher Q_w is sought after and from the result, this can be achieved by increasing α and λ. Similarly, increasing these parameters will also raise C_f.

For all the figures that illustrated Q_w at various parameters, jagged lines are spotted for the x values that are in close proximity to the stagnation point $(x=0)$. However, the lines started to smooth out as the flow moves towards the middle of the cylinder. This instability is absent for the case of boundary layer flow in Chapter 4 and free convection problem in Chapter 5 but is only discovered when mixed convection is considered. Since velocity of fluid and heat transfer coefficient are proportional (Kakac et al., 2002), when the velocity of the flow drops to zero at the front stagnation point, the transfer rate will also approach zero. At this point, due to no motion in the fluid, convection cannot occur, and conduction becomes more dominant. The transition between these modes of heat transfer could cause instability to flow and further interaction between the buoyancy force from the mixed convection and the conduction-dominated heat transfer might add up to the unsteadiness.

Table 6.1 The momentum equation and boundary conditions of problems involved for result validation

Author	**Model**
Present	$(1+K_1)f''' + ff'' - f'^2 + 1 + \lambda\theta + K\left(2f'f''' - ff^{iv} - f''^2\right)$ $+K_1 h - M\left(f'-1\right)\sin^2\alpha = 0$ with boundary conditions $f(0) = f'(0) = 0, \quad \theta(0) = 1, \quad h(0) = -\frac{1}{2}f''(0)$ $f' \to 1, \quad f'' \to 0, \quad \theta \to 0, \quad h = 0 \quad \text{as } y \to \infty$
Merkin (1977)	$f''' + ff'' - f'^2 + 1 + \lambda\theta = 0$ with boundary conditions $f(0) = f'(0) = 0, \quad \theta(0) = 1$ $f' \to 1, \quad \theta \to 0, \text{ as } y \to \infty$

Table 6.1 Continued

Author	Model
Nazar et al. (2003)	$\left(1+K_1\right) f''' + ff'' - f'^2 + 1 + \lambda\theta + Kh' = 0$ with boundary conditions $f(0) = f'(0) = 0, \quad \theta(0) = 1, \quad h(0) = -\frac{1}{2} f''(0)$ $f' \to 1, \quad \theta \to 0, \quad h \to 0 \quad \text{as } y \to \infty$
Anwar et al. (2008)	$f''' + ff'' - f'^2 + 1 + \lambda\theta + K\left(2f' f''' - ff^{iv} - f''^2\right) = 0$ with boundary conditions $f(0) = f'(0) = 0, \quad \theta(0) = 1$ $f' \to 1, \quad f'' \to 0, \quad \theta \to 0 \quad \text{as } y \to \infty$

Table 6.2 Comparative values of $f''(0)$ at $\Pr = 1$ and $K = K_1 = M = 0$

	Merkin (1977)			**Nazar et al. (2003)**			**Present**		
λ / ***x***	**-1**	**0**	**1**	**-1**	**0**	**1**	**-1**	**0**	**1**
0.0	0.0000	0.0000	0.0000	0.0000	0.0000	0.0000	0.0000	0.0000	0.0000
0.2	0.1257	0.2427	0.3436	0.1252	0.2421	0.3430	0.1275	0.2427	0.3452
0.4	0.2266	0.4627	0.6639	0.2242	0.4602	0.6610	0.2273	0.4628	0.6643
0.6	0.2784	0.6393	0.9398	0.2731	0.6337	0.9335	0.2825	0.6393	0.9433
0.8	0.2554	0.7552	1.1538	0.2463	0.7461	1.1432	0.2574	0.7552	1.1543
1.0	0.1069	0.7982	1.2938	0.0890	0.7855	1.2785	0.1215	0.7981	1.2977
1.2		0.7615	1.3541		0.7460	1.3343		0.7613	1.3535
1.4		0.6429	1.3356		0.6256	1.3121		0.6425	1.3385
1.6		0.4405	1.2459		0.4229	1.2200		0.4383	1.2431
1.8		0.1069	1.0986		0.0833	1.0728		0.1060	1.0996
2.0			0.9117			0.8880			0.9060
2.2			0.7063			0.6866			0.7054
2.4			0.5048			0.4900			0.4967
2.6			0.3287			0.3215			0.3272
2.8			0.1979			0.1949			0.1894
3.0			0.1292			0.1355			0.1305
π			0.1206			0.1325			0.1215

Table 6.3 Comparative values of Q_w at $\Pr = 1$ and $K = K_1 = M = 0$

	Merkin (1977)			Nazar et al. (2003)			Present		
x \ λ	-1	0	1	-1	0	1	-1	0	1
0.0	0.5067	0.5705	0.6156	0.5080	0.5710	0.6160	0.5067	0.5705	0.6156
0.2	0.5018	0.5668	0.6115	0.5022	0.5668	0.6125	0.5041	0.5686	0.6140
0.4	0.4865	0.5564	0.6028	0.4862	0.5560	0.6031	0.4870	0.5570	0.6042
0.6	0.4594	0.5391	0.5885	0.4584	0.5380	0.5880	0.4614	0.5403	0.5903
0.8	0.4160	0.5145	0.5686	0.4140	0.5130	0.5673	0.4172	0.5150	0.5696
1.0	0.3326	0.4826	0.5435	0.3259	0.4808	0.5414	0.3424	0.4836	0.5446
1.2		0.4426	0.5133		0.4406	0.5105		0.4428	0.5135
1.4		0.3928	0.4785		0.3909	0.4750		0.3937	0.4788
1.6		0.3280	0.4394		0.3262	0.4354		0.3286	0.4389
1.8		0.2114	0.3967		0.2049	0.3924		0.2266	0.3964
2.0			0.3509			0.3465			0.3499
2.2			0.3029			0.3002			0.3026
2.4			0.2540			0.2515			0.2531
2.6			0.2061			0.2040			0.2062
2.8			0.1634			0.1636			0.1629
3.0			0.1354			0.1397			0.1365
π			0.1306			0.1380			0.1307

Table 6.4 Comparative values of $f''(0)$ and $-\theta'(0)$ at $\Pr = 1$ and $K_1 = M = 0$ at various K and λ

K	$\lambda = 1$				$\lambda = -1$			
	Anwar et al (2008)		**Present**		**Anwar et al (2008)**		**Present**	
	$f''(0)$	$-\theta'(0)$	$f''(0)$	$-\theta'(0)$	$f''(0)$	$-\theta'(0)$	$f''(0)$	$-\theta'(0)$
0	1.736738	0.615601	1.736761	0.615612	0.651118	0.509534	0.648911	0.506688
0.01	1.718552	0.613861	1.718552	0.613861	0.643624	0.505705	0.643624	0.505705
0.1	1.580229	0.600089	1.580229	0.600089	0.601190	0.497588	0.601190	0.497588
0.2	1.464141	0.587800	1.464141	0.587800	0.562568	0.489810	0.562568	0.489810
0.3	1.372892	0.577594	1.372892	0.577594	0.530390	0.483012	0.530390	0.483012
0.4	1.298364	0.568851	1.298364	0.568851	0.502993	0.476970	0.502993	0.476970
0.5	1.235808	0.561198	1.235808	0.561198	0.479271	0.471533	0.479271	0.471533
0.6	1.182212	0.554389	1.182212	0.554389	0.458452	0.466588	0.458452	0.466588
0.7	1.135550	0.548256	1.135550	0.548256	0.439978	0.462056	0.439978	0.462056
0.8	1.094396	0.542677	1.094396	0.542677	0.423434	0.457872	0.423434	0.457872
0.9	1.057711	0.537559	1.057711	0.537559	0.408500	0.453987	0.408500	0.453987
1	1.024719	0.532833	1.024719	0.532833	0.394929	0.450362	0.394929	0.450362
2	0.810695	0.498821	0.810695	0.498821	0.304357	0.423419	0.304357	0.423419
3	0.694301	0.477261	0.694301	0.477261	0.254015	0.405786	0.254015	0.405786
4	0.617991	0.461601	0.617991	0.461601	0.221003	0.392827	0.221003	0.392827
5	0.562865	0.449394	0.562865	0.449394	0.197308	0.382679	0.197308	0.382679
8	0.458930	0.423929	0.458930	0.423929	0.153389	0.361509	0.153389	0.361509
10	0.415342	0.412127	0.415342	0.412127	0.135426	0.351747	0.135426	0.351747

Table 6.5 Variations of C_f and Q_w for various values of *K*, *K*1, *M* and α at $\Pr = 21$

K	K_1	M	λ	α	C_f	Q_w
1	0.5	0.5	1	$\pi/6$	0.880805	1.504045
2	0.5	0.5	1	$\pi/6$	0.706572	1.399927
3	0.5	0.5	1	$\pi/6$	0.609618	1.333863
4	0.5	0.5	1	$\pi/6$	0.545340	1.285967
5	0.5	0.5	1	$\pi/6$	0.498570	1.248667
0.5	1	0.5	1	$\pi/6$	1.137399	1.634937
0.5	1.5	0.5	1	$\pi/6$	1.247696	1.686556
0.5	2	0.5	1	$\pi/6$	1.381323	1.745195
0.5	2.5	0.5	1	$\pi/6$	1.543941	1.811722
0.5	3	0.5	1	$\pi/6$	1.741915	1.886763
0.5	0.5	1	1	$\pi/6$	1.117672	1.622148
0.5	0.5	2	1	$\pi/6$	1.184745	1.651009
0.5	0.5	3	1	$\pi/6$	1.247688	1.676768
0.5	0.5	4	1	$\pi/6$	1.307176	1.700045
0.5	0.5	5	1	$\pi/6$	1.363719	1.721289
0.5	0.5	1	-2	$\pi/6$	0.382369	1.302741
0.5	0.5	1	-1	$\pi/6$	0.675802	1.450591
0.5	0.5	1	0	$\pi/6$	0.911582	1.547469
0.5	0.5	1	1	$\pi/6$	1.117672	1.622148
0.5	0.5	1	2	$\pi/6$	1.304386	1.683820
0.5	0.5	1	1	$\pi/4$	1.184745	1.651009
0.5	0.5	1	1	$\pi/3$	1.247688	1.676768
0.5	0.5	1	1	$\pi/2$	1.307176	1.700045

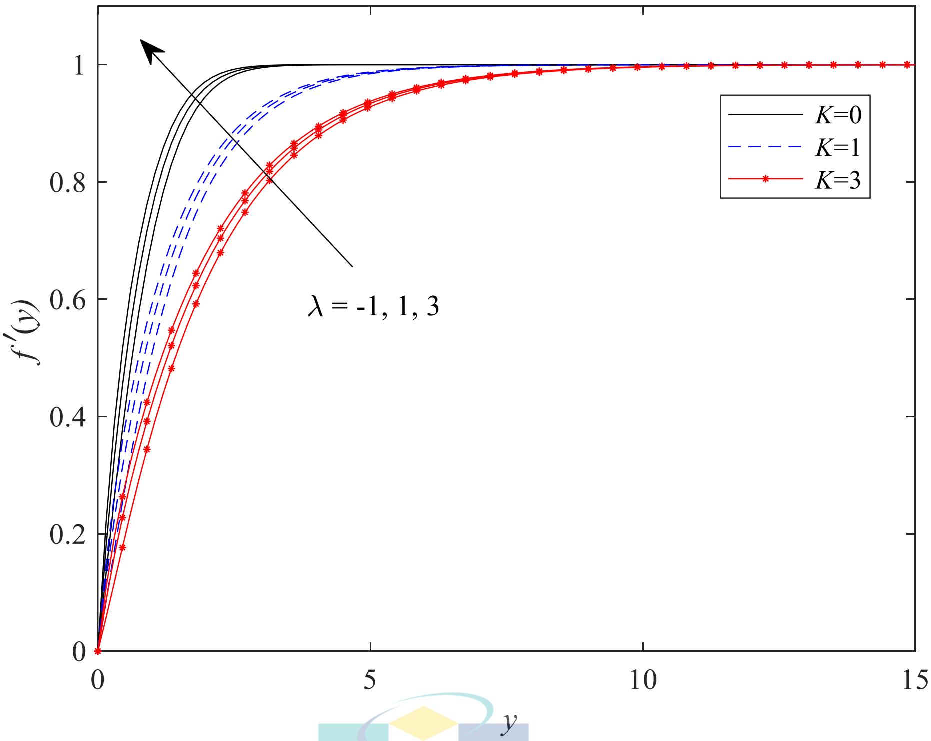

Figure 6.2 Variation of $f'(y)$ for various values of K and λ at $K_1 = M = 0.5$ and $\alpha = \pi/6$

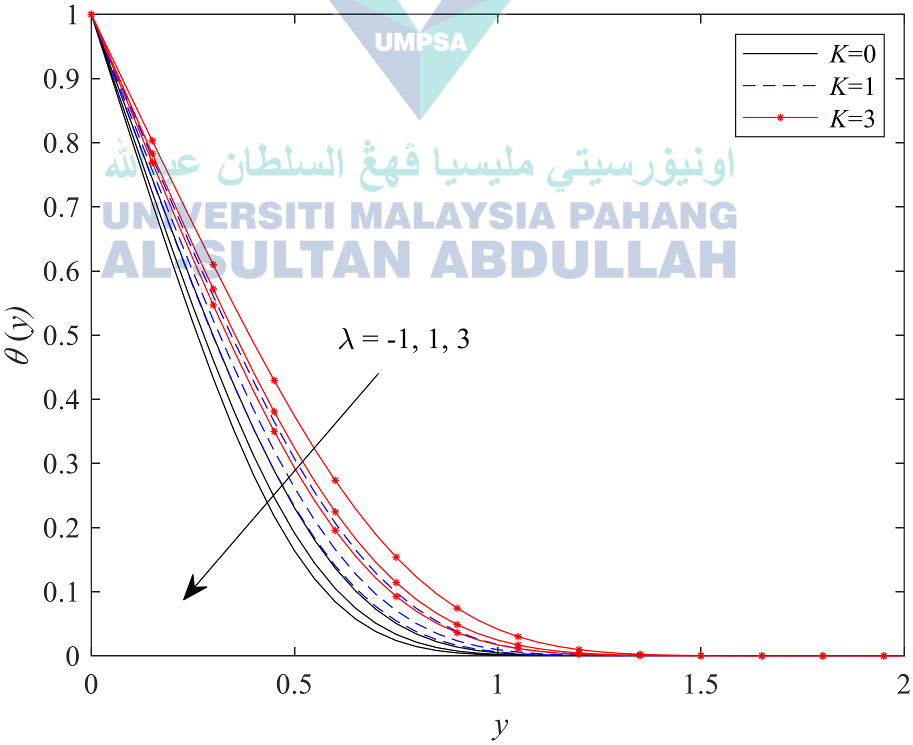

Figure 6.3 Variation of $\theta(y)$ for various values of K and λ at $K_1 = M = 0.5$ and $\alpha = \pi/6$

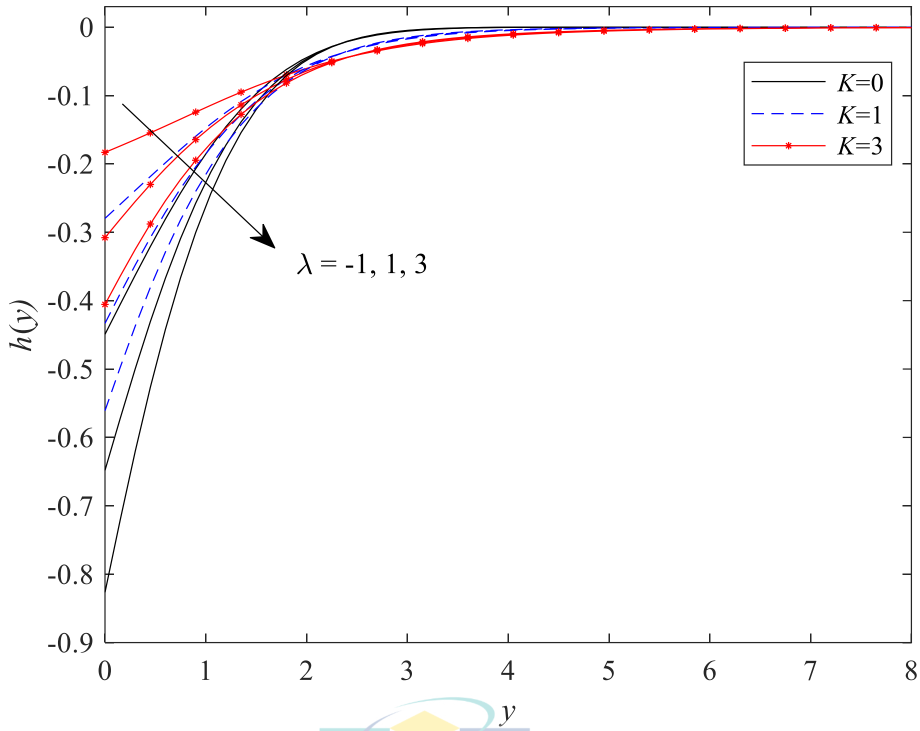

Figure 6.4 Variation of $h(y)$ for various values of K and λ at $K_1 = M = 0.5$ and $\alpha = \pi/6$

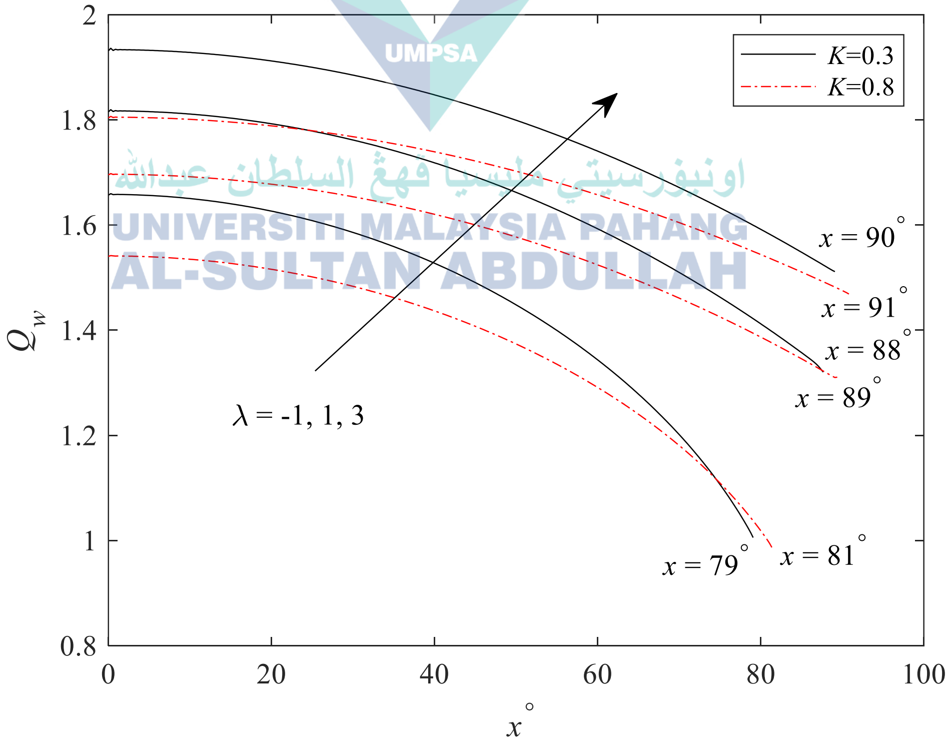

Figure 6.5 Variation of Q_w for various values of K and λ at $K_1 = M = 0.5$ and $\alpha = \pi/6$

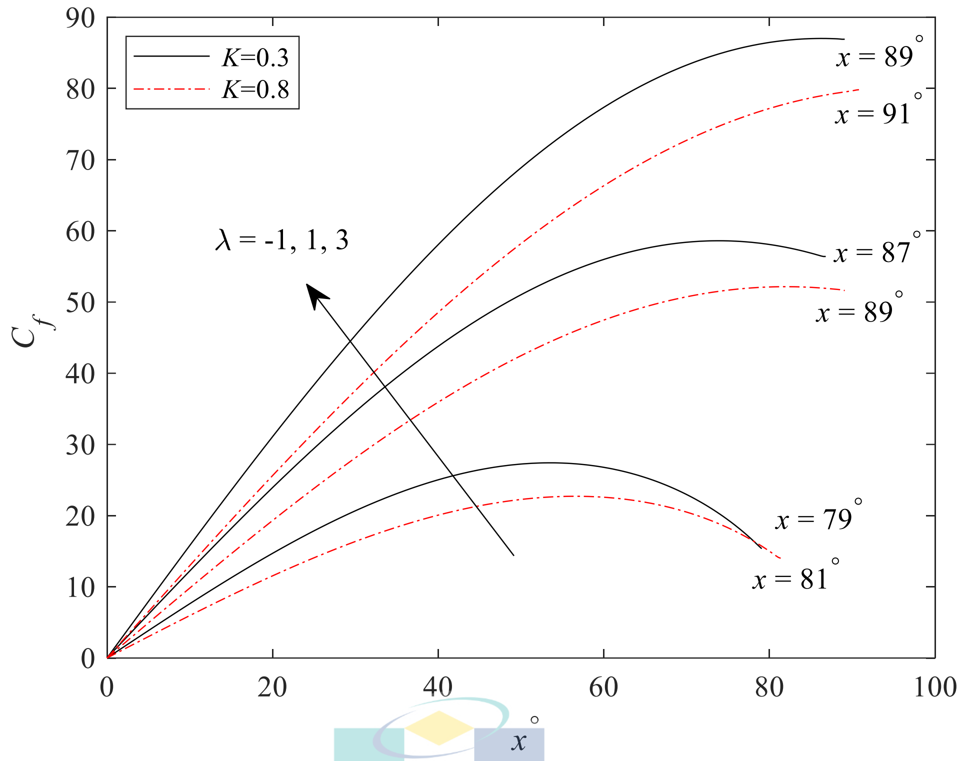

Figure 6.6 Variation of C_f for various values of K and λ at $K_1 = M = 0.5$ and $\alpha = \pi/6$

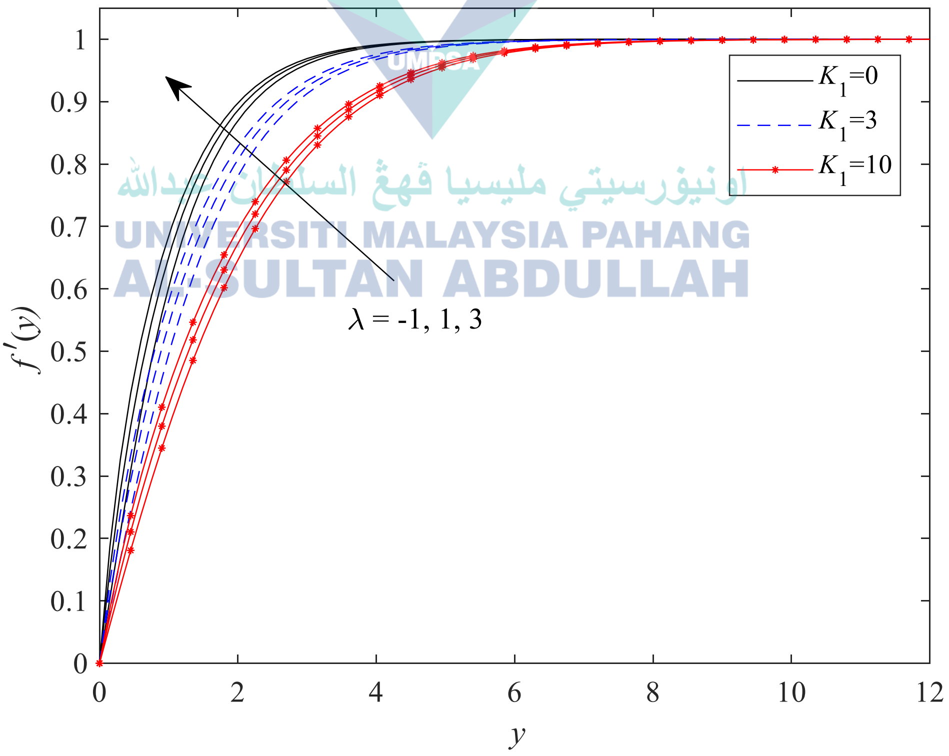

Figure 6.7 Variation of $f'(y)$ for various values of K_1 and λ at $K = M = 0.5$ and $\alpha = \pi/6$

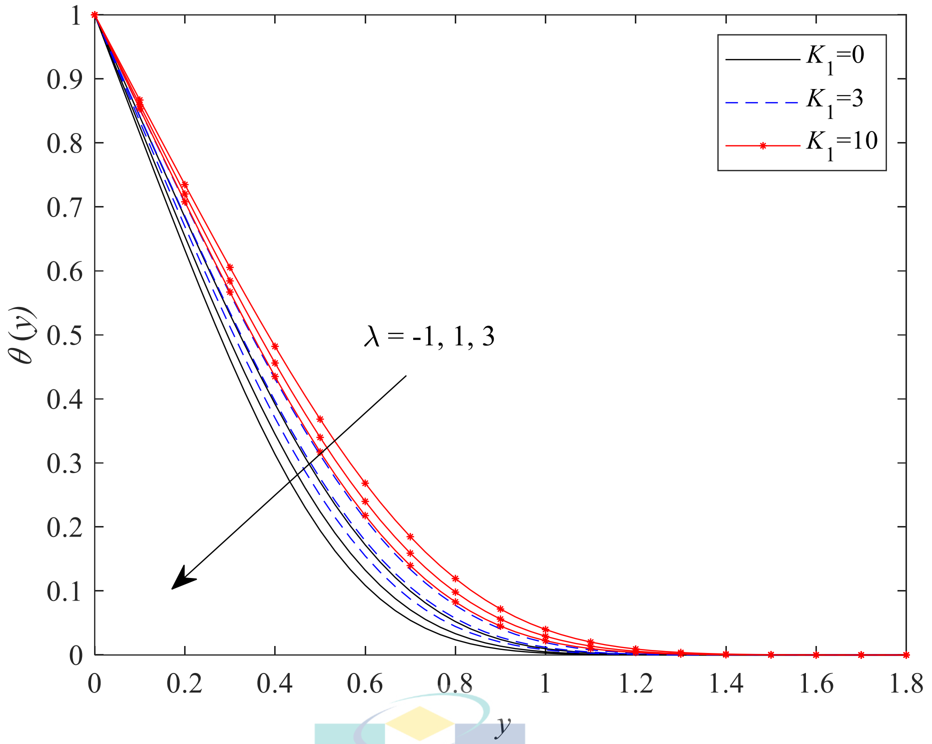

Figure 6.8 Variation of $\theta(y)$ for various values of K_1 and λ at $K = M = 0.5$ and $\alpha = \pi/6$

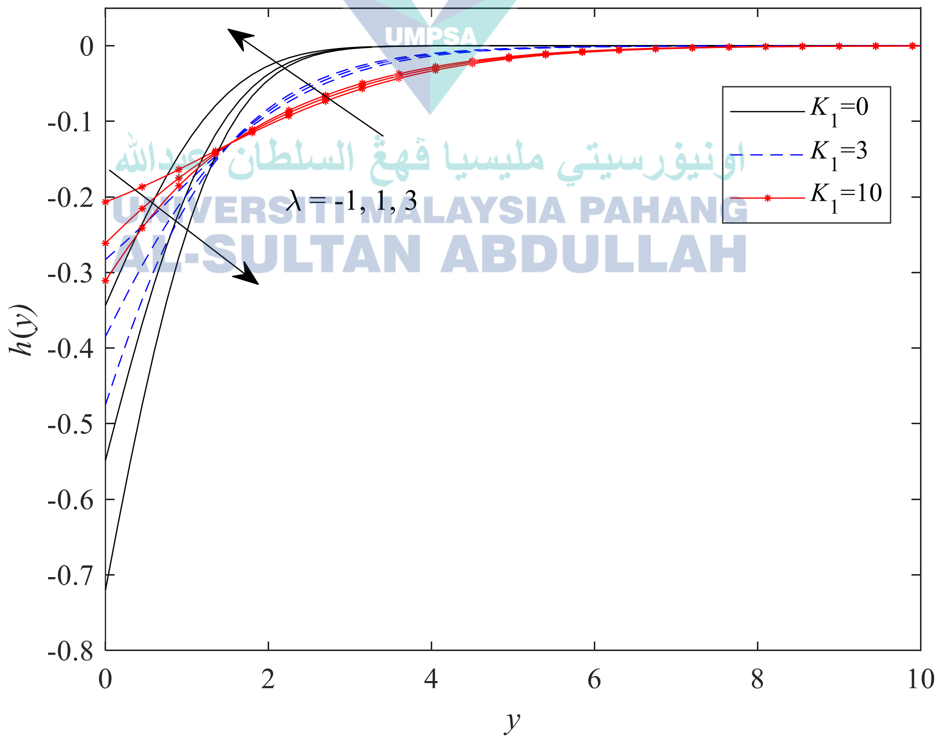

Figure 6.9 Variation of $h(y)$ for various values of K_1 and λ at $K = M = 0.5$ and $\alpha = \pi/6$

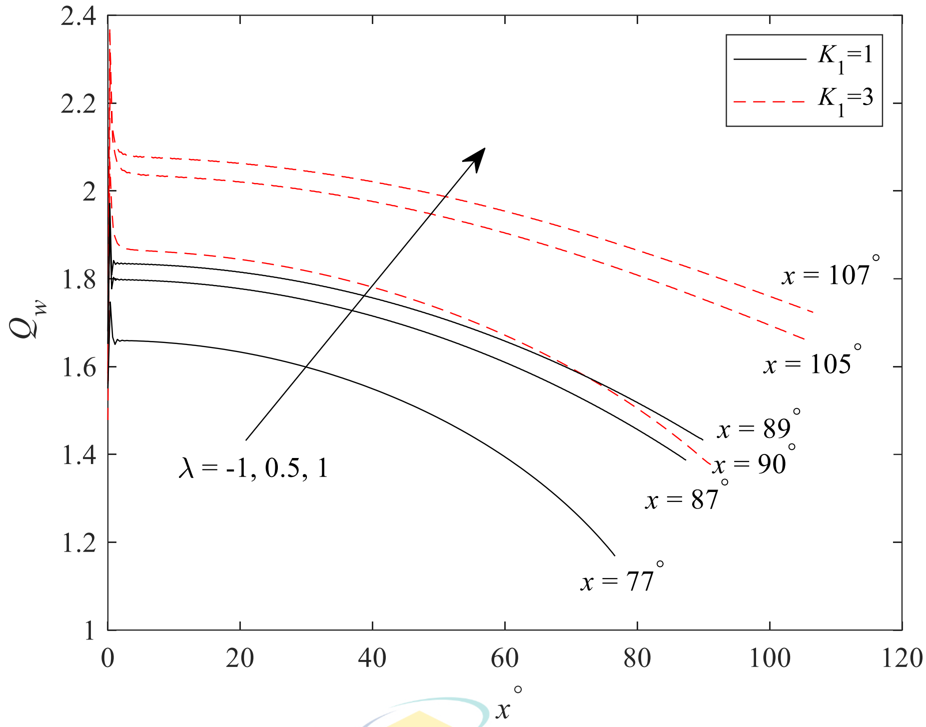

Figure 6.10 Variation of Q_w for various values of K_1 and λ at $K = M = 0.01$ and $\alpha = \pi/6$

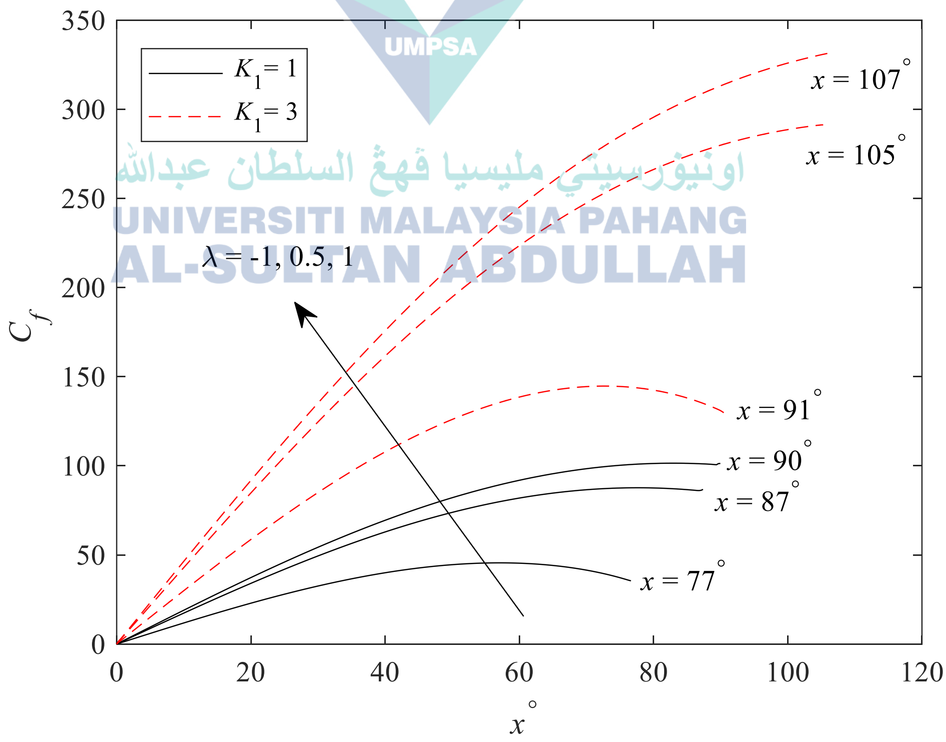

Figure 6.11 Variation of C_f for various values of K_1 and λ at $K = M = 0.01$ and $\alpha = \pi/6$

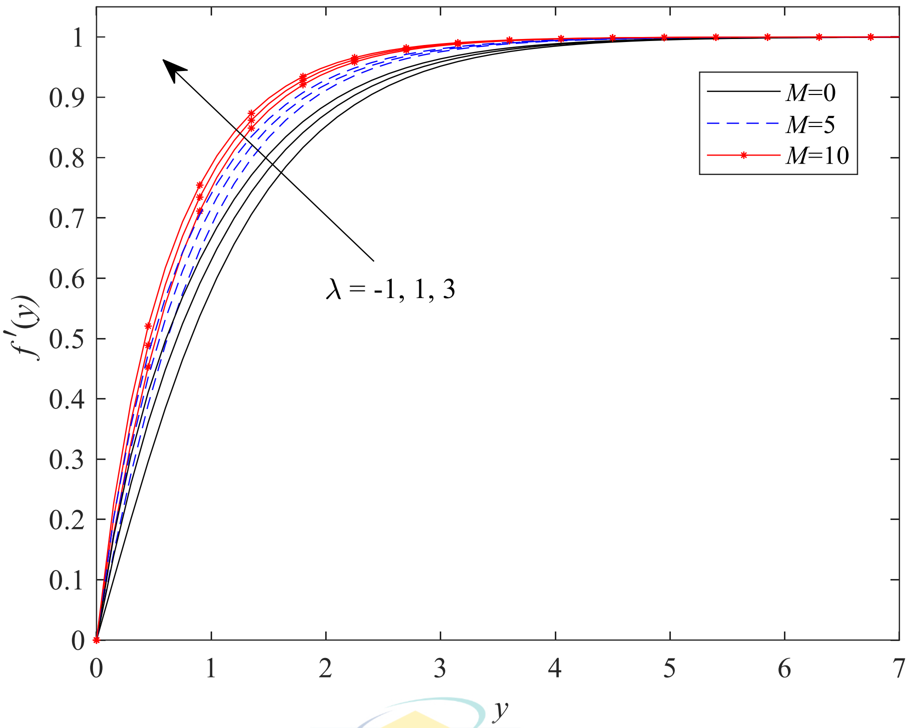

Figure 6.12 Variation of $f'(y)$ for various values of M and λ at $K = K_1 = 0.5$ and $\alpha = \pi/6$

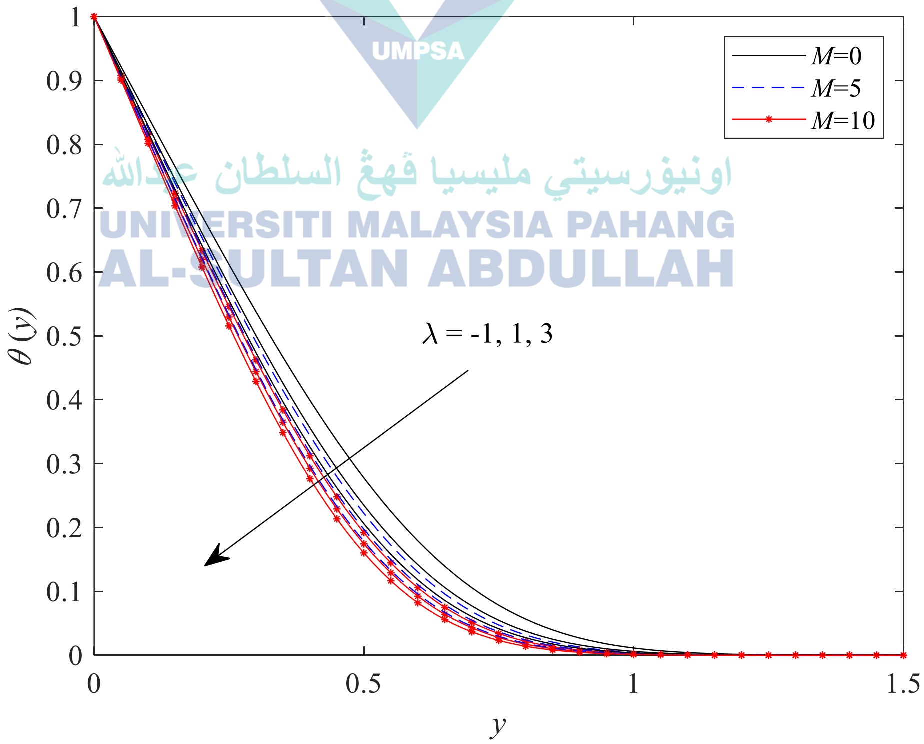

Figure 6.13 Variation of $\theta(y)$ for various values of M and λ at $K = K_1 = 0.5$ and $\alpha = \pi/6$

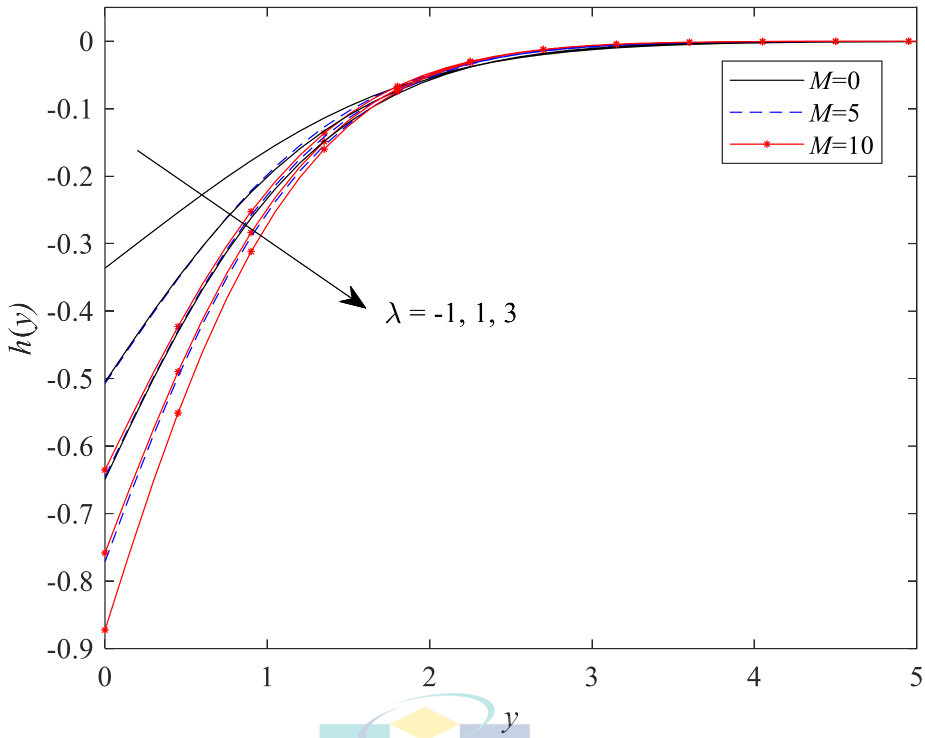

Figure 6.14 Variation of $h(y)$ for various values of M and λ at $K = K_1 = 0.5$ and $\alpha = \pi/6$

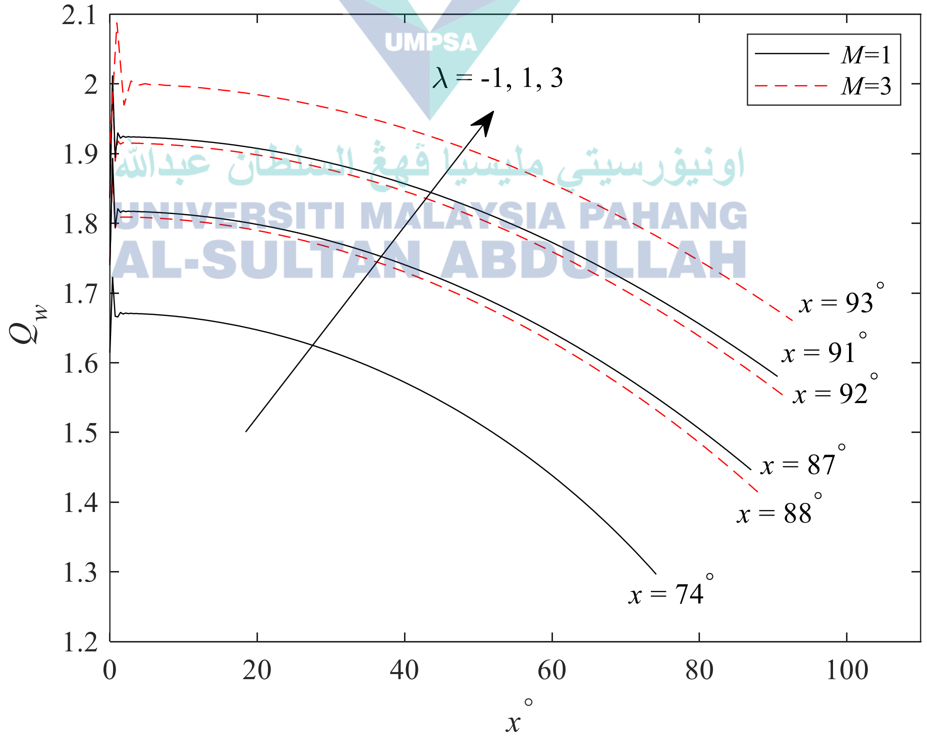

Figure 6.15 Variation of Q_w for various values of M and λ at $K = K_1 = 0.5$ and $\alpha = \pi/6$

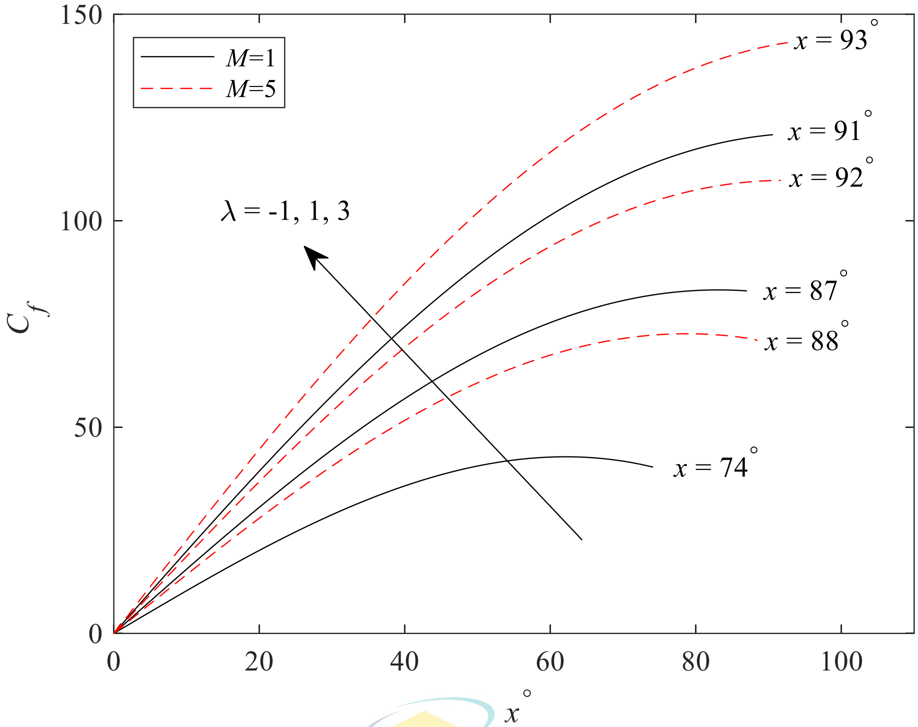

Figure 6.16 Variation of C_f for various values of M and λ at $K = K_1 = 0.01$ and $\alpha = \pi/6$

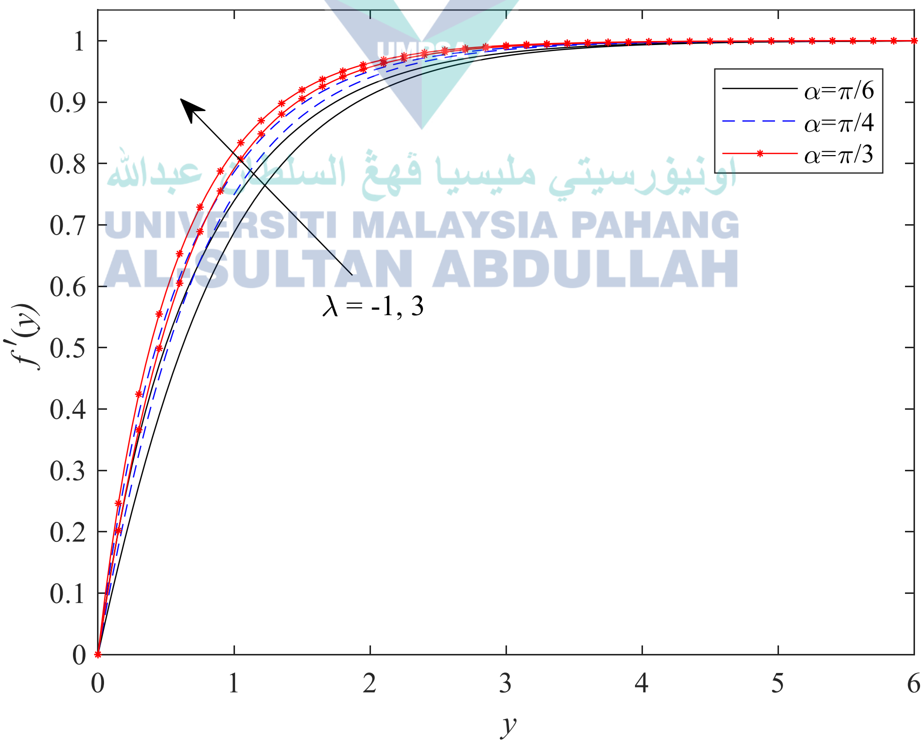

Figure 6.17 Variation of $f'(y)$ for various values of α and λ at $K = K_1 = 0.01$

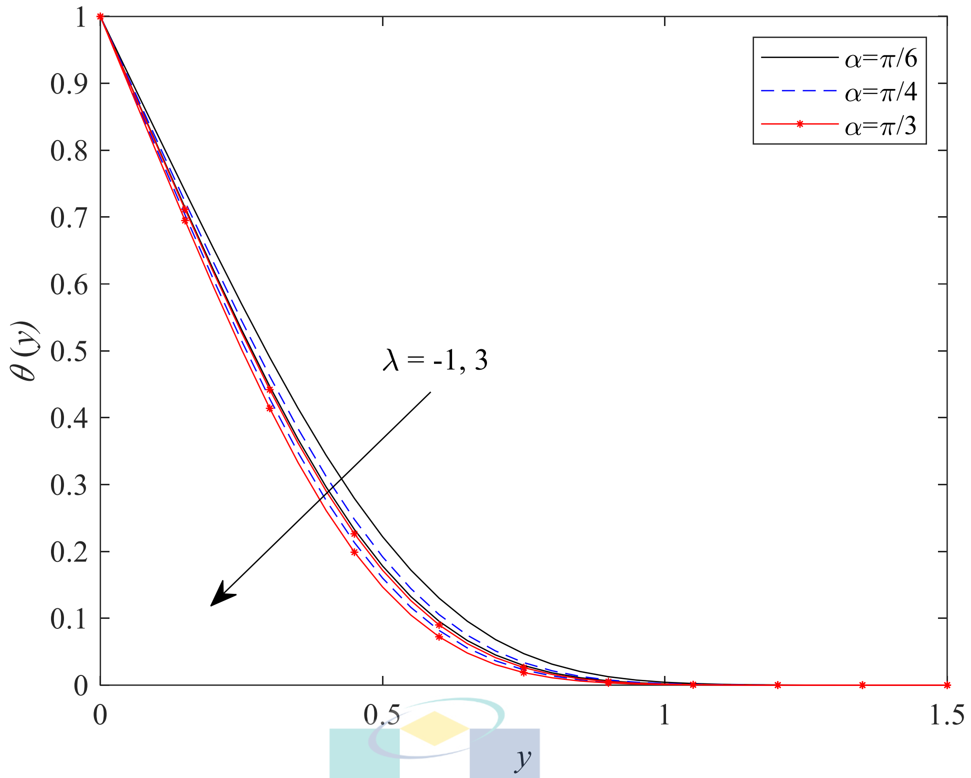

Figure 6.18 Variation of $\theta(y)$ for various values of α and λ at $K = K_1 = M = 0.5$

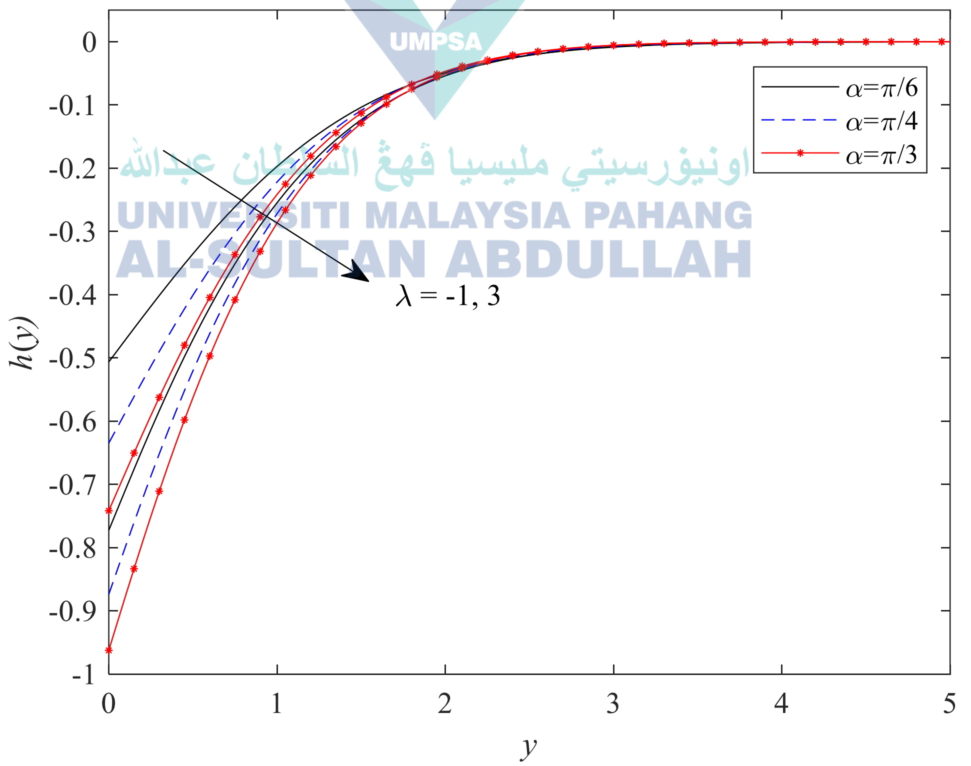

Figure 6.19 Variation of $h(y)$ for various values of α and λ at $K = K_1 = M = 0.5$

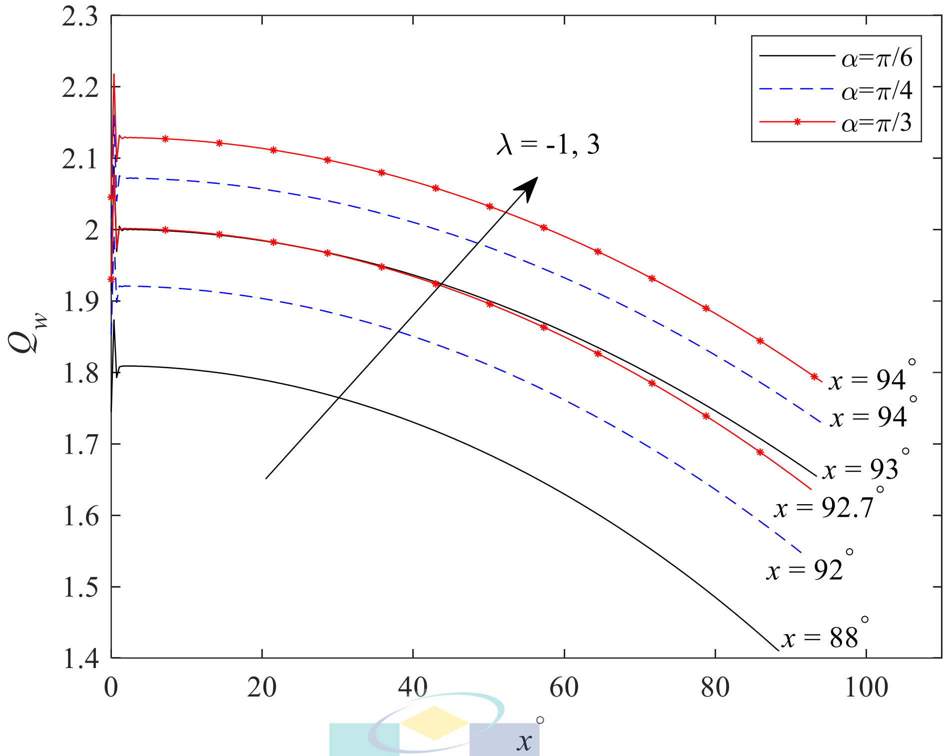

Figure 6.20 Variation of Q_w for various values of α and λ at $K = K_1 = M = 0.01$

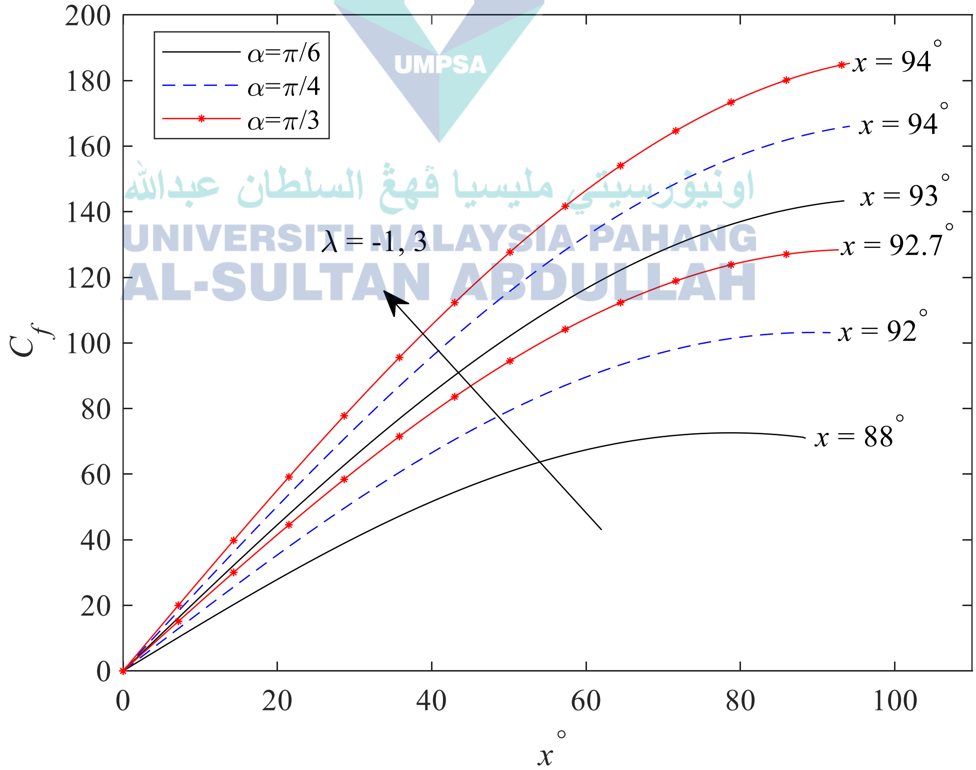

Figure 6.21 Variation of C_f for various values of α and λ at $K = K_1 = M = 0.01$

6.4 Summary

In this chapter, the numerical solution of the mixed convection boundary layer flow of viscoelastic micropolar fluid over a circular cylinder has been evaluated. The parameters that were varied to identify their effect on the flow are similar as the previous problems with an additional mixed convection parameter, λ. The formulation for the problem is displayed in Table 6.7 while the outcome of this investigation is summarized in Table 6.6 along with the following statements:

i. Increasing the values of all parameters, K, K_1, M, α and λ can delay boundary layer separation.

ii. As λ gets reasonably large, the inclined angle no longer has any effect on the boundary layer separation.

iii. Instability is observed for the graphs of heat transfer at the stagnation point of the circular cylinder.

Table 6.6 Summary of present results for mixed convection boundary layer flow of viscoelastic micropolar on a horizontal circular cylinder

Distribution	$K\uparrow$	$K_1\uparrow$	$M\uparrow$	$\alpha\uparrow$	$\lambda\uparrow$
f'	$\downarrow$	$\downarrow$	$\uparrow$	$\uparrow$	$\uparrow$
h	$\uparrow$	$\uparrow\downarrow$	$\downarrow$	$\downarrow$	$\downarrow$
θ	$\uparrow$	$\uparrow$	$\downarrow$	$\downarrow$	$\downarrow$
C_f	$\downarrow$	$\uparrow$	$\uparrow$	$\uparrow$	$\uparrow$
Q_w	$\downarrow$	$\uparrow$	$\uparrow$	$\uparrow$	$\uparrow$

$\uparrow$ increase $\downarrow$ decrease

Table 6.7 Solution procedure for mathematical formulation for mixed convection boundary layer flow of viscoelastic micropolar on a horizontal circular cylinder

Steps	Equation
Governing equations	$\frac{\partial u}{\partial x}+\frac{\partial u}{\partial y}=0$ $u\frac{\partial u}{\partial x}+v\frac{\partial u}{\partial y}=u_e\frac{\partial u_e}{\partial x}+(1+K_1)\frac{\partial^2 u}{\partial y^2}+\lambda\theta\sin x+K_1\frac{\partial H}{\partial y}$ $-M\left(u-u_e\right)\sin^2\alpha+K\left(\frac{\partial}{\partial x}\left(u\frac{\partial^2 u}{\partial y^2}\right)+v\frac{\partial^3 u}{\partial y^3}-\frac{\partial u}{\partial y}\frac{\partial^2 u}{\partial x\partial y}\right)$ $u\frac{\partial H}{\partial x}+v\frac{\partial H}{\partial y}=-K_1\left(2H+\frac{\partial u}{\partial y}\right)+\left(1+\frac{K_1}{2}\right)\frac{\partial^2 H}{\partial y^2}$ $u\frac{\partial \theta}{\partial x}+v\frac{\partial \theta}{\partial y}=\frac{1}{\Pr}\frac{\partial^2 \theta}{\partial y^2}$
Boundary conditions	$u(0)=v(0)=0,\quad \theta(0)=1,\quad H(0)=-\frac{1}{2}\frac{\partial u}{\partial y}$ $u\to u_e(x),\quad \frac{\partial u}{\partial y}\to 0,\quad \theta\to 0,\quad H\to 0\quad \text{as}\quad y\to\infty$
Non-similarity transformation	$\psi=xf(x,y),\ H=xh(x,y),\ \theta=\theta(x,y)$
Ordinary differential equations	At stagnation point: $(1+K_1)f'''+f\,f''-f'^2+1+\lambda\theta+K\left(2f'f'''-f\,f^{iv}-f''^2\right)$ $+K_1h'-M\left(f'-1\right)\sin^2\alpha=0$ $\left(1+\frac{K_1}{2}\right)h''+f\,h'-f'h-K_1\left(2h+f''\right)=0$ $\frac{1}{\Pr}\theta''+f\,\theta'=0$
Transformed boundary conditions	$f(0)=f'(0)=0,\quad \theta(0)=1,\quad h(0)=-\frac{1}{2}f''(0)$ $f'\to 1,\quad f''\to 0,\quad \theta\to 0,\quad h=0\quad \text{as}\ y\to\infty$

CHAPTER 7

FREE CONVECTION BOUNDARY LAYER FLOW OF VISCOELASTIC MICROPOLAR FLUID OVER A SPHERE WITH ALIGNED MHD EFFECT

7.1 Introduction

The flow of viscoelastic micropolar fluid over a horizontal circular cylinder has been the subject of the previous three chapters. In Chapters 7 and 8, the sphere in solid form that will serve as the pivotal bluff body are described. It is worth highlighting that a geometrical difference between circular cylinder and sphere exists. Despite the similarity between the schematic diagrams in Figures 4.1 and 7.1, there is an additional variable, $\bar{r}$ being considered for the sphere, which represents the radial distance between any point on the sphere surface and the centre. While the boundary layer flow of circular cylinder is two-dimensional, the flow on the sphere is three-dimensional as it occurs in all directions on the curved surface. For circular cylinder, the flow travels parallel to the axis at every point. In addition, the stagnation point of a sphere is at the front centre of the sphere and as for the circular cylinder, there are definite front and rear stagnation points.

Building upon the groundbreaking research of Huang and Chen (1987), this problem extends the analysis of the micropolar model by Nazar and Amin (2002). The formulation of the problem is similar to the previous chapters where the dimensional PDEs are transformed to dimensionless form by employing the non-dimensional and non-similarity transformation. Then, the carved-out equations are solved using the Keller-box method to identify the distinguished characteristics of the flow from the velocity, temperature, microrotation and magnetic profiles, as well as the skin friction coefficient and heat transfer at assorted parameters.

7.2 Mathematical Formulation

The schematic diagram for free convection flow of viscoelastic micropolar fluid over a sphere is illustrated in Figure 7.1.

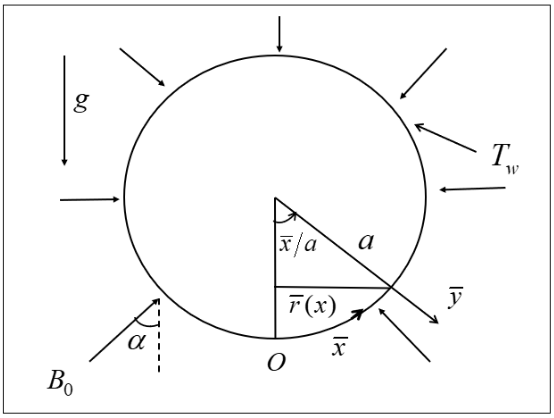

Figure 7.1 Schematic diagram for free convection boundary layer flow of viscoelastic micropolar fluid over sphere.

The dimensional momentum, angular momentum and energy equations are as written in Equations (5.1), (4.2) and (3.79), respectively, while the continuity equation is:

$$\frac{\partial}{\partial x}(\bar{r}\,\bar{u})+\frac{\partial}{\partial y}(\bar{r}\,\bar{v})=0 \qquad 7.1$$

where $\bar{r}$ is the radial distance from the centre of the sphere to a point in the fluid, defined as $\bar{r}(\bar{x})=a\sin(\bar{x}/a)$. The governing equations associated with this problem are subjected to the boundary conditions in Equation (5.2). Then, the same set of non-dimensional variables as listed in Equation (5.3), with an additional variable, $r=\bar{r}/a$ are substituted into the equations to retrieve the dimensionless form of the governing equations. As a result, Equation (7.1) is transformed to:

$$\frac{\partial}{\partial x}(r\,u)+\frac{\partial}{\partial y}(r\,v)=0 \qquad 7.2$$

while the dimensionless momentum, angular momentum and energy equations are transformed to Equations (5.4), (4.10) and (5.5) bounded by the conditions in Equation

(5.6). Following Nabwey et al. (2022), the non-similarity transformation variables that are befitting for this problem are:

$$\psi = xr(x)\,f(x,y), \qquad H = xh(x,y), \qquad \theta = \theta(x,y) \tag{7.3}$$

with the stream function, ψ defined as

$$u = \frac{1}{r}\frac{\partial \psi}{\partial y}, \quad v = -\frac{1}{r}\frac{\partial \psi}{\partial x} \tag{7.4}$$

Equation (7.2) is inevitably satisfied by the transformation variables while the remaining equations are reduced to the subsequent non-linear ODEs, subjected to the boundary conditions in Equation (5.11).

$$\begin{aligned}
&(1+K_1)\frac{\partial^3 f}{\partial y^3} - \left(\frac{\partial f}{\partial y}\right)^2 + \left(1 + x\frac{\cos x}{\sin x}\right) f \frac{\partial^2 f}{\partial y^2} + \theta\frac{\sin x}{x} + K_1\frac{\partial h}{\partial y} - M\frac{\partial f}{\partial y}\sin^2\alpha \\
&+K\left[2\frac{\partial f}{\partial y}\frac{\partial^3 f}{\partial y^3} - \left(1 + x\frac{\cos x}{\sin x}\right)\left(f\frac{\partial^4 f}{\partial y^4} + \left(\frac{\partial^2 f}{\partial y^2}\right)^2\right)\right] \\
&= Kx\left[\frac{\partial f}{\partial x}\frac{\partial^4 f}{\partial y^4} - \frac{\partial^2 f}{\partial x\partial y}\frac{\partial^3 f}{\partial y^3} - \frac{\partial f}{\partial y}\frac{\partial^4 f}{\partial x\partial y^3} + \frac{\partial^2 f}{\partial y^2}\frac{\partial^3 f}{\partial x\partial y^2}\right] + x\left(\frac{\partial f}{\partial y}\frac{\partial^2 f}{\partial x\partial y} - \frac{\partial f}{\partial x}\frac{\partial^2 f}{\partial y^2}\right)
\end{aligned} \tag{7.5}$$

$$\frac{1}{\Pr}\frac{\partial^2\theta}{\partial y^2} + \left(1 + x\frac{\cos x}{\sin x}\right) f \frac{\partial \theta}{\partial y} = x\left(\frac{\partial f}{\partial y}\frac{\partial \theta}{\partial x} - \frac{\partial f}{\partial x}\frac{\partial \theta}{\partial y}\right) \tag{7.6}$$

$$\left(1 + \frac{K_1}{2}\right)\frac{\partial^2 h}{\partial y^2} + \left(1 + x\frac{\cos x}{\sin x}\right) f \frac{\partial h}{\partial y} - \frac{\partial f}{\partial y}h - K_1\left(2h + \frac{\partial^2 f}{\partial y^2}\right) = x\left(\frac{\partial f}{\partial y}\frac{\partial h}{\partial x} - \frac{\partial f}{\partial x}\frac{\partial h}{\partial y}\right) \tag{7.7}$$

Near the lower stagnation point where $x \approx 0,$ Equations (7.5) to (7.7) are reduced to the succeeding ordinary differential equations, bounded by the conditions in Equation (5.14).

$$(1+K_1)\,f''' - f'^2 + 2ff'' + \theta + K_1 h' - Mf'\sin^2\alpha + 2K\left(f'f''' - ff^{iv} - f''^2\right) = 0 \tag{7.8}$$

$$\frac{1}{\Pr}\theta'' + 2f\theta' = 0 \tag{7.9}$$

$$\left(1+\frac{K_1}{2}\right)h'' + 2f\,h' - f'h - K_1\left(2h + f''\right) = 0 \qquad 7.10$$

The physical quantities of principal interest in terms of skin friction coefficient and heat transfer remain the same as in Equations (4.23) and (5.15).

7.3 Results and Discussion

The non-linear PDEs in Equations (7.8) to (7.10) bounded by the conditions in Equation (5.14) are solved via Keller-box method, coded in the Fortran language before the figures are plotted using MATLAB. The results are analysed and discussed for diverse values of parameters K, K_1, M and α to provide further understanding on the constraining force that each parameter possesses on the behaviour of the flow. Prior to the evaluation, validation with previous published results listed in Table 7.1 had been conducted and the similarity between the figures are verified.

The results are compared to another four models representing medley of fluids for which the degenerate case of their momentum equations and the accompanying boundary conditions would reduce exactly to the same equation as this problem when $K = K_1 = M = 0$. The initial comparison are done with the results from Huang and Chen (1987), Nazar and Amin (2002) as well as Mohamed et al. (2019) who also applied the Keller-box method to solve their free convection problem on viscous, micropolar and nanofluid, respectively. The heat transfer coefficient at various positions on the sphere from the studies are displayed in Table 7.2, all demonstrating high degree of consistency.

Further validation is done by comparing the heat transfer coefficient at $K_1 = 1$ and $K_1 = 2$ when the other parameters are set to 0 with the micropolar fluid models by Nazar and Amin (2002) as well as Bég et al. (2011) who also included the Soret and Dufour effects in their model. The figures shown in Table 7.3 indicate reasonable agreement to support the reliability of the present result. Moreover, from the table it can be seen that that moving forward from the front stagnation point, Q_w decreases and higher K_1 also reduces the heat transfer coefficient. After the results are verified, values of $f''(0)$ and Q_w at diverse values of parameters involved in this problem are generated as in Table

7.4. The table reveals that both values are suppressed by the increase in value of all parameters when the others are held constant.

From the result, parameters K and K_1 have similar effect on the profiles and coefficients in general, except for the skin friction coefficient. When K_1 and C_f are positively correlated, K and C_f showed contradict behaviour as shown in Figures 7.6 and 7.11, respectively. Higher K indicates higher elasticity which in turn could reduce the shear stress hence, reducing the skin friction on the boundary layer. The surge of K_1, however added more freedom for the rotation near that could increase momentum changes on the wall as well as the skin friction coefficient. The same pattern can be observed from the velocity profiles of K and K_1 in Figures 7.2 and 7.7 where f' would decrease to a certain maximum value near the wall before it increases and approaches to 0. Prior to the convergence, there is a turning point where the relationship between K and K_1 with the velocity changes from being inversely proportional to being positively correlated.

It is also shown in Figures 7.5 and 7.10 that rising K and K_1 reduce heat transfer at the surface. However, the resistant nature of the fluid enhanced by increasing K and K_1 could cause the fluid motion to resist thermal conduction hence causing heat to build up on the surface thus increasing the temperature of the wall. From the microrotation profiles, h increases when K and K_1 escalate before it reaches the turning point where the effect of the parameter is barely significant as displayed in Figures 7.4 and 7.9.

Apparently, from Figures 7.12 to 7.16, it can be observed that M and α have the same effect on the free convection boundary layer flow. Since increasing M indicates rising the strength of magnetic field, therefore, in this case, it implies that the strength of the magnetic field and the aligned angles are proportionate. As expected, the parameters have retarding effect on f' as the profile decreases when the magnetic field becomes stronger. Conversely, the magnetic effect fuelled the microrotation that causes h to elevate. The energized rotation of the microelements undoubtedly could be one of the heat generator sources at the wall and as a result, θ increases.

Meanwhile, as the magnetic field opposes and slows down the velocity, C_f also declines which implies reduced of drag force on the surface in contact with the fluid when the magnetic field intensified. The same behaviour can be observed for Q_w in Figure 7.15. The decrease of Q_w could be caused by several factors. For instance, slower fluid motion means less efficient convective heat transfer from the surface to the fluid. Besides that, the magnetic field may cause the boundary layer to thicken, creating a larger insulating layer that impedes heat transfer and lastly, the induced currents in the fluid can lead to Joule heating, which might counteract with some of the cooling effects, further complicating the heat transfer dynamics.

As opposed to the analysis in Chapter 5, where the boundary layer separation is prominent, for the problem of free convection over sphere, the separation is not affected by the parameters. Unlike the horizontal circular cylinder, there is no definite rear stagnation point, so the flow remains intact until further back of the sphere. Similar results in free convection study have been recorded by Alkasasbeh (2022) where the separation of the micropolar ferrofluid flow only occurred at $x \approx 120^{\circ}$. In this problem, the separation occurred at $x = 116^{\circ}$ despite the changes in values of the parameters. The fact that separation occurs at a consistent angle regardless of parameter changes suggests that for this problem the separation is primarily governed by the geometry rather than fluid properties.

Table 7.1 The momentum equation and boundary conditions of problems involved for result validation.

Author	Model
Present	$(1+K_1)f''' - f'^2 + 2ff'' + \theta + K_1 h' - Mf' \sin^2\alpha$ $+2K\left(f' f''' - ff^{iv} - f''^2\right) = 0$ with boundary conditions $f(0) = f'(0) = 0,\ \theta(0) = 1,\ h(0) = -\frac{1}{2}f''(0)$ $f' \to 0,\ f'' \to 0,\ \theta \to 0,\ h \to 0,$ as $y \to \infty$
Huang and Chen (1987)	$f''' - f'^2 + \left[1 + \tilde{\alpha}(X) + \tilde{\beta}(X)\right]ff'' + \frac{\sin X}{\xi}\theta = \xi\left(f'\frac{\partial f'}{\partial \xi} - f''\frac{\partial f}{\partial \xi}\right)$ with boundary conditions $f'(0) = 0,\ \theta(0) = 1$ $f' \to 0,\ \theta \to 0,$ as $y \to \infty$
Nazar and Amin (2002)	$(1+K_1)f''' + 2ff'' - f'^2 + \theta + K_1 h' = 0$ with boundary conditions $f(0) = f'(0) = 0,\ \theta(0) = 1,\ h(0) = -\frac{1}{2}f''(0)$ $f' \to 0,\ \theta \to 0,\ h \to 0,$ as $y \to \infty$
Bég et all (2011)	$(1+K_1)f''' + 2ff'' - f'^2 + \theta + N\phi + K_1 h' = 0$ with boundary conditions $f(0) = f'(0) = 0,\ \theta(0) = 1,\ h(0) = -\frac{1}{2}f''(0),\ \phi(0) = 1$ $f' \to 0,\ \theta \to 0,\ h \to 0,\ \phi \to 1$ as $y \to \infty$
Mohamed et al (2019)	$f''' + 2ff'' - f'^2 + \theta + \chi\phi = 0$ with boundary conditions $f(0) = f'(0) = 0,\ \theta(0) = 1,\ h(0) = -\frac{1}{2}f''(0)$ $f' \to 0,\ \theta \to 0,\ h \to 0$ as $y \to \infty$

Table 7.2 Comparison values of Q_w at different x when Pr=0.7

x	$K_1 = 1$			$K_1 = 2$		
	Nazar and Amin (2002)	**Bég et al (2011)**	**Present**	**Nazar and Amin (2002)**	**Bég et al (2011)**	**Present**
0°	0.4166	0.4165	0.4309	0.3927	0.393	0.4114
10°	0.4156	0.4154	0.4299	0.3917	0.3921	0.4105
20°	0.4128	0.4126	0.4270	0.3891	0.3894	0.4077
30°	0.408	0.4078	0.4215	0.3847	0.385	0.4024
40°	0.4014	0.4014	0.4152	0.3786	0.3789	0.3964
50°	0.3928	0.3925	0.4063	0.3705	0.3709	0.3879
60°	0.3822	0.3818	0.3952	0.361	0.3611	0.3773
70°	0.3696	0.3695	0.3824	0.3491	0.3493	0.3652
80°	0.3547	0.3545	0.3669	0.3353	0.3355	0.3504
90°	0.3374	0.3369	0.3489	0.3192	0.3195	0.3332
100°	-	-	0.3282	-	-	0.3136
110°	-	-	0.3045	-	-	0.2911
120°	-	-	0.2775	-	-	0.2655

Table 7.3 Values of Q_w for various x at $K_1 = 1$ and $K_1 = 2$ when Pr = 0.7

x	**Huang and Chen (1987)**	**Nazar and Amin (2002)**	**Mohamed et al (2019)**	**Present Result**
0	0.4574	0.4576	0.4576	0.4576
$\pi/18$	0.4563	0.4565	0.4565	0.4566
$\pi/9$	0.4532	0.4533	0.4533	0.4535
$\pi/6$	0.4480	0.4480	0.4480	0.4482
$2\pi/9$	0.4407	0.4405	0.4406	0.4408
$5\pi/18$	0.4312	0.4308	0.4310	0.4312
$\pi/3$	0.4194	0.4198	0.4195	0.4198
$7\pi/18$	0.4053	0.4046	0.4053	0.4051
$4\pi/9$	0.3886	0.3879	0.3886	0.3890
$\pi/2$	0.3694	0.3684	0.3692	0.3689
$5\pi/9$	-	-	0.3469	0.3474
$11\pi/18$	-	-	0.3215	0.3221
$2\pi/3$	-	-	0.2925	0.2931
$13\pi/18$	-	-	0.2594	0.2601

Table 7.4 Values of $f''(0)$ and $-\theta'(0)$ for various values of K, K_1, M and α at $\Pr = 21$

K	***K*₁**	**M**	***α***	***f*″(0)**	**-*θ*′(0)**
1	1	1	$\pi/6$	0.241162	1.112736
2	1	1	$\pi/6$	0.222639	1.077637
3	1	1	$\pi/6$	0.208610	1.050144
4	1	1	$\pi/6$	0.197393	1.027543
5	1	1	$\pi/6$	0.188100	1.008360
1	1.5	1	$\pi/6$	0.218445	1.083598
1	2	1	$\pi/6$	0.200540	1.057798
1	2.5	1	$\pi/6$	0.185903	1.034715
1	3	1	$\pi/6$	0.173637	1.013877
1	3.5	1	$\pi/6$	0.163163	0.994920
1	1	2	$\pi/6$	0.234873	1.091056
1	1	3	$\pi/6$	0.229741	1.073139
1	1	4	$\pi/6$	0.225339	1.057630
1	1	5	$\pi/6$	0.221446	1.043803
1	1	6	$\pi/6$	0.217933	1.031232
1	1	1	$\pi/4$	0.234873	1.091056
1	1	1	$\pi/3$	0.229741	1.073139
1	1	1	$\pi/2$	0.225339	1.057630

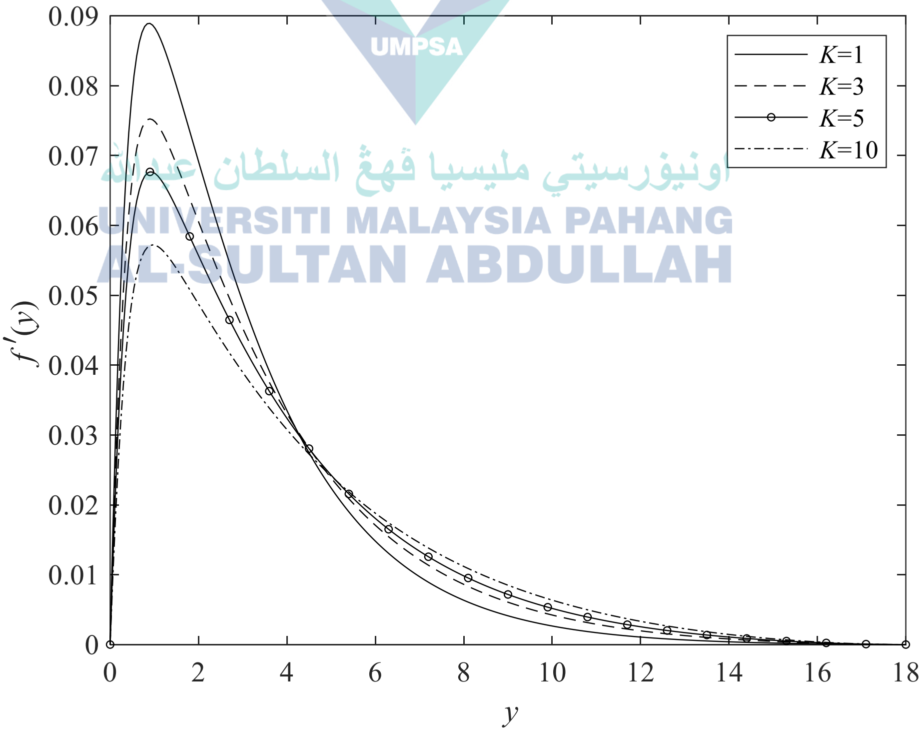

Figure 7.2 Variation of $f'(y)$ for various values of K at $K_1 = M = 0.5$ and $\alpha = \pi/6$

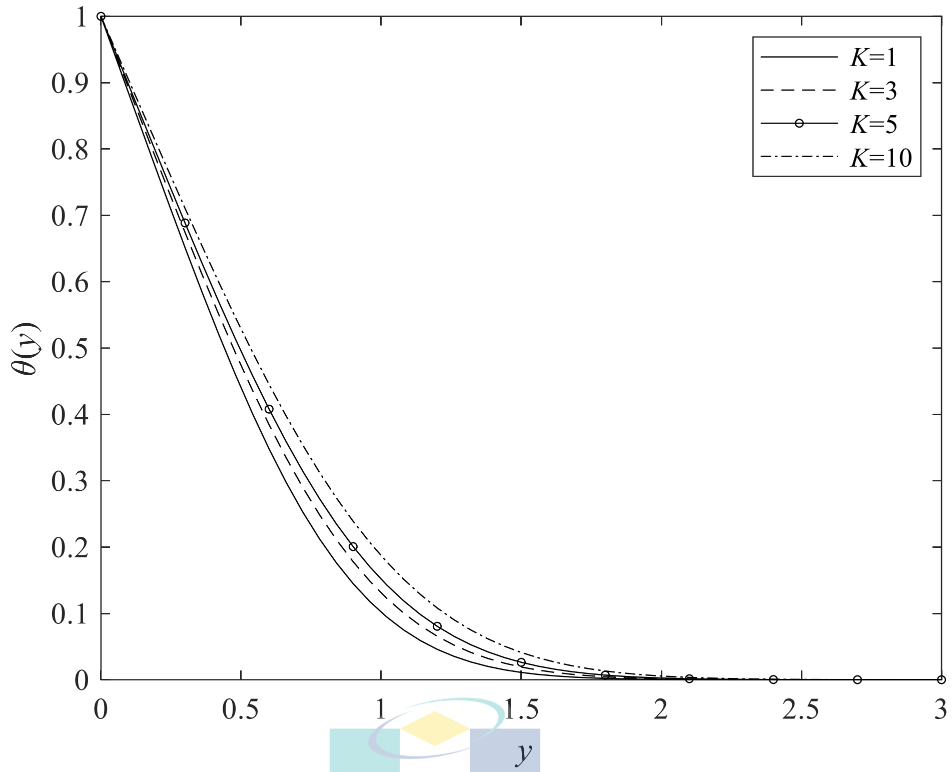

Figure 7.3 Variation of $\theta(y)$ for various values of K at $K_1 = M = 0.5$ and $\alpha = \pi/6$

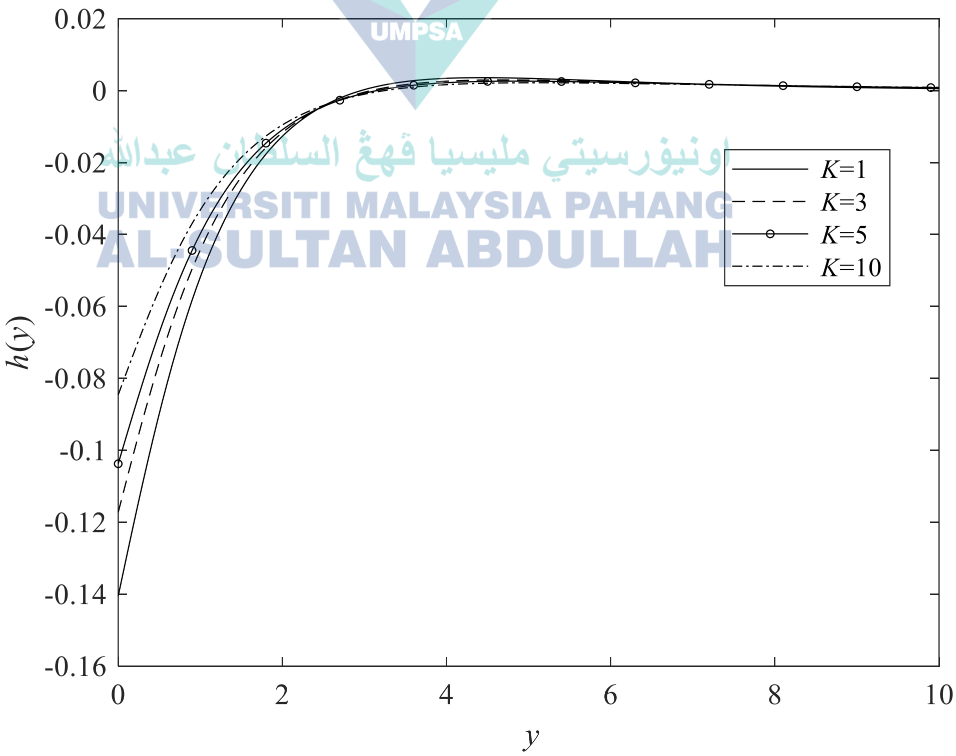

Figure 7.4 Variation of $h(y)$ for various values of K at $K_1 = M = 0.5$ and $\alpha = \pi/6$

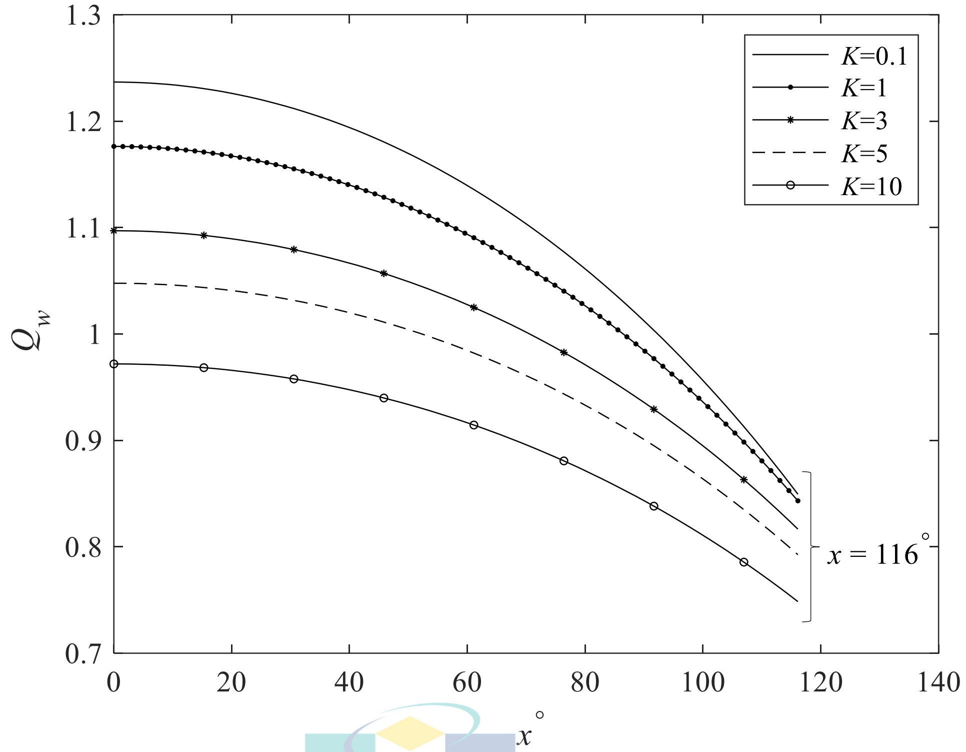

Figure 7.5 Variation of Q_w for various values of K at $K_1 = M = 0.5$ and $\alpha = \pi/6$

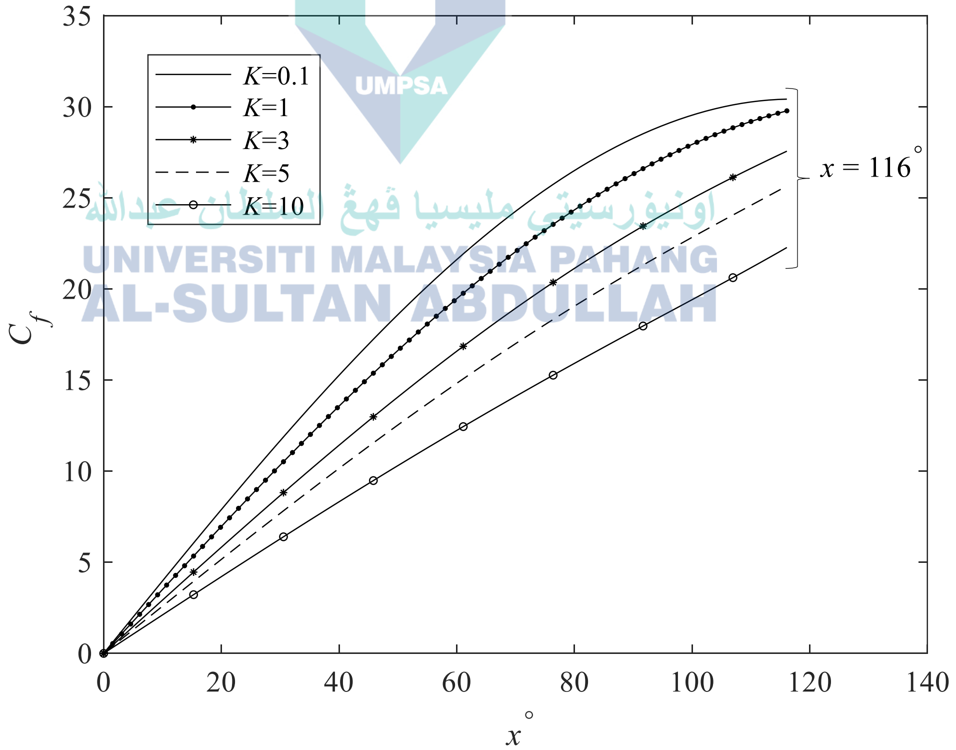

Figure 7.6 Variation of C_f for various values of K at $K_1 = M = 0.5$ and $\alpha = \pi/6$

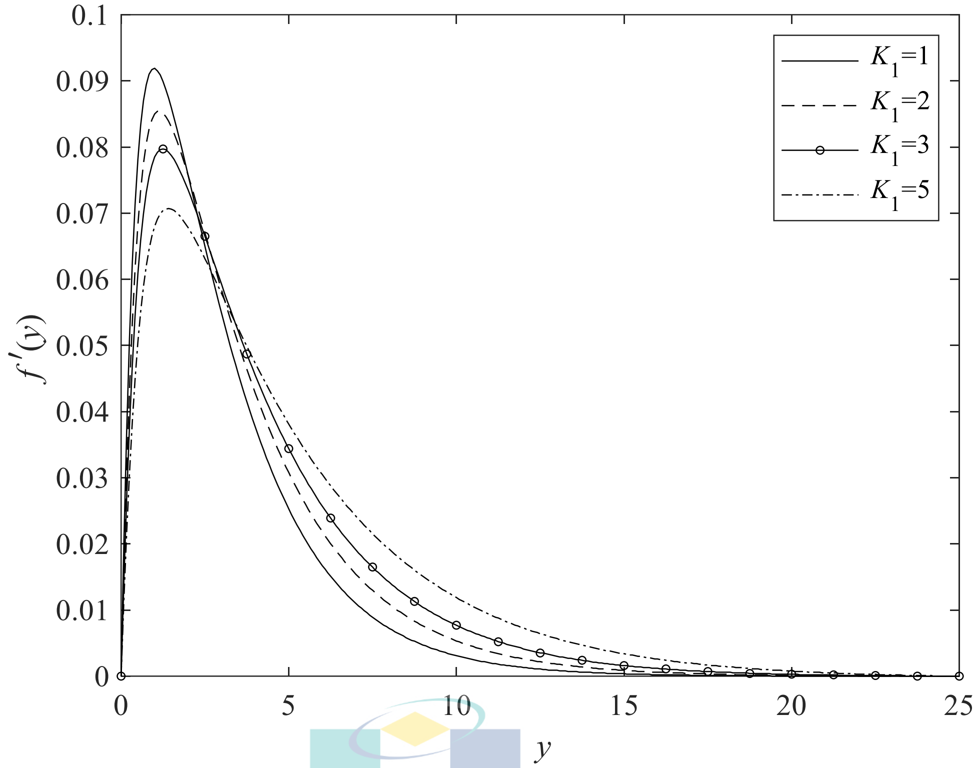

Figure 7.7 Variation of $f'(y)$ for various values of K_1 at $K = M = 0.5$ and $\alpha = \pi/6$

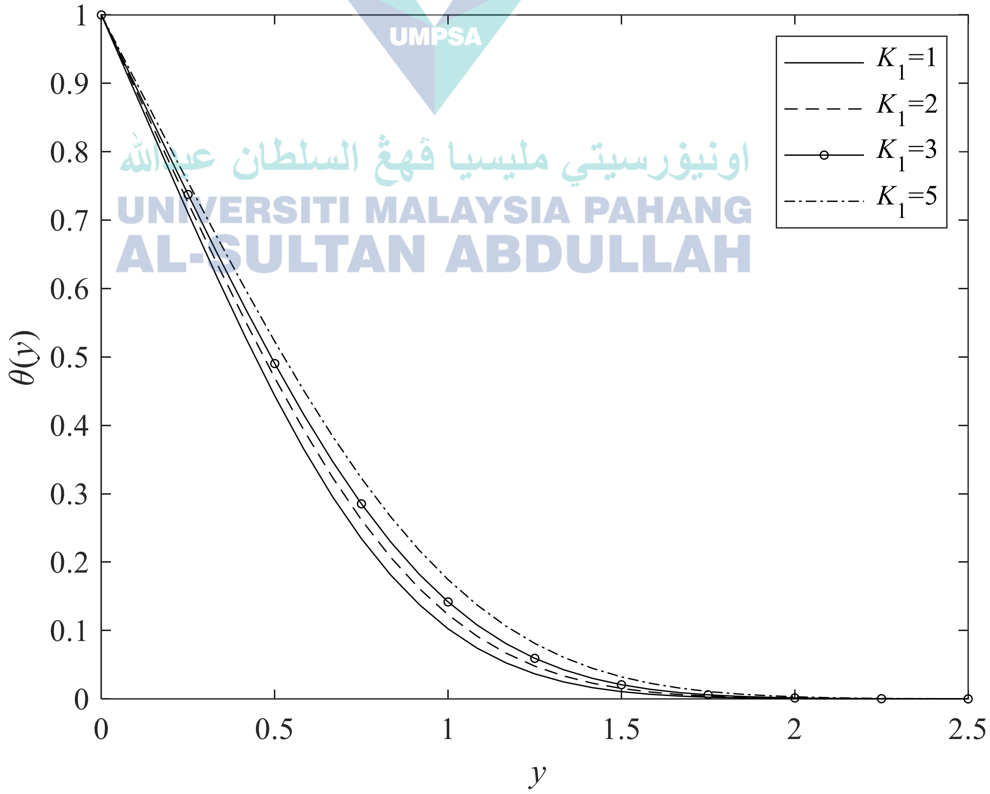

Figure 7.8 Variation of $\theta(y)$ for various values of K_1 at $K = M = 0.5$ and $\alpha = \pi/6$

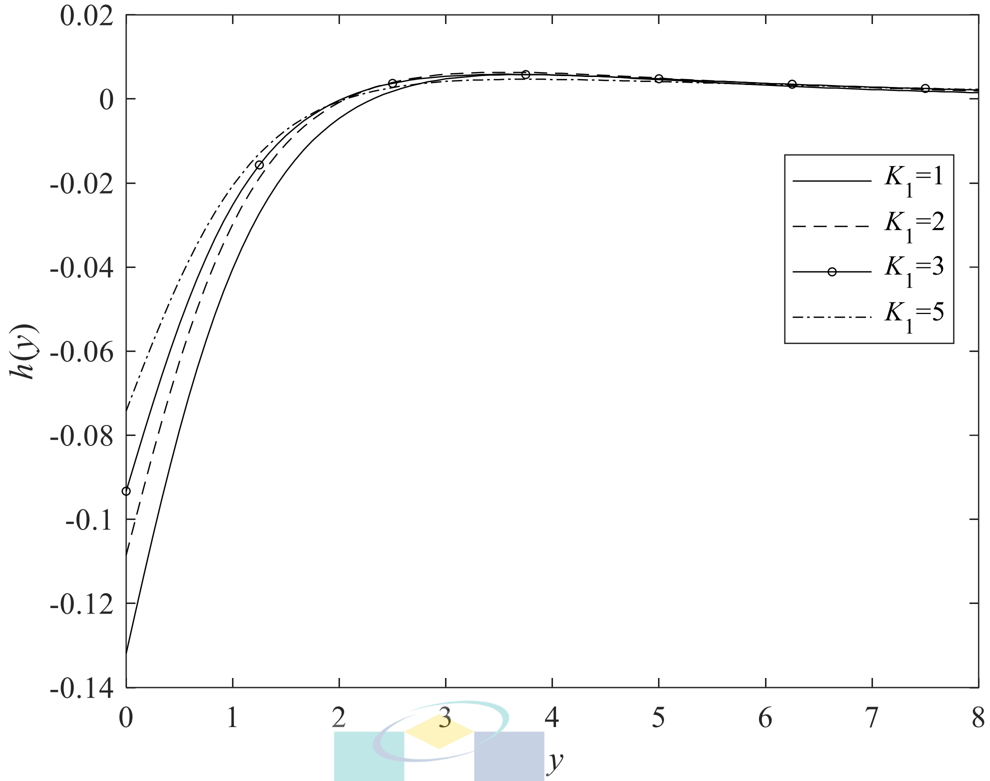

Figure 7.9 Variation of $h(y)$ for various values of K_1 at $K = M = 0.5$ and $\alpha = \pi/6$

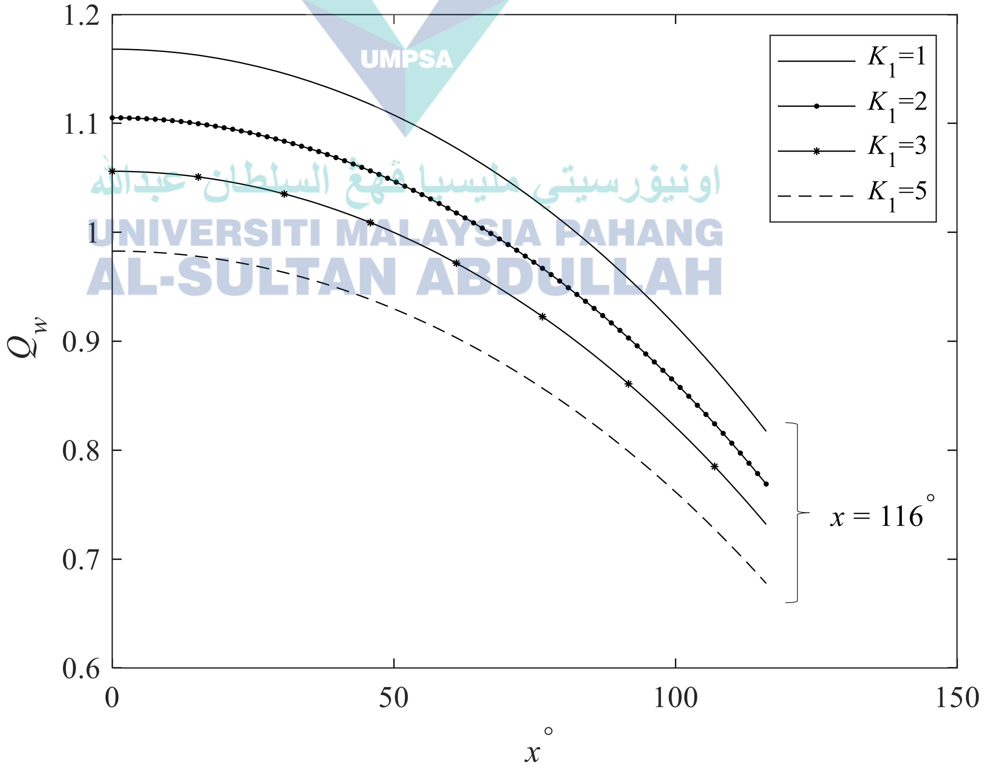

Figure 7.10 Variation of Q_w for various values of K_1 at $K = M = 0.5$ and $\alpha = \pi/6$

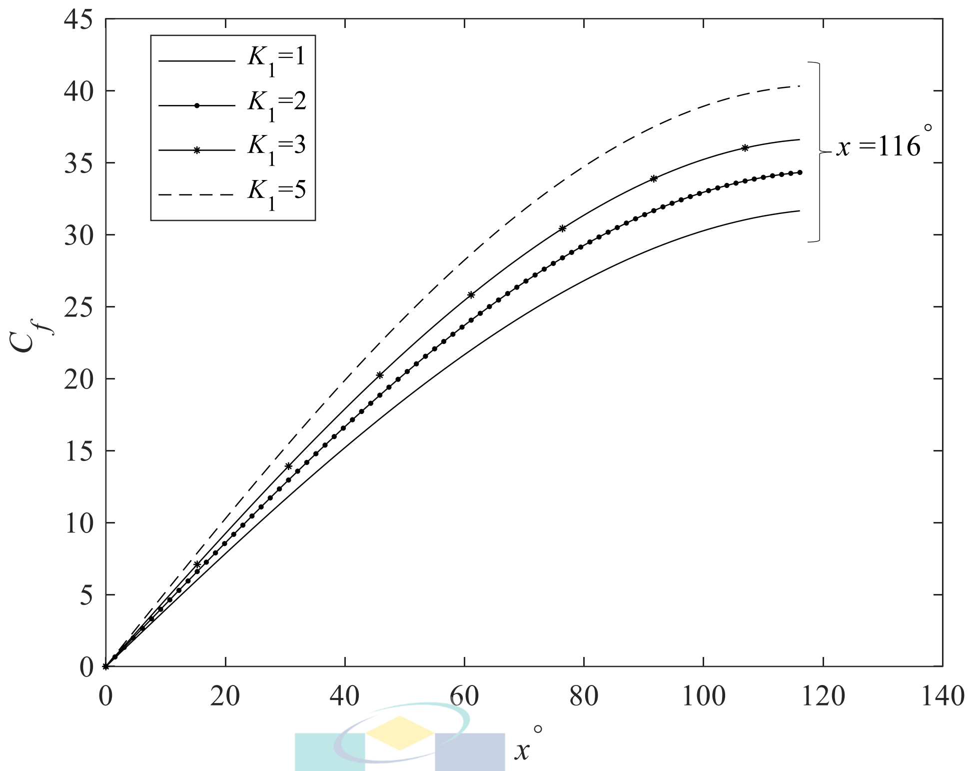

Figure 7.11 Variation of C_f for various values of K_1 at $K = M = 0.5$ and $\alpha = \pi/6$

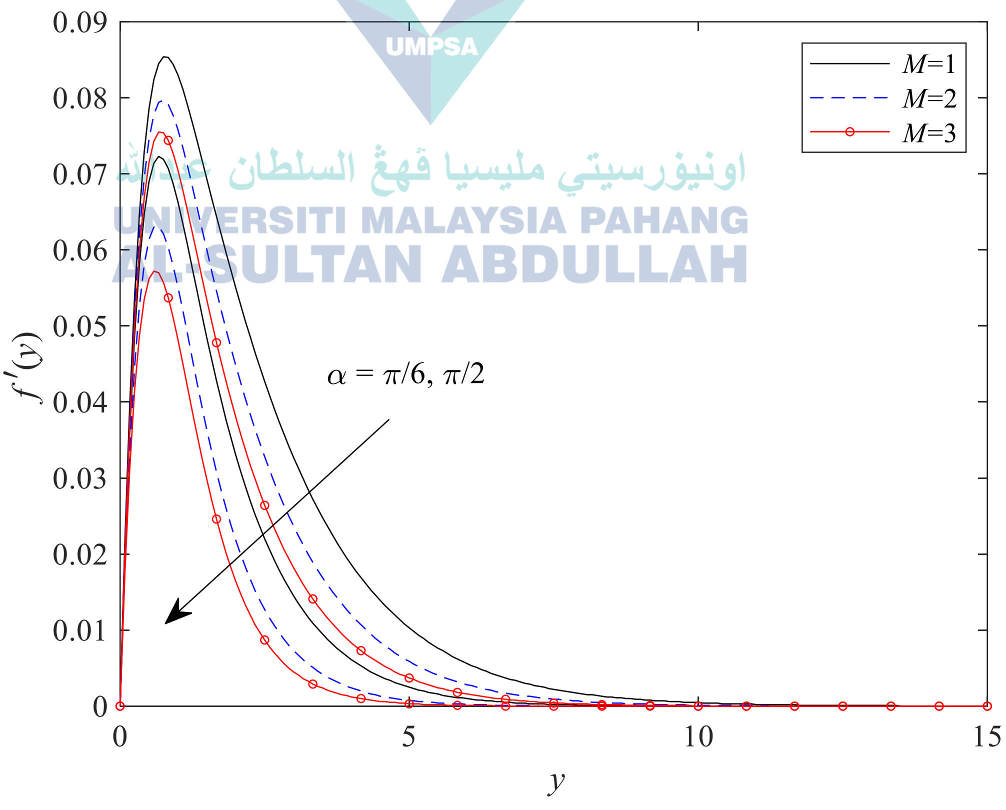

Figure 7.12 Variation of $f'(y)$ for various values of M and α at $K = K_1 = 0.5$

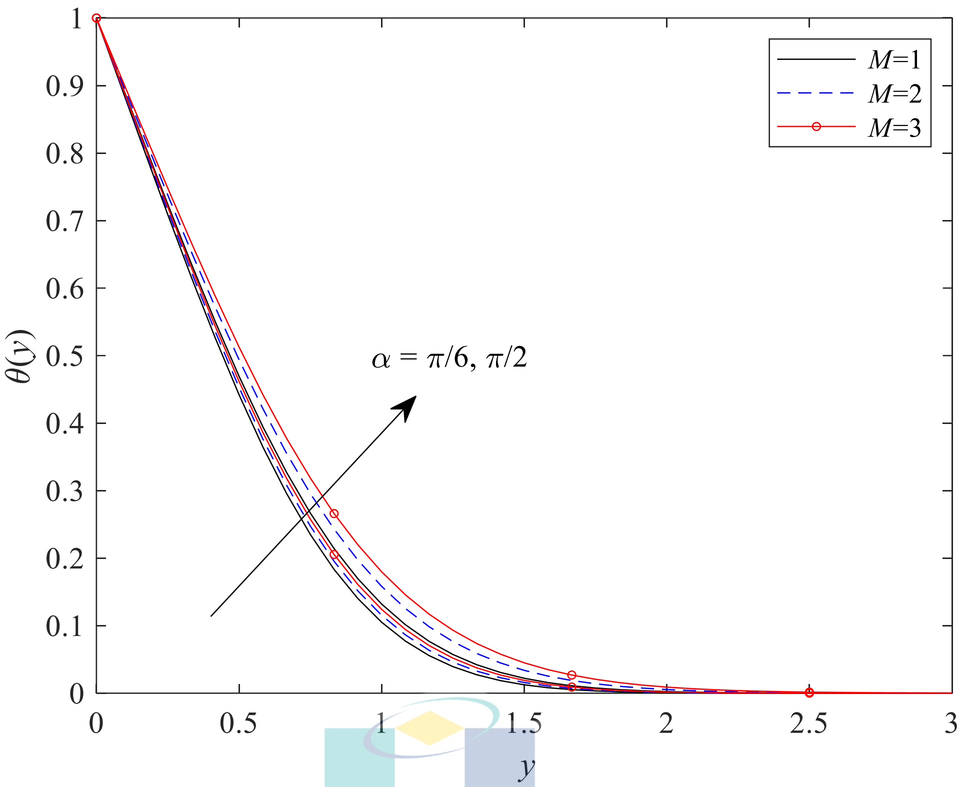

Figure 7.13 Variation of $\theta(y)$ for various values of M and α at $K = K_1 = 0.5$

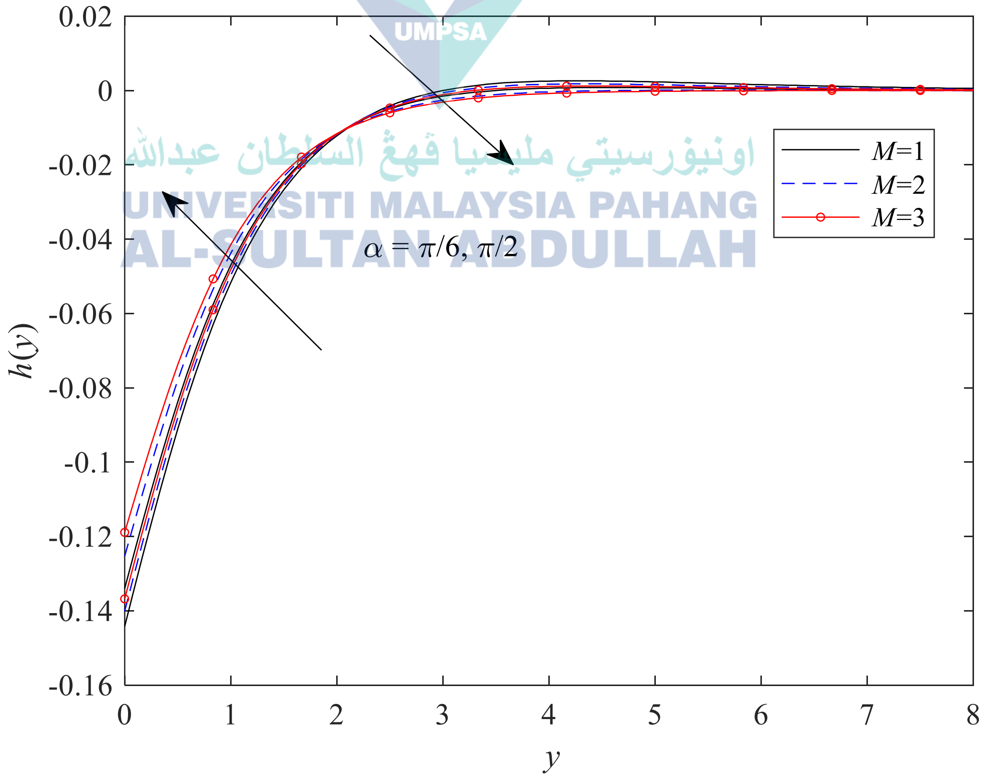

Figure 7.14 Variation of $h(y)$ for various values of M and α at $K = K_1 = 0.5$

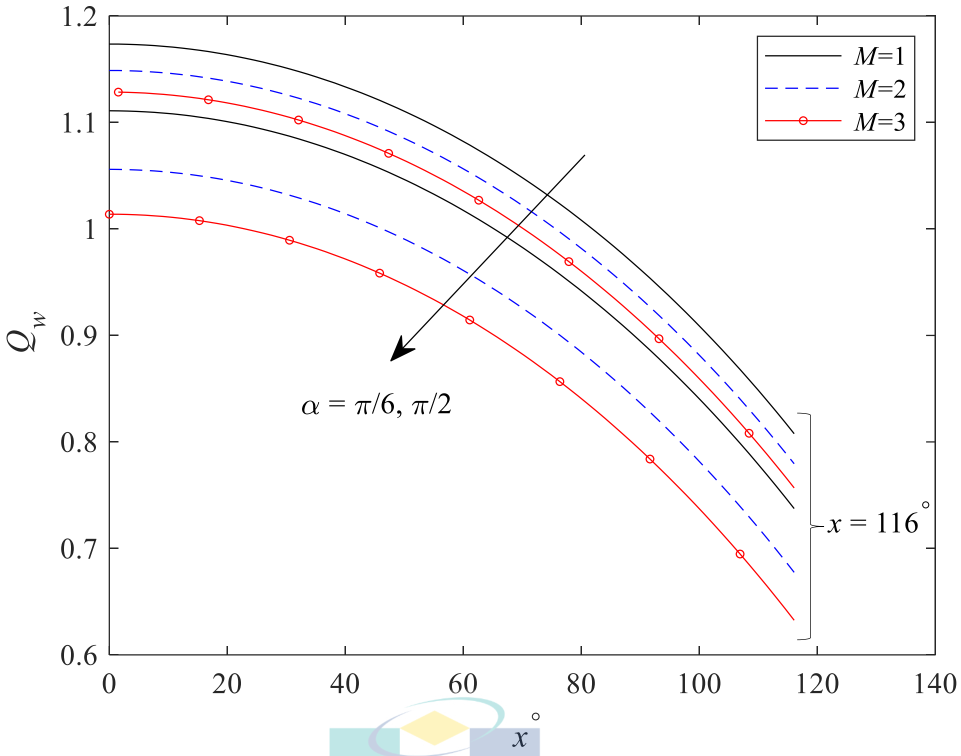

Figure 7.15 Variation of Q_w for various values of M and α at $K = K_1 = 0.5$

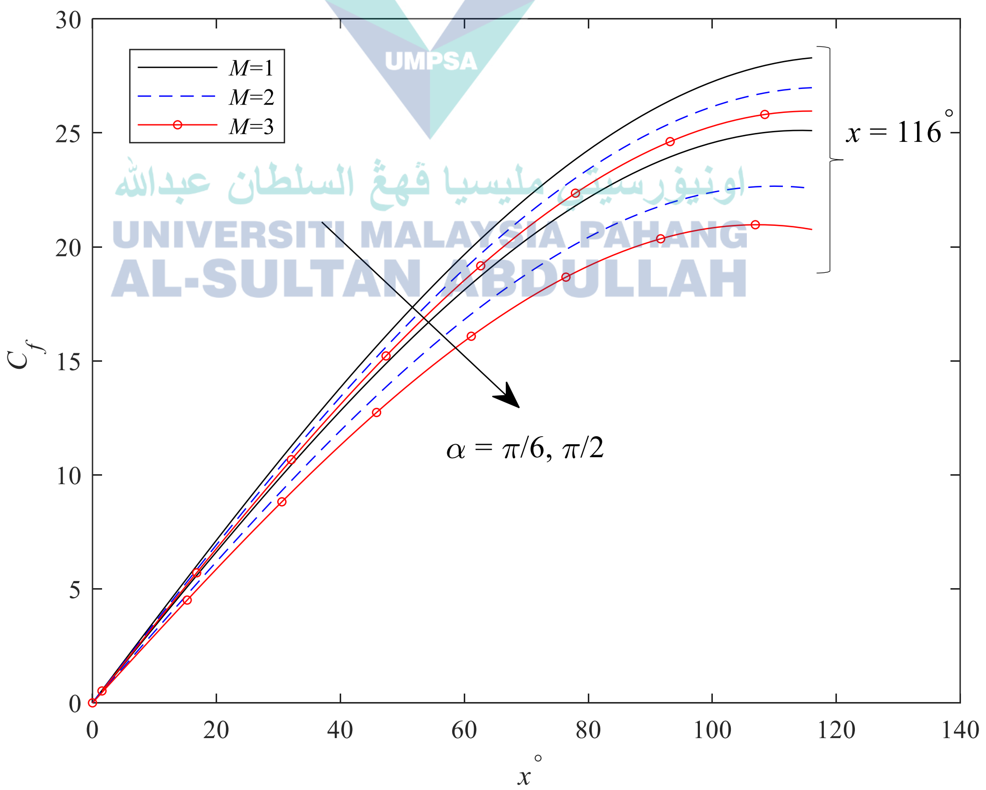

Figure 7.16 Variation of C_f for various values of M and α at $K = K_1 = 0.5$

7.4 Summary

The evaluation of the numerical solution for free convection boundary layer flow of viscoelastic micropolar fluid over a sphere has been presented in this chapter. The formulated governing equation for this problem is as displayed in Table 7.6. The same parameters as discussed in Chapter 5 have been analysed over different geometries and the observed outcomes are follows:

i. The velocity profile is enhanced by M and α where it decreases then increases for K and K_1.

ii. The microrotation are boosted by the rise in values of all parameters before the deflection point where the pattern reversed.

iii. Temperature profile is positively correlated to all parameters.

iv. All parameters are inversely proportional to the heat transfer and skin friction coefficient except for K_1 and heat transfer coefficient that are directly proportional.

v. All parameters have no effect on boundary layer separation.

Table 7.5 Summary of present results for mixed convection boundary layer flow of viscoelastic micropolar on a sphere

Distribution	$K\uparrow$	$K_1\uparrow$	$M\uparrow$	$\alpha\uparrow$
f'	$\downarrow\uparrow$	$\downarrow\uparrow$	$\downarrow$	$\downarrow$
h	$\uparrow\downarrow$	$\uparrow\downarrow$	$\uparrow\downarrow$	$\uparrow\downarrow$
θ	$\uparrow$	$\uparrow$	$\uparrow$	$\uparrow$
C_f	$\downarrow$	$\uparrow$	$\downarrow$	$\downarrow$
Q_w	$\downarrow$	$\downarrow$	$\downarrow$	$\downarrow$

$\uparrow$ increase $\downarrow$ decrease

Table 7.6 Summary of solution procedure for mathematical formulation for free convection boundary layer flow of viscoelastic micropolar on a sphere

Steps	Equations
Governing equations	$\frac{\partial}{\partial x}(r\,u)+\frac{\partial}{\partial y}(r\,v)=0$ $u\frac{\partial u}{\partial x}+v\frac{\partial u}{\partial y}=(1+K_1)\frac{\partial^2 u}{\partial y^2}+K\left[\frac{\partial}{\partial x}\left(u\frac{\partial^2 u}{\partial y^2}\right)+v\frac{\partial^3 u}{\partial y^3}-\frac{\partial u}{\partial y}\frac{\partial^2 u}{\partial x\partial y}\right]$ $+\theta\sin(x)+K_1\frac{\partial H}{\partial y}-Mu\sin^2\alpha$ $u\frac{\partial N}{\partial x}+v\frac{\partial N}{\partial y}=-K_1\left(2N+\frac{\partial u}{\partial y}\right)+\left(1+\frac{K_1}{2}\right)\frac{\partial^2 N}{\partial y^2}$ $u\frac{\partial \theta}{\partial x}+v\frac{\partial \theta}{\partial y}=\frac{1}{\Pr}\frac{\partial^2 \theta}{\partial y^2}$
Boundary conditions	$u=v=0,\ \theta=1,\ H=-\frac{1}{2}\frac{\partial u}{\partial y}\ \text{ on }\ y=0$ $u\to 0,\ \frac{\partial u}{\partial y}\to 0,\ \theta\to 0,\ H\to 0\ \text{ as }\ y\to\infty$
Non-similarity transformation	$\psi=xr(x)f(x,y),\ \ H=xh(x,y),\ \ \theta=\theta(x,y)$
Ordinary differential equations	At stagnation point: $(1+K_1)f'''-f'^2+2ff''+\theta+K_1h'-Mf'\sin^2\alpha$ $+2K\left(f'f'''-ff^{iv}-f''^2\right)=0$ $\frac{1}{\Pr}\theta''+2f\theta'=0$ $\left(1+\frac{K_1}{2}\right)h''+2f\,h'-f'h-K_1(2h+f'')=0$
Transformed boundary conditions	$f(0)=f'(0)=0,\ \theta(0)=1,\ h(0)=-\frac{1}{2}f''(0)$ $f'\to 0,\ \ f''\to 0,\ \theta\to 0,\ h\to 0\ \text{ as }\ y\to\infty$

CHAPTER 8

MIXED CONVECTION BOUNDARY LAYER FLOW OF VISCOELASTIC MICROPOLAR FLUID OVER SPHERE WITH ALIGNED MHD EFFECT

8.1 Introduction

This chapter expanded the core interest in Chapter 7 by divulging into the problem of mixed convection flow of viscoelastic micropolar fluid over a sphere with aligned magnetic effect. While drawing from a broad range of studies, this problem particularly relies on the comprehensive reviews on viscous fluid model by Mohamed et al. (2016), micropolar fluid model by Nazar et al. (2003) and viscoelastic model as presented by Dasman et al. (2013).

After the result obtained using the Keller-box method are validated with the listed main references, they are presented and evaluated to comprehend the manner of the boundary layer fluid flow. The physical insight of the significant parameters that have been discussed in Chapter 7, on top of the mixed convection parameters are visibly demonstrated in the velocity, temperature and microrotation profiles as well as the heat transfer and skin friction coefficients. At the end of the chapter, the overall finding is outlined. For thi

8.2 Mathematical Formulation

Consider a heated sphere of temperature T_w with radius a, immersed in viscoelastic micropolar fluid of ambient temperature T_∞ as shown in Figure 8.1. Similar to the previous problems, the governing equations of this problems are made up of continuity, momentum, energy and angular momentum equations. The continuity, energy and angular momentum equations are as stated in Equations (7.1), (3.79) and (4.2), respectively while the momentum equation is

$$\bar{u}\frac{\partial \bar{u}}{\partial \bar{x}}+\bar{v}\frac{\partial \bar{u}}{\partial \bar{y}}=\bar{u}_e\frac{\partial \bar{u}_e}{\partial \bar{x}}+\left(\frac{\mu+\kappa}{\rho}\right)\frac{\partial^2 \bar{u}}{\partial \bar{y}^2}+\frac{k_0}{\rho}\left[\frac{\partial}{\partial \bar{x}}\left(\bar{u}\frac{\partial^2 \bar{u}}{\partial \bar{y}^2}\right)+\bar{v}\frac{\partial^3 \bar{u}}{\partial \bar{y}^3}+\frac{\partial \bar{u}}{\partial \bar{y}}\frac{\partial^2 \bar{v}}{\partial \bar{y}^2}\right]$$
$$+g\beta\left(T-T_\infty\right)\sin\left(\frac{\bar{x}}{a}\right)+\frac{\kappa}{\rho}\frac{\partial \bar{H}}{\partial \bar{y}}-\frac{\sigma}{\rho}\left(\bar{u}-\bar{u}_e\right)B^2\sin^2\alpha \qquad 8.1$$

The equations are subjected to the boundary conditions as follows

$$\begin{aligned}&\bar{u}=\bar{v}=0, \quad T=T_w, \quad \bar{H}=-\frac{1}{2}\frac{\partial \bar{u}}{\partial \bar{y}} \quad \text{on } \bar{y}=0,\\ &\bar{u}=\bar{u}_e\left(\bar{x}\right), \quad \frac{\partial \bar{u}}{\partial \bar{y}}=0, \quad T=T_\infty, \quad \bar{H}=0 \quad \text{as } \bar{y}\to\infty\end{aligned} \qquad 8.2$$

where the velocity outside the boundary layer, $\bar{u}_e$ is defined as $\bar{u}_e(\bar{x})=\frac{3}{2}U_\infty\sin\left(\frac{\bar{x}}{a}\right)$.

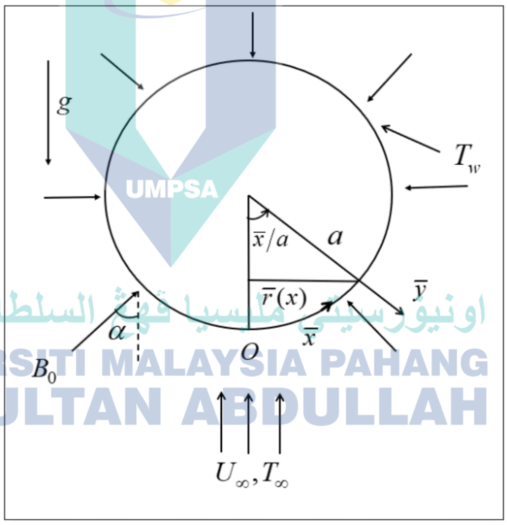

Figure 8.1 Schematic diagram for mixed convection boundary layer flow of viscoelastic micropolar fluid over sphere.

Then, the variables as listed in Equation (6.3) are utilised to convert the governing equations into dimensionless form. As a result, the continuity, angular momentum and energy equations are transformed into Equations (7.2), (4.10) and (5.5), while the momentum equation changes into

$$u\frac{\partial u}{\partial x}+v\frac{\partial u}{\partial y}=u_e\frac{\partial u_e}{\partial x}+\left(1+K_1\right)\frac{\partial^2 u}{\partial y^2}+K\left[\frac{\partial}{\partial x}\left(u\frac{\partial^2 u}{\partial y^2}\right)+v\frac{\partial^3 u}{\partial y^3}+\frac{\partial u}{\partial y}\frac{\partial^2 v}{\partial y^2}\right]$$
$$+\lambda\theta\sin x+K_1\frac{\partial H}{\partial y}-M\left(u-u_e\right)\sin^2\alpha \qquad 8.3$$

The associated dimensionless boundary conditions are as follows.

$$u=v=0,\quad \theta=1,\quad H=-\frac{1}{2}\frac{\partial u}{\partial y}\quad \text{on } y=0,$$
$$u_e=\frac{3}{2}\sin x,\quad \frac{\partial u}{\partial y}=0,\quad \theta=0,\quad H=0\quad \text{as } y\to\infty \qquad 8.4$$

The same non-similarity transformation variable from Equation (7.3) is applied to the equations that satisfy the continuity equation in Equation (7.2), while the energy and angular momentum equations evolved into Equations (7.6) and (7.7). As for the momentum equation, it is modified to

$$\left(1+K_1\right)\frac{\partial^3 f}{\partial y^3}-\left(\frac{\partial f}{\partial y}\right)^2+\frac{9}{4}\frac{\sin x}{x}\cos x+\lambda\frac{\sin x}{x}\theta+K_1\frac{\partial h}{\partial y}-M\left(\frac{\partial f}{\partial y}-\frac{3}{2}\frac{\sin x}{x}\right)\sin^2\alpha$$
$$+\left(1+\frac{x}{\sin x}\cos x\right)f\frac{\partial^2 f}{\partial y^2}+K\left[2\frac{\partial f}{\partial y}\frac{\partial^3 f}{\partial y^3}-\left(1+\frac{x}{\sin x}\cos x\right)\left(f\frac{\partial^4 f}{\partial y^4}+\left(\frac{\partial^2 f}{\partial y^2}\right)^2\right)\right] \qquad 8.5$$
$$=x\left(\frac{\partial f}{\partial y}\frac{\partial^2 f}{\partial x\partial y}-\frac{\partial f}{\partial x}\frac{\partial^2 f}{\partial y^2}\right)-Kx\left(\frac{\partial f}{\partial x}\frac{\partial^4 f}{\partial y^4}-\frac{\partial^3 f}{\partial y^3}\frac{\partial^2 f}{\partial x\partial y}-\frac{\partial f}{\partial y}\frac{\partial^4 f}{\partial x\partial y^3}+\frac{\partial^2 f}{\partial y^2}\frac{\partial^3 f}{\partial x\partial y^2}\right)$$

and the boundary conditions are

$$f(0)=f'(0)=0,\quad \theta(0)=1,\quad h(0)=-\frac{1}{2}f''(0)$$
$$f'=\frac{3}{2}\frac{\sin x}{x},\quad f''=0,\quad \theta=0,\quad h=0\quad \text{as } y\to\infty \qquad 8.6$$

At $x\approx 0$, Equations (7.6) and (7.7) are translated into Equations (7.9) and (7.10), respectively, whilst the momentum equation is reduced to a fourth-order ODE in the form

$$(1+K_1)f''' - f'^2 + \frac{9}{4} + \lambda\theta + K_1 h - M\left(f' - \frac{3}{2}\right)\sin^2\alpha + 2ff'' + 2K\left(f'f''' - ff^{iv} - f''^2\right) = 0 \qquad 8.7$$

with boundary conditions

$$\begin{gathered} f(0) = f'(0) = 0, \quad \theta(0) = 1, \quad h(0) = -\frac{1}{2}f''(0) \\ f' = \frac{3}{2}, \quad f'' = 0, \quad \theta = 0, \quad h = 0 \quad \text{as } y \to \infty \end{gathered} \qquad 8.8$$

Following Nazar et al. (2003) and Dasman et al. (2013), the local skin friction coefficient and local wall heat transfer coefficient are defined as

$$C_f = \frac{a}{U_\infty}\mathrm{Re}^{-1/2}\left[(\mu+\kappa)\frac{\partial \bar{u}}{\partial \bar{y}} + \kappa\bar{H}\right], \quad Q_w = -\frac{a}{k(T_w - T_\infty)}\mathrm{Re}^{-1/2}\left(\frac{\partial T}{\partial \bar{y}}\right) \qquad 8.9$$

Applying the non-dimensional equations in Equation (8.3), the final outcome of the coefficients are as stated in Equations (4.23) and (5.15).

8.3 Results and Discussion

Using the Keller-box method, the computational solution is developed using Fortran language to solve the PDE in Equations (7.6), (7.7) and (8.5) bounded to the condition in (8.6). The numerical results acquired is supposed to provide the physical insights of the parameters involved in this study, namely K, K_1, M, α and λ. The numerical solution that starts at the front stagnation point of the sphere extends round the sphere until it reaches the boundary layer separation.

The results are verified by comparing the present results to the limiting case of the problems listed in Table 8.1. Even though other three studies were centred around different types of fluid where Nazar et al. (2003), Mohamed et al. (2016) and Yasin et al. (2022) investigated on micropolar, viscous and ferrofluid, respectively, as the key parameters for these studies are set to zero, the momentum equations in the governing equation are indistinguishable. Comparison of $f''(0)$ and $-\theta'(0)$ values at various λ

between the present study and the study by Nazar et al. (2003) is shown in Table 8.2 where the figures are congruous. This is further supported by Figures 8.1 and 8.2 that show low discrepancies between the values of $f''(0)$ and $-\theta'(0)$ from both studies at $K_1 = 1,$ while at $K_1 = 0,$ the lines from both graphs overlap, indicating identical figures.

Further authentication is done by comparing present $-\theta'(0)$ values to Mohamed et al. (2016) and Yasin et al. (2022). Then, the results for diverse λ at different points on the sphere were presented. The results from all three problems, as displayed in Table 8.3 demonstrated high agreement between the values which denotes that they are analogous. Upon validation, more results are generated in Table 8.4 to obtain an overview of how varying the individual parameters would affect the behaviour of the flow. Apparently, the result suggests solid connection between the momentum and thermal transport as parallel change is observed for C_f and Q_w as the parameters are varied. Both coefficients showed a decline when K and K_1 increased in values, while rising M, α and λ caused the value of the coefficients to elevate.

It is evident form the Figures 8.4, 8.7 and 8.8 that f', C_f and Q_w are at their peak for the biggest value of λ and smallest K. The same observation on f' was recorded by Dasman et al. (2013), claiming that viscoelastic fluid has thicker velocity boundary layer compared to Newtonian fluid. It is observed across all problems that high K retards fluid velocity due to its resistive nature. While θ is enhanced by opposing flow and high K value, h experiences reversal effect at relatively high K. In close proximity of the wall, h is highest when K is the largest in opposing flow but after the reversal point, the opposite is observed, and it stood out that the effect of λ on h had reduced significantly as the flow moved towards the free stream. The exact same pattern can also be observed for parameter K_1 in Figure 8.11 for the microrotation profile.

Moreover, it is also shown in Figures 8.6 and 8.7 that the flow detached from the sphere wall in advance when $\lambda < 0$ and in low viscoelasticity. This early detachment could be due to the reduced viscoelastic effects, which typically help the fluid adhere to surfaces. With lower viscoelasticity, the fluid is less able to resist deformation and separation. Moreover, the micropolar effects might become more dominant in low viscoelasticity conditions, potentially promoting earlier separation due to microrotations. It is also notable that when $\lambda > 0$ and $K > 2$, the value of parameter K is no longer relevant as a determining factor for the boundary layer separation. Strong assisting flow combined with high viscoelasticity may create a flow regime where further increases in viscoelastic effects no longer significantly impact the boundary layer behaviour.

Similar to the results proposed by Nazar et al. (2003), growth of K_1 value promotes rise of C_f and decrease Q_w in assisting flow. The figures also suggest that assisting flow brings the separation points towards the middle of the sphere and the point and the separation can be further delayed using small K_1 value. It is also apparent that f' and θ demonstrate opposing behaviour. The velocity profiles in Figure 8.9 increases as λ increases and K_1 decreases, whereas the opposite set up values is required to maximize θ as shown in Figure 8.10.

The illustrations in Figures 8.14 to 8.21 describe the effect of M and α on the boundary layer flow. It comes off that both parameters affect the flow in the same manner. Increasing α when $\lambda > 0$ would boost f', C_f and Q_w while smaller angle in opposing flow enhances θ and h before the deflection. Again, as observed in other parameters, after the reversal point, both parameters seemed to have little to no effect on the flow anymore.

Apparently, the deflection pattern in h that was observed across all the problems are actually common in micropolar fluid study and other studies had also revealed the same flow behavior, for example, Na and Pop (1997), Rana et al. (2021), and Dasman et al. (2021), just to name a few. However, none of them actually discussed the pattern in detail. Since the microrotation profile is unique for micropolar fluid, the microrotation must have been a contributing factor. From the result, it appears that the microrotation profile can be manipulated by the parameters at the boundary layer, but the effect was diminished towards the free stream.

At the wall, viscous forces are dominant due to the no-slip condition, and the level of viscosity dictated the resistance level of the flow due to the microrotation where higher viscosity would lead to stronger resistance. However, at the outer boundary layer, viscous forces are no longer superior, so microrotation would also decrease which is consistent to the boundary condition $h(\infty)=0.$ It could be due to this reason that not much changes can be observed in the profile after the reversal especially for λ.

Table 8.1 The momentum equation and boundary conditions of problems involved for result validation.

Author	Model
Present	$(1+K_1)f''' - f'^2 + \frac{9}{4} + \lambda\theta + K_1 h - M\left(f' - \frac{3}{2}\right)\sin^2\alpha + 2ff''$ $+2K\left(f'f''' - ff^{iv} - f''^2\right) = 0$ with boundary conditions $f(0) = f'(0) = 0, \quad \theta(0) = 1, \quad h(0) = -\frac{1}{2}f''(0)$ $f' = \frac{3}{2}, \quad f'' = 0, \quad \theta = 0, \quad h = 0 \quad \text{as } y \to \infty$
Nazar et al (2003)	$(1+K_1)f''' + 2ff'' - f'^2 + K_1 h' + \lambda\theta + \frac{9}{4} = 0$ with boundary conditions $f(0) = f'(0) = 0, \quad \theta(0) = 1, \quad h(0) = -\frac{1}{2}f''(0)$ $f' \to \frac{3}{2}, \quad \theta \to 0, \quad h \to 0 \quad \text{as } y \to \infty$
Mohamed et al (2016)	$f''' + 2ff'' - f'^2 + \frac{9}{4} + \lambda\theta = 0$ with boundary conditions $f(0) = f'(0) = 0, \quad \theta(0) = 1$ $f' \to \frac{3}{2}, \quad \theta \to 0 \quad \text{as } y \to \infty$
Yasin et al (2022)	$\frac{1}{(1-\phi)^{2.5}\left[1-\phi+(\phi\rho_s)/(\rho_f)\right]}f''' + \frac{(1-\phi)\rho_f + \phi(\rho\beta)_s/\beta_f}{(1-\phi)\rho_f + \phi\rho_s}\lambda\theta$ $+2ff'' - f'^2 + \frac{9}{4} - \frac{\sigma_{ff}/\sigma_f}{1-\phi+\phi(\rho_s/\rho_f)}M\left(f' - \frac{3}{2}\right) = 0$ with boundary conditions $f(0) = f'(0) = 0, \quad \theta(0) = 1$ $f' \to \frac{3}{2}, \quad \theta \to 0 \quad \text{as } y \to \infty$

Table 8.2 Values of $f''(0)$ and $-\theta'(0)$ for various values of λ at $K = K_1 = M = 0$ and $\Pr = 0.7$

λ	$f''(0)$ Nazar et al (2003)	$f''(0)$ Present	$-\theta'(0)$ Nazar et al (2003)	$-\theta'(0)$ Present
-4	0.5028	0.500858	0.6534	0.652840
-3	1.0700	1.068461	0.7108	0.710288
-2	1.5581	1.556534	0.7529	0.752399
-1	2.0016	1.999974	0.7870	0.786567
0	2.4151	2.413345	0.8162	0.815716
1	2.8064	2.804472	0.8463	0.841346
2	3.1804	3.178171	0.8648	0.864346
3	3.5401	3.537672	0.8857	0.885291
4	3.8880	3.885274	0.9050	0.904578
5	4.2257	4.222687	0.9230	0.922494
6	4.5546	4.551229	0.9397	0.939253
7	4.8756	4.871941	0.9555	0.955021
8	5.1896	5.185665	0.9704	0.969929
9	5.4974	5.493094	0.9846	0.984081
10	5.7995	5.794807	0.9981	0.997564
20	8.5876	8.579000	1.1077	1.107074

Table 8.3 Comparison values of $-\theta'(x)$ with previous published results for various x and λ at $K = K_1 = M = 0$ and $\Pr = 0.7$

x	Mohamed at al (2016)			Yasin et al (2022)			Present		
	-1	0	1	-1	0	1	-1	0	1
0°	0.786	0.815	0.841	0.786	0.815	0.841	0.782	0.816	0.841
10°	0.781	0.810	0.836	0.781	0.810	0.836	0.782	0.811	0.837
30°	0.742	0.774	0.802	0.742	0.774	0.802	0.743	0.775	0.803
50°	0.662	0.703	0.735	0.664	0.704	0.736	0.663	0.703	0.735
70°	0.536	0.595	0.635	0.535	0.594	0.636	0.534	0.594	0.635
90°	-	0.441	0.507	-	0.441	0.507	-	0.440	0.509
100°	-	0.329	0.431	-	0.324	0.431	-	0.326	0.430

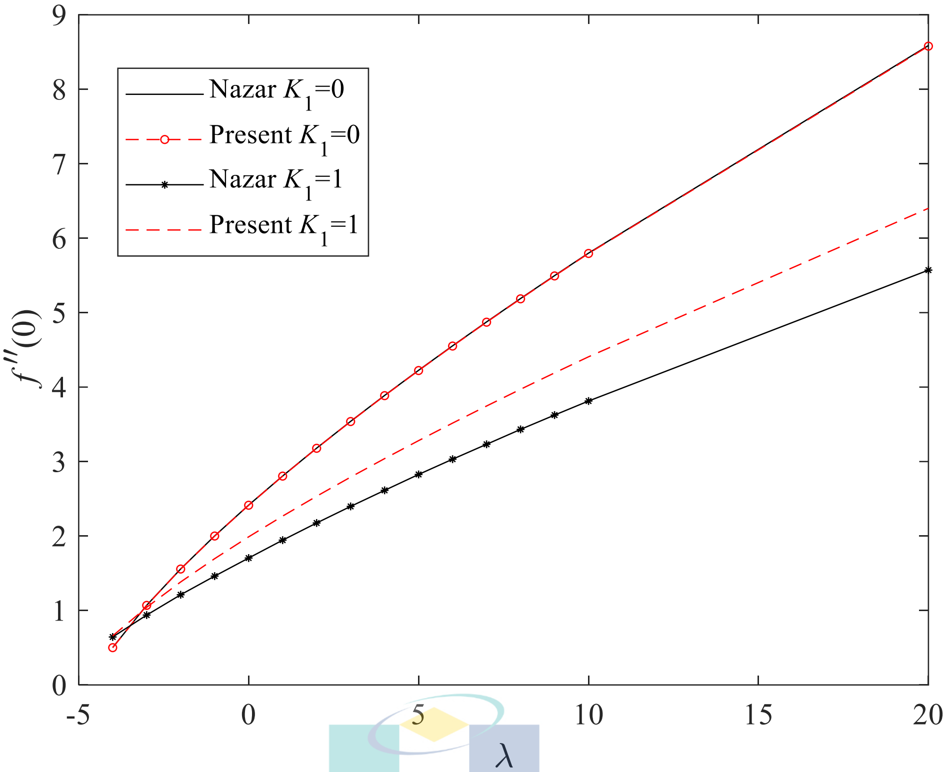

Figure 8.2 Comparison of $f''(0)$ at different K_1

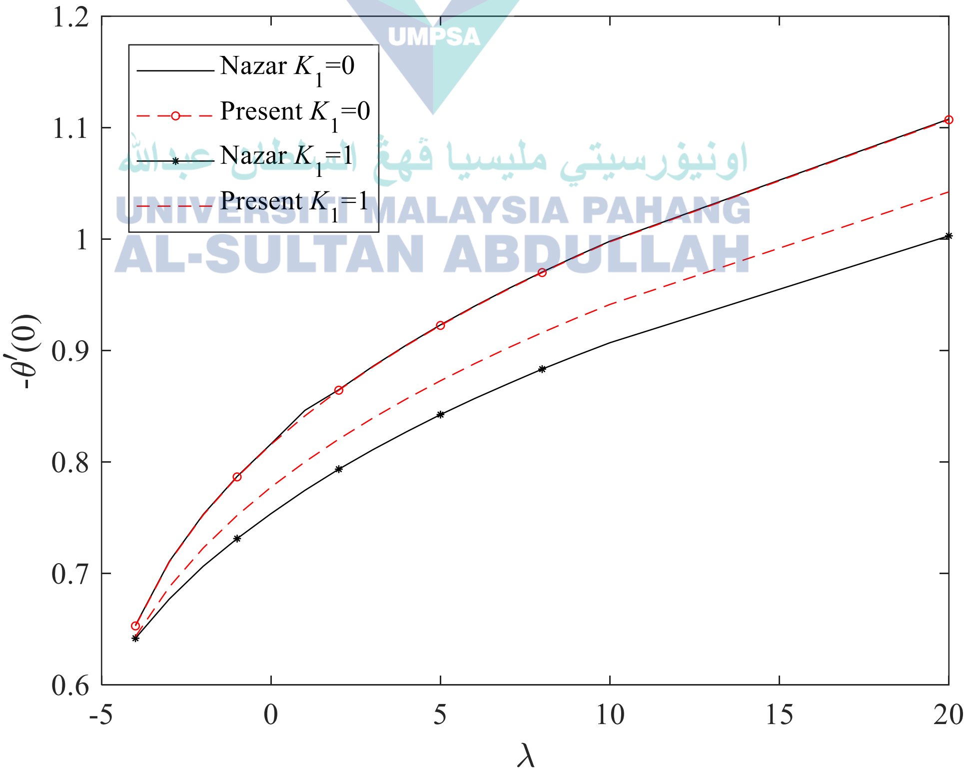

Figure 8.3 Comparison of $-\theta'(0)$ values at different K_1

Table 8.4 Values of C_f and Q_w for various values of K, K_1, M, λ and α at $\Pr = 21$

K	K_1	M	λ	α	C_f	Q_w
1	1	1	1	$\pi/6$	1.694681	2.191746
2	1	1	1	$\pi/6$	1.287269	2.003420
3	1	1	1	$\pi/6$	1.078451	1.890096
4	1	1	1	$\pi/6$	0.946413	1.810224
5	1	1	1	$\pi/6$	0.853401	1.749137
1	1.5	1	1	$\pi/6$	1.654535	2.175706
1	2	1	1	$\pi/6$	1.616444	2.160101
1	2.5	1	1	$\pi/6$	1.580661	2.145112
1	3	1	1	$\pi/6$	1.547120	2.130774
1	3.5	1	1	$\pi/6$	1.515659	2.117073
1	1	2	1	$\pi/6$	1.772823	2.222066
1	1	3	1	$\pi/6$	1.847441	2.250155
1	1	4	1	$\pi/6$	1.918965	2.276339
1	1	5	1	$\pi/6$	1.987746	2.300874
1	1	6	1	$\pi/6$	2.054076	2.323969
1	1	1	-2	$\pi/6$	1.317794	2.084211
1	1	1	-1	$\pi/6$	1.449626	2.123084
1	1	1	0	$\pi/6$	1.574924	2.158743
1	1	1	2	$\pi/6$	1.809651	2.222513
1	1	1	3	$\pi/6$	1.920431	2.251367
1	1	1	1	$\pi/4$	1.772823	2.222066
1	1	1	1	$\pi/3$	1.847441	2.250155
1	1	1	1	$\pi/2$	1.918965	2.276339

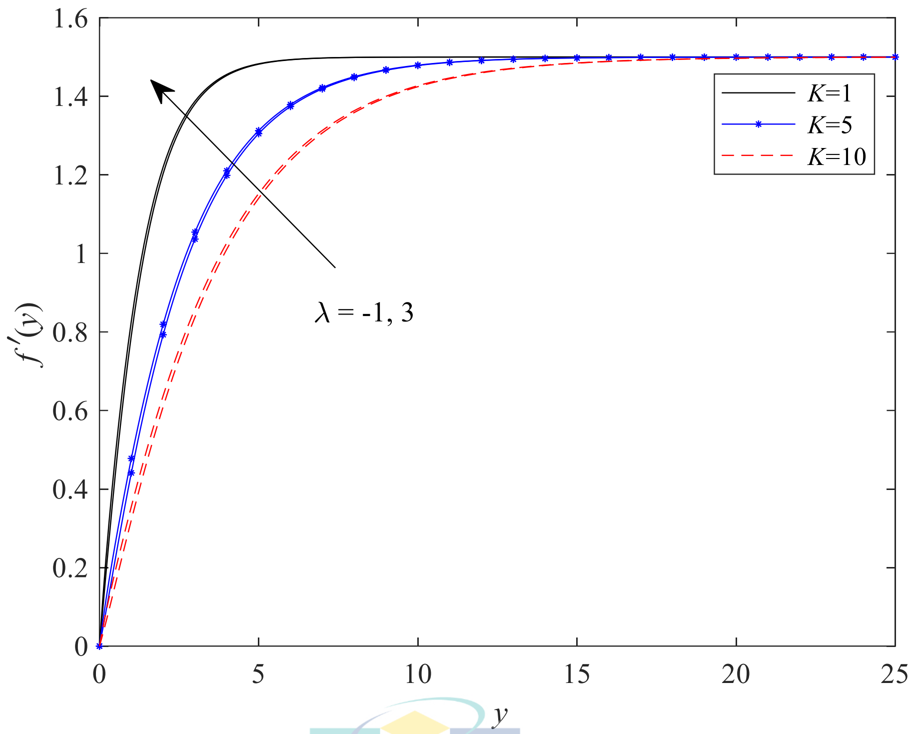

Figure 8.4 Variation of $f'(y)$ for various values of K and λ at $K_1 = 1, M = 0.5$ and $\alpha = \pi/6$

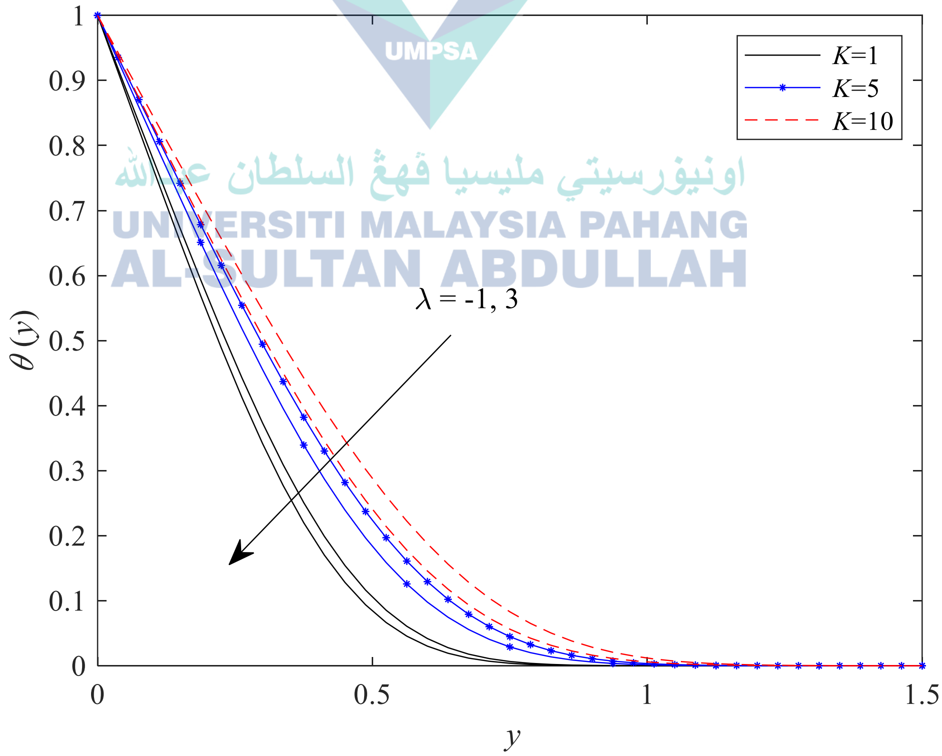

Figure 8.5 Variation of $\theta(y)$ for various values of K and λ at $K_1 = 1, M = 0.5$ and $\alpha = \pi/6$

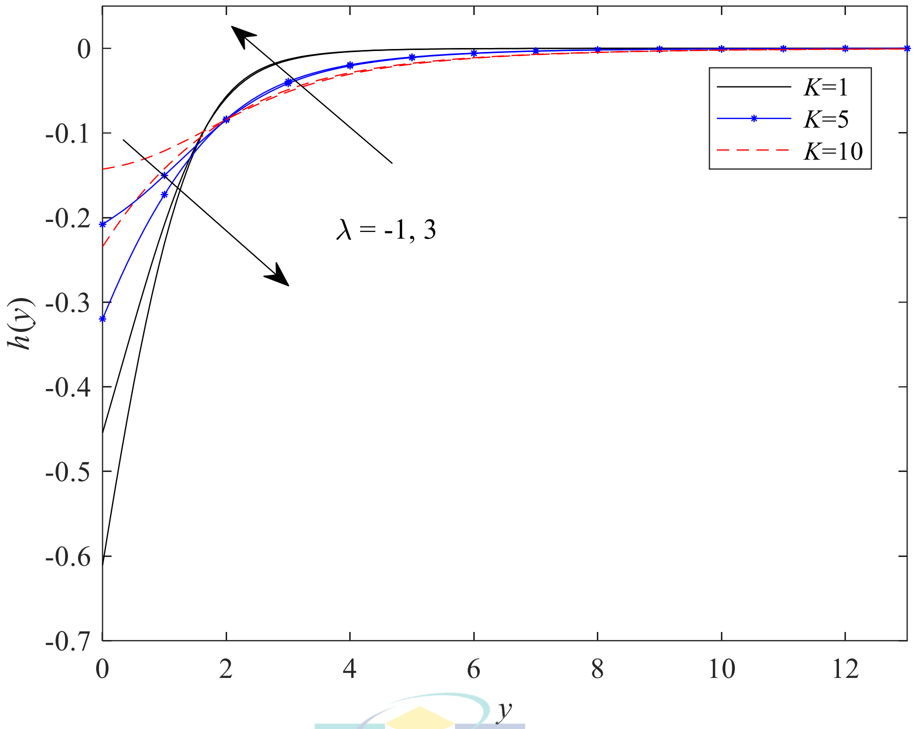

Figure 8.6 Variation of $h(y)$ for various values of K and λ at $K_1 = 1, M = 0.5$ and $\alpha = \pi/6$

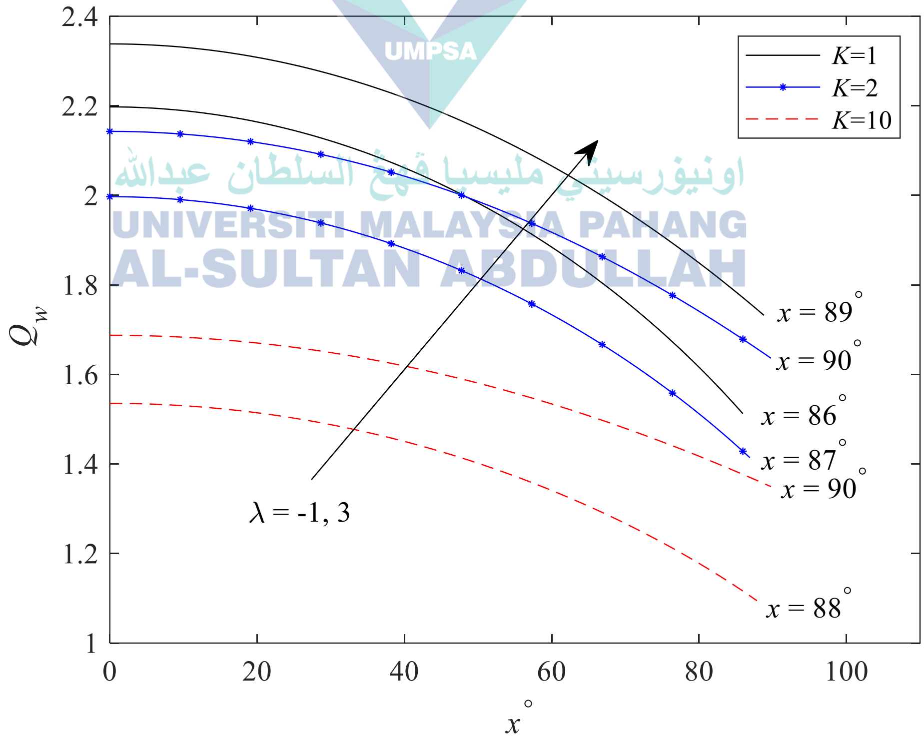

Figure 8.7 Variation of Q_w for various values of K and λ at $K_1 = 1, M = 0.5$ and $\alpha = \pi/6$

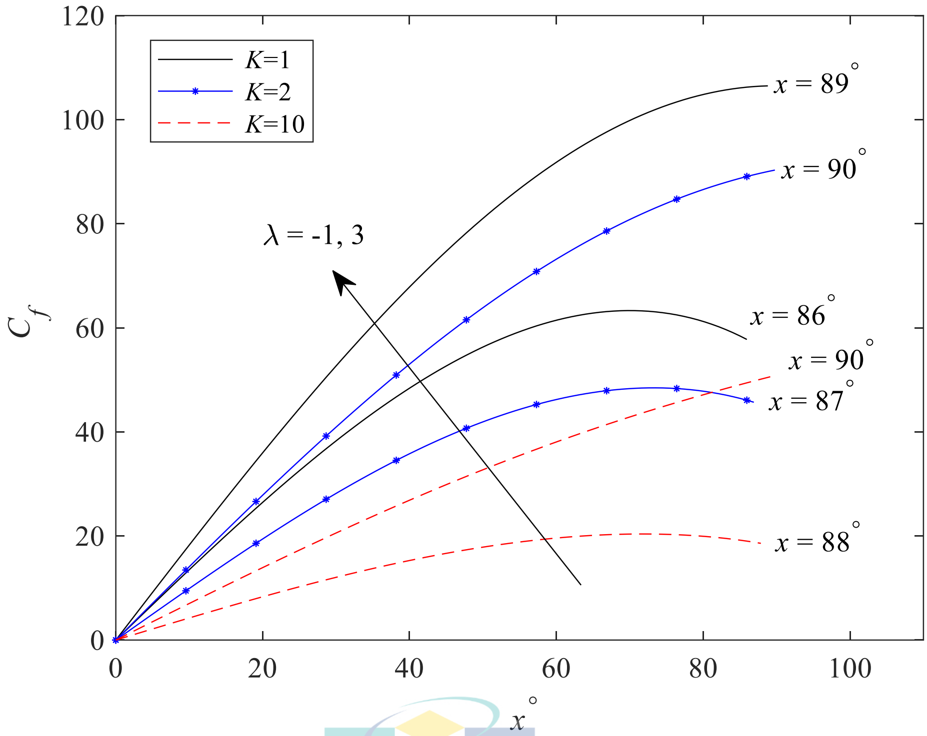

Figure 8.8 Variation of C_f for various values of K and λ at $K_1 = 1, M = 0.5$ and $\alpha = \pi/6$

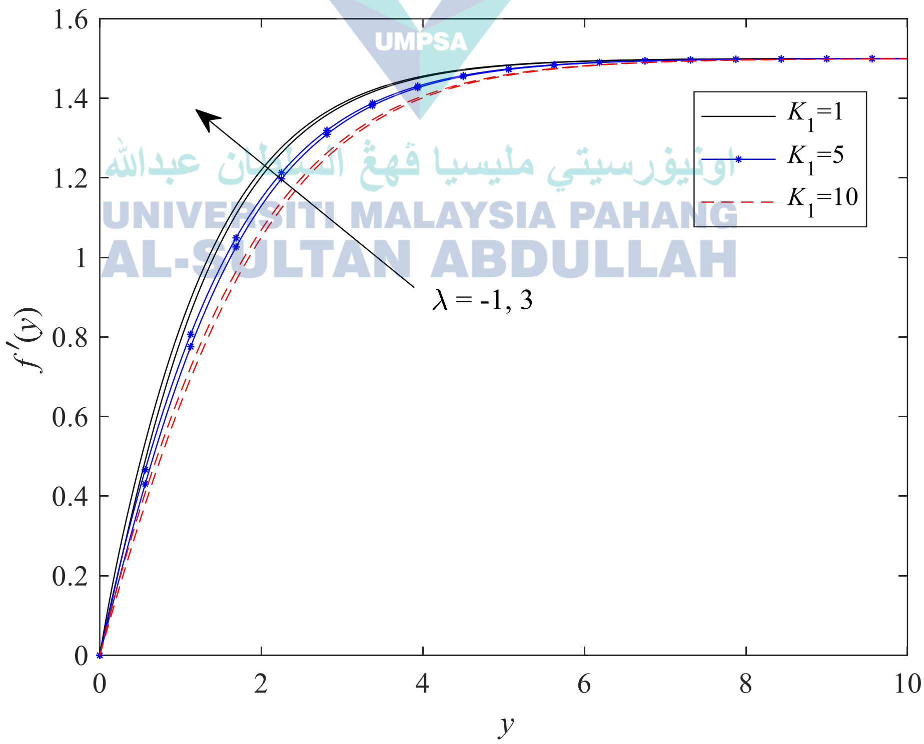

Figure 8.9 Variation of $f'(y)$ for various values of K_1 and λ at $K = 1, M = 0.5$ and $\alpha = \pi/6$

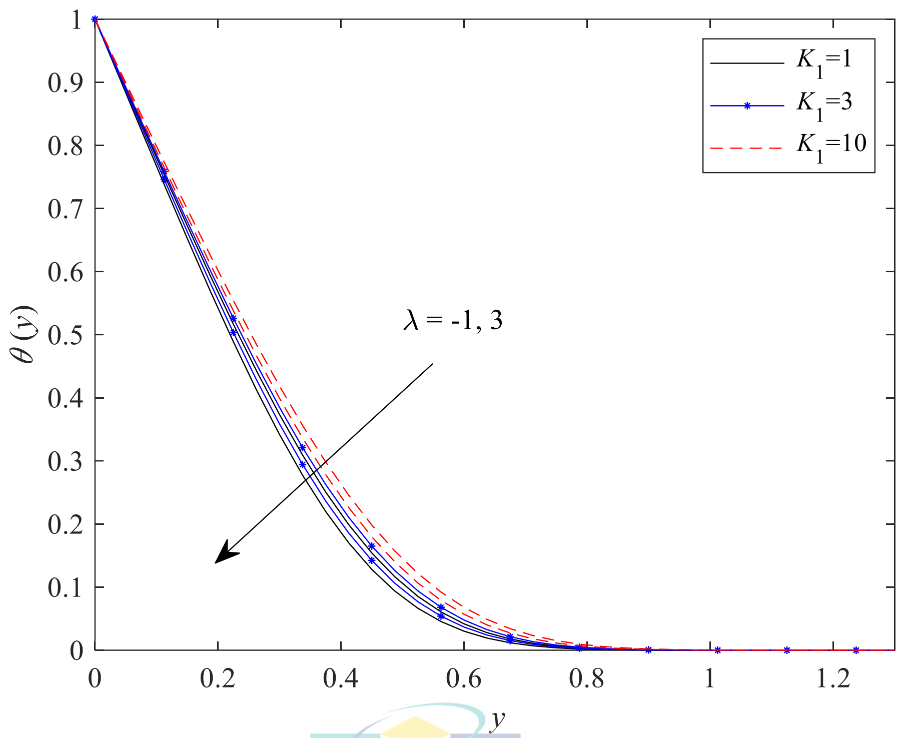

Figure 8.10 Variation of $\theta(y)$ for various values of K_1 and λ at $K=1, M=0.5$ and $\alpha=\pi/6$

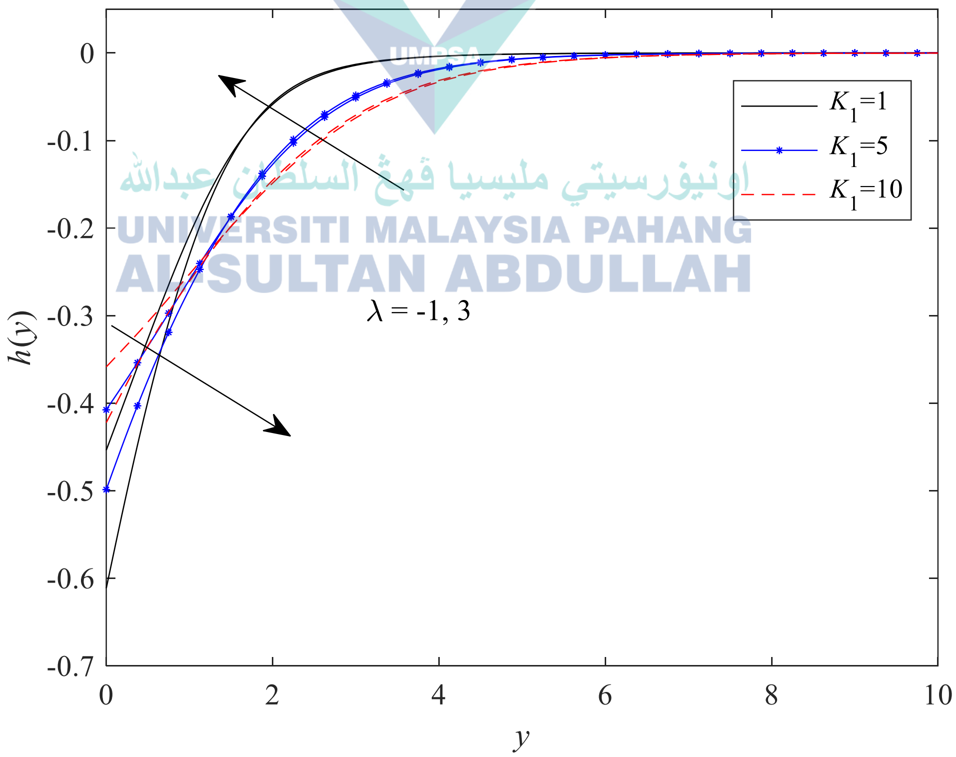

Figure 8.11 Variation of $h(y)$ for various values of K_1 and λ at $K=1, M=0.5$ and $\alpha=\pi/6$

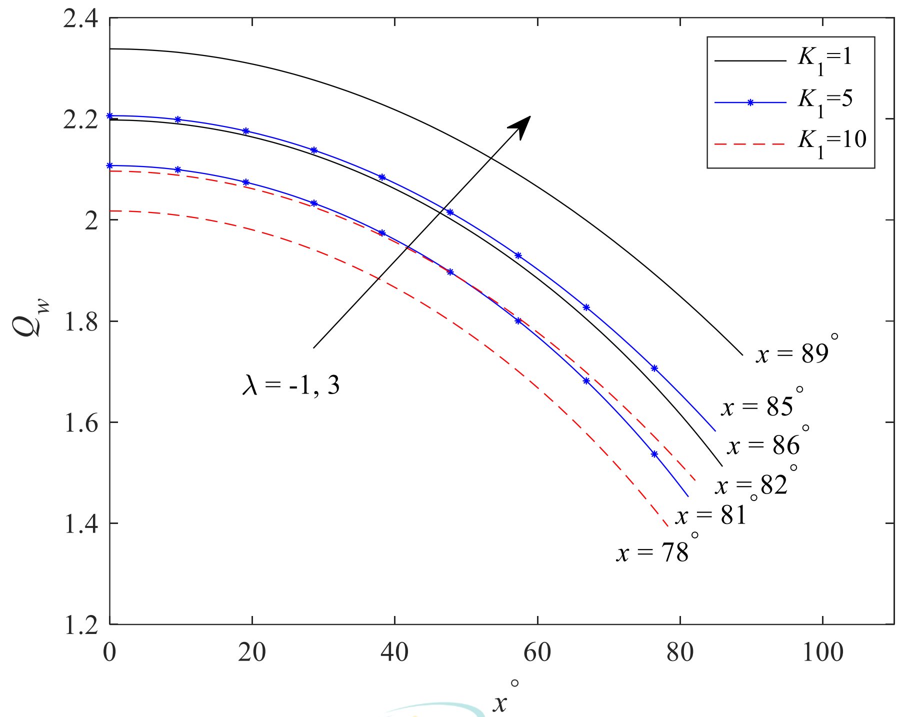

Figure 8.12 Variation of Q_w for various values of K_1 and λ at $K=1, M=0.5$ and $\alpha=\pi/6$

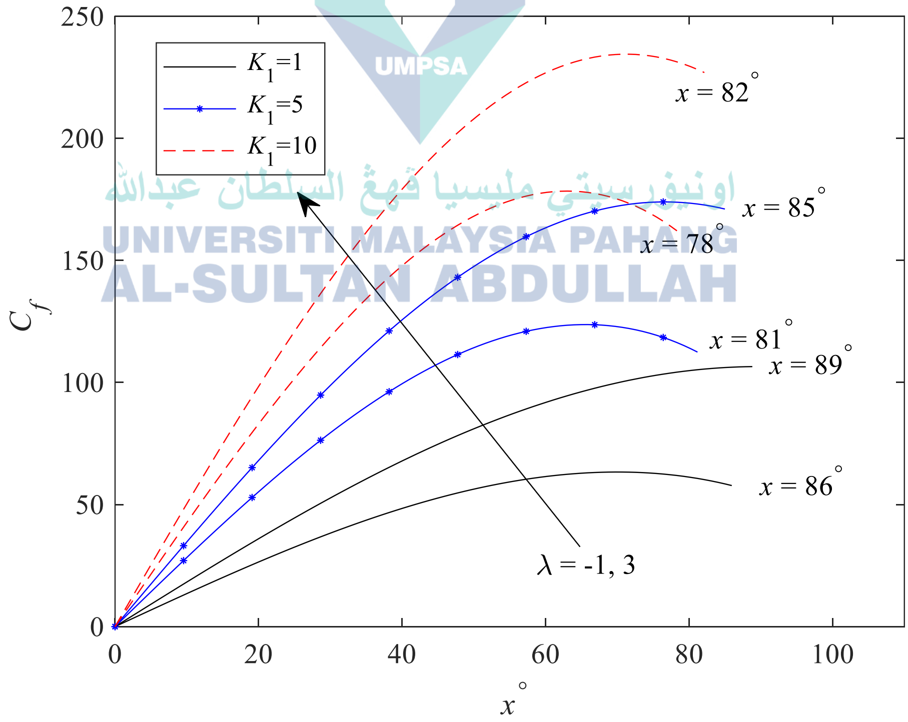

Figure 8.13 Variation of C_f for various values of K_1 and λ at $K=1, M=0.5$ and $\alpha=\pi/6$

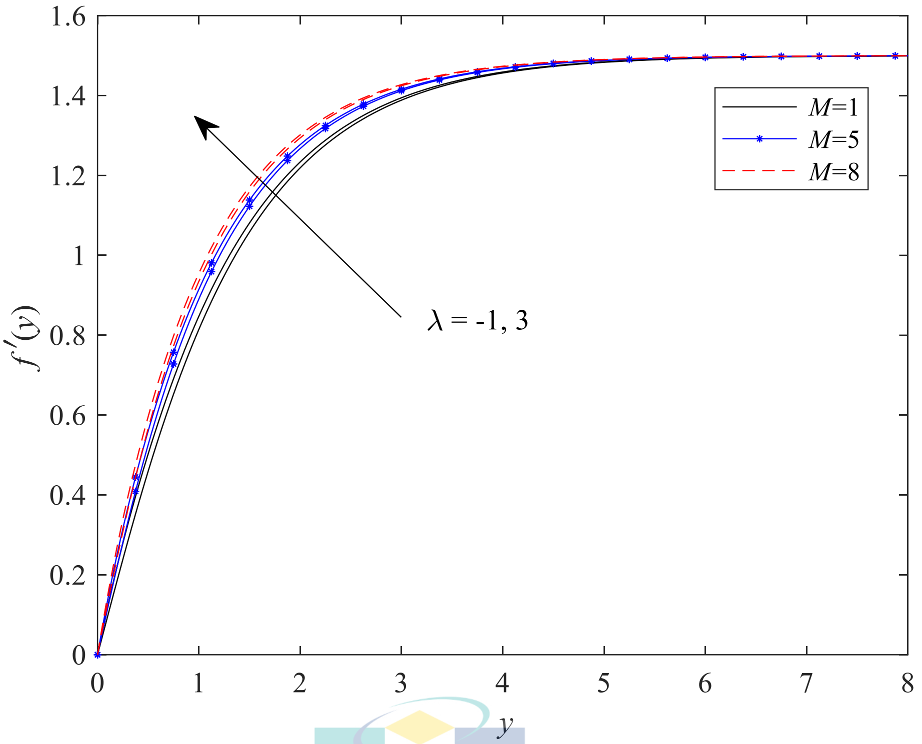

Figure 8.14 Variation of $f'(y)$ for various values of M and λ at $K = K_1 = 1$ and $\alpha = \pi/6$

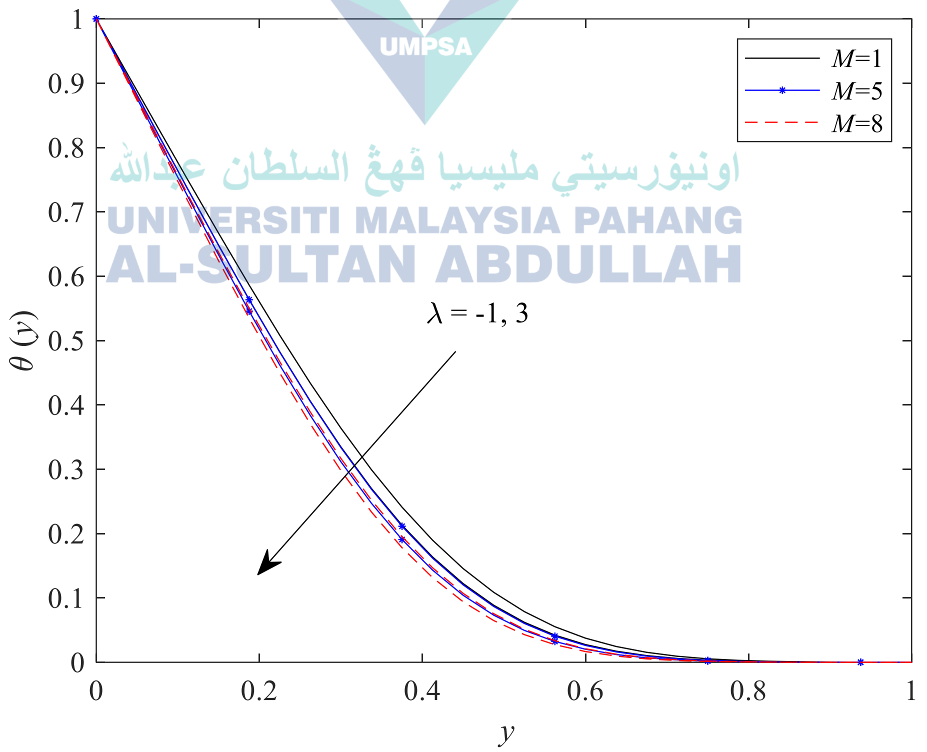

Figure 8.15 Variation of $\theta(y)$ for various values of M and λ at $K = K_1 = 1$ and $\alpha = \pi/6$

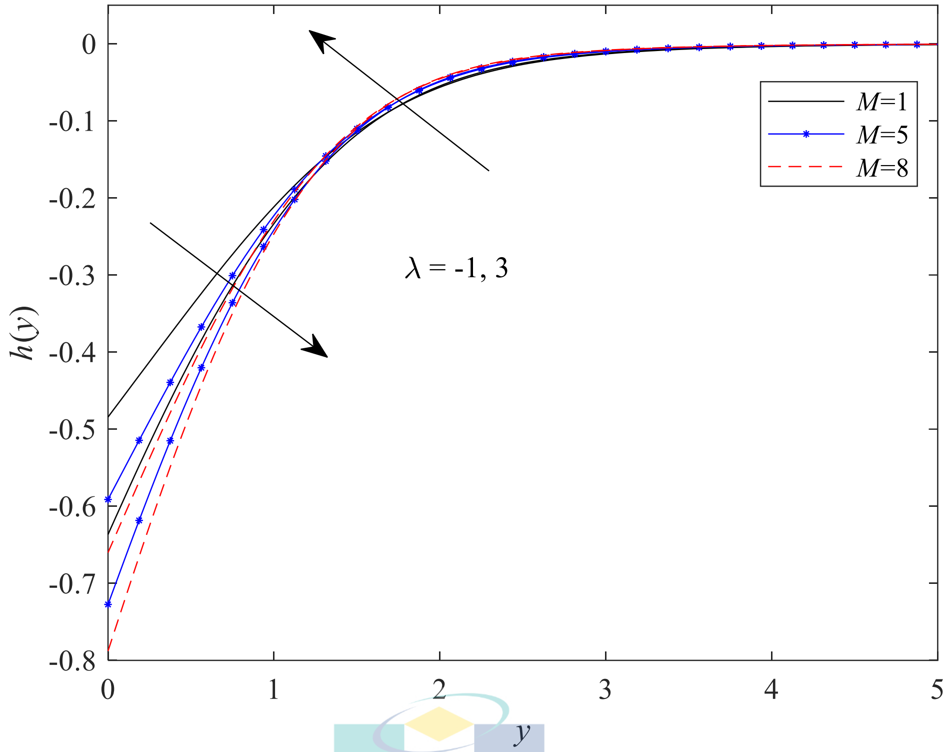

Figure 8.16 Variation of $h(y)$ for various values of M and λ at $K = K_1 = 1$ and $\alpha = \pi/6$

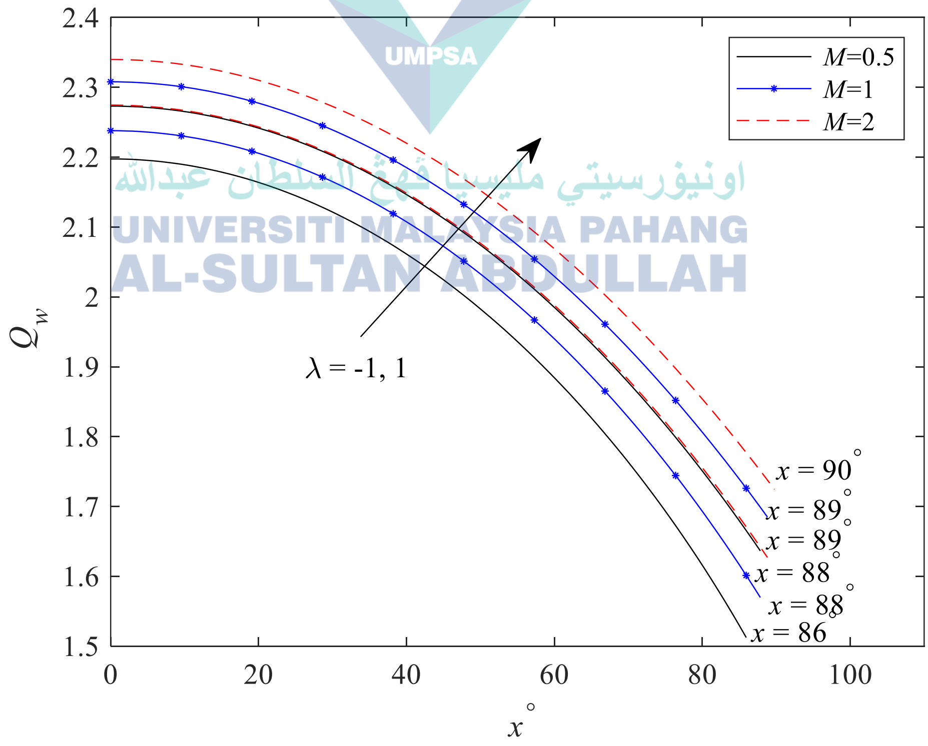

Figure 8.17 Variation of Q_w for various values of M and λ at $K = K_1 = 1$ and $\alpha = \pi/6$

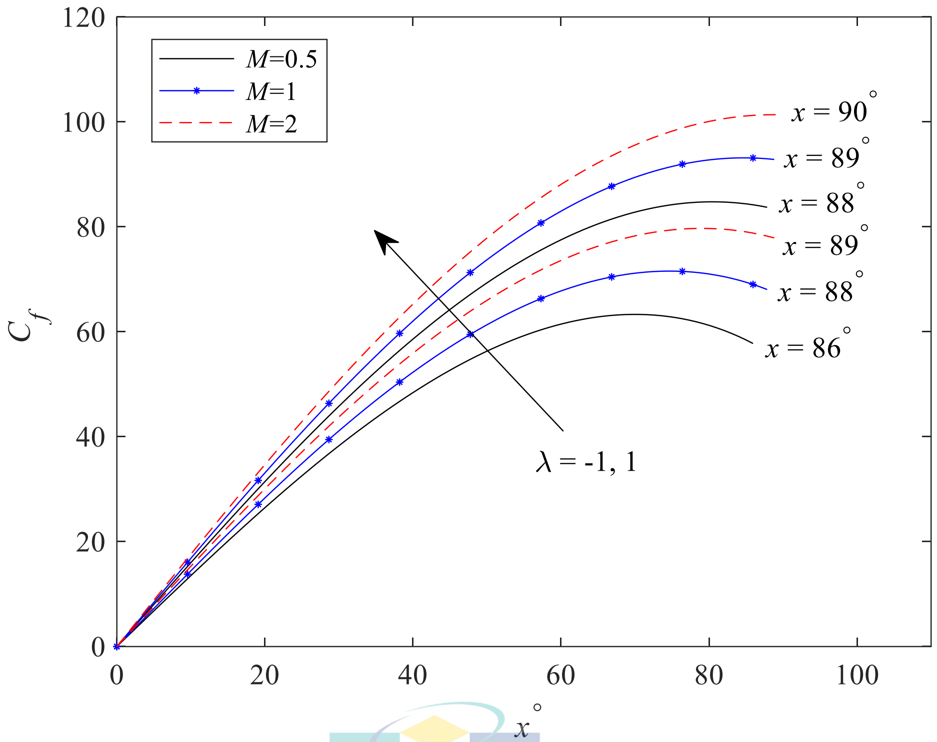

Figure 8.18 Variation of C_f for various values of M and λ at $K = K_1 = 1$ and $\alpha = \pi/6$

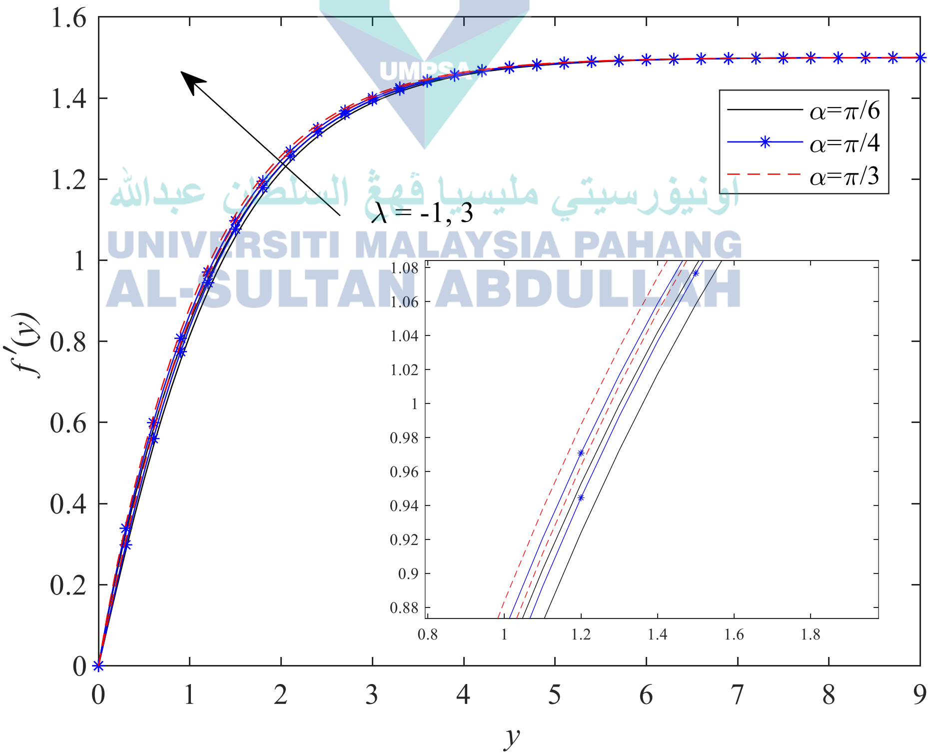

Figure 8.19 Variation of $f'(y)$ for various values of α and λ at $K = K_1 = M = 1$

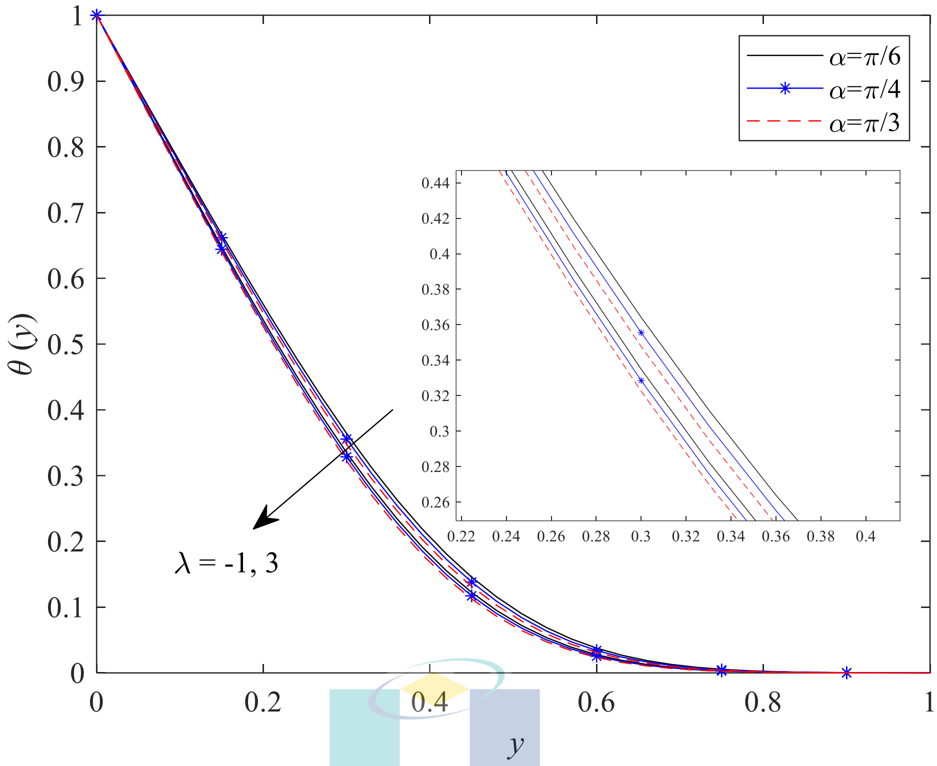

Figure 8.20 Variation of $\theta(y)$ for various values of α and λ at $K = K_1 = M = 1$

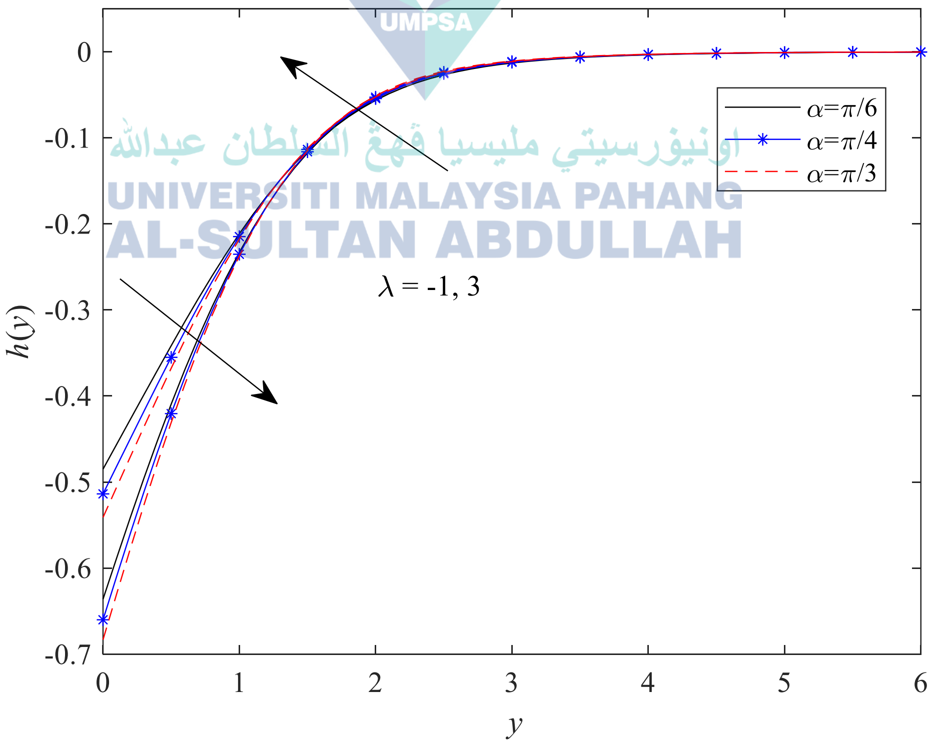

Figure 8.21 Variation of $h(y)$ for various values of α and λ at $K = K_1 = M = 1$

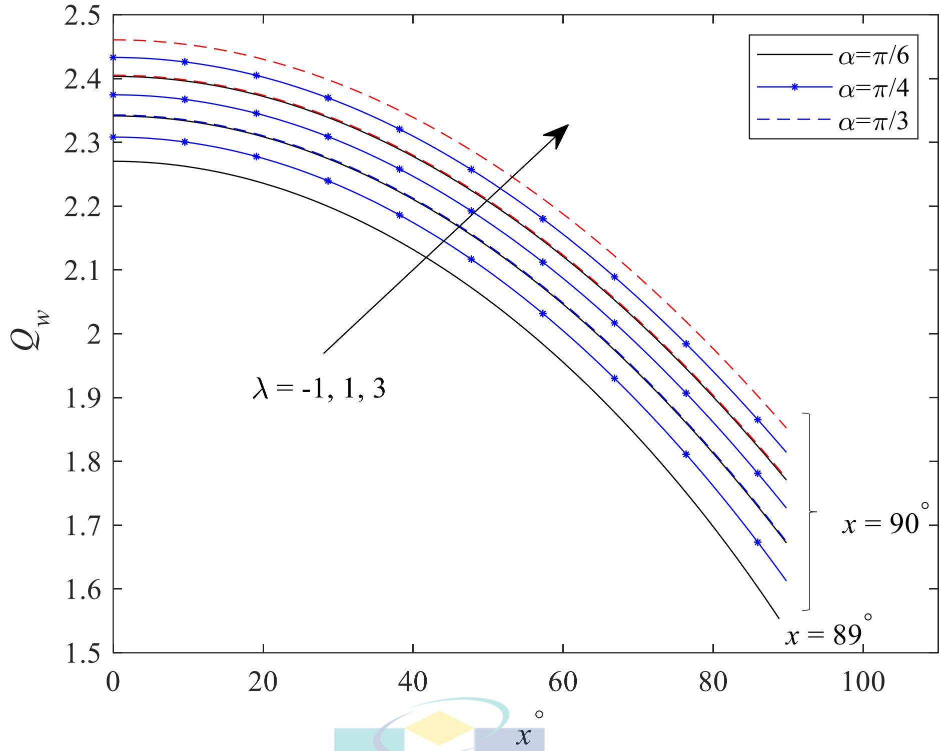

Figure 8.22 Variation of Q_w for various values of α and λ at $K = K_1 = M = 1$

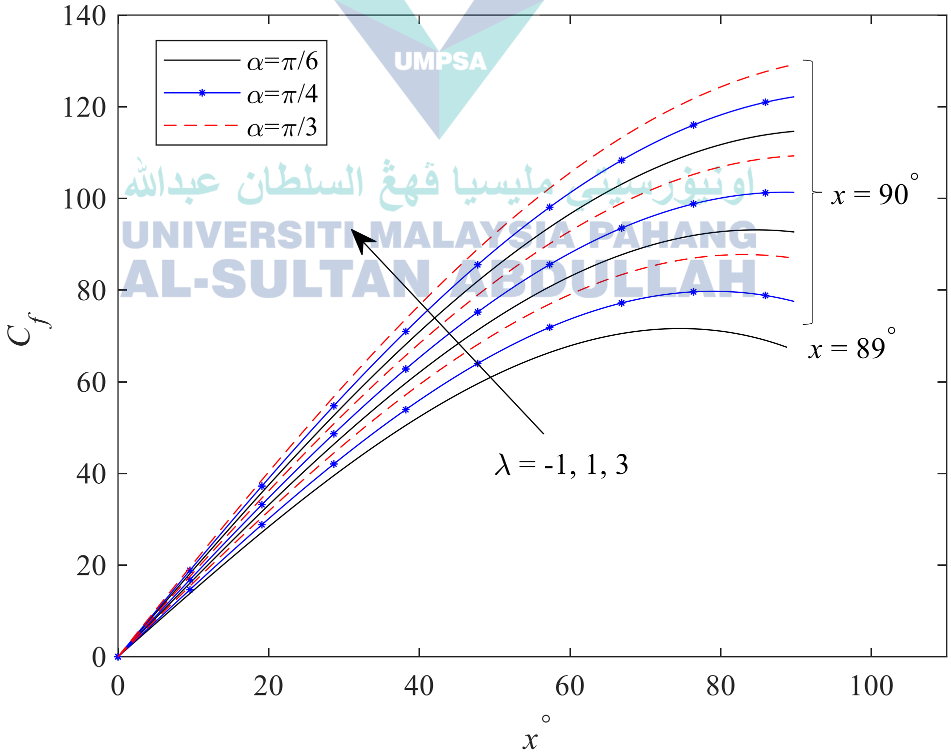

Figure 8.23 Variation of C_f for various values of α and λ at $K = K_1 = M = 1$

8.4 Summary

In this chapter, the behavior flow of mixed convection boundary layer flow of viscoelastic micropolar fluid over a sphere has been examined. The governing equations that were solved in the analysis are displayed in Table 8.6. Section 8.3 presents an analysis of the observed and discussed effect resulting from the interaction between the mixed convection parameter and the viscoelastic, micropolar, magnetic, and aligned angle parameters. The summary of the effect is shown in Table 8.5 and in light of the results, the findings of the investigations are as follows.

i. Velocity profile increases as the other parameters increase, except for K and K_1.

ii. Heat transfer and skin friction coefficients are enhanced by assisting flow in general. They increase when M and α increase and decrease when K rises. However, when skin friction is intensified by the growth of K_1, the opposite is observed for heat transfer.

iii. Microrotation profile is heightened by the increasing K and K_1 and receded as M and α grow, before the turning point when the pattern reversed.

iv. The parameters K and K_1 have boosting effect on temperature profile but M and α show the contradiction.

v. The parameter λ, is positively correlated with velocity, heat transfer and skin fiction coefficients while the relationship is the opposite with temperature profile and microrotation profile near the wall.

Table 8.5 Summary of present results for mixed convection boundary layer flow of viscoelastic micropolar on a sphere

Distribution	$K\uparrow$	$K_1\uparrow$	$M\uparrow$	$\alpha\uparrow$	$\lambda\uparrow$
f'	↓	↓	↑	↑	↑
h	↑↓	↑↓	↓↑	↓↑	↓↑
θ	↑	↑	↓	↓	↓
C_f	↓	↑	↑	↑	↑
Q_w	↓	↓	↑	↑	↑

↑ increase ↓ decrease

Table 8.6 Solution procedure for mathematical formulation for mixed convection boundary layer flow of viscoelastic micropolar on a sphere

Steps	**Equation**
Governing equations	$\frac{\partial}{\partial x}(r\,u)+\frac{\partial}{\partial y}(r\,v)=0$ $u\frac{\partial u}{\partial x}+v\frac{\partial u}{\partial y}=u_e\frac{\partial u_e}{\partial x}+K\left[\frac{\partial}{\partial x}\left(u\frac{\partial^2 u}{\partial y^2}\right)+v\frac{\partial^3 u}{\partial y^3}+\frac{\partial u}{\partial y}\frac{\partial^2 v}{\partial y^2}\right]$ $+(1+K_1)\frac{\partial^2 u}{\partial y^2}+\lambda\theta\sin x+K_1\frac{\partial H}{\partial y}-M(u-u_e)\sin^2\alpha$ $u\frac{\partial H}{\partial x}+v\frac{\partial H}{\partial y}=-K_1\left(2H+\frac{\partial u}{\partial y}\right)+\left(1+\frac{K_1}{2}\right)\frac{\partial^2 H}{\partial y^2}$ $u\frac{\partial \theta}{\partial x}+v\frac{\partial \theta}{\partial y}=\frac{1}{\Pr}\frac{\partial^2\theta}{\partial y^2}$
Boundary conditions	$u(0)=v(0)=0,\quad \theta(0)=1,\quad H(0)=-\frac{1}{2}\frac{\partial u}{\partial y}$ $u_e=\frac{3}{2}\sin x,\quad \frac{\partial u}{\partial y}=0,\quad \theta=0,\quad H=0\quad \text{as}\;\; y\to\infty$
Non-similarity transformation	$\psi=xr(x)f(x,y),\;\; H=xh(x,y),\;\; \theta=\theta(x,y)$
Ordinary differential equations	At stagnation point: $(1+K_1)f'''-f'^2+\frac{9}{4}+\lambda\theta+K_1h-M\left(f'-\frac{3}{2}\right)\sin^2\alpha+2ff''$ $+2K\left(f'f'''-ff^{iv}-f''^2\right)=0$ $\frac{1}{\Pr}\theta''+2f\theta'=0$ $\left(1+\frac{K_1}{2}\right)h''+2fh'-f'h-K_1(2h+f'')=0$
Transformed boundary conditions	$f(0)=f'(0)=0,\;\; \theta(0)=1,\;\; h(0)=-\frac{1}{2}f''(0)$ $f'\to\frac{3}{2},\;\; f''\to 0,\;\; \theta\to 0,\;\; h\to 0\;\; \text{as}\;\; y\to\infty$

CHAPTER 9

CONCLUSION

9.1 Introduction

This chapter concludes the finding of this study that have been disclosed in Chapter 4 to 8 as well as suggests some insights that could be useful for prospect studies in the near future.

9.2 Summary of Thesis

This thesis consists of a total of five proposed problems related to boundary layer flow of viscoelastic micropolar fluid with an addition of aligned magnetic effect over bluff body. The thesis begins with a pilot study considering only the flow of the viscoelastic micropolar fluid with magnetic effect over a circular cylinder without energy. Once the idea has been established, different modes of convection, namely free and mixed convection were considered as presented in Chapters 5 and 6, respectively. Afterward, another bluff body in the form of sphere is introduced for the case of free and mixed convection as discussed in Chapters 7 and 8.

Chapter 1 lays the foundation and rationale of the thesis where the background of study is introduced by providing necessary context to understand the research problem. This chapter offers a conceptual framework for understanding the research and findings that will be discussed in the following chapters. It is followed by Chapter 2 that unveils the context and background that frame the original research. This chapter illustrates how the current study is based on prior research, but also acknowledging the limits and unanswered questions that highlight the gap in knowledge, so motivating the undertaking of this study. Once the idea has been established, a mathematical representation of the governing equations is provided in Chapter 3, which includes the continuity, momentum, angular momentum and energy equations based on the conservation laws and fluid mechanics principles.

Subsequently, the intricate governing equations were simplified by employing boundary layer and Boussinesq approximations, followed by the application of a suitable non-similarity transformation to reduce the equations to solvable partial differential equations (PDEs). Near the stagnation point, these equations were converted to a set of ODEs. Both DEs were incorporated in Fortran, the programming language used to develop the Keller-box method algorithm. Then, the numerical solution of the problems was plotted in MATLAB to yield the graphical description of the flow behaviour. The effect of the parameters on the boundary layer flow were then discussed in detail for each problem.

The first problem in Chapter 4 serves as the preliminary study and sneak preview of the viscoelastic micropolar flow behavior over circular cylinder. The effect of parameters K, K_1, M and α on the velocity and microrotation profiles as well as the skin fraction coefficient was analysed. From the literature review, it had been acknowledged that viscoelastic fluid model by itself is already intricate to solve as the momentum equation is a non-linear fourth order DE. Adding another element like micropolar on top of that with a bluff body for the geometry, added another layer of complexity in terms of the derivation and the mathematical algorithm. Therefore, once the solution for this chapter has been verified, it provides access to the proceeding problems.

In Chapter 5, energy equation is included in the governing equations where free convection problem was considered. The same parameters in Chapter 5 were evaluated with additional temperature profile and heat transfer coefficient as a result from the augmented variable, θ. The problem was then further extended in Chapter 6 by investigating the mixed convection problem, hence implying the existence of the mixed convection parameter, λ. For this problem, the combination effect of λ with other parameters in terms of which coupling could boost or retard the profiles and physical quantities was also explored.

Moving on to Chapters 7 and 8, these problems are analogous to the problem in Chapter 5 and 6, respectively, but using sphere geometry instead of horizontal circular cylinder. The same approach was taken as the previous problems, so this allows an analysis of the impact of the geometry on the fluid flow behaviour and heat transfer under the same conditions. Even though the model and parameters might look similar, but the flow behaviour differed as the physical models of the bodies were non-identical, resulting in substantial variances in boundary layer development, wake structure, stability, separation and other hydrodynamic factors.

In general, K and K_1 had retarding effects on velocity profile but showed positive relationship with the microrotation profile. Meanwhile, M and α demonstrated the same effect on the flow throughout all problems indicating that they are directly proportional. Since the increase of M represents stronger magnetic field, for these problems, it is possible to conclude that the magnetic field was optimized when the angle is perpendicular to the flow at $\alpha = \pi/2$. However, the results had also established that both of them could be the limiting factors of the other.

Across the problems, it can be observed the existence of a turning point for angular velocity profiles, but such deflection does not exist for the velocity profiles. The velocity profile starts at zero at the surface due to no-slip condition and smoothly approaches the free stream velocity as the flow moves away from the surface, typically resulting in a monotonic curve without a turning point. In contrast, the angular velocity at the surface is directly proportional to the skin friction which means that the rotational motion of fluid particles near the surface is influenced by the shear stress experienced at the boundary. Moving away from the surface, the spinning motion from the surface tries to spread upward, potentially making particles spin faster but simultaneously, the rest of the fluid resists this spinning motion, trying to slow it down. Therefore, the turning point is likely where the two competing effects reached equilibrium. At this point, the surface-induced rotation reaches its maximum influence before the fluid's inherent resistance begins to dominate, causing the angular velocity to decrease towards zero in free stream.

For both types of geometry, the boundary layer separation was delayed in free convection but occurred much earlier in mixed convection. It is also evident that for the case of circular cylinder, the parameters had control over the flow separation but for sphere, they had little significance. The comparison from results in Chapters 6 and 8 suggests that at the stagnation point, the boundary layer flow of viscoelastic micropolar fluid was more stable over sphere as opposed to circular cylinder. These results are expected to provide an insight into the microscale boundary layer behaviours of viscoelastic micropolar fluid over circular cylinder and sphere. The models and simulations could potentially guide the design of fluidic devices and systems involving complex fluid rheology where experimental trial-and-error poses financial, safety, or feasibility risks.

9.3 Suggestions for Future Research

This study attempted to explore in detail the steady two-dimensional flow free and mixed convection of viscoelastic micropolar fluid with aligned MHD effect by incorporating constant wall temperature as the heating condition. Presented here are some suggestions that are anticipated to improve and widen the research area that might appeal to other researchers and practitioners.

i. Employment of other surface thermal conditions such as Newtonian heating, constant surface heat flux, convective boundary condition, time-dependent surface temperature and surface radiation
ii. Explore other geometrical bluff body including rectangular prism, disk, cube and semi-circular cylinder.
iii. Taking into account other captivating effect, for example, Soret and Dufour, electro hydrodynamics as well as melting and solidification.
iv. Analyse other types of flow that involve viscoelastic or micropolar such as viscoelastic jets, viscoelastic films, micropolar ferrofluid and reactive micropolar flow.
v. Consider two-phase flow problem involving either micropolar or viscoelastic fluid. For instance, biofluids-liquid that could represents blood (micropolar) and saline solution (viscoelastic) or viscoelastic polymer-polymer as separated flow of two melted viscoelastic polymer.

REFERENCES

Abbas, N., Shatanawi, W., & Shatnawi, T. A. (2024). Thermodynamic analysis of micropolar-casson fluid flow with PST and PHF heating condition over a curved stretching surface. *Ain Shams Engineering Journal*, *15*(7), 102778.

Abbas, Z., Wang, Y., Hayat, T., & Oberlack, M. (2008). Hydromagnetic flow in a viscoelastic fluid due to the oscillatory stretching surface. *International Journal of Non-Linear Mechanics*, *43*(8), 783-793.

Abdul Rahman Mohd Kasim. (2014). *Convective Boundary Layer Flow of Viscoelastic Fluid* Universiti Teknologi Malaysia].

Abdullah, I., & Norsarahaida, A. (2010). A micropolar fluid model of blood flow through a tapered artery with a stenosis. *Mathematical Methods in the Applied Sciences*, *33*, 1910-1923. https://doi.org/10.1002/mma.1303

Ahmadi, G. (1976). Stability of a micropolar fluid layer heated from below. *International Journal of Engineering Science*, *14*(1), 81-89. https://doi.org/https://doi.org/10.1016/0020-7225(76)90058-6

Ahmed, Z., Saleem, S., Nadeem, S., & Khan, A. U. (2021). Squeezing Flow of Carbon Nanotubes-Based Nanofluid in Channel Considering Temperature-Dependent Viscosity: A Numerical Approach. *Arabian Journal for Science and Engineering*, *46*(3), 2047-2053. https://doi.org/10.1007/s13369-020-04981-x

Al-Sharifi, H., Kasim, A., & Hussanan, A. (2023). Numerical investigation of Casson micropolar fluid over a stretching sheet with convective boundary condition. AIP Conference Proceedings,

Al-Sharifi, H., Kasim, A., Salleh, M., & Shafie, S. (2017). Effect of aligned magnetohydrodynamics on convective boundary layer flow of Jeffrey micropolar fluid with Newtonian heating across a stretching sheet. AIP Conference Proceedings,

Al-Waeli, A. H. A., Chaichan, M. T., Kazem, H. A., Sopian, K., & Safaei, J. (2018). Numerical study on the effect of operating nanofluids of photovoltaic thermal system (PV/T) on the convective heat transfer. *Case Studies in Thermal Engineering*, *12*, 405-413. https://doi.org/https://doi.org/10.1016/j.csite.2018.05.011

Alao, S., Salawu, S. O., Oderinu, R. A., Oyewumi, A. A., & Akinola, E. I. (2024). Investigation of thermal radiation and viscous heating effects on the hydromagnetic reacting micropolar fluid species flowing past a stretchy plate in permeable media. *International Journal of Thermofluids*, *22*, 100600.

Alfven, H. (1942). Existence of electromagnetic-hydrodynamic waves. *Nature*, *150*(3805), 405-406.

Ali, A., Umar, M., Bukhari, Z., & Abbas, Z. (2020). Pulsating flow of a micropolar-Casson fluid through a constricted channel influenced by a magnetic field and Darcian porous medium: A numerical study. *Results in Physics*, *19*, 103544. https://doi.org/https://doi.org/10.1016/j.rinp.2020.103544

Ali, L., Ali, B., & Ghori, M. B. (2022). Melting effect on Cattaneo–Christov and thermal radiation features for aligned MHD nanofluid flow comprising microorganisms to leading edge: FEM approachImage 1. *Computers & Mathematics with Applications, 109*, 260-269. https://doi.org/https://doi.org/10.1016/j.camwa.2022.01.009

Ali, M., Hanı, U., & Alam, M. S. (2024). MHD boundary layer micropolar fluid flow over a stretching wedge surface: Thermophoresis and brownian motion effect. *Journal of Thermal Engineering, 10*(2), 330-349. https://doi.org/10.18186/thermal.1448609

Alkasasbeh, H. (2022). Mathematical modeling of MHD flow of hybrid micropolar ferrofluids about a solid sphere. *Frontiers in Heat and Mass Transfer (FHMT), 18*.

Alkasasbeh, H. T., Al Faqih, F. M., Alizadeh, A. A., Abderrahmane, A., Ali F. M., Zekri, H., Toghraie, D., Mourad, A., Guedri, K., & Younis, O. (2023). Computational modeling of hybrid micropolar nanofluid flow over a solid sphere. *Journal of Magnetism and Magnetic Materials, 569*, 170444. https://doi.org/https://doi.org/10.1016/j.jmmm.2023.170444

Alzahrani, J., Vaidya, H., Prasad, K. V., Rajashekhar, C., Mahendra, D. L., & Tlili, I. (2022). Micro-polar fluid flow over a unique form of vertical stretching sheet: Special emphasis to temperature-dependent properties. *Case Studies in Thermal Engineering, 34*, 102037. https://doi.org/https://doi.org/10.1016/j.csite.2022.102037

Amjad, M., Zehra, I., Nadeem, S., & Abbas, N. (2021). Thermal analysis of Casson micropolar nanofluid flow over a permeable curved stretching surface under the stagnation region. *Journal of Thermal Analysis and Calorimetry, 143*(3), 2485-2497. https://doi.org/10.1007/s10973-020-10127-w

Anderson, J. D. (2005). Ludwig Prandtl's boundary layer. *Physics Today, 58*(12), 42-48.

Andersson, H. I. (1992). MHD flow of a viscoelastic fluid past a stretching surface. *Acta Mechanica, 95*(1), 227-230. https://doi.org/10.1007/BF01170814

Anwar, I., Amin, N., & Pop, I. (2008). Mixed convection boundary layer flow of a viscoelastic fluid over a horizontal circular cylinder. *International Journal of Non-Linear Mechanics, 43*(9), 814-821. https://doi.org/https://doi.org/10.1016/j.ijnonlinmec.2008.04.008

Arakeri, J. H., & Shankar, P. (2000). Ludwig Prandtl and boundary layers in fluid flow. *Resonance, 5*(12), 48-63.

Arfken, G. B., Griffing, D. F., Kelly, D. C., & Priest, J. (1984). chapter 23 - Heat Transfer. In G. B. Arfken, D. F. Griffing, D. C. Kelly, & J. Priest (Eds.), *International Edition University Physics* (pp. 430-443). Academic Press. https://doi.org/https://doi.org/10.1016/B978-0-12-059858-8.50028-5

Ariel, P. D. (2002). On extra boundary condition in the stagnation point flow of a second grade fluid. *International Journal of Engineering Science, 40*(2), 145-162. https://doi.org/https://doi.org/10.1016/S0020-7225(01)00031-3

Arifin, N. S. B. (2019). Two-Phase Mixed Convection Flow Over A Vertical Stretching Sheet With Aligned Magnetic Field And Newtonian Heating.

Ariman, T., & Cakmak, A. S. (1968). Some basic viscous flows in micropolar fluids. *Rheologica Acta*, *7*(3), 236-242. https://doi.org/10.1007/BF01985784

Arjun, K. S., & Kumar, R. (2017). Performance Index in MHD Duct Nanofluid Flow Past a Bluff Body at High Re. *Journal of Mechanical Engineering/Strojniški Vestnik, 63*(4).

Asmat, F., Khan, W. A., Usman, Shamshuddin, M. D., Salawu, S. O., & Bouye, M. (2023). Thermal analysis in an electrically conducting fluid with multiple slips and radiation along a plate: A case study of Stokes' second problem. *Case Studies in Thermal Engineering*, *44*, 102831. https://doi.org/https://doi.org/10.1016/j.csite.2023.102831

Aurangzaib, Sharif Uddin, M., Bhattacharyya, K., & Shafie, S. (2016). Micropolar fluid flow and heat transfer over an exponentially permeable shrinking sheet. *Propulsion and Power Research, 5*(4), 310-317. https://doi.org/https://doi.org/10.1016/j.jppr.2016.11.005

Azizah Tukiran, N., & Ishak, A. (2012). Micropolar fluid flow over a shrinking sheet. *Meccanica, 47*. https://doi.org/10.1007/s11012-011-9439-8

Badami, M. M., Riasi, A., & Sadeghy, K. (2021). Numerical analysis of laminar viscoelastic fluid hammer phenomenon in an axisymmetric pipe. *Journal of the Brazilian Society of Mechanical Sciences and Engineering, 43*(8), 396. https://doi.org/10.1007/s40430-021-03113-2

Bafakeeh, O. T., Al-Khaled, K., Khan, S. U., Abbasi, A., Ganteda, C., Khan, M. I., Guedri, K., & Eldin, S. M. (2023). On the Bioconvective Aspect of Viscoelastic Micropolar Nanofluid Referring to Variable Thermal Conductivity and Thermo-Diffusion Characteristics. *Bioengineering, 10*(1), 73. https://www.mdpi.com/2306-5354/10/1/73

Beard, D., & Walters, K. (1964). Elastico-viscous boundary-layer flows I. Two-dimensional flow near a stagnation point. Mathematical Proceedings of the Cambridge Philosophical Society,

Bearman, P. (1997). Bluff body hydrodynamics. NAS Twenty-First Symposium on Naval Hydrodynamics,

Beg, O., Beg, T., Kadir, A., Leonard, H., Malysheva, L., Khan, U., & El Gendy, M. (2022). Numerical simulation of biomagnetic micropolar blood flow with the Rosensweig ferromagnetic formulation.

Beg, O. A., Ramachandra Prasad, V., Vasu, B., Bhaskar Reddy, N., Li, Q., & Bhargava, R. (2011). Free convection heat and mass transfer from an isothermal sphere to a micropolar regime with Soret/Dufour effects. *International Journal of Heat and Mass Transfer, 54*(1), 9-18. https://doi.org/https://doi.org/10.1016/j.ijheatmasstransfer.2010.10.005

Bejan, A. (2013). *Convection heat transfer*. John wiley & sons.

Bhukta, D., Dash, G. C., & Mishra, S. R. (2014). Heat and Mass Transfer on MHD Flow of a Viscoelastic Fluid through Porous Media over a Shrinking Sheet. *International Scholarly Research Notices, 2014*, 572162. https://doi.org/10.1155/2014/572162

Bibi, M., Zeeshan, A., Malik, M. Y., & Rehman, K. U. (2019). Numerical investigation of the unsteady solid-particle flow of a tangent hyperbolic fluid with variable thermal conductivity and convective boundary. *The European Physical Journal Plus, 134*(6), 298. https://doi.org/10.1140/epjp/i2019-12651-9

Bilal, S., Rehman, K. U., & Malik, M. Y. (2017). Numerical investigation of thermally stratified Williamson fluid flow over a cylindrical surface via Keller box method. *Results in Physics*, *7*, 690-696. https://doi.org/https://doi.org/10.1016/j.rinp.2017.01.032

Biswas, G. (2003). *Introduction to Fluid Mechanics and Fluid Machines, 2e*. Tata McGraw-Hill Education.

Biswas, P., Jony, A. H., & Islam, A. (2012). MHD micropolar fluid flow through vertical plate with heat generation. *Academic Research International*, *2*(1), 60-74.

Blasius, H. (1908). Boundary Layer in Fluid, Fluids with Less Friction, Z Math. *Phys, 56*, 1-37.

Bodart, C., & Crochet, M. J. (1994). The time-dependent flow of a viscoelastic fluid around a sphere. *Journal of Non-Newtonian Fluid Mechanics, 54*, 303-329. https://doi.org/https://doi.org/10.1016/0377-0257(94)80029-4

Boodoo, C. (2024). Micropolar Fluid Flows Past a Porous Shell: A Model for Drug Delivery Using Porous Microspheres. *European Journal of Engineering and Technology Research*, *9*(3), 1-7.

Bourgin, P., & Tichy, J. A. (1989). The effect of an additional boundary condition on the plane creeping flow of a second-order fluid. *International Journal of Non-Linear Mechanics*, *24*(6), 561-569. https://doi.org/https://doi.org/10.1016/0020-7462(89)90020-6

Bujurke, N. M., Biradar, S. N., & Hiremath, P. S. (1987). Second-order fluid flow past a stretching sheet with heat transfer. *Zeitschrift für angewandte Mathematik und Physik ZAMP*, *38*(4), 653-657. https://doi.org/10.1007/BF00946345

Buresti, G., & Piccardo, G. (2022). Bluff-Body Aerodynamics: Research Challenges from Wind Engineering. 50+ Years of AIMETA, Cham.

Cebeci, T., & Bradshaw, P. (1984). *Physical and computational aspects of convective heat transfer*.

Cebeci, T., Clark, R. W., Chang, K. C., Halsey, N. D., & Lee, K. (1986). Airfoils with separation and the resulting wakes. *Journal of Fluid Mechanics*, *163*, 323-347. https://doi.org/10.1017/S0022112086002318

Chandna, O. P., Barron, R. M., & Chew, K. T. (1982). Hodograph transformations and solutions in variably inclined MHD plane flows. *Journal of Engineering Mathematics*, *16*(3), 223-243. https://doi.org/10.1007/BF00042718

Chen, T. S., & Mucoglu, A. (1977). Analysis of mixed forced and free convection about a sphere. *International Journal of Heat and Mass Transfer, 20*(8), 867-875. https://doi.org/http://dx.doi.org/10.1016/0017-9310(77)90116-8

Cheng, C. Y. (2008). Natural convection heat and mass transfer from a sphere in micropolar fluids with constant wall temperature and concentration. *International Communications in Heat and Mass Transfer, 35*(6), 750-755.

Coleman, N. (2010). A Derivation of the Navier-Stokes Equations.

Cotter, C. S., Smolarkiewicz, P. K., & Szczyrba, I. N. (2002). A viscoelastic fluid model for brain injuries. *International Journal for Numerical Methods in Fluids, 40*(1-2), 303-311. https://doi.org/10.1002/fld.287

Dandapat, B. S., & Gupta, A. S. (1989). Flow and heat transfer in a viscoelastic fluid over a stretching sheet. *International Journal of Non-Linear Mechanics, 24*(3), 215-219. https://doi.org/https://doi.org/10.1016/0020-7462(89)90040-1

Dasman, A., Kasim, A. R. M., Waini, I., & Khashi'ie, N. S. (2021). Numerical Solution for Boundary Layer Flow of a Dusty Micropolar Fluid Due to a Stretching Sheet with Constant Wall Temperature. *Journal of Advanced Research in Fluid Mechanics and Thermal Sciences, 87*(1), 30-40.

Dasman, A., Kasim, M., Rahman, A., Mohammad, N. F., Mangi, A., & Shafie, S. (2013). Mixed Convection Boundary Layer Flow of Viscoelastic Fluids Past a Sphere. Defect and Diffusion Forum,

Davidson, P. A. (2016). The World of Metallurgical MHD. In P. A. Davidson (Ed.), *Introduction to Magnetohydrodynamics* (2 ed., pp. 307-316). Cambridge University Press. https://doi.org/DOI: 10.1017/9781316672853.015

Dawar, A., Shah, Z., Kumam, P., Alrabaiah, H., Khan, W., Islam, S., & Shaheen, N. (2020). Chemically reactive MHD micropolar nanofluid flow with velocity slips and variable heat source/sink. *Scientific Reports, 10*(1), 20926.

Denn, M. M. (1990). Issues in Viscoelastic Fluid Mechanics. *Annual Review of Fluid Mechanics, 22*(1), 13-32. https://doi.org/10.1146/annurev.fl.22.010190.000305

Dixon, V. A., & Woods, L. C. (1976). On the structure of oblique hydromagnetic shock waves. *Plasma Physics, 18*(8), 627-640. https://doi.org/10.1088/0032-1028/18/8/005

Eringen, A. C. (1964). Simple microfluids. *International Journal of Engineering Science, 2*(2), 205-217. https://doi.org/http://dx.doi.org/10.1016/0020-7225(64)90005-9

Eringen, A. C. (1966). Theory of Micropolar Fluids. *Journal of Mathematics and Mechanics, 16*(1), 1-18. www.jstor.org/stable/24901466

Eringen, A. C. (2001). *Microcontinuum field theories: II. Fluent media* (Vol. 2). Springer Science & Business Media.

Faltas, M. S., Sherief, H. H., & Ibrahim, M. A. (2020). Darcy–Brinkman Micropolar Fluid Flow through Corrugated Micro-Tube with Stationary Random Model. *Colloid Journal, 82*(5), 604-616. https://doi.org/10.1134/S1061933X20050075

Florea, O. A., & Roşca, I. C. (2015). Stokes' second problem for a micropolar fluid with slip. *Plos one, 10*(7), e0131860.

Frossling, N. (1958). Calculation by series expansion of the heat transfer in laminar, constant-property boundary layers at nonisothermal surfaces. *Arkiv Fysik, 14*.

Gaffar, S. A., Bég, O. A., & Prasad, V. R. (2020). Mathematical modeling of natural convection in a third-grade viscoelastic micropolar fluid from an isothermal inverted cone. *Iranian Journal of Science and Technology, Transactions of Mechanical Engineering, 44*(2), 383-402.

Garg, V. K., & Rajagopal, K. R. (1990). Stagnation point flow of a non-newtonian fluid. *Mechanics Research Communications*, *17*(6), 415-421.

Ghani, M., & Rumite, W. (2021). Keller-box scheme to mixed convection flow over a solid sphere with the effect of mhd. *MUST: Journal of Mathematics Education, Science and Technology*, *6*(1), 97-120.

Goldsworthy, F. A. (1961). Magnetohydrodynamic flows of a perfectly conducting, viscous fluid. *Journal of fluid Mechanics, 11*(4), 519-528.

Guedri, K., Mahmood, Z., Fadhl, B. M., Makhdoum, B. M., Eldin, S. M., & Khan, U. (2023). Mathematical analysis of nonlinear thermal radiation and nanoparticle aggregation on unsteady MHD flow of micropolar nanofluid over shrinking sheet. *Heliyon, 9*(3).

Habib, D., Salamat, N., Abdal, S. H. S., & Ali, B. (2022). Numerical investigation for MHD Prandtl nanofluid transportation due to a moving wedge: Keller box approach. *International Communications in Heat and Mass Transfer*, *135*, 106141. https://doi.org/https://doi.org/10.1016/j.icheatmasstransfer.2022.106141

Habib, D., Salamat, N., Hussain, S., Abdal, S., Hussein, A. K., & Ali, B. (2024). Variable viscosity effects on dynamic of non-Newtonian fluid nanofluid over a paraboloid of revolution via Keller box method. *The European Physical Journal Plus, 139*(5), 1-19.

Hayat, T., Abbas, Z., & Pop, I. (2008). Mixed convection in the stagnation point flow adjacent to a vertical surface in a viscoelastic fluid. *International Journal of Heat and Mass Transfer, 51*, 3200-3206. https://doi.org/10.1016/j.ijheatmasstransfer.2007.05.032

Heruska, M. W., Watson, L. T., & Sankara, K. K. (1986). Micropolar flow past a porous stretching sheet. *Computers & Fluids, 14*(2), 117-129.

Hieber, C. A., & Gebhart, B. (1969). Mixed convection from a sphere at small Reynolds and Grashof numbers. *Journal of Fluid Mechanics*, *38*(1), 137-159. https://doi.org/10.1017/S0022112069000097

Holbourn, A. H. S. (1943). Mechanics Of Head Injuries. *The Lancet, 242*(6267), 438-441. https://doi.org/https://doi.org/10.1016/S0140-6736(00)87453-X

Hossain, M., Das, S., & Pop, I. (1996). MHD free convection flow near rotating axisymmetric round-nosed bodies. *Magnetohydrodynamics, 32*(1), 63-67.

Hosseinzadeh, K., Roghani, S., Mogharrebi, A. R., Asadi, A., Waqas, M., & Ganji, D. D. (2020). Investigation of cross-fluid flow containing motile gyrotactic microorganisms and nanoparticles over a three-dimensional cylinder. *Alexandria Engineering Journal*, *59*(5), 3297-3307. https://doi.org/https://doi.org/10.1016/j.aej.2020.04.037

Hsiao, K. L. (2017). Micropolar nanofluid flow with MHD and viscous dissipation effects towards a stretching sheet with multimedia feature. *International Journal of Heat and Mass Transfer, 112*, 983-990.

Huang, M. J., & Chen, C. K. (1987). Laminar Free Convection From a Sphere With Blowing and Suction. *Journal of Heat Transfer, 109*(2), 529-532. https://doi.org/10.1115/1.3248117

Idowu, A., & Falodun, B. (2020). Variable thermal conductivity and viscosity effects on non-Newtonian fluids flow through a vertical porous plate under Soret-Dufour influence. *Mathematics and Computers in Simulation, 177*, 358-384.

Ilias, M. R., Rawi, N. A., & Shafie, S. (2016). MHD Free Convection Flow and Heat Transfer of Ferrofluids over a Vertical Flat Plate with Aligned and Transverse Magnetic Field. *Indian Journal of Science and Technology, 9*. https://doi.org/10.17485/ijst/2016/v9i36/97347

Ilias, M. R., Rosli, N. N., Ishak, S. S., David, V. D., Shafie, S., & Abd Rahman, M. N. (2023). Radiation and Nanoparticles Shape Effect on Aligned MHD Jeffrey Hybrid Nanofluids Flow and Heat Transfer over a Stretching Inclined Plate. *Journal of Advanced Research in Applied Mechanics, 109*(1), 84-102.

Incropera, F. P., DeWitt, D. P., Bergman, T. L., & Lavine, A. S. (1996). *Fundamentals of heat and mass transfer* (Vol. 6). Wiley New York.

Ishak, A. (2010). Thermal boundary layer flow over a stretching sheet in a micropolar fluid with radiation effect. *Meccanica, 45*(3), 367-373. https://doi.org/10.1007/s11012-009-9257-4

Ishak, A., Nazar, R., & Pop, I. (2006). Moving wedge and flat plate in a micropolar fluid. *International Journal of Engineering Science, 44*(18), 1225-1236. https://doi.org/https://doi.org/10.1016/j.ijengsci.2006.08.005

Jafar, A. B., Shafie, S., & Ullah, I. (2019). Magnetohydrodynamic Boundary Layer Flow of a Viscoelastic Fluid Past a Nonlinear Stretching Sheet in the Presence of Viscous Dissipation Effect. *Coatings, 9*(8), 490. https://www.mdpi.com/2079-6412/9/8/490

Javed, M. F., Khan, M. I., Khan, N. B., Muhammad, R., Rehman, M. U., Khan, S. W., & Khan, T. A. (2018). Axisymmetric flow of Casson fluid by a swirling cylinder. *Results in Physics, 9*, 1250-1255. https://doi.org/https://doi.org/10.1016/j.rinp.2018.04.015

Jones, J., & Lewis, M. (1968). On the streamline motion of elastico-viscous liquids in rotating channels. *Rheologica Acta, 7*(4), 307-316.

Josserand, J., Marty, P., & Alemany, A. (1993). Pressure and drag measurements on a cylinder in a liquid metal flow with an aligned magnetic field. *Fluid Dynamics Research, 11*(3), 107-117. https://doi.org/10.1016/0169-5983(93)90010-8

Kainz, M. P., Greiner, A., Hinrichsen, J., Kolb, D., Comellas, E., Steinmann, P., Budday, S., Terzano, M., & Holzapfel, G. A. (2023). Poro-viscoelastic material parameter identification of brain tissue-mimicking hydrogels [Original Research]. *Frontiers in Bioengineering and Biotechnology, 11*. https://doi.org/10.3389/fbioe.2023.1143304

Kakac, S., Liu, H., & Pramuanjaroenkij, A. (2002). *Heat exchangers: selection, rating, and thermal design*. CRC press.

Kakac, S., Yener, Y., & Pramuanjaroenkij, A. (2013). *Convective heat transfer*. CRC press.

Kapur, J. N. (1962). Flow of Reiner-Rivlin fluids in a magnetic field. *Applied Scientific Research, Section B, 10*(3), 183-194. https://doi.org/10.1007/BF02923436

Kasim, A., Mohammad, N., Aurangzaib, A., & Shafie, S. (2013). MHD mixed convection flow of viscoelastic fluid embedded in porous medium. *Malaysian Journal of Fundamental and Applied Sciences, 9*(1).

Kasim, A., Mohammad, N., Aurangzaib, A., & Shafie, S. (2013). Natural convection boundary layer flow past a sphere with constant heat flux in viscoelastic fluid. *Jurnal Teknologi, 62*(3).

Kasim, A., Mohammad, N., & Aurangzaib, S. S. (2012). Natural convection boundary layer flow of a viscoelastic fluid on solid sphere with Newtonian heating. *Data Processing, 329*, 2142.

Kasim, A. M., Mohammad, N., & Shafie, S. (2011). Effect of Heat Generation on Free Convection Boundary Layer Flow of a Viscoelastic Fluid Past a Horizontal Circular Cylinder with Constant Surface Heat Flux, 5th Int. Conf. *Research and Education in Mathematics (ICREM5), Bandung, Indonesia*.

Kasim, A. R. M., Admon, M. A., & Shafie, S. (2011). Free convection boundary layer flow of a viscoelastic fluid in the presence of heat generation. *Momentum, 10*(6).

Katopodes, N. D. (2019). Chapter 5 - Viscous Fluid Flow. In N. D. Katopodes (Ed.), *Free-Surface Flow* (pp. 324-426). Butterworth-Heinemann.

Keller, H. B., & Cebeci, T. (1972). Accurate numerical methods for boundary-layer flows. II: Two dimensional turbulent flows. *AIAA Journal, 10*(9), 1193-1199.

Khan, M., Ahmed, J., Ali, W., & Nadeem, S. (2020). Chemically reactive swirling flow of viscoelastic nanofluid due to rotating disk with thermal radiations. *Applied Nanoscience, 10*, 5219-5232.

Khan, N. A., Alshammari, F. S., Tavera Romero, C. A., Sulaiman, M., & Mirjalili, S. (2021). An Optimistic Solver for the Mathematical Model of the Flow of Johnson Segalman Fluid on the Surface of an Infinitely Long Vertical Cylinder. *Materials, 14*(24), 7798. https://www.mdpi.com/1996-1944/14/24/7798

Khan, U., Zaib, A., Ishak, A., Sherif, E.-S. M., Waini, I., Chu, Y.-M., & Pop, I. (2022). Radiative mixed convective flow induced by hybrid nanofluid over a porous vertical cylinder in a porous media with irregular heat sink/source. *Case Studies in Thermal Engineering, 30*, 101711. https://doi.org/https://doi.org/10.1016/j.csite.2021.101711

Koribilli, N., Aravamudan, K., & Aditya Varadhan, M. U. S. V. (2011). Quantifying Enhancement in Heat Transfer Due to Natural Convection During Canned Food Thermal Sterilization in a Still Retort. *Food and Bioprocess Technology, 4*(3), 429-450. https://doi.org/10.1007/s11947-009-0232-9

Kudenatti, R. B., & Amrutha, H. (2022). MHD boundary layer flow of viscoelastic fluid over a wedge in porous medium. *Archive of Applied Mechanics, 92*(12), 3983-3998.

Kumar, N. N., Sastry, D. R. V. S. R. K., & Shaw, S. (2022). Irreversibility analysis of an unsteady micropolar CNT-blood nanofluid flow through a squeezing channel with activation energy-Application in drug delivery. *Computer Methods and Programs in Biomedicine, 226*, 107156. https://doi.org/https://doi.org/10.1016/j.cmpb.2022.107156

Kumari, M., Takhar, H. S., & Nath, G. (1995). Nonsimilar mixed convection flow of a non-Newtonian fluid past a vertical wedge. *Acta Mechanica, 113*(1), 205-213. https://doi.org/10.1007/BF01212643

Li, B., Wang, C., & Chen, J. (2020). A Frequency-Correcting Method for a Vortex Flow Sensor Signal Based on a Central Tendency. *Sensors, 20*(18), 5379. https://www.mdpi.com/1424-8220/20/18/5379

Lien, F. S., & Chen, C. K. (1987). Mixed convection of micropolar fluid about a sphere with blowing and suction. *International Journal of Engineering Science, 25*(7), 775-784.

Lin, H. T., & Yu, W. S. (1988). Free Convection on a Horizontal Plate With Blowing and Suction. *Journal of Heat Transfer, 110*(3), 793-796. https://doi.org/10.1115/1.3250564

Lin, H. T., & Chen, C. C. (1988). Mixed convection on vertical plate for fluids of any prandtl number. *Wärme - und Stoffübertragung, 22*(3), 159-168.

Lukaszewicz, G. (1999). *Micropolar Fluids Theory and Applications* (1 ed.). Birkhäuser Basel. https://doi.org/10.1007/978-1-4612-0641-5

Ma, M., Ouyang, J., & Wang, X. (2023). Numerical study of viscoelastic flow around an oscillating circular cylinder. *Physics of Fluids, 35*(3). https://doi.org/10.1063/5.0141254

Mahat, R., Saqib, M., Ulah, I., Shafie, S., & Isa, S. M. (2022). Magnetohydrodynamics Mixed Convection of Viscoelastic Nanofluid Past a Circular Cylinder with Constant Heat Flux. *CFD letters, 14*(9), 52-59.

Mahat, R., Shafie, S., & Januddi, F. (2021). Numerical analysis of mixed convection flow past a symmetric cylinder with viscous dissipation in viscoelastic nanofluid. *CFD letters, 13*(2), 12-28.

Majid, N. A., Mohammad, N. F., Kasim, A. R. M., & Shafie, S. (2019). Forced convective of micropolar fluid on a stretching surface of another quiescent fluid. *MATEMATIKA: Malaysian Journal of Industrial and Applied Mathematics*.

Mehmood, Z., Mehmood, R., & Iqbal, Z. (2017). Numerical Investigation of Micropolar Casson Fluid over a Stretching Sheet with Internal Heating. *Communications in Theoretical Physics, 67*(4), 443. https://doi.org/10.1088/0253-6102/67/4/443

Mehta, R. D. (1985). Aerodynamics of Sports Balls. *Annual Review of Fluid Mechanics, 17*(1), 151-189. https://doi.org/10.1146/annurev.fl.17.010185.001055

Merkin, J. (1976). Free convection boundary layer on an isothermal horizontal cylinder. American Society of Mechanical Engineers and American Institute of Chemical Engineers, Heat Transfer Conference, St. Louis, Mo., Aug. 9-11, 1976, ASME 5 p.,

Merkin, J. (1977). Mixed convection from a horizontal circular cylinder. *International Journal of Heat and Mass Transfer, 20*(1), 73-77.

Merkin, J., & Pop, I. (1988). A note on the free convection boundary layer on a horizontal circular cylinder with constant heat flux. *Heat and Mass Transfer, 22*(1), 79-81.

Miklavcic, M., & Wang, C. Y. (2006). VISCOUS FLOW DUE TO A SHRINKING SHEET. *Quarterly of Applied Mathematics, 64*(2), 283-290. http://www.jstor.org/stable/43638726

Minaeian, A., Nili-Ahmadabadi, M., & Norouzi, M. (2020). Forced convective heat transfer of nonlinear viscoelastic flows over a circular cylinder at low Reynolds inertia regime. *Communications in Nonlinear Science and Numerical Simulation, 83*, 105134. https://doi.org/https://doi.org/10.1016/j.cnsns.2019.105134

Misra, J. C., Shit, G. C., & Rath, H. J. (2008). Flow and heat transfer of a MHD viscoelastic fluid in a channel with stretching walls: Some applications to haemodynamics. *Computers & Fluids, 37*(1), 1-11. https://doi.org/https://doi.org/10.1016/j.compfluid.2006.09.005

Mohamed, M. K. A., Ishak, A., Rosli, W. M. H. W., Soid, S. K., & Alkasasbeh, H. T. (2023). MHD Natural Convection Flow of Casson Ferrofluid over a Vertical Truncated Cone. *Journal of Advanced Research in Fluid Mechanics and Thermal Sciences, 112*(1), 94-105.

Mohamed, M. K. A., Noar, N. A. Z. M., Salleh, M. Z., & Ishak, A. (2019). Free convection boundary layer flow on a solid sphere in a nanofluid with viscous dissipation. *Malaysian Journal of Fundamental and Applied Sciences, 15*(3), 381-388.

Mohamed, M. K. A., Sarif, N. M., Noar, N., Salleh, M. Z., & Ishak, A. (2016). Viscous dissipation effect on the mixed convection boundary layer flow towards solid sphere. *Trans. Sci. Technol, 3*(1-2), 59-67.

Molla, M. M., Hossain, M. A., & Paul, M. C. (2006). Natural convection flow from an isothermal horizontal circular cylinder in presence of heat generation. *International Journal of Engineering Science, 44*(13-14), 949-958.

Mucoglu, A., & Chen, T. S. (1978). Mixed Convection about a Sphere with Uniform Surface Heat Flux. *Journal of Heat Transfer, 100*(3), 542-544. https://doi.org/10.1115/1.3450846

Muhammad, T., Waqas, H., Khan, S. A., Ellahi, R., & Sait, S. M. (2021). Significance of nonlinear thermal radiation in 3D Eyring–Powell nanofluid flow with Arrhenius activation energy. *Journal of Thermal Analysis and Calorimetry, 143*(2), 929-944. https://doi.org/10.1007/s10973-020-09459-4

Mukutadze, A., Opatskikh, A., & Prikhodko, V. (2022). Micropolar Lubricants in a Bearing with a Low-Melting Base Ring Coating and a Porous Slider Surface Coating. Proceedings of the 7th International Conference on Industrial Engineering (ICIE 2021) Volume I 7, Na, T. Y., & Pop, I. (1997). Boundary-layer flow of a micropolar fluid due to a stretching wall. *Archive of Applied Mechanics*, *67*, 229-236.

Nabwey, H. A., Rashad, A. M., El-Hakiem, A. M. A., & Alshber, S. I. (2022). Effectiveness of Newtonian Heating on Magneto-Free Convective Flow of Polar Nanofluid across a Solid Sphere. *Fractal and Fractional, 6*(2).

Nath, D., Pujari, P. C., Jain, A., & Rastogi, V. (2021). Drag reduction by application of aerodynamic devices in a race car. *Advances in Aerodynamics, 3*(1), 1-20.

Nath, G. (1975). Similar solutions for the incompressible laminar boundary layer with pressure gradient in micropolar fluids. *Rheologica Acta, 14*(9), 850-857. https://doi.org/10.1007/BF01521414

Nath, G. (1976, 1976/05/01). Nonsimilar incompressible laminar boundary-layer flows in micropolar fluids. *Rheologica Acta, 15*(5), 209-214. https://doi.org/10.1007/BF01521119

Nazar, R., & Amin, N. (2002). Free Convection Boundary Layer On An Isothermal Sphere In A Micropolar Fluid. *International Communications in Heat and Mass Transfer, 29*(3), 377-386. https://doi.org/https://doi.org/10.1016/S0735-1933(02)00327-5

Nazar, R., Amin, N., & Pop, I. (2002). Free convection boundary layer on an isothermal horizontal circular cylinder in a micropolar fluid. *Heat Transfer, 2*, 525-530.

Nazar, R., Amin, N., & Pop, I. (2003). Mixed convection boundary layer flow about an isothermal sphere in a micropolar fluid. *International Journal of Thermal Sciences, 42*(3), 283-293. https://doi.org/http://dx.doi.org/10.1016/S1290-0729(02)00027-3

Nazar, R., Pop, I., & Amin, N. (2003). Mixed convection boundary-layer flow from a horizontal circular cylinder in micropolar fluids: case of constant wall temperature. *International Journal of Numerical Methods for Heat & Fluid Flow, 13*(1), 86-109. https://doi.org/10.1108/09615530310456778

Nazar, R. M. (2004). *Mathematical models for free and mixed convection boundary layer flows of micropolar fluids* Universiti Teknologi Malaysia].

Nazemi, A., Baou, M., Jabari-Moghadam, A., & Norouzi, M. (2019). A numerical study on viscoelastic boundary layer on flat plate. *Journal of the Brazilian Society of Mechanical Sciences and Engineering, 42*(1), 11. https://doi.org/10.1007/s40430-019-2087-y

Oertel, H. (2010). Fundamental equations of fluid mechanics. In *Prandtl-Essentials of Fluid Mechanics* (pp. 265-343). Springer.

Oldroyd, J. G. (1950). On the formulation of rheological equations of state. *Proceedings of the Royal Society of London. Series A. Mathematical and Physical Sciences, 200*(1063), 523-541.

Ozisik, M. N. (1985). *Heat transfer: a basic approach* (Vol. 1). McGraw-Hill New York.

Padet, J., Cotta, R. M., Mladin, E. C., & Padet, C. (2015). Mixed thermal convection: fundamental issues and analysis of the planar case. *Anais da Academia Brasileira de Ciências, 87*, 1865-1885.

Papanastasiou, T., Georgiou, G., & Alexandrou, A. N. (2021). *Viscous fluid flow*. CRC press.

Parkinson, G. (1971). Wind-induced instability of structures. *Philosophical Transactions of the Royal Society of London. Series A, Mathematical and Physical Sciences*, *269*(1199), 395-413.

Peddieson, J. (1970). Boundary Layer Theory For A Micropolar Fluid.

Pimenta, F., & Alves, M. A. (2021). Conjugate heat transfer in the unbounded flow of a viscoelastic fluid past a sphere. *International Journal of Heat and Fluid Flow*, *89*, 108784. https://doi.org/https://doi.org/10.1016/j.ijheatfluidflow.2021.108784

Plan, E. L. C. VI M., Yeomans, J. M., & Doostmohammadi, A. (2020). Active matter in a viscoelastic environment. *Physical Review Fluids*, *5*(2), 023102. https://doi.org/10.1103/PhysRevFluids.5.023102

Poulikakos, D., & Renken, K. (1987). Forced convection in a channel filled with porous medium, including the effects of flow inertia, variable porosity, and Brinkman friction.

Prandtl, L. (1928). Motion of fluids with very little viscosity.

Prasad, K. M., & Yasa, P. R. (2021). Micropolar fluid flow in tapering stenosed arteries having permeable walls. *Malaysian journal of mathematical sciences*, *15*(1), 157-171.

Rajagopal, K. R., Na, T., & Gupta, A. (1984). Flow of a viscoelastic fluid over a stretching sheet. *Rheologica Acta*, *23*, 213-215.

Raman, R., Dewang, Y., & Raghuwanshi, J. (2018). A review on applications of computational fluid dynamics. *2*.

Ramzan, M., Farooq, M., Hayat, T., & Chung, J. D. (2016). Radiative and Joule heating effects in the MHD flow of a micropolar fluid with partial slip and convective boundary condition. *Journal of Molecular Liquids*, *221*, 394-400. https://doi.org/https://doi.org/10.1016/j.molliq.2016.05.091

Ramzan, M., Saeed, A., Dawar, A., Lone, S. A., Kumam, P., & Watthayu, W. (2022). Applications of solar radiation toward the slip flow of a non-Newtonian viscoelastic hybrid nanofluid over a rotating disk. *ZAMM-Journal of Applied Mathematics and Mechanics/Zeitschrift für Angewandte Mathematik und Mechanik*, *102*(12), e202200127.

Rana, P., Mahanthesh, B., Nisar, K. S., Swain, K., & Devi, M. (2021). Boundary layer flow of magneto-nanomicropolar liquid over an exponentially elongated porous plate with Joule heating and viscous heating: a numerical study. *Arabian Journal for Science and Engineering*, *46*, 12405-12415.

Rashad, A. M., Khan, W. A., El-Kabeir, S. M. M., & El-Hakiem, A. M. A. (2019). Mixed Convective Flow of Micropolar Nanofluid across a Horizontal Cylinder in Saturated Porous Medium. *Applied Sciences*, *9*(23), 5241. https://www.mdpi.com/2076-3417/9/23/5241

Rauf, A., Shah, N. A., Mushtaq, A., & Botmart, T. (2023). Heat transport and magnetohydrodynamic hybrid micropolar ferrofluid flow over a non-linearly stretching sheet. *AIMS Math, 8*(1), 164-193.

Reddy, S. R. R., Jakeer, S., & Rupa, M. L. (2023). ANN model of three-dimensional micropolar dusty hybrid nanofluid flow with coriolis force: biomedical applications. *Indian Journal of Physics*, *97*(13), 3801-3825. https://doi.org/10.1007/s12648-023-02737-5

Rock, A., Hincapie, R. E., Tahir, M., Langanke, N., & Ganzer, L. (2020). On the Role of Polymer Viscoelasticity in Enhanced Oil Recovery: Extensive Laboratory Data and Review. *Polymers*, *12*(10), 2276. https://www.mdpi.com/2073-4360/12/10/2276

Rosaidi, N. A., Ab Raji, N. H., Ibrahim, S. N. H. A., & Ilias, M. R. (2022). Aligned magnetohydrodynamics free convection flow of magnetic nanofluid over a moving vertical plate with convective boundary condition. *Journal of Advanced Research in Fluid Mechanics and Thermal Sciences, 93*(2), 37-49.

Sadiq, M. A., Khan, A. U., Saleem, S., & Nadeem, S. (2019). Numerical simulation of oscillatory oblique stagnation point flow of a magneto micropolar nanofluid [10.1039/C8RA09698H]. *RSC Advances*, *9*(9), 4751-4764. https://doi.org/10.1039/C8RA09698H

Saeed, A., Alsubie, A., Kumam, P., Nasir, S., Gul, T., & Kumam, W. (2021). Blood based hybrid nanofluid flow together with electromagnetic field and couple stresses. *Scientific Reports*, *11*(1), 12865. https://doi.org/10.1038/s41598-021-92186-z

Saha, A. K., Muralidhar, K., & Biswas, G. (2000). Experimental study of flow past a square cylinder at high Reynolds numbers. *Experiments in Fluids, 29*(6), 553-563. https://doi.org/10.1007/s003480000123

Saleem, A., Kiani, M. N., Nadeem, S., Akhtar, S., Ghalambaz, M., & Issakhov, A. (2021). Electroosmotically driven flow of micropolar bingham viscoplastic fluid in a wavy microchannel: application of computational biology stomach anatomy. *Computer Methods in Biomechanics and Biomedical Engineering*, *24*(3), 289-298. https://doi.org/10.1080/10255842.2020.1827236

Saleem, M., Hossain, M. A., & Saha, S. C. (2012). Mixed Convection Flow of Micropolar Fluid in an Open Ended Arc-Shape Cavity. *Journal of Fluids Engineering*, *134*(9). https://doi.org/10.1115/1.4007268

Salleh, M. Z., Nazar, R., & Pop, I. (2012). Numerical solutions of free convection boundary layer flow on a solid sphere with Newtonian heating in a micropolar fluid [journal article]. *Meccanica*, *47*(5), 1261-1269. https://doi.org/10.1007/s11012-011-9510-5

Sankara, K., & Watson, L. (1985). Micropolar flow past a stretching sheet. *Zeitschrift für angewandte Mathematik und Physik ZAMP*, *36*, 845-853. https://doi.org/10.1007/BF00944898

Sarpkaya, T. (1961). Flow of non-Newtonian fluids in a magnetic field. *AIChE Journal*, *7*(2), 324-328.

Schlichting, H., & Gersten, K. (2016). *Boundary-layer theory*. Springer.

Schlichting, H., & Kestin, J. (1960). *Boundary layer theory*. McGraw-Hill. https://books.google.com.my/books?id=gtXjoAEACAAJ

Sekhar, T. V. S., Sivakumar, R., Kumar, H., & Ravi kumar, T. V. R. (2007). Effect of aligned magnetic field on the steady viscous flow past a circular cylinder. *Applied Mathematical Modelling, 31*(1), 130-139. https://doi.org/https://doi.org/10.1016/j.apm.2005.08.011

Shabbir, T., Mushtaq, M., Ijaz Khan, M., & Hayat, T. (2020). Modeling and numerical simulation of micropolar fluid over a curved surface: Keller box method. *Computer Methods and Programs in Biomedicine, 187*, 105220.

Shah, Z., Islam, S., Ayaz, H., & Khan, S. (2019). Radiative Heat and Mass Transfer Analysis of Micropolar Nanofluid Flow of Casson Fluid Between Two Rotating Parallel Plates With Effects of Hall Current. https://doi.org/10.1115/1.4040415]

Sharma, S., Lambha, S., Mittal, V., & Verma, R. (2023). Micropolar lubricant effects on the performance of partial journal bearings. *Proceedings of the Institution of Mechanical Engineers, Part J: Journal of Engineering Tribology*, 13506501231161379.

Siddiqa, S., Begum, N., Hossain, M. A., Abrar, M. N., Gorla, R. S. R., & Al-Mdallal, Q. (2021). Effect of thermal radiation on conjugate natural convection flow of a micropolar fluid along a vertical surface. *Computers & Mathematics with Applications*, *83*, 74-83. https://doi.org/https://doi.org/10.1016/j.camwa.2020.01.011

Singh, J., & Nayak, P. (2023). pH-responsive polymers for drug delivery: Trends and opportunities. *Journal of Polymer Science*.

Sparrow, E., & Lee, L. (1976). Analysis of mixed convection about a horizontal cylinder. *International Journal of Heat and Mass Transfer, 19*(2), 229-232.

Subramanian, R. (2019a). Navier-Stokes Equation: Principle of Conservation of Momentum.

Subramanian, R. (2019b). Some Elementary Aspects of Boundary Layer Theory.

Sun, F., Wen, X., Si, X., Xie, C., Li, B., Cao, L., & Zhu, J. (2024). Numerical simulations of the Oldroyd-B fluid flow around triangular cylinders with different orientations. *Journal of Non-Newtonian Fluid Mechanics, 326*, 105204.

Svorcan, J., Wang, J. M., & Griffin, K. P. (2022). Current state and future trends in boundary layer control on lifting surfaces. *Advances in Mechanical Engineering, 14*(7), 16878132221112161. https://doi.org/10.1177/16878132221112161

Tamoor, M., Waqas, M., Khan, M. I., Alsaedi, A., & Hayat, T. (2017). Magnetohydrodynamic flow of Casson fluid over a stretching cylinder. *Results in Physics, 7*, 498-502. https://doi.org/https://doi.org/10.1016/j.rinp.2017.01.005

Tani, I. (1977). History of Boundary Layer Theory. *Annual Review of Fluid Mechanics, 9*(1), 87-111. https://doi.org/10.1146/annurev.fl.09.010177.000511

Tipei, N. (1979). Lubrication With Micropolar Liquids and Its Application to Short Bearings. *Journal of Lubrication Technology, 101*(3), 356-363. https://doi.org/10.1115/1.3453375

Tschoegl, N. W. (1989). Energy Storage and Dissipation in a Linear Viscoelastic Material. In N. W. Tschoegl (Ed.), *The Phenomenological Theory of Linear Viscoelastic Behavior: An Introduction* (pp. 443-488). Springer Berlin Heidelberg. https://doi.org/10.1007/978-3-642-73602-5_9

Veena, N., Dinesh, P. A., Abraham, A., & Idicula, J. J. (2023). Viscoelastic dielectric liquid flow over a horizontal stretching sheet. *Journal of Thermal Analysis and Calorimetry*. https://doi.org/10.1007/s10973-023-12480-y

Verma, P., & Govardhan, M. (2011). Flow behind bluff bodies in side-by-side arrangement. *Journal of Engineering Science and Technology, 6*, 745-768.

Vijaya, R. B., Prasad, K. M., & Umadevi, C. (2016). A mathematical model for micropolar fluid flow through an artery with the effect of stenosis and post stenotic dilatation. *Applications and Applied Mathematics: An International Journal (AAM), 11*(2), 12.

Vilchevskaya, A. E., Vilchevskaya, E. N., Müller, W. H., & Eremeyev, V. A. (2023). Modeling of blood flow in the framework of micropolar theory. *Continuum Mechanics and Thermodynamics*, 1-23.

Wakif, A. (2020). A Novel Numerical Procedure for Simulating Steady MHD Convective Flows of Radiative Casson Fluids over a Horizontal Stretching Sheet with Irregular Geometry under the Combined Influence of Temperature-Dependent Viscosity and Thermal Conductivity. *Mathematical Problems in Engineering, 2020*, 1675350. https://doi.org/10.1155/2020/1675350

Wang, C. Y. (1990). Liquid Film On An Unsteady Stretching Surface. *Quarterly of Applied Mathematics, 48*(4), 601-610. http://www.jstor.org/stable/43637666

Wang, L., & Chu, X. (2023). An extended CFD-DEM model based on micropolar fluid and its application in geological engineering. *Computers and Geotechnics, 154*, 105133. https://doi.org/https://doi.org/10.1016/j.compgeo.2022.105133

Watkins, S. (2010). Aerodynamic noise and its refinement in vehicles. In X. Wang (Ed.), *Vehicle Noise and Vibration Refinement* (pp. 219-234). Woodhead Publishing. https://doi.org/https://doi.org/10.1533/9781845698041.3.219

Willson, A. J. (1970). Boundary layers in micropolar liquids. *Mathematical Proceedings of the Cambridge Philosophical Society, 67*(2), 469-476. https://doi.org/10.1017/S0305004100045746

Yagmur, S., Dogan, S., Aksoy, M. H., Canli, E., & Ozgoren, M. (2015). Experimental and Numerical Investigation of Flow Structures around Cylindrical Bluff Bodies. *EPJ Web of Conferences, 92*, 02113. https://doi.org/10.1051/epjconf/20159202113

Yanovych, V., Duda, D., & Uruba, V. (2021). Structure turbulent flow behind a square cylinder with an angle of incidence. *European Journal of Mechanics - B/Fluids, 85*, 110-123. https://doi.org/https://doi.org/10.1016/j.euromechflu.2020.09.003

Yasin, S. H. M., Mohamed, M. K. A., Ismail, Z., & Salleh, M. Z. (2020). MHD free convection boundary layer flow near the lower stagnation point flow of a horizontal circular cylinder in ferrofluid. *IOP Conference Series: Materials Science and Engineering, 736*(2), 022117. https://doi.org/10.1088/1757-899x/736/2/022117

Yasin, S. H. M., Mohamed, M. K. A., Ismail, Z., Widodo, B., & Salleh, M. Z. (2022). Numerical Investigation of Ferrofluid Flow at Lower Stagnation Point over a Solid Sphere using Keller-Box Method. *Journal of Advanced Research in Fluid Mechanics and Thermal Sciences, 94*(2), 200-214.

Yasmin, A., Ali, K., & Ashraf, M. (2020). Study of heat and mass transfer in MHD flow of micropolar fluid over a curved stretching sheet. *Scientific Reports, 10*(1), 4581.

Yuge, T. (1960). Experiments on Heat Transfer From Spheres Including Combined Natural and Forced Convection. *Journal of Heat Transfer, 82*(3), 214-220. https://doi.org/10.1115/1.3679912

Zakaria, K. A., & Amin, N. S. (2014). The Lorentz Force. *International Journal of Scientific and Innovative Mathematical Research (IJSIMR), 2*(4), 378-380.

Zhou, P. B. (1993). Finite difference method. In *Numerical Analysis of Electromagnetic Fields* (pp. 63-94). Springer.

Zohuri, B. (2018). Chapter 5 First Law of Thermodynamics. In B. Zohuri (Ed.), *Physics of Cryogenics* (pp. 119-163). Elsevier. https://doi.org/https://doi.org/10.1016/B978-0-12-814519-7.00005-7

Zu-gan, Q., & Zhang-ji, L. (1987). Lubrication theory for micropolar fluids and its application to a journal bearing with finite length. *Applied Mathematics and Mechanics, 8*(7), 655-665. https://doi.org/10.1007/BF02458263

APPENDIX

Appendix A: Fortran algorithm

This is the Fortran algorithm for the problem mixed convection boundary layer flow of viscoelastic micropolar fluid past a horizontal circular cylinder with aligned magnetic effect

```
      program autobox

      parameter(nx=1001,ny=1001,neq=8,neq1=9)
      implicit real*8(a-h,o-z)
      real*8 x(nx),y(ny),sol(neq,nx,ny), xtemp(nx),ytemp(ny),
     +hh(nx)
      real*8 tf, ts, tm
      character*20 fname
      common /kbox1/sol,x,y,sfric,hh
      common /data/gamma,zkay,omega,Pr,ampli,pi,fw,M

      print*,'Problem Viscoelastic Micropolar fluid'
        xmax=6
      kx=301
      do 11 i=1,kx
      xtemp(i)=dble(i-1)*xmax/dble(kx-1)
   11 continue
        ymax=8
      ky=301
            do 20 i=1,ky
            ytemp(i)=dble(i-1)*ymax/dble(ky-1)
   20 continue

      nsub=1
      if((kx-1)*nsub+1.gt.nx)then
      print*,'No.of points too large'
      print*,'kx=',kx
      print*,'nx=',nx
      print*,'==>',(kx-1)*nsub+1
      stop
      end if
      do 21 i=1,kx-1
      ii=(i-1)*nsub+1
      do 22 j=1,nsub
      x(ii+j-1)=xtemp(i)+(xtemp(i+1)-xtemp(i))*dble(j-1)/dble(nsub)
   22 continue
   21 continue
      x((kx-1)*nsub+1)=xtemp(kx)
      kx=(kx-1)*nsub+1

      nsub=1
      if((ky-1)*nsub+1.gt.ny)then
      print*,'No.of points too large'
      print*,'ky=',ky
      print*,'ny=',ny
      print*,'==>',(ky-1)*nsub+1
```

```
      stop
      end if
      do 27 i=1,ky-1
      ii=(i-1)*nsub+1
      do 28 j=1,nsub
      y(ii+j-1)=ytemp(i)+(ytemp(i+1)-ytemp(i))*dble(j-1)/dble(nsub)
   28 continue
   27 continue
      y((ky-1)*nsub+1)=ytemp(ky)
      ky=(ky-1)*nsub+1

      dx=xmax/dble(kx-1)
      kperiod=2.000001/dx

      fw=0.5
       M=1
      omega=1
       zkay=0.5
      Pr=21
      tol=1.d-10
       maxits=50
      pi=4.d0*datan(1.d0)
      call kbox(kx,ky,tol,maxits,kperiod)

  876 format(1000(1x,f11.6))
*
      print*,'File for shear stress result?'
      read*,fname
      if(fname.eq.'no')goto 35
      open(10,file=fname)
      do 878 i=1,kx
      write(10,876) x(i), sol(3,i,1), -sol(6,i,1)

  878 continue

   35 continue

        print*,'file name for velocity/temperature?'
      read*,fname
      if(fname.eq.'no')goto 42
      open(10,file=fname)
      do 668 i=1,kx,100
        write(10,871)i,x(i)
  871 format(1x,i5,1x,f11.6)
       do 667 j=1,ky
        write(10,876) y(j),sol(2,i,j),sol(5,i,j),sol(7,i,j)
  667   continue
 668   continue
        close(10)
   42   continue

      read*,nans
      if(nans.eq.1)then
   40 continue
      print*,'Which variable?'
      read*,nvar
      if(nvar.eq.0)stop
```

```
      call rufcon(sol,nx,ny,kx,ky,nvar)
      goto 40
      end if
*
      stop
      end

              subroutine kbox(kx,ky,tol,maxits,kperiod)
              implicit real*8(a-h,o-z)
              parameter(nx=1001,ny=1001,neq=8,neq1=9)
              real*8 y(ny),x(nx),dy(ny),yy(ny),hh(nx)
              real*8 yb(neq,ny),yi(neq,ny),dyi(neq,ny)
              real*8 a(neq,neq,ny),b(neq,neq,ny),c(neq,neq,ny),
     +        rhs(neq,ny)
              real*8 sol(neq,nx,ny)
              real*8 ymvec(neq),yvec(neq),ypvec(neq)
              real*8 ybmvec(neq),ybvec(neq),ybpvec(neq)
              real*8 amat(neq,neq),bmat(neq,neq),cmat(neq,neq),
     +        rhsvec(neq)
*
              common /kbox1/sol,x,y,sfric,hh
              common /data/gamma,zkay,omega,Pr,ampli,pi,fw,M
              common /bits/xx,dx,yvalm,yvalp,dym,dyp

               print*,'maxits,tol,n,K,w,Prandtl,amplitud,R'
               print*,maxits,tol,gamma,zkay,omega,Pr,ampli,M
               do 10 k=1,ky
               do 10 i=1,neq
               yi(i,k)=0.d0
               yb(i,k)=0.d0
   10        continue
             do 15 k=1,ky
             yi(2,k)=1.d0-dexp(-y(k))
             yi(1,k)=y(k)+dexp(-y(k))-1.d0
             yi(3,k)=dexp(-y(k))
   15        continue
             do 20 k=1,ky-1
             yy(k)=0.5d0*(y(k)+y(k+1))
             dy(k)=y(k+1)-y(k)
   20        continue

             do 999 ibox=1,kx
             if(ibox.eq.1)then
             xx=x(1)
             dx=1.d0
             else
             xx=0.5d0*(x(ibox-1)+x(ibox))
             dx=x(ibox)-x(ibox-1)
             end if

             do 990 kits=1,maxits
             do 30 k=1,ky
             kp=k+1
             km=k-1
             if(k.eq.1)km=1
             if(k.eq.ky)kp=ky
             do j=1,neq
               ymvec(j)=yi(j,km)
```

```
            yvec(j)=yi(j,k)
            ypvec(j)=yi(j,kp)
            ybmvec(j)=yb(j,km)
            ybvec(j)=yb(j,k)
            ybpvec(j)=yb(j,kp)
          end do
          yvalm=yy(km)
          yvalp=yy(k)
          dym=dy(km)
          dyp=dy(k)
          kval=k

      call calcmats(amat,bmat,cmat,ymvec,yvec,ypvec,ybmvec,ybvec,
     +ybpvec,rhsvec,ibox,kval,ky)
*
          do 50 i=1,neq
          do 50 j=1,neq
            a(i,j,k)=amat(i,j)
            b(i,j,k)=bmat(i,j)
            c(i,j,k)=cmat(i,j)
   50     continue
            do 60 i=1,neq
            rhs(i,k)=rhsvec(i)
   60     continue
   30   continue

            call btdma(a,b,c,rhs,dyi,ky,det)
*
            dymax=0.d0
            rfact=1.d0
*           if(kits.gt.5)rfact=0.7d0
            do 70 i=1,neq
            do 70 k=1,ky
            chek=dabs(dyi(i,k))
            if(chek.gt.dymax)dymax=chek
            yi(i,k)=yi(i,k)+dyi(i,k)*rfact
   70   continue

            if(dymax.lt.tol)then
            ibl=iblend(yi,ky)

         write(6,998)ibox,kits,y(ibox), yi(2,1), yi(5,1)

  998     format(1x,i4,1x,i3,5(1x,f10.6),1x,i3,1x,f10.6)
                goto 991
                end if
  990   continue
             print*,ibox,xx,' Not converged ',maxits
             kx=ibox-1
             return
  991   continue
*
             do 80 i=1,neq
             do 80 k=1,ky
             yb(i,k)=yi(i,k)
             sol(i,ibox,k)=yi(i,k)
   80   continue
  999      continue
```

```
      return
      end

      subroutine btdma(a,b,c,rhs,y,n,det)
      implicit real*8(a-h,o-z)
      parameter(nx=1001,ny=1001,neq=8,neq1=9)
*
      real*8 a(neq,neq,ny),b(neq,neq,ny),c(neq,neq,ny)
      real*8 rhs(neq,ny),y(neq,ny)
      real*8 gerhs(neq,neq1),gemat(neq,neq),gesol(neq,neq1)

    do 10 kk=1,n-1
    do 20 i=1,neq
       gerhs(i,neq1)=rhs(i,kk)
    do 20 j=1,neq
       gerhs(i,j)=c(i,j,kk)
       gemat(i,j)=b(i,j,kk)
20   continue
      call gausse(gemat,gesol,gerhs,neq,neq1,det)
      do 30 i=1,neq
      rhs(i,kk)=gesol(i,neq1)
      do 30 j=1,neq
      c(i,j,kk)=gesol(i,j)
30   continue
      do 40 i=1,neq
      do 40 k=1,neq
      temp=0.d0
      do 50 j=1,neq
      temp=temp+a(i,j,kk+1)*c(j,k,kk)
50     continue
        b(i,k,kk+1)=b(i,k,kk+1)-temp
40   continue
      do 60 i=1,neq
      temp=0.d0
      do 70 j=1,neq
      temp=temp+a(i,j,kk+1)*rhs(j,kk)
70     continue
      rhs(i,kk+1)=rhs(i,kk+1)-temp
60   continue
10   continue
*
      do 80 i=1,neq
      gerhs(i,neq1)=rhs(i,n)
      do 80 j=1,neq
      gerhs(i,j)=b(i,j,n)
      gemat(i,j)=b(i,j,n)
80  continue
      call gausse(gemat,gesol,gerhs,neq,neq1,det)
     do 90 i=1,neq
       y(i,n)=gesol(i,neq1)
90  continue
     do 100 kk=n-1,1,-1
     do 110 i=1,neq
     temp=rhs(i,kk)
     do 120 j=1,neq
     temp=temp-c(i,j,kk)*y(j,kk+1)
120    continue
     y(i,kk)=temp
```

```
 110    continue
 100    continue
             return
             end

             subroutine rufcon(a,nxm,nym,kx,ky,nvar)
             parameter(nx=1001,ny=1001,neq=8,neq1=9)
             implicit real*8(a-h,o-z)
             real*8 a(neq,nxm,nym)
             character*1 c(nx)
             character*1 ch(11)
             ch(1)='0'
             ch(2)='1'
             ch(3)='2'
             ch(4)='3'
             ch(5)='4'
             ch(6)='5'
             ch(7)='6'
             ch(8)='7'
             ch(9)='8'
             ch(10)='9'
             ch(11)='t'
             c(kx+1)=' '
             print*,'Basic (1) or pert (0)'
             read*,npb
             kxy=kx*ky
             amax=biggest(a,nxm,nym,kx,ky,nvar,npb)
             amin=smallest(a,nxm,nym,kx,ky,nvar,npb)
             print*,'psimax,min=',amax,amin
             if(nvar.eq.1)then
             print*,'OK?'
             read*,nans
             if(nans.eq.0)then
             print*,'max min ='
             read*,amax,amin
             end if
             end if
             adiff=amax-amin
             if(adiff.ne.0.)adiff=1./adiff
*
             nfact=kx/130+1
             do 30 j=1,ky
             jj=ky-j+1
             do 10 i=1,kx/nfact
             if(npb.eq.1)then
              x=1.5+10.*(a(nvar,i*nfact,jj)-amin)*adiff
             else
              x=1.5+10.*(a(nvar,i*nfact,jj)-amin-a(nvar,1,jj))*adiff
             end if
      n=x
      if(n.gt.11)c(i)='T'
      if(n.lt.1)c(i)='Z'
      if(n.ge.1.and.n.le.11)c(i)=ch(n)
      if(npb.eq.1)then
      if(a(nvar,i*nfact,jj).gt.amax)c(i)='T'
      if(a(nvar,i*nfact,jj).lt.amin)c(i)='Z'
      else
      if(a(nvar,i*nfact,jj)-a(nvar,1,jj).gt.amax)c(i)='T'
```

```
      if(a(nvar,i*nfact,jj)-a(nvar,1,jj).lt.amin)c(i)='Z'
      end if
   10 continue
      m=kx/nfact
      if(m.gt.130)m=130
      write(6,20)(c(k),k=1,m)
   20 format(1x,200a1)
   30 continue
      return
      end

      double precision function smallest(a,nxm,nym,kx,ky,nvar,npb)
      parameter(nx=1001,ny=1001,neq=8,neq1=9)
      implicit real*8(a-h,o-z)
      real*8 a(neq,nxm,nym)
      if(npb.eq.1)then
      z=a(nvar,1,1)
      else
      z=0.d0
      end if
      do 10 i=1,kx
      do 10 j=1,ky
      if(npb.eq.1)then
      val=a(nvar,i,j)
      else
      val=a(nvar,i,j)-a(nvar,1,j)
      end if
      if(z.gt.val)z=val
   10 continue
      smallest=z
      return
      end

      double precision function biggest(a,nxm,nym,kx,ky,nvar,npb)
      parameter(nx=1001,ny=1001,neq=8,neq1=9)
      implicit real*8(a-h,o-z)
      real*8 a(neq,nxm,nym)
      if(npb.eq.1)then
      z=a(nvar,1,1)
      else
      z=0.d0
      end if
      do 10 i=1,kx
      do 10 j=1,ky
      if(npb.eq.1)then
      val=a(nvar,i,j)
      else
      val=a(nvar,i,j)-a(nvar,1,j)
      end if
      if(z.lt.val)z=val
   10 continue
      biggest=z
      return
      end

      subroutine gausse(a,x,b,n,nvec,det)
      implicit real*8(a-h,o-z)
      real*8 a(n,n),b(n,nvec),x(n,nvec)
```

```
      if(n.eq.1)then
      do 700 i=1,nvec
      x(1,i)=b(1,i)/a(1,1)
  700 continue
      return
      end if
*
      eps=1.d-20
      do 10 k=1,(n-1)
      kpvt=k
      kp1=k+1
      do 35 i=kp1,n
      if (abs(a(kpvt,k)).lt.abs(a(i,k))) kpvt=i
   35 continue
      if (abs(a(kpvt,k)).lt.eps) goto 50
      if (kpvt.eq.k) goto 25
      do 45 jcol=k,n
      save=a(k,jcol)
      a(k,jcol)=a(kpvt,jcol)
      a(kpvt,jcol)=save
   45 continue
      do 710 iii=1,nvec
      save=b(k,iii)
      b(k,iii)=b(kpvt,iii)
      b(kpvt,iii)=save
  710 continue
      goto 25
   50 print*,'Sorry, the matrix is singular, i.e. det=0.'
      print*,'Gaussian Elimination does not work.'
      return
   25 do 15 i=k+1,n
      q=-a(i,k)/a(k,k)
      a(i,k)=0.d0
      do 20 j=k+1,n
      a(i,j)=a(i,j)+q*a(k,j)
   20 continue
      do 720 iii=1,nvec
      b(i,iii)=b(i,iii)+q*b(k,iii)
  720 continue
   15 continue
   10 continue
      det=1.d0
      do 70 i=1,n
      det=det*a(i,i)
   70 continue

      do 730 iii=1,nvec
      x(n,iii)=b(n,iii)/a(n,n)
  730 continue
      do 75 i=n-1,1,-1
      do 740 iii=1,nvec
      s=0.d0
      do 80 j=i+1,n
      s=s+a(i,j)*x(j,iii)
   80 continue
      x(i,iii)=(b(i,iii)-s)/a(i,i)
  740 continue
```

```
   75 continue
      return
      end

      subroutine calcmats(amat,bmat,cmat,ym,y,yp,ybm,yb,
     +ybp,rhs,ibox,kval,ky)
      parameter(nx=1001,ny=1001,neq=8,neq1=9)
      implicit real*8(a-h,o-z)
      real*8 ym(neq),y(neq),yp(neq),ybm(neq),yb(neq),ybp(neq)
      real*8 tempm(neq),temp(neq),tempp(neq),rhseps(neq)
      real*8 amat(neq,neq),bmat(neq,neq),cmat(neq,neq),rhs(neq)

      common /bits/xx,dx,yvalm,yvalp,dym,dyp

      eps=1.d-6
      call calcrhs(rhs,ym,y,yp,ybm,yb,ybp,ibox,kval,ky)

  901 format(100(1x,f12.6))
      do 10 i=1,neq
*
      do 20 j=1,neq
      tempm(j)=ym(j)
      temp(j)=y(j)
      tempp(j)=yp(j)
   20 continue
      tempm(i)=tempm(i)+eps
      call calcrhs(rhseps,tempm,temp,tempp,ybm,yb,ybp,ibox,kval,ky)
      do 30 j=1,neq
      amat(j,i)=-(rhseps(j)-rhs(j))/eps
   30 continue
*
      do 40 j=1,neq
      tempm(j)=ym(j)
      temp(j)=y(j)
      tempp(j)=yp(j)
   40 continue
      temp(i)=temp(i)+eps
      call calcrhs(rhseps,tempm,temp,tempp,ybm,yb,ybp,ibox,kval,ky)
      do 50 j=1,neq
      bmat(j,i)=-(rhseps(j)-rhs(j))/eps
   50 continue
*
      do 60 j=1,neq
      tempm(j)=ym(j)
      temp(j)=y(j)
      tempp(j)=yp(j)
   60 continue
      tempp(i)=tempp(i)+eps
      call calcrhs(rhseps,tempm,temp,tempp,ybm,yb,ybp,ibox,kval,ky)
      do 70 j=1,neq
      cmat(j,i)=-(rhseps(j)-rhs(j))/eps
   70 continue
*
   10 continue
      return
      end

      subroutine calcrhs(rhs,ym,y,yp,ybm,yb,ybp,ibox,kval,ky)
```

```fortran
      parameter(nx=1001,ny=1001,neq=8,neq1=9)
      implicit real*8(a-h,o-z)
      real*8 rhs(neq),ym(neq),y(neq),yp(neq),ybm(neq),yb(neq),ybp(neq)
      real*8 avem(neq),avep(neq)
      real*8 diffxm(neq),diffxp(neq),diffym(neq),diffyp(neq)
*
      common /data/gamma,zkay,omega,Pr,ampli,pi,fw,M
      common /bits/xval,dx,yvalm,yvalp,dym,dyp
*
      do 10 i=1,neq
      if(ibox.eq.1)then
      avem(i)=(ym(i)+y(i))/2.d0
      avep(i)=(y(i)+yp(i))/2.d0
      diffxm(i)=0.d0
      diffxp(i)=0.d0
      diffym(i)=(y(i)-ym(i))/dym
      diffyp(i)=(yp(i)-y(i))/dyp
      else
      avem(i)=(ym(i)+y(i)+ybm(i)+yb(i))/4.d0
      avep(i)=(y(i)+yp(i)+yb(i)+ybp(i))/4.d0
      diffxm(i)=(ym(i)+y(i)-ybm(i)-yb(i))/(2.d0*dx)
      diffxp(i)=(yp(i)+y(i)-ybp(i)-yb(i))/(2.d0*dx)
      diffym(i)=(y(i)-ym(i)+yb(i)-ybm(i))/(2.d0*dym)
      diffyp(i)=(yp(i)-y(i)+ybp(i)-yb(i))/(2.d0*dyp)
      end if
   10 continue
*
      if(ibox.eq.1)then
      if(kval.eq.1)then
      rhs(1)=y(1)
      rhs(2)=y(2)
      rhs(3)=y(5)-1.d0
      rhs(4)=y(7)+(1.d0/2.d0)*y(3)
      else
      rhs(1)=-diffym(1)+avem(2)
      rhs(2)=-diffym(2)+avem(3)
      rhs(3)=diffym(6)+ Pr*avem(1)*avem(6)
      rhs(4)=-diffym(7)+avem(8)
      end if
*
      if(kval.eq.ky)then
      rhs(5)=y(2)-1.d0
      rhs(6)=y(3)
      rhs(7)=y(5)
      rhs(8)=y(7)
      else
      rhs(5)=-diffyp(5)+avep(6)
      rhs(6)=(1.d0+fw)*avep(4)+avep(1)*avep(3)-avep(2)*avep(2)
     + - zkay*(-2.d0*avep(2)*avep(4)
     + + avep(3)*avep(3)+avep(1)*diffyp(4))-(1.d0/1.d0)*M*(avep(2)-
1.d0)
     + + 1.d0+omega*avep(5)+fw*avep(8)
      rhs(7)=-diffyp(3)+avep(4)
      rhs(8)=(1.d0+(1.d0/2.d0)*fw)*diffyp(8)+avep(1)*avep(8)
     +-avep(2)*avep(7)-fw*(2.d0*avep(7)+avep(3))
      end if

      else
```

```
      if(kval.eq.1)then
      rhs(1)=y(1)
      rhs(2)=y(2)
      rhs(3)=y(5)-1.d0
      rhs(4)=y(7)+(1.d0/2.d0)*y(3)
      else
      rhs(1)=-diffym(1)+avem(2)
      rhs(2)=-diffym(2)+avem(3)
      rhs(3)=diffym(6)+ Pr*avem(1)*avem(6)
     +-xval*Pr*(avem(2)*diffxm(5)-diffxm(1)*avem(6))
      rhs(4)=-diffym(7)+avem(8)
      end if
*
      if(kval.eq.ky)then
      rhs(5)=y(2)-sin(xval)/xval
      rhs(6)=y(3)
      rhs(7)=y(5)
      rhs(8)=y(7)
      else
      rhs(5)=-diffyp(5)+avep(6)
      rhs(6)=avep(4)+avep(1)*avep(3)-avep(2)*avep(2)+fw*avep(8)
     + + (sin(xval)*cos(xval)/xval) + omega*avep(5)* sin(xval)/xval
     + + zkay*(2.d0*avep(2)*avep(4))
     + - avep(3)*avep(3) - avep(1)*diffyp(4)
     + +  xval*( diffxp(2)*avep(4)+avep(2)*diffxp(4)
     + - diffxp(1)*diffyp(4)-  avep(3)*diffxp(3) )  )
     + -(1.d0/1.d0)*M*(avep(2)-sin(xval)/xval)
     + -  xval* ( avep(2)*diffxp(2)-diffxp(1)*avep(3) )
      rhs(7)=-diffyp(3)+avep(4)
      rhs(8)=(1.d0+(1.d0/2.d0)*fw)*diffyp(8)+avep(1)*avep(8)
     + - avep(2)*avep(7)-fw*(2.d0*avep(7)+avep(3))
     + - xval*(avep(2)*diffxp(7)-diffxp(1)*avep(8))

      end if
      end if
      return
      end

      integer function iblend(yi,ky)
      parameter(nx=1001,ny=1001,neq=8,neq1=9)
      implicit real*8(a-h,o-z)
      real*8 yi(neq,ny)
*
      ibl=0
      do 10 i=2,ky
      if(dabs(yi(2,i)-1.d0).lt.1.d-2)then
      ibl=i
      goto 20
      end if
      ibl=i
   10 continue
   20 continue
      iblend=ibl
      return
      end
```